



HAL
open science

Energy-based variational modelling of adiabatic shear band structure

Shaopu Su

► **To cite this version:**

Shaopu Su. Energy-based variational modelling of adiabatic shear band structure. Solid mechanics [physics.class-ph]. Ecole Centrale de Nantes (ECN), 2012. English. NNT: . tel-00797178

HAL Id: tel-00797178

<https://theses.hal.science/tel-00797178v1>

Submitted on 5 Mar 2013

HAL is a multi-disciplinary open access archive for the deposit and dissemination of scientific research documents, whether they are published or not. The documents may come from teaching and research institutions in France or abroad, or from public or private research centers.

L'archive ouverte pluridisciplinaire **HAL**, est destinée au dépôt et à la diffusion de documents scientifiques de niveau recherche, publiés ou non, émanant des établissements d'enseignement et de recherche français ou étrangers, des laboratoires publics ou privés.

Ecole Centrale de Nantes

ÉCOLE DOCTORALE

Sciences Pour l'Ingénieur, Géosciences, Architecture

Année 2012

Thèse de DOCTORAT

Spécialité: GÉNIE MÉCANIQUE

Présentée et soutenue publiquement par:

SHAOPU SU

le 28 Novembre 2012

à l'École Centrale de Nantes

TITRE

**MODÉLISATION DES BANDES DE CISAILLEMENT
ADIABATIQUE PAR UNE APPROCHE ÉNERGÉTIQUE
VARIATIONNELLE**

JURY

Président:	M. MERCIER Sébastien	Professeur, Université de Lorraine
Rapporteur:	M. LEROY Yves	Directeur de Recherche CNRS, ENS Paris
	M. LONGÈRE Patrice	Professeur, ISAE, Toulouse
Examineur:	M. RACINEUX Guillaume	Professeur, École Centrale de Nantes
	M. STAINIER Laurent	Professeur, École Centrale de Nantes

Directeur de thèse: STAINIER Laurent

Laboratoire: GEM, École Centrale de Nantes

N° ED 498-248

Résumé :

Une Bande de Cisaillement Adiabatique (BCA) est une bande étroite associée à de grandes déformations et de hautes températures dans les matériaux ductiles. Il est bien établi que les BCAs impliquent souvent une dépendance au maillage dans la simulation numérique du phénomène localisé. Pour contourner cette difficulté, des modèles de discontinuités ont été proposés et largement appliqués en ingénierie. Cependant, des conditions cruciales doivent être vérifiées afin de développer ces modèles, telles que des descriptions précises des profils physiques, des relations de comportement dans des approches multi-physiques et surtout une capacité de prédiction de la largeur de bande. Sans discrétisation du domaine physique, on propose un nouveau modèle de la structure de BCA basé sur une approche énergétique variationnelle, incluant l'élasticité, l'écrouissage, la conduction de chaleur et la condition limite thermique. Les lois de comportement sont transformées en un problème d'optimisation mathématique par rapport à un ensemble de scalaires. A l'aide d'expressions canoniques de profils de déplacement et de température, la largeur de bande et la température centrale sont calculées en tant que des variables internes du potentiel incrémental total en régime stationnaire et transitoire. Comme application de notre modélisation variationnelle 1D à la localisation de cisaillement, on étend et propose une modélisation variationnelle à deux échelles en introduisant un "élément de localisation de la déformation". Contrairement aux travaux existant, des déformations plastiques et des températures non homogènes sont prises en compte par les expressions analytiques canoniques, et l'évolution de la largeur de bande est calculée comme un problème d'optimisation d'une fonctionnelle énergétique. Une dérivation variationnelle valide sa faisabilité théorique. De même, une implémentation d'élément fini est également dérivée et donne une bonne fondation pour une future mise en oeuvre.

Mots clés: Approche énergétique variationnelle, Couplage thermo-mécanique, Thermo-visco-plasticité, Bandes de cisaillement adiabatique

Abstract :

An Adiabatic Shear Band (ASB) is a relatively narrow band presenting large deformation and high temperature, occurring in various ductile materials. It is well established that ASBs can cause mesh dependence in the numerical simulation of this localization phenomenon. In this respect, several discontinuous models have been proposed and widely applied for overcoming this difficulty. Yet some crucial conditions are substantially required to build and improve these models, such as the accurate description of physical profiles, additional constitutive relations in multi-physical approaches and the prevision of bandwidth evolution. Without a mesh to discretize the physical domain, we propose a new energy-based variational model for adiabatic shear banding structure, including elasticity, work hardening, heat conduction and thermal boundary condition. Balance and constitutive equations are transformed into a mathematical optimization problem with respect to a limited set of scalars. Consequently by means of canonical expressions of displacement and temperature profiles, the bandwidth and central temperature can be accurately tracked as internal variables of the total incremental potential in steady and transient state. As an application of our 1D variational modelling for shear localization, we extend it and propose a variational two-scale model resorting to a strain localization element. Compared to existing work, the advantage of our approach is that an inhomogeneous plastic deformation and temperature distribution in the localized region are introduced by canonical analytical expressions. Moreover bandwidth evolution can be accurately calculated by the optimization of an incremental potential. The variational derivation theoretically validates the feasibility of our two-scale modelling. Furthermore finite element implementation is derived and gives a good base for future implementation.

Keywords: Variational method, Thermo-mechanical coupling, Thermo-visco-plasticity, Adiabatic shear bands

Discipline : Sciences de l'Ingénieur

Ecole Centrale de Nantes

ÉCOLE DOCTORALE

Sciences Pour l'Ingénieur, Géosciences, Architecture

Année 2012

Thèse de DOCTORAT

Spécialité: GÉNIE MÉCANIQUE

Présentée et soutenue publiquement par:

SHAOPU SU

le 28 Novembre 2012

à l'École Centrale de Nantes

TITRE

Energy-based variational modelling of adiabatic shear band structure

JURY

Président:	M. MERCIER Sébastien	Professeur, Université de Lorraine
Rapporteur:	M. LEROY Yves	Directeur de Recherche CNRS, ENS Paris
	M. LONGÈRE Patrice	Professeur, ISAE, Toulouse
Examineur:	M. RACINEUX Guillaume	Professeur, École Centrale de Nantes
	M. STAINIER Laurent	Professeur, École Centrale de Nantes

Directeur de thèse: STAINIER Laurent

Laboratoire: GEM, École Centrale de Nantes

N° ED 498-248

Acknowledgments

Over the past three years in France, I have received a lot of support, encouragement and assistances from a number of sources in my work and my life. Words are weak and inadequate to express my appreciation in this text.

First of all, I offer my sincerest gratitude to my supervisor: Laurent Stainier, who provides many guidances with his patience and serious attitude for the research. It is rightly him to introduce me to the research world of thermo-mechanical coupling. His outstanding expertise and distinctive advice make me enjoy working with him and benefit a lot. When I did my PHD in the first year, communication problem and the weak background of the thesis cause a lot of inconveniences for him. He always takes them and solves the problems that I met with great patience. He never gives me up, but continuously gives me the high confidence. Without his good supervision, my thesis can not be finished and would be poorer.

I extend my appreciation to Professor Sébastien Mercier giving me a lot of assistances in my thesis. The chapter 2 is the work with his collaboration during the study time in Metz. Although we worked together in a short time, I have a great pleasure to study with him because of his dedicated attitude to work, the kindness and the humorous. In addition, some expensive advices contribute a lot to my thesis.

I want to offer my large gratitude to my colleagues in the Simulation & Structure group, especially for the persons in my office: Augusto Selke Emmel, Jean-Charles Guldner, Mathieu Foca and Raphaël Allais. They gave me lots of help in my work, my study of language and my life in France. The completion of the thesis can not be done without their advices in the manuscript. I think it is my fortunate to work in this cheerful and friendly office. Moreover, a lot of thanks are given to Thibault Gorris, Loïc Giraldi, Kevin Moreau, Olivier Zahm for their assistances in compiling the thesis, computer operation and code programming. In addition, The discussions with the professors Anthony Nouy, Eduardo Alberto Fancello and Nicolas Chevaugéon provide me good inspirations in my research.

Thanks a lot to the finance support of my study abroad: China Scholarship Council. Since admitted as a member of this PHD programme in 2009, my Chinese friends, also my comrades have accompanied me in these years. We encouraged and supported each other, making me not feel lonely when staying in abroad.

Last but not the least, I am grateful to the support of my family and my friend Jiang Hui in China. It is a hard time to live without their accompanies, and the three years' abroad life also make me realize their importances in my heart. They offer me lots of

encouragement in my three years of PHD life. My courage can not insist without their support.

We might as well say that this is an emotional thesis with many visible and invisible efforts from a great number of people.

Shaopu SU

September 2012

Abstract

An Adiabatic Shear Band (ASB) is a relatively narrow band presenting large deformation and high temperature, occurring in various ductile materials. It is well established that ASBs can cause mesh dependence in the numerical simulation of this localization phenomenon. In this respect, several discontinuous models have been proposed and widely applied for overcoming this difficulty. Yet some crucial conditions are substantially required to build and improve these models, such as the accurate description of physical profiles, additional constitutive relations in multi-physical approaches and the prevision of bandwidth evolution.

Without a mesh to discretize the physical domain, we propose a new energy-based variational model for adiabatic shear banding structure, including elasticity, work hardening, heat conduction and thermal boundary condition. Balance and constitutive equations are transformed into a mathematical optimization problem with respect to a limited set of scalars. Consequently by means of canonical expressions of displacement and temperature profiles, the bandwidth and central temperature can be accurately tracked as internal variables of the total incremental potential in steady and transient state.

Based on this thermo-mechanical coupled variational framework, we can verify the generality of the proposed analytical approach with respect to constitutive models, as illustrated through various thermal softening laws. The corresponding influence of material parameters is also analysed in the study. We can show that the onset of ASBs is easier for small strain rate sensibility exponent, high thermal softening coefficient and high-speed loading. In addition, we numerically validated that thermal conduction is a noticeable parameter in the final term of ASBs formation, influencing the size of bandwidth. Considering that it is difficult to keep an isothermal boundary condition of the layer undergoing high strain rate, the additional heat exchange on the boundary is included in the variational models. Moreover, a formula for exchange coefficient is numerically fitted and conveniently applied in the calculation of the transient state, which ensures the independence of bandwidth on structure size. Accounting for work hardening and elasticity, we propose a new thermo-elasto-viscoplastic model of shear localization for the widely used Johnson-Cook law in engineering. A new loading/unloading condition, stemming as a Kuhn-Tucker relation, is introduced for this variational model. The stress evolution and the influence of cyclic loading on the formation of ASB are analysed, presenting a good correspondence with simulations by finite element method.

As an application of our 1D variational modelling for shear localization, we extend it and propose a variational two-scale model resorting to a strain localization element. Com-

pared to existing work, the advantage of our approach is that an inhomogeneous plastic deformation and temperature distribution in the localized region are introduced by canonical analytical expressions. Moreover bandwidth evolution can be accurately calculated by the optimization of an incremental potential. The variational derivation theoretically validates the feasibility of our two-scale modelling. Furthermore finite element implementation is derived and gives a good base for future implementation.

Keywords: Variational method, Thermo-mechanical coupling, Thermo-visco-plasticity, Adiabatic shear bands

Résumé

Une Bande de Cisaillement Adiabatique (BCA) est une bande étroite associée à de grandes déformations et de hautes températures dans les matériaux ductiles. Il est bien établi que les BCAs impliquent souvent une dépendance au maillage dans la simulation numérique du phénomène localisé. Pour contourner cette difficulté, des modèles de discontinuités ont été proposés et largement appliqués en ingénierie. Cependant, des conditions cruciales doivent être vérifiées afin de développer ces modèles, telles que des descriptions précises des profils physiques, des relations de comportement dans des approches multi-physiques et surtout une capacité de prédiction de la largeur de bande.

Sans discrétisation du domaine physique, on propose un nouveau modèle de la structure de BCA basé sur une approche énergétique variationnelle, incluant l'élasticité, l'écrouissage, la conduction de chaleur et la condition limite thermique. Les lois de comportement sont transformées en un problème d'optimisation mathématique par rapport à un ensemble de scalaires. À l'aide d'expressions canoniques de profils de déplacement et de température, la largeur de bande et la température centrale sont calculées en tant que des variables internes du potentiel incrémental total en régime stationnaire et transitoire.

Basée sur le cadre variationnel en thermomécanique couplée, la généralité des formulations analytiques proposées par rapport aux modèles constitutives est vérifiée sur différentes lois d'adoucissement thermique. Les influences correspondantes des paramètres du matériau sont analysées dans cette étude. On observe qu'il est facile de provoquer l'apparition de BCAs dans les matériaux ayant un petit exposant de sensibilité à la vitesse de déformation, un coefficient élevé d'adoucissement thermique et une vitesse de chargement élevée. En outre, on valide numériquement que la conduction thermique est un paramètre remarquable dans la dernière phase de la formation de BCA, qui influence la largeur de bande. En considérant qu'une bande soumise à de grandes vitesses de déformation garde difficilement une condition isotherme aux frontières, l'échange de chaleur supplémentaire est ensuite incluse dans la modélisation variationnelle. On propose une formule du coefficient d'échange, qui joue un effet important en régime transitoire par une méthode d'ajustement polynomial, garantissant l'indépendance de la largeur de bande par rapport à la taille de la structure. En incluant l'écrouissage et l'élasticité dans le modèle de Johnson-Cook, un nouveau modèle thermique élasto-viscoplastique de BCA est proposé pour analyser les évolutions de contrainte sous un chargement cyclique, aussi bien que l'influence de chargement en BCA. Les résultats correspondent bien aux simulations par la méthode des éléments finis.

Comme application de notre modélisation variationnelle 1D à la localisation de ci-

saillement, on étend et propose une modélisation variationnelle à deux échelles en introduisant un “élément de localisation de la déformation”. Contrairement aux travaux existant, des déformations plastiques et des températures non homogènes sont prises en compte par les expressions analytiques canoniques, et l’évolution de la largeur de bande est calculée comme un problème d’optimisation d’une fonctionnelle énergétique. Une dérivation variationnelle valide sa faisabilité théorique. De même, une implémentation d’élément fini est également dérivée et donne une bonne fondation pour une future mise en oeuvre.

Mots clés: Approche énergétique variationnelle, Couplage thermo-mécanique, Thermo-visco-plasticité, Bandes de cisaillement adiabatique

Contents

Acknowledgments	i
Abstract	iii
Résumé	v
Contents	vii
1 Introduction	1
1.1 Adiabatic shear bands	3
1.2 State-of-the-art	4
1.2.1 Experiments	5
1.2.2 Theoretical analysis	8
1.2.3 Numerical implication	14
1.3 Energy-based variational method	17
1.4 Thesis outline	20
2 Variational modelling in steady state	23
2.1 General framework	25
2.1.1 Variational formulation in thermo-mechanical coupling	25
2.1.2 Rayleigh-Ritz method	29
2.2 Couette flow and thermal layer	30
2.3 Thermal Couette flow	31
2.3.1 Analytical solutions	31
2.3.2 Variational formulations	32
2.4 Fully formed adiabatic shear band	34
2.4.1 Analytical solutions	36
2.4.2 Variational modelling with Rayleigh-Ritz method	37
2.4.3 Results and analysis	40
2.4.4 Extension to various constitutive relations	43
2.4.5 Thermal boundary condition	48
2.5 Conclusions	53

3	Variational modelling in transient state	55
3.1	Variational updates	58
3.1.1	Variational framework	58
3.1.2	Finite element method	61
3.2	Thermo-visco-plastic variational modelling	63
3.2.1	Variational modelling for exponential softening law	63
3.2.2	Influence of material parameters	70
3.2.3	Extension to various constitutive model	75
3.2.4	Variational modelling with hardening	76
3.2.5	Variational modelling with thermal boundary condition	81
3.3	Thermo-elasto-visco-plastic variational modelling	85
3.3.1	Variational modelling	86
3.3.2	Numerical validation	89
3.3.3	Average stress analysis	94
3.4	Conclusions	96
4	Variational two-scale modelling in 2D/3D	99
4.1	Mesh dependence in standard FEM	102
4.2	Variational two-scale method	108
4.2.1	Discontinuous approaches	108
4.2.2	Variational two-scale modelling	114
4.3	Finite element implementation	118
4.3.1	Finite element modelling	118
4.3.2	Thermo-mechanical flux	121
4.4	Conclusions	124
5	Conclusions and perspectives	127
5.1	Conclusions	127
5.2	Discussion and future work	129
	Conclusions et perspectives	131
A	Verification of variational modelling	135
B	Additional derivation in interface element	137
	List of Figures	141
	List of Tables	145
	Bibliography	147

Chapter 1

Introduction

Abstract :

In thermo-visco-plastic materials, adiabatic shear localization occurs easily when they are subjected to intense impact loading. Since Tresca first observed this phenomenon during the forging of a platinum bar, it has attracted a considerable attention from researchers as a precursor to cracks. This chapter will give a detailed description of adiabatic shear bands, and illustrate its study status from the experimental, theoretical analysis and numerical simulation points of view in the last several decades, pointing out the advantages of our approach to this thermo-mechanical coupled problem.

Résumé :

Les bandes de cisaillement adiabatique (BCA) apparaissent souvent dans les matériaux thermo-visco-plastique soumises aux chargements impacts intenses. Leur formation suscite un grand intérêt en vue des applications en dynamique des matériaux depuis elle est observée pendant le forgeage d'une barre de platine. Ce chapitre présente brièvement une description des BCAs, et illustre leur cadre d'étude pendant des dernières décennies compte tenu des développements des expériences, des analyses théoriques et des simulations numériques, puis indique des avantages de notre approche pour modéliser le problème de BCA.

Contents

1.1	Adiabatic shear bands	3
1.2	State-of-the-art	4
1.2.1	Experiments	5
1.2.1.1	Split Hopkinson Bar	5
1.2.1.2	Kalthoff's experiment	6
1.2.1.3	Thick-walled compression and torsion experiments	7
1.2.2	Theoretical analysis	8
1.2.2.1	Critical condition	9
1.2.2.2	Band profiles	9
1.2.2.3	Band width	11
1.2.3	Numerical implication	14
1.2.3.1	Finite element method	14
1.2.3.2	Meshless method	15
1.2.3.3	Extended finite element method	16
1.3	Energy-based variational method	17
1.4	Thesis outline	20

1.1 Adiabatic shear bands

Adiabatic shear instability is an ordinary phenomenon in ductile materials undergoing high strain rate loading. Under strong impacts, a lot of heat and intense strain accompanying inelastic deformation form in localized zones in a short time, which we call adiabatic shear bands. Since first observed and correctly interpreted by Tresca in the 19th century, shear bands have drawn a great attention in the research community on its initiation, propagation and formation. In general, adiabatic shear band is the result of thermo-mechanical instability appearing at large deformation and high temperature in the narrow regions, usually a few tens of micrometers width. Thus the existence of jump distance makes it seem as a singular surface due to its thin thickness between two sides of the band. Yet from the experiment photos in microscopic state it still represents a good continuity in the materials, the traction can transform from one side to the other side in that region. FIG.1.1 is the shear band observed in the bulk material under the optical microscope [Odeshi et al., 2006].

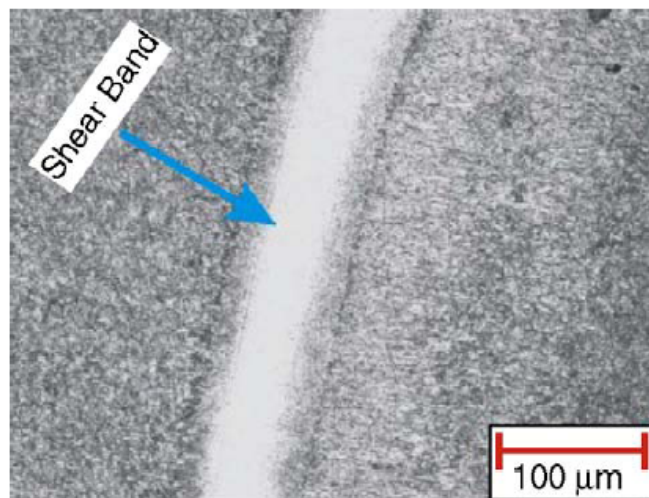


Figure 1.1: Adiabatic shear band in the bulk material ([Odeshi et al., 2006])

The localized band frequently occurs in a wide range of metals, alloys, fractured and granular ceramics, polymers and ductile single crystals during high shearing rate process. This failure mechanism has been observed in ballistic penetration, metal forming, explosive-metal interaction and shock loading. Similarly, if we neglect thermal softening in civil engineering, the localized regions presenting in rocks and concrete can be seen as isothermal shear bands. Physically, the formation of adiabatic shear bands is an interactive process: an increase in strain rate in a weaker zone causes a local increase in temperature which in turn, causes a further increase in strain rate [Molinari and Clifton, 1987] for a thermal softening material. The high temperature (several hundreds degrees) and enormous deformation are the main characters of adiabatic shear bands. The reason why we call it adiabatic is that the formation of band is so short that the heat exited from the band is negligible compared with the concentrated part in the band. However, it is a misnomer

about this phenomenon. Many experiments confirm that the thermal conduction has an important effect in the final stage of its formation. Once the instability and localization set in, the gradient of temperature on the boundary will influence the bandwidth and the central temperature, thus the material is no longer adiabatic. This is also why we should consider the conduction in numerical simulation.

Although the profiles of localized band are continuous in fully microscopic physics of material, large inhomogeneous distributions of temperature and strain rate cause the damage of material properties in localization region. Furthermore, voids and micro-cracks appear gradually in the evolution of adiabatic shear bands, and accelerate catastrophic failure. FIG.1.2 is the micro-structure in the localized shear zone of Ti-6Al-4V alloy obtained by [Bai et al., 1994]. Thus many researchers regard this domain as a precursor to the rupture of the material. Normally it should be deleterious to the performance of material in the mind of most researchers, yet recently Magness [Magness et al., 1994] proposed that adiabatic shear failure contrarily enhance the performance of U3/4Ti as a penetrator material [Wright, 2002]. Better understanding of shear bands' formation, propagation and behavior is also of interest in the development of metal forming and optimum design.

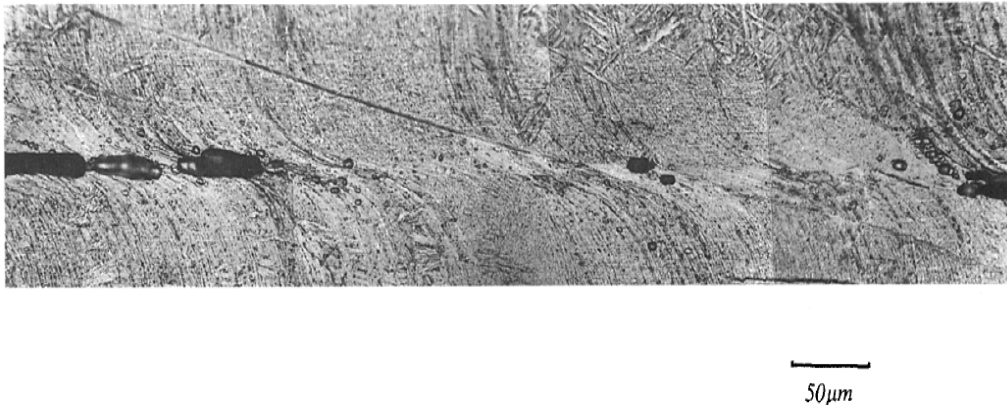


Figure 1.2: Voids and micro-cracks (Ti-6Al-4V alloy [Bai et al., 1994]) in adiabatic shear band

1.2 State-of-the-art

For this coupled thermo-mechanical problem characterized by large deformation localized in tens of micrometres and high temperature close to melting point, experiments or numerical simulation present many challenges. Here we give a short overview of the research of adiabatic shear bands in last several decades.

1.2.1 Experiments

In general, the experimental structures for the investigation of adiabatic shear bands mainly concentrate in the following types: Split Hopkinson Bar in one-dimensional test, Kalthoff's experiment, collapse of thick-walled cylinder and thick-walled torsion experiments.

1.2.1.1 Split Hopkinson Bar

Split Hopkinson Bar is the most widely used device to test the form of stress-strain diagram at high-strain rate loading, and we call it one dimensional experiment owing to its loading at one direction. Roughly speaking, it is divided into three variations according to the loading states: tension, compression and torsion. The specimen must be short and ductile enough that it can come into equilibrium state when the high impacting forces are acted on the two bars during the early part of loading pulse. Usually the dynamic force is uniformly subjected to the materials, thus once the shear localization happens, all the bands will propagate at the same time.

The formation of adiabatic shear bands (ASBs) in hat-shaped specimen operated by split Hopkinson pressure bar is mostly referenced in the area of shear localization. Since firstly introduced by Meyer and Manwaring [Meyer and Manwaring, 1986], this technique has been widely and successfully applied in the analysis of different material properties under the occurrence of shear localization at high strain rate loading. For instance, Longère [Longère et al., 2005] presented the formation of ASBs in hard structural steel to validate their thermal elastic-viscoplastic constitutive model with viscous deterioration. The influences of geometry sizes on stress rate in Ti-6Al-4V are also investigated at quasi-static and dynamic impacting by Peirs [Peirs et al., 2008], and it is found that the width of the shear region and the radius of the corners play an important role in their constitutive relations. Besides these, the dynamic effect of adiabatic shearing on its propagation and fracture behaviour is studied for AISI 4340 steel at high compressive strain-rate [Odeshi et al., 2005]. They point out that the bands are inherently very hard and brittle, and exhibit a tendency to brittle fracture, causing fast propagation speed. Critical condition is also a hotspot in experimental view. Li [Li et al., 2003] obtained that the critical strain rate for failure was $\dot{\epsilon}_c = 2000s^{-1}$ in titanium alloy-Ti17 though impacting cylindrical and conical frustum specimens.

Dynamic torsion experiment concerning hat-shaped specimen also contributes a lot in the examination of ASB [Bai et al., 1994, Ranc et al., 2008]. FIG.1.3 is the formation process of ASB and the corresponding stress-strain curve of Ti-6Al-4V [Liao and Duffy, 1998] tested by dynamic torsional experiment. In the first stage, material experiences an homogeneous elastic and plastic deformation, and arrives at the maximum shear stress with further hardening. Subsequently, strain softening plays a gradually important effect (in the second stage), and then influences the magnitudes of stress, which dropped suddenly due to thermal softening (in the third stage). Meanwhile the variation of temperature also passes three stages: from unapparent increase to gradually slow changes, finally arriving at a large and fast increase. In general, ASBs form prior to or at the start of sudden drop

in stress.

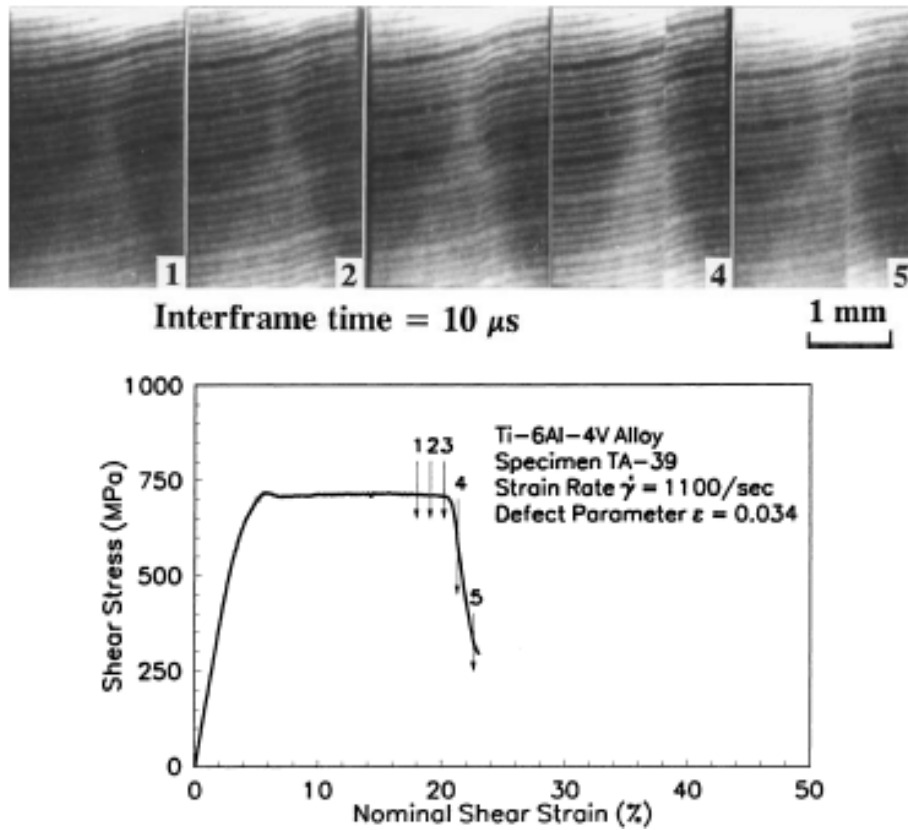


Figure 1.3: Stress-strain curves at High-speed photographs of the grid pattern(Ti-6Al-4V alloy in [Liao and Duffy, 1998])

The other three experimental structures: Kalthoff's experiment, collapse of thick-walled cylinder and thick-walled torsion experiments, customarily capture the features of two-dimensional growth and propagation of one or several adiabatic shear bands.

1.2.1.2 Kalthoff's experiment

Kalthoff's experiment is a structure to examine the initiation and propagation of ASBs in a target plate with one or two pre-notch undergoing a high impacting velocity. Three special kinds of behaviours may appear in the process: stable-brittle-ductile, brittle and ductile. The failure modes depend on impacting speed and material types. Guduru [Guduru et al., 2001] studied the evolution of dynamic ASBs in pre-fatigued single edge notched specimen for C300 maraging steel. The shearing band has an initial width about $100\mu\text{m}$, and later localized temperature starts to diffuse in that region, then displays 'hot spots' distribution in front of crack tip along the length of a well-developed shear band. These experimental results are contrary to the widely used theoretical models assuming that temperature fields have a laminate structure within ASBs.

Ballistic impact is a mostly well-known example to examine and investigate the formation and micro-structural property of ASBs. For Ti-6Al-4V targets, Li [Li et al., 2010] found that two types of ASB existed in the impacted process: deformed bands and transformed bands (white-etching bands are also classified in transformed bands). Martinez [Martinez et al., 2007] studied the plug formation in the targets at velocities from 633 m/s to 1027 m/s . The characteristically white-band thickness bands varied from 5 μm -40 μm with the incidence of ASBs increasing with impact velocity, but decreased with the loading time.

1.2.1.3 Thick-walled compression and torsion experiments

Compression-torsion Kolsky bar was developed by Chichili and Ramesh in 1999 to address the ASBs in materials. Notched thick-walled cylinders subjected to dynamic compression and torsion were examined to investigate the occurrence of dynamic shearing localization in α -titanium [Chichili et al., 2004]. They observed the phenomenon of planar dislocation motion, twinning or sub-grains near to the band tip.

Recently a lot of contributions were devoted to the investigation of multiple shear bands in view of satisfying industrial need. Nesterenko developed thick-walled cylinder specimen [Nesterenko et al., 1998] to investigate their spacing in Ti-6Al-4V, titanium, copper and FCC materials, and a typical feature of self organisation is observed in the evolution of bands. Xue [Xue et al., 2003, Xue et al., 2004] obtained that the spacing of shear bands in stainless steel was expressed as:

$$L = \frac{\sum_i L_{i,i-1}}{n_i} \frac{R_{f0}}{R_f}$$

where R_{f0} is the radius of specimen at the initiation of the shear band, and R_f is the final radius at any larger effective strain. $L_{i,i-1}$ is defined as the spacing between i th and $i-1$ th shear bands.

As we said in the first part, material damage originates from the localization zone. Due to high temperature and large deformation produced in a short time, the occurrence of micro-cracks, voids is unavoidable, necessarily causing a reduction of material mechanical ability. It is important to emphasize that the constitutive behaviour within a shear band is influenced by micro-structural details. So recently some legitimate constitutive relations about shear band are also introduced in microscopic scale ([Hong et al., 2010]). Consequently, for the sake of predicting accurately the occurrence of ASBs, many engineers try to look into the formation of ASBs in microscopic structure.

Xue [Xue et al., 2002] indicated that shear bands are favoured initiation sites for failure for Ti-6Al-4V alloy, occurring by void nucleation, growth, and coalescence inside the thermally softening regions. Furthermore, the work in [Xue et al., 2008] investigated the micro grains effects in 304 stainless steels through electron backscatter diffraction technology (EBSD), showing that shear-induced deformation structure was sensitive to initial micro-structure and local orientation of ASBs. Moreover in micro-structure mechanisms, Murr [Murr et al., 2009] pointed out that the ASB evolution in micro-structural stage is

accompanied by the evolution of the dark deformation bands, and the cracks nucleating and propagating within the ASBs were observed to increase from 8% to 87% of the ASB length with increasing impact velocity.

Meyers et al [Meyers et al., 2001, Meyers et al., 2003] used hat-shaped specimen and thick-walled cylinder to investigate the micro-structural evolution in stainless steel. Using compression test performed by UCSD's recovery Hopkinson bar, Nemat-Nasser investigated the dependence of flow stress on strain rates (from quasi-static to dynamic cases) and initial temperature (77-1000 K) in three different types of micro-structure of Titanium alloys [Nemat-Nasser et al., 2001]. The results show that only the initial micro-structural features affect the threshold stress and the athermal part of flow stress, and the initial temperature has more influences on the flow stress than that of strain rate. Moreover based on their work [Nemat-Nasser and Li, 1998], a physical constitutive model was also applied to predict the performance of material, which gave a good development to the numerical simulation of adiabatic shear band in titanium alloys.

In fact, many experiments illustrate that the existence of adiabatic shear band has a large influence to material entire property. However, due to its tiny bandwidth and inhomogeneous high temperature distribution, experiment is not sufficient to capture the characters of adiabatic shear band, such as the investigation and measure of temperature in the band. Thus the research in the views of theory and numerical algorithm gets considerable interests to mechanics and materials communities.

1.2.2 Theoretical analysis

For coupled thermo-mechanical problems, the main equations governing adiabatic shear banding structure are simply described as follows:

$$\rho_0 \dot{v} - \sigma_{,y} = 0$$

$$\rho_0 C \dot{\theta} - k \theta_{,yy} = \beta D_{int}$$

i.e. conservation law of momentum and balance of energy. Here ρ_0 is material density, C and k are thermal capacity and thermal conductivity. v and θ are velocity and temperature, and σ is stress. The right hand side of second equation presents the intrinsic dissipation D_{int} , denoted as $D_{int} = \sigma \dot{\epsilon}^P$. Taylor-Quinney coefficient β exhibits the ratio of plastic work transformed to heat. Normally it is treated as a constant, chosen between 80% and 100%. Since the shear band localization is so narrow compared with the other dimensions, one-dimensional theoretical analysis of ASBs is considered as a canonical problem that captures much of the observed phenomena. Actually its existence often shows how the physical and geometric parameters are organized.

In the process of ASB formation, the competition between thermal softening and material hardening determines the different term of the development of shear strain localization. In the first stage, material hardening presents a dominant effect in this part, therefore equivalent stress increases slowly. With the time increased, the speed of the temperature increasing is eventually rapid, and thermal softening enhances and passes away the

hardening part, the material enters into instability. Then the uniqueness of mechanical response is lost. Correspondingly stress decreases slowly, the form of shear band is gradually clear. Yet when a critical strain reaches, the stress suddenly has a large descend. Heat conduction cannot be ignored in the final term, determining the stable size of shear region. Afterwards stress decreases again slowly or arrives at steady state for some materials without hardening work, then one or multiple fully shear bands form. Generally speaking, all the theoretical analysis turn around the three stages: critical conditions, profiles of deformation and temperature and instability analysis.

1.2.2.1 Critical condition

The critical conditions of the transformation from stability to instability attract lots of interests in mathematical and mechanical points of view. As Molinari described, there are two fundamental questions regarding the stability analysis [Molinari and Clifton, 1987]: the conditions of shear localization occurrence and the nominal critical shear when the catastrophic process occurs. In general, linear perturbation method and bifurcation analysis are two widely used methods to predict these phenomenons. For the adiabatic and quasi-static problem, the work in [Clifton and Molinari, 1983] gave the onset and evolution of ASB with respect to different constitutive laws, especially including the work hardening factor. Moreover, they [Molinari and Clifton, 1987] obtain the critical strain γ^c at which the localization becomes catastrophic for two boundary conditions (constant stress value and constant velocity value). Wright [Wright, 2002] also gave an approximated expression to scale the defect for the timing of localization. In addition, using perturbation method, Batra [Batra and Wei, 2007] considered the damage factor and analysed critical strains for a heat-conducting, strain-rate hardening, and thermal softening initiation and propagation.

1.2.2.2 Band profiles

In the final term of ASB evolution, one or several fully formed shear bands appear clearly. Wright [Wright, 2002] noticed that the strain rate became essentially independent of time at this stage, and although the temperature and stress continue to evolve, the changes are very slow. FIG.1.4 gives out the profile of temperature measured across an adiabatic shear band at a late stage of deformation, the shape of temperature is alike 'cusp'. Therefore a part of work concentrates on pursuing a theoretical distribution of deformation and temperature in shear localization. In the modelling of describing a fully formed shear band, Leroy [Leroy and Molinari, 1992] proposed the following mixed boundary conditions to illustrate a more comprehensive ASB:

$$\begin{aligned} [\theta_{,y} + \frac{1}{\alpha}(\theta - \theta_0)]|_d &= 0 \\ [(v - v_0) - \phi(\tau - \bar{\tau})]|_d &= 0 \end{aligned}$$

A mixed boundary condition of temperature is described in the first formula, α is a film parameter to decide whether the problem is in adiabatic term ($\alpha = \infty$) or in isothermal

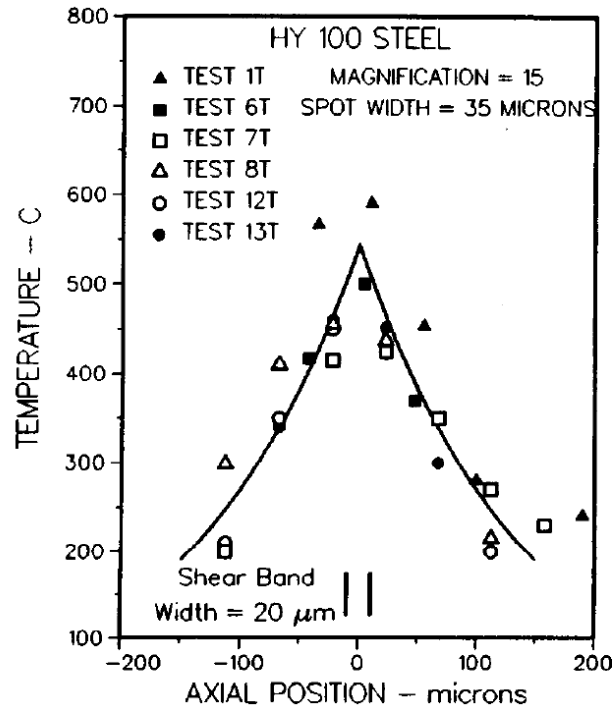


Figure 1.4: Temperature profile measured across an ASB at a late stage of deformation [Marchand and Duffy, 1988])

term ($\alpha = 0$), and the corresponding convection rate on the boundary. The second boundary condition regards to the loading type: when $\phi = 0$, it defines a Dirichlet problem; similarly a Neumann problem is described when $\phi = \infty$. For an isothermal problem, Bodin [Bodin, 1996] analysed that the influence of ϕ in the mixed condition limits on the stability of steady state. There was always a solution in the steady state for thermo-mechanical equations when loading as velocity form. Yet for the loading in the term of force, it exists a critical shear stress τ^* to decide the occurrence of stable state. According to [Leroy and Molinari, 1992], the shear band in a torsional Kolsky bar does not tend towards the stable steady state. Moreover, they derived the profiles of velocity and temperature on exponential law as follows:

$$v = \frac{m Z}{\beta k \tau} \tanh\left(\frac{Z}{2} y\right)$$

$$\theta = \theta_b + \frac{m}{\beta} \log\left[\operatorname{sech}^2\left(\frac{Z}{2} y\right)\right]$$

where Z is a parameter calculated by the thermal and mechanical boundary conditions. We understand that the bandwidth is denoted as $\frac{2}{Z}$. θ_b is the temperature in central band. Obviously, these formulas are similar to the canonical aspects proposed later by Wright [Wright and Ravichandran, 1997]. Shear band was analysed as a surface of discontinuity,

and they use the characteristic length scale δ as:

$$\delta = \left(\frac{2mk}{s\lambda a}\right)^{\frac{1}{2}} [1 + O(m_c)] \quad (1.1)$$

to illustrate the canonical explicit formulas of velocity and temperature for arbitrary flow laws, only if the material parameters satisfy some certain conditions. As an extension of this work, Wright also verified the feasibility of canonical formulas on the widely used constitutive relations: power law, Johnson-Cook model, Zerilli and Armstrong law, MTS model and Bodner and Partom law. Yet work hardening was neglected or considered as a constant in all the mechanical models.

1.2.2.3 Band width

Although shear band appears as a discontinuity surface at macroscopic scale due to its tiny length, lots of researchers try to find its actual width for the sake of approximating the mesh size in the numerical simulations. Beyond the predictions in the experimental structures, some theoretical results are also obtained. So far there is not an exact scale definition of band width, and many papers merely use it to measure the distance of velocity jump and temperature rapid variation (1.1). Additionally, Wright [Wright and Ockendon, 1992] defined the band width δ as

$$\delta = \left(\frac{1-m}{2m} \frac{-\partial\sigma_0/\partial\theta}{k} b^m\right)^{-1/(1-m)} v_0^{-\frac{1+m}{1-m}}$$

for a material with linear softening but no hardening. Here $\sigma_0 = k_0(1 - \alpha\theta)$, m, k, b are the material parameters, v_0 is the imposed velocity. They pointed out that band width was the distance from the center of the band at which the strain rate is less than the maximum value by a factor ($e^{0.9/(1-m)}$), and it is inversely proportional to v_0 , but independent to structure size.

In microscopic measurement, Dinzart [Dinzart and Molinari, 1998] described that there were two characteristic length scales in a localization area as in FIG.1.5. Besides the shear band width presenting the large strain rate and high velocity, a length of heat affected zone (HAZ) (FIG.1.5) surrounds the band. Due to temperature increase in that region, lower strains and local annealing make the HAZ less hardened. Considering the existence of HAZ, the band width is obtained as:

$$w = 2x_r \cong 6\sqrt{2m} \frac{k_0\theta_0}{v_0 a \tau_0}$$

where x_r is defined by the strain rate as following:

$$\begin{cases} \frac{\dot{\gamma}(x)}{\dot{\gamma}(0)} = \left(1 - \frac{a-\xi}{2} x^2\right)^{-1/m}, & \text{for } 0 < x < x_i \\ \frac{\dot{\gamma}(x)}{\dot{\gamma}(0)} = p_0(x - x - r)^2, & \text{for } x_i < x < x_r \end{cases}$$

In addition, it is $3\sqrt{2}$ times to the size of the result that Wright derived, and they validated that their approximation was better closer to the experimental solution.

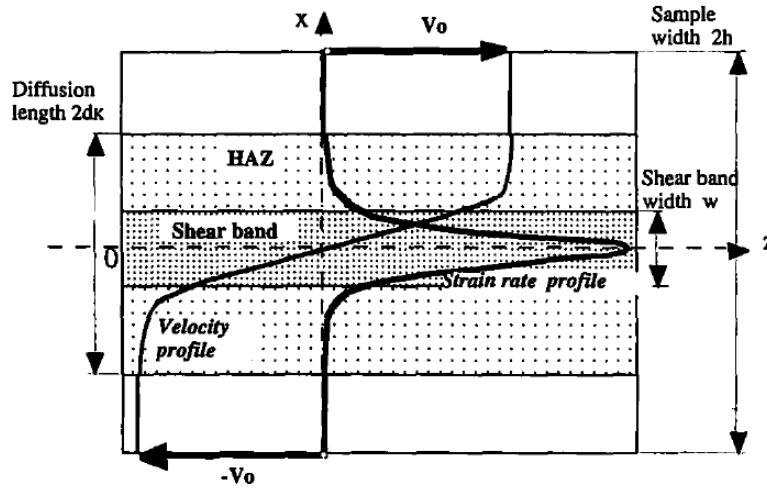


Figure 1.5: Schematic view of thin-walled tube ([Dinzart and Molinari, 1998])

Some engineers also define bandwidths according to the mechanical profiles. Batra [Batra and Ko, 1992] chose the length when the stress had dropped to 85% of its peak values as band width, and analysed its evolution in twelve materials obeying on Johnson-Cook model ([Batra and Kim, 1992]).

Dynamic shear localization in one dimension is also a hot spot in theoretical analysis. Most of work is based on the negligence of inertia and work hardening in constitutive relations to simplify the localized problem, even some neglect thermal conduction for treating the temperature as an internal variable in calculation. As illustrated in experimental analysis, adiabatic state merely occurs in the first stage: the stress has a small perturbation, and the corresponding strain rate can be considered as linear form. Yet afterwards thermal conduction factor will be dominant to the distribution of velocity, temperature and stress.

Some theories in Fluid mechanics are also applied to analyse the character of ASBs, such as boundary layer: a layer of fluid produced by the effect of viscosity. Normally outside of the layer, the velocity keeps constant, yet the velocity has a large change in the layer. This property makes lots of researchers regard the ASBs phenomenon as an application of boundary layer theory. For a particular material which constitutive relation is similar to exponential law, Dilello [Dilello and Olmstead, 1997] considered the zone of velocity jump as a boundary layer having non-zero thickness. They derived the expressions of transient velocity, stress gradient and temperature, as well the evolution of thermal boundary layer obtained as a measure of shear band thickness. Moreover elasticity is included in the model. The bandwidth is as following:

$$\Delta(t) = m\delta(t) = \left\{ \frac{\lambda a}{2m} s(0,t) \dot{\gamma}[s(0,t), \theta(0,t)] \right\}^{-1/2}$$

where $\delta(t)$ is a transient boundary layer thickness, λ , a , m are the material parameters; and $s(0,t)$, $\dot{\gamma}(0,t)$, $\theta(0,t)$ are the stress, plastic strain rate and temperature on the central part of slab. Furthermore, they extended this method to the thermo-viscoplastic materials sat-

isfying a typical Johnson-Cook model([Dilellio and Olmstead, 2003]), yet no hardening coefficient was considered.

Considering the existence of two length scales in the profiles of temperature and velocity through numerical results, Glimm [Glimm et al., 1996] considered the ASBs structure on the quasi-static core of shear band surrounded by thermal layer. Hence the solutions of thermo-mechanical fields are separated as two parts: one is similar to the results of Leroy [Leroy and Molinari, 1992] for quasi-static fields, the other is merely controlled by heat equation because of constant stress, velocity and zero plastic strain rate. The half-width of ASB was defined from the temperature profiles:

$$\delta = \left(\frac{2km}{a(\theta_c)\sigma_{c,v,y}(y_c)} \right)^{1/2}$$

where $a(\theta_c) = -g'(\theta_c)/g(\theta_c)$. $g(\theta)$ is thermal softening part in constitutive relation, and the subscript c means choosing the values at the center. The result is similar to the characteristic length in [Wright and Ravichandran, 1997].

As a hot topic in the present research of ASB, it would be well if we simply talk about shear band spacing when referring to shear band width. It is a length scale for multiple shear banding, such as in thin-tube wall and cylinder collapse. Usually, linear perturbation analysis is a popular method to characterize the shear band spacing, when the stress has a slight decline in the second stage. Wright ([Wright, 1995, Wright and Ockendon, 1996]), Molinari([Molinari, 1997]), Zhou([Zhou et al., 2006]) and Batra([Chen and Batra, 1999, Batra and Wei, 2006, Batra and Chen, 1999]) proposed different formulas for certain flow relations, thereby giving a good prediction for the experiments and numerical simulations. In [Batra and Wei, 2006], they referred that the shear band width was controlled by heat diffusion and shear band spacing by momentum diffusion, and an approximate relation between bandwidths and spacing was deduced in their work.

In theoretical analysis, a two-dimensional work is always a large challenge for mechanical engineers, so these works are rare and cherished. The first two-dimensional analysis was studied by Wright [Wright, 2002]. They studied a steady shear band in the near-tip fields of antiplane motion, here power rate hardening is considered. The speed of an ASB propagation was estimated for a perfectly plastic materials [Wright, 2003], which depends on the material state ahead of the tip of fully localized band. Gioia [Gioia and Ortiz, 1996] applied the boundary layer theory to investigate a shear localization structure in a plate with a crack, which is impacted at a high velocity by a flat-ended, rigid projectile. Accounting for the inertia effect, work hardening and convection, and applying the stability criterion, they regarded the occurrence of shear band as an outcome of material incapability of supporting steady boundary layers. The profiles of velocity, temperature and plastic strain energy were studied in steady and transient state, as well as the propagation speed of ASB. In addition, correspondent to experimental results, shear band tip speed keeps at a constant when impacted on steady velocity. Using variational method, Mercier [Mercier, 1997] analysed this stationary velocity of 2D ASB propagation in the layer subjected to a simple shearing velocity, moreover the transition length can also be solved though two nonlinear equations.

For shear localization problems, the thermo-viscoplastic material represents complicated constitutive relations with thermal softening and the large displacement jump in tens of micrometers of bandwidth. Furthermore, as an important part to determine the steady size of bandwidths, thermal conduction brings lots of difficulties in theoretical analysis. Although good approximations are observed to describe the characteristics of ASB in the foregoing work, most of the results need to be resourced to the simplifications of material modelling, such as lost of work hardening, elasticity or conduction. So far one dimensional ASB is always a popular subject compared to that on 2D/3D in theoretical analysis. Meanwhile it is far less studied and uncompleted in the propagation of ASB, especially since engineers discovered that the temperature distribution represents hot spot phenomenon. So kinds of questions in ASB analysis urge the researchers to proceed from insufficient 1D ASB to 2D or 3D simulation. Naturally for the sake of building the generality of constitutive models, numerical simulation is an efficient way that many researchers preferred adopting to achieve the reliability and accuracy of ASB analysis.

1.2.3 Numerical implication

Shear localization is a common phenomenon in engineering since it is discovered by Tresca. As a precursor to the fracture of materials, its research attracts a lot of interests and some popular numerical methods are all applied to simulate this localized problem, but also encounters some difficulties.

1.2.3.1 Finite element method

Since Finite Element Method (FEM) is developed by Olgierd Zienkiewicz in 1947 for solving the simple elastic problem, it has been a strongly numerical technique for finding an approximation of partial differential equations. It may well experience a relatively mature development and wide application in the last several decades. Therefore naturally engineers earlier applied it to solve the shear localization problem in thermo-mechanical coupling.

As we all known, large strains accumulate inside a shear band with the equivalent plastic strain increasing, simultaneously the temperature fields are rapidly increasing, involving that the central band practically arrives at the melting point, and then the corresponding damage and failure are following. So different types of mechanical phenomena happening in tens of micrometers give a large challenge to the simulation of surrounding material behaviour in shear localization. Apparently due to these striking features, strong mesh-alignment sensitivity of elements is coming in standard FEM. For the accurate implication of FEM, we should set fine mesh or refine the mesh ([Batra and Ko, 1992]) step by step in the localization. Physically, the mesh size is set as the same order of minimum band thickness. Moreover, the mesh direction in localized zone should follow with the band interfaces to avoid mesh distortion. Briefly reviewed, the initiation, formation of ASB [Wilson and Batra, 1998], and their propagation [Zhang, 1994], finally the transitions from ASB to fracture [Teng et al., 2007] are also simulated by standard

finite element method. Batra [Wilson and Batra, 1998] studied the dynamic plane strain, axisymmetric deformations of a tungsten heavy alloy block subjected to a plane strain compression, pointing out that the plastic strain distribution in these narrow regions of intense localization is non uniform. Peirs analysed the influences of the geometry structure to shear localization profiles in hat-shaped specimen by ALE adaptive meshing technique, which avoids the mesh alignment [Peirs et al., 2010]. However, the tiny shear band width needs the enormous number of elements to capture the characters of ASB, thus it makes the computational time unacceptable, especially for 3D ASB.

In general, a shear localization phenomenon is concentrated in tens of micrometers which caused a discontinuity in macro-scale view, yet the other part is relatively homogeneous. Many engineers try to embed the discontinuous element in the standard FEM to solve this localized problem. For the rate-independent materials obeying on small displacement theory, Ortiz [Ortiz et al., 1987] proposed this method at the earliest to enhance the performance of isoparametric elements for localized failure problem, resolving the limitation of designed mesh. Afterwards accounting for large-scale plasticity, Ortiz [Ortiz and Pandolfi, 1999] developed a finite-deformation cohesive element in 3D to separate the crack fronts part in 1999. Beyond their work, Belyschko [Belytschko et al., 1988] enriched the strain fields by discontinuous element for shear bands, and considered the bandwidth as a material parameter to avoid mesh dependence. Through a critical bandwidth as a condition to introduce a bifurcation, Oliver [Oliver et al., 1999] developed a strong discontinuity approach to analyse the initiation and propagation of strain localization part. In addition, when the bandwidth tends to zero, it turns to recover a strong discontinuity.

Yet all the forwarding work are referred to mechanical problem without thermal part. Needleman [Needleman and Tvergaard, 1992] applied the embedding enriched elements to the J2 plastic localization in metals with weak discontinuities. Regarding ASB as an anisotropic mechanical degradation process, Longère [Longère et al., 2005] introduced regular and singular state variables at the representative volume element to present ASB, here considering average localized fields, i.e. uniform temperature and strain, and performed the initiation and propagation of ASB in 3D hat shaped specimen. This multi-scale model has a weak mesh dependency, yet thermal conduction is neglected. Recently based on thermo-mechanical variational potentials and considering finite kinematics with thermal conduction, Yang [Yang et al., 2005] resourced to cohesive element and developed it to emulate the discontinuous strain/temperature fields. Here band width works as an optimization parameter in the models. This technique easily gets rid of the default of mesh alignment and distortion in standard FEM, but strain profiles are thought as homogeneous in the discontinuous element. How to accurately illustrate the characters of localization is still a considerable work.

1.2.3.2 Meshless method

A priori, strain localization element should be set to match the ASB orientation. So for some mechanisms such as cylinder with multiple shear bands, this technique will be

helpless without the aid of experiments. Comparatively, meshless method is a suitable method in the independence of shear band path.

Since Li [Li and Liu, 2000] firstly applied mesh-free Galerkin method in strain localization phenomena in 2000, a series of studies on bifurcation [Li et al., 2000, Li et al., 2001] and adiabatic shear band [Li et al., 2002], even their dynamic propagation property in micro-structure, are presented with the advantage of relieving mesh alignment sensitivity. A criteria for dynamic ASB propagation is proposed in Kirchhoff experiment [Medyanik et al., 2007], and they also described the distribution of temperature presenting the hot spot phenomenon through this meshless method. On the other hand, recently based on Smoothed Particle Hydrodynamics method, which has the same predecessor as Meshfree method, Batra proposed the modified smoothed particle method to analyse the localization problem in axisymmetric Taylor impact test ([Batra and Zhang, 2008]). The corresponding validation by FEM are presented in [Batra and Zhang, 2004]. Yet these models on the basis of meshless method are unable to escape the firstly approximation of shear band width. We should set inhomogeneous density of nodes for the accuracy resolution. For bypassing this problem, Rabczuk [Rabczuk and Samaniego, 2008, Rabczuk et al., 2007] embedded strong discontinuity in shear band model combined with meshless method, yet thermal conduction is neglected.

1.2.3.3 Extended finite element method

Extended finite element method is a developed FEM by enriching the discontinuous spaces [Moës et al., 1999]. It is initially proposed to solve the crack propagation problem, and the enrichments of solution spaces effectively alleviate the difficulties of simulating discontinuous surfaces by standard FEM. Naturally, its challenging feature that does not need to remesh the structure makes this method widely applied to the discontinuity and localization problems, such as adiabatic shear band.

Evidently, an important factor in XFEM is to introduce an appropriate enrichment for localization zone, by coincidence which is well treated in theoretical analysis. Some simplified form are correspondingly applied in a limited number of references. Using the temperature distribution derived by Wright, Areias and Belytschko used a Heaviside function to enrich the displacement and temperature profiles in localization, which formulas are all considered linear in enrichment [Areias and Belytschko, 2006, Areias and Belytschko, 2007]. For tracking the evolution of shear localization, linear perturbation analysis was analysed as a condition to embed enrichment. As expected, it obtained a good mesh-independent effect in several examples of shear band formation. In addition, they pointed out that the bandwidth can be obtained through the minimum incremental work criterion, as described in [Grady, 1994].

Besides the default of mesh dependence, the numerical simulation of thermo-mechanical localization problem also encountered other difficulties such as model quality, damage or interactions between multiple bands. To some extent, it is always complicated to find a good constitutive model [Khan et al., 2004, Love and Batra, 2006] to present the initiation, propagation and stability of the discontinuous spaces. Some engineers try to use two

models to describe this process: one for the first and second stage as the foregoing stated and the other for the stress dropping suddenly. Moreover, the criteria for ASB initiation and propagation is still an open noteworthy question. In the most of the numerical approaches, it is necessary to know an approximate domain of shear band width to avoid the expensive calculation. So predicting the localized length in thermo-viscoplastic materials is prerequisite to proceed the dynamic evolution of shear localization, and consequently benefits to the improvement of the material manufacturing, such as metals, alloys and polymers.

Arrived here, we restated that the development of adiabatic shear band in the last decades from the experiment, theoretical analysis and numerical simulation points of view. Every aspect has its character in the research of ASB, yet also has its hardly resolved points needed to be looked out. Here by means of the results in three domains and adopting every relatively advantage, we will use an optimized method, with the character parameters of ASB, to describe the profiles of the band and simulate the formation of ASB. This optimization has a strong mathematical background: energy-based variational method.

1.3 Energy-based variational method

Variational method is a popular approximated method to find the optimization values of a function in quantum mechanics. It is widely applied in physics, statics, control theory as well as economics. In simple terms of mechanical view, this method used the calculus of variations to adjust the variational parameters with regard to displacement, stress or temperature, thus observed the minimum or maximum of energy well correspondent to thermo-mechanical conservation laws. In addition, variational principle is a connected bridge of the equality between lowest potential and continuum mechanical balances.

In general, variational principle is an optimization approach to describe the state and dynamical boundary value problem. Normally the quantity to be optimized does not employ the governing equations, yet it can reflect and yield the physical processes. Its feature is to provide the governing equations as some stationary conditions, which is effective to carry out a common mathematical approach. In addition, error estimation and coordinate transformation are relatively more simple to the problem described by these principles. Virtual power principle is widely known around in mechanics as the cornerstone of the development in numerical methods. In short, it is originated from the basic equations of equilibrium with mechanical boundary conditions. Hamilton principle is a statement that variational method can determine the dynamics of the physical system by an unique function, which contains all the informations of problem.

Although choosing the same deformational energy as an optimized formula, theoreticians proposed different variational principles to express the multi-physical boundary value problem. Hu-Washizu-Fraeijs principle is the most general canonical principle of elasticity expressing the optimized quantity through three fields: displacement, strain and stress. All the boundary conditions can be included in the scalar function $\phi(u, \varepsilon, \sigma)$, gen-

erally the boundary value problem can be written as follows:

$$\inf_{u, \varepsilon, \sigma} \phi(u, \varepsilon, \sigma)$$

u represents displacement, ε and σ are separately strain and stress. Through the calculus of variations, the observed Euler-Lagrange equations are equivalent to conservation laws. In one case, if imagining that the comparability condition is satisfied beforehand and applying Legendre transformation in Hu-Washizu-Fraeijs principle, Hellinger-Reissner principle was proposed by expressing the problem as an optimization with regarding to two fields: displacement and stress. In a general way, the corresponding constitutive relation and equilibrium equations are obtained at the stationary point of the quantity. Introducing Lagrangian multipliers, HE [He, 1997] proved the equivalence between Hellinger-Reissner and Hu-Washizu principles in elasticity. Generally, it is the effective basis for developing the mixed and hybrid finite element, which has a better approximation about stress than other numerical methods. In similar case, if we suppose that the compatibility conditions and equilibrium equations are known, minimum complementary energy principle is merely built as an optimization regarding to the stress.

Here we prefer to assign the minimum potential energy principle to build the variational modelling. Taking an elastic mechanical problem with finite deformation as an example, we define φ as configuration and W as energy density. So the deformation energy can be written as [Stainier, 2006]:

$$\mathcal{U}(\varphi) = \int_{B_0} W(\nabla_0 \varphi^T \nabla_0 \varphi) dV$$

and the energy from external forces are defined:

$$\mathcal{W}(\varphi) = \int_{B_0} \rho_0 \bar{b} \cdot \varphi dV + \int_{\partial_\sigma B_0} \bar{t} \cdot \varphi dA$$

where ρ_0 is mass density, \bar{b} is body force and \bar{t} as imposed force. Supposing the comparability condition and constitutive relations are satisfied, the boundary value problem via variational principle is described as

$$\inf_{\varphi_{adm}} (\mathcal{U}(\varphi) - \mathcal{W}(\varphi))$$

Its stationary point with respect to φ is correspondent to the conservation of momentum in elasticity.

As many reference stated, the variational form of equations is very convenient for the numerical simulations, and the uniqueness and existence of the solutions in the problem are easily analysed in mathematical view. By means of this energy-based variational method, we emphasize that a physical problem is transformed to a mathematical optimization, and then a series of optimization algorithms can be applied in the analysis of physical fields. However, how can we determine the existence of potential and its variational formulation to be optimized, meanwhile reflecting well the physical signification?

In the physical system, every boundary value problem obeys on the following list of conservation laws [Belytschko et al., 2000]:

- Conservation of mass

$$\frac{d}{dt} \int_V \rho dv = \oint_S \rho(u_n - \mathbf{v} \cdot \mathbf{n}) ds$$

where ρ is mass density, $u_n - \mathbf{v} \cdot \mathbf{n}$ is the relative normal speed between the surface and the material, 0 for material volume and $u_n = 0$ for control volume.

- Conservation of linear momentum

$$\frac{d}{dt} \int_V \rho \mathbf{v} dv = \oint_S \rho \mathbf{v}(u_n - \mathbf{v} \cdot \mathbf{n}) ds + \oint_S \mathbf{t} ds + \int_V \rho \mathbf{b} dv$$

where \mathbf{t} is the density of surface tractions, and \mathbf{b} is the density of body forces.

- Conservation of angular momentum

$$\frac{d}{dt} \int_V \mathbf{x} \times \rho \mathbf{v} dv = \oint_S \mathbf{x} \times \rho \mathbf{v}(u_n - \mathbf{v} \cdot \mathbf{n}) ds + \oint_S \mathbf{x} \times \mathbf{t} ds + \int_V \mathbf{x} \times \rho \mathbf{b} dv$$

- Conservation of energy (first law of thermodynamics)

$$\frac{d}{dt} \int_V \rho(e + \frac{1}{2} \mathbf{v}^2) dv = \oint_S \rho(e + \frac{1}{2} \mathbf{v}^2)(u_n - \mathbf{v} \cdot \mathbf{n}) ds + \oint_S (\mathbf{v} \cdot \mathbf{t} - q) ds + \int_V \rho(\mathbf{v} \cdot \mathbf{b} + r) dv$$

where e is the internal energy per unit mass; q is heat flux leaving the volume; r is an energy source per unit mass; n is normal direction.

- Clausius-Duhem Inequality (second law of thermodynamics)

$$\frac{d}{dt} \int_V \rho \eta dv \geq \rho \eta(u_n - \mathbf{v} \cdot \mathbf{n}) ds + \oint_S -\frac{\mathbf{q} \cdot \mathbf{n}}{T} ds + \int_V \frac{\rho r}{T} dv$$

where T is the absolute temperature, and η is the internal entropy density per unit mass.

Furthermore, a boundary value problem is described as the above governing equations including material constitutive relations and compatibility conditions. According to variational method and multiplying a small constraint but arbitrary variation $\mathfrak{v} \in \mathcal{V} = \mathfrak{v} \in R^3 | \mathfrak{v} = 0$ on BC (Boundary Conditions) in the equations, we can obtain the weak form of the problem. For instance, for the mechanical problem:

$$\text{Div} \mathbf{P} + \rho_0 \mathbf{B} = 0 \quad \text{where } \mathbf{P} \cdot \mathbf{N} = \boldsymbol{\tau} \text{ on } L$$

where $\boldsymbol{\tau}$ is the traction on the boundary L . The weak form is defined as:

$$\text{Find } \boldsymbol{\varphi} \in \mathcal{P} \quad \text{such that } G(\boldsymbol{\varphi}, \mathfrak{v}) = 0 \quad \text{for all } \mathfrak{v} \in \mathcal{V}$$

where

$$G(\boldsymbol{\varphi}, \mathfrak{v}) = \int_V (\mathbf{P} : \text{GRAD} \mathfrak{v} - \rho_0 \mathbf{B} \cdot \mathfrak{v}) dV - \int_L \boldsymbol{\tau} \cdot \mathfrak{v} dL$$

where $\varphi \in \mathcal{P} = \varphi \in R^3 | \varphi = \varphi_d$ on BC. If the physical fields and \mathfrak{t} are C^1 , the weak form is equivalent to the strong form.

In view of the weak form, Marsden [Marsden and Hughes, 1983] pointed out that if and only if

$$D_1 G(\varphi, \mathfrak{t}) \cdot \xi = D_1 G(\varphi, \xi) \cdot \mathfrak{t} \quad \text{for all } \varphi \in \mathcal{P} \text{ and } \mathfrak{t}, \xi \in \mathcal{V}$$

there is a potential E making $DE(\varphi) \cdot \mathfrak{t} = G(\varphi, \mathfrak{t})$, and its corresponding form is

$$E(\varphi) = \int_0^1 G(t\varphi, \varphi) dt$$

thereby a formulation embodying equilibrium equations, material behaviors and boundary conditions are built in the variational framework. Apparently, the weak form of conservation laws is a basis to build the variational pseudo-potential, yet simultaneously we should guaranty its symmetry.

In 1999, Ortiz and Stainier [Ortiz and Stainier, 1999] obtained a variational formulation for general viscoplastic solids with respect to different dissipative relations in finite deformation regime. They developed a constitutive update modelling as an optimization to a scalar function with a set of internal variables, including Hemholtz free energy, conjugate inelastic potential and viscous part. The according constitutive updates can be defined as a minimum of incremental pseudo-potential about deformation over the time step. We can say that this work represents a new and active research area, the applications of this variational structure to general dissipative materials are continuously developed [Stainier et al., 2002]. For instance, constitutive viscoelastic formulations are as following provided to embody the nonlinear viscous behaviour based on this theoretical framework[Fancello et al., 2006, Stainier et al., 2005].

Recently considering temperature effect, a variational formulation of coupled thermo-mechanical boundary-value problems was proposed by Yang et al [Yang et al., 2006]. In their work, they skilfully introduced the equilibrium temperature in the formula, making the weak form symmetry. In addition, the characteristic of this formulation is allowing to describe the thermal and mechanical balance equations, including irreversible and dissipative behaviors, as an optimization of energy-based variational form. Indeed, beyond unifying a wide range of constitutive models in a common framework, the variational formulation also presents the interesting mathematical properties, like symmetry of its bilinear form, which is an important feature comparing with the alternative coupled thermo-mechanical formulations. Applying this variational formulation, Stainier [Stainier and Ortiz, 2010] successfully presented an experimental validation of three thermo-viscoplastic materials: aluminium alloy, α -Titanium and Tantalum. These theoretical conclusions will be used to build our variational modelling for adiabatic shear bands structure.

1.4 Thesis outline

Based on the strongly coupled thermo-mechanical variational formulation proposed by Yang, we aim at building an energy-based modelling of adiabatic shear band structure,

and accurately analysing the physical profiles of the layer subjected to a simple shearing velocity. Sufficiently combined with the foregoing theoretical work, we introduce the discontinuities of velocity and temperature to describe the profiles of shear localization. Meanwhile considering the mixed heat exchange boundary condition, we improve the material modelling and propose a mathematical structure with thermal boundary conditions to approximate the transfer coefficient, which of a numerical formula is fitted with respect to structure size. In addition, not only this modelling works on the various thermal softening and rate-dependency laws widely used in the engineering, but also besides work hardening and heat conduction, elasticity is skilfully considered as the optimization of pseudo-potential with the unknown characteristic parameters. Some examples will show the feasibility of the modelling. Based on this variational framework for shear localization problems, we propose a variational two-scale modelling, and give its finite element implementation.

In CHAP.2, we present an energy-based variational modelling of a fully formed shear band in steady state, and verify our optimized modelling by analytical solution and finite element method. Variational framework is simply introduced in the first part, which gives a basis to build our variational modelling in the second part. Then as an application of our modelling in steady state, we introduce the maximum temperature as an optimized parameter in variational framework grounded on the analytical formulas for exponential law, thereby avoiding the dependence of the modelling on material parameters. Here two examples (power law and Johnson-Cook model) will verify this good aspect of our modelling. As a final part, a new variational modelling with thermal boundary conditions is proposed and analysed to alleviate the dependence on structure size.

The corresponding variational modelling in transient state is introduced in CHAP.3. In the first part, an incremental update of variational modelling is demonstrated for general dissipative solids. Briefly, we also introduce the update framework of finite element method based on variational method, as a comparing tool for the problem subjected to a simple shearing force. Starting from simplicity, the variational formulations in exponential softening law, power law and Johnson-Cook law (with hardening coefficient) are gradually derived for thermo-viscoplastic materials, verifying the feasibility of our modelling on various constitutive relations. In the results analysis, the evolutions of band width and maximum temperature in exponential law are presented and validated by FEM. Furthermore, taking a widely applied model in engineering: Johnson-Cook law, we build our variational modelling including elasticity, work hardening and heat conduction, which lays the groundwork for the extension of the modelling from 1D ASB to 2D ASB.

The principle work in CHAP.4 is to propose a variational two-scale method for shear localization problem. As we know, the difficulty of numerical simulation in adiabatic shear band mainly exists in three domains: mesh dependence, model quality and interaction between multiple bands. We neglect the influence of micro-structure, such as micro-crack, void and material damage. The modelling we proposed is concentrated on solving the mesh dependence problem. Firstly based on the variational finite element method, we use an example of a pre-notched bar undergoing a constant velocity, to point out the mesh-dependence problem for standard FEM in shear localization simulation. Then inserting a

strong discontinuous element in standard FEM, we propose a variational two-scale model for ASB structure in 2D or 3D through interface elements. Meanwhile the framework of finite element discretization is derived. Although no numerical implementation is presented, we can verify the feasibility of two-scale modelling in theory.

Chapter 2

Variational modelling in steady state

Abstract :

We propose an energy-based variational modelling of adiabatic shear band in thermo-viscoplastic materials. The classical one-dimensional slab sustaining a stationary simple shear mode of deformation is analyzed by a Rayleigh-Ritz method, where the discontinuities of velocity and temperature can be parametrized by measures of shear band width and central temperature. Indeed, this formulation works for various material constitutive models, which will be illustrated by two popular constitutive models (power law and Johnson-Cook law) and verified by variational Finite Element Method.

Résumé :

Une modélisation de la bande de cisaillement adiabatique basée sur une approche énergétique variationnelle est proposée. Une couche classique ayant une propriété thermo-viscoplastique soumise à une sollicitation de cisaillement simple est analysée par la méthode Rayleigh-Ritz. La formulation des profils de vitesse et de température, paramétrées par des mesures de la largeur de bande et de la température centrale, fonctionne pour des lois de comportement diverses. En utilisant la méthode des éléments finis, on valide cet aspect par la loi de puissance et la loi de Johnson-Cook.

Contents

2.1	General framework	25
2.1.1	Variational formulation in thermo-mechanical coupling	25
2.1.2	Rayleigh-Ritz method	29
2.2	Couette flow and thermal layer	30
2.3	Thermal Couette flow	31
2.3.1	Analytical solutions	31
2.3.2	Variational formulations	32
2.4	Fully formed adiabatic shear band	34
2.4.1	Analytical solutions	36
2.4.2	Variational modelling with Rayleigh-Ritz method	37
2.4.2.1	Shear band width and penalty method	37
2.4.2.2	Shear band width and central temperature	39
2.4.3	Results and analysis	40
2.4.4	Extension to various constitutive relations	43
2.4.4.1	Power law	43
2.4.4.2	Johnson-Cook model	46
2.4.5	Thermal boundary condition	48
2.5	Conclusions	53

For thermo-mechanical localization problem, adiabatic shear bands (ASBs) can arrive at a steady state in the final stage if the materials without hardening subject to a constant velocity. When the fluctuations of the profiles of velocity and temperature are quite small and tend to zero, we call that the physics is in steady case. At this state, adiabatic shear bands are fully formed accompanying the large deformation and high temperature at macroscopic scale.

In present chapter, we aim at building an energy-based variational modelling for this fully formed shear band to analyse the shear localization in one dimension. The study is organized as follows: the variational approach for the thermo-mechanical problem is firstly restated. We validate the theory by considering classical problems such as Couette flow, thermal conduction in a layer and non-Newtonian thermal-Couette flow. In section 4, the fully formed adiabatic shear band is considered and the formulation in [Leroy and Molinari, 1992] is adopted. The thermo-viscoplastic modelling not only inherits the advantage of the thermo-mechanical coupled variational approach, but also predicts the shear band width and central temperature in an adiabatic shear band based on a continuum theory. Exact results of [Leroy and Molinari, 1992] are retrieved. Meanwhile, effects of material parameters (thermal softening, strain-rate sensibility on these two features) are analysed by this variational method. As an extension, different constitutive laws, power law and Johnson-Cook law, are adopted to evaluate the characters of ASB. Since theoretical analysis is difficult to give an accurate solution for general constitutive behaviors, a variational-based FEM numerically predicts the evolutions of velocity and temperature, and up to the steady state. It is shown that the results obtained by variational models are in good agreement with FEM. Based on this variational modelling, we introduce heat exchange on the boundary to consistent the bandwidth with different specimen sizes. A corresponding curve fitting of transfer coefficient is analysed with respect to structure size.

2.1 General framework

2.1.1 Variational formulation in thermo-mechanical coupling

Thermo-mechanical coupling is a common phenomenon in solid mechanics, and their effects are of importance in the structure manufacturing. For general dissipative materials, the coupling between mechanics and thermotics easily provokes some localization zones associated with large deformation and high temperature, e.g. the formation of ASBs. Their occurrences are a precursor to material macroscopic fracture. Here we will describe this phenomenon as a strong-coupled boundary value problem. Within the world of metallurgy and materials science, it does not seem unreasonable to apply standard continuum mechanics [Wright, 2002] for adiabatic shear band. Thus the five conservation laws should be obeyed in ASB structure: conservation of mass, conservation of linear momentum, conservation of angular momentum, conservation of energy and the Clausius-Duhem inequality. The corresponding finite constitutive equations for thermo-mechanical coupling

can be given ([Yang et al., 2006]) as follows:

$$\begin{aligned} \text{Div}\mathbf{P} + \rho_0\mathbf{B} &= \rho_0\dot{\mathbf{V}} \\ \mathbf{F}\mathbf{P}^T &= \mathbf{P}\mathbf{F}^T \\ \dot{E} &= \mathbf{P} \cdot \dot{\mathbf{F}} + \rho_0 Q - \text{Div}\mathbf{H} \\ \dot{\gamma} &\equiv \rho_0\dot{\eta} - \frac{\rho_0 Q}{T} + \text{Div}\frac{\mathbf{H}}{T} \geq 0 \end{aligned}$$

where ρ_0 is mass density per unit undeformed volume; \mathbf{B} is body force density per unit mass; Q and \mathbf{H} are the specified heat source per unit mass and the outward heat flux. T is the absolute temperature, and η is the specific entropy, defined as follows:

$$\rho_0\eta = -\frac{\partial W}{\partial T}$$

here Helmholtz free energy W is assumed to be existed. According to the definition of W and using Legendre-Frenchel transform, the internal energy density E is defined as:

$$E = \sup_T [\rho_0\eta T + W]$$

which has the property:

$$T = \frac{\partial E}{\partial(\rho_0\eta)}$$

For general standard dissipative and irreversible materials, the coupling terms between mechanics and thermotics originate from the softening of plastic stress in the constitutive relations and the dissipation including viscoelasticity and viscoplasticity parts. We consider the general pseudo-potential dissipation Δ , defined as:

$$\Delta = \psi^*(\dot{\mathbf{Z}}; \mathbf{Z}, T) + \phi^*(\dot{\mathbf{F}}; \mathbf{F}, T) - \chi(\mathbf{H}; T)$$

there ψ^* , ϕ^* and χ are the kinetic potential, viscous potential (Kelvin-Voigt viscoelasticity) and conduction potential. \mathbf{Z} represents the internal variables, for instance, cumulated plastic strain for thermal viscoplastic material. \mathbf{F} is the deformation gradient and $\mathbf{F} = \text{Grad}\phi$. We choose \mathbf{P} as the first Piola-Kirchhoff stress conjugate to \mathbf{F} , defined as:

$$\mathbf{P} = \frac{\partial W}{\partial \mathbf{F}} + \frac{\partial \phi^*}{\partial \dot{\mathbf{F}}}$$

The alternate representations of constitutive relations can similarly be obtained with the use of the conjugate pairs of stress-strain tensors (Cauchy stress-Cauchy-green strain, second Piola-Kirchhoff stress -Green-Lagrange finite strain...). We suppose the force conjugate to the cumulated plastic deformation as Y :

$$Y = -\frac{\partial W}{\partial \mathbf{Z}} = \frac{\partial \psi^*}{\partial \dot{\mathbf{Z}}}$$

where ψ^* is a dual pseudo-potential obtained from a Legendre-Fenchel transform of kinetic potential ψ , defined as:

$$\psi^* = \sup_Y \{Y\dot{\mathbf{Z}} - \psi\} \quad \text{and} \quad \dot{\mathbf{Z}} = \frac{\partial \psi}{\partial Y}$$

Convexity of ψ verifies the following properties of ψ^* :

$$\psi^* \geq 0; \quad \psi^* \text{ convex}; \quad \psi^*(0) = 0$$

which will be the sufficient conditions for verifying the second law of thermodynamics.

Therefore for thermo-visco-plasticity material, the first law of thermodynamics can also be written as:

$$\rho_0 C \dot{T} = T \frac{\partial^2 W}{\partial T \partial \mathbf{F}} : \dot{\mathbf{F}} + T \frac{\partial^2 W}{\partial T \partial \dot{\mathbf{Z}}} : \dot{\mathbf{Z}} + \mathcal{D}^{int} + \rho_0 Q - \text{Div} \mathbf{H}$$

where C is heat capacity, defined as the ratio of heat energy transferred to the increase of temperature:

$$\rho_0 C = -T \frac{\partial^2 W}{\partial T^2}$$

which depends on the state variables in physical system and temperature, yet we always choose it as a constant in the numerical calculation. The intrinsic dissipation \mathcal{D}^{int} is stated as $Y\dot{\mathbf{Z}}$. In finite plastic strains, Stainier [Stainier and Ortiz, 2010] provided an accuracy formulation of the Taylor-Quinney parameter to calculate the ratio of intrinsic dissipation converted to total plastic power in the variational framework. In contrast, engineers regard it as a priori definition.

As a consequence, the second law of thermodynamics can be simplified as:

$$\frac{1}{T} Y \dot{\mathbf{Z}} - \frac{1}{T^2} \mathbf{H} \cdot \nabla T \geq 0$$

Clearly if the material is thermo-elastic material, Biot conduction ($H = -\lambda \nabla T$) can directly satisfy this inequality. λ is thermal conductivity. Yet for the thermo-viscoplastic materials, the satisfaction of the law needs that the kinetic potential ψ^* is convex, which is rightly an intrinsic character of ψ^* in our variational framework.

Based on the aforementioned described thermodynamic framework, we summarize the energy-based variational formulation of the coupled thermo-mechanical boundary-value problem proposed by Yang [Yang et al., 2006]. The potential for general standard dissipative materials is stated as follows:

$$\begin{aligned} \Phi [\phi, T, \dot{\eta}, \dot{\mathbf{Z}}] &= \int_B \left[\dot{E} - \rho_0 T \dot{\eta} + \Delta \left(\frac{T}{\Theta} \dot{\mathbf{F}}, \frac{T}{\Theta} \dot{\mathbf{Z}}, -\frac{1}{T} \text{Grad} T \right) \right] dV \\ &\quad - \int_B \rho_0 \mathbf{B} \cdot \phi dV - \int_{\partial_\tau B} \bar{\mathbf{T}} \cdot \phi dS \\ &\quad + \int_B \rho_0 Q \log \frac{T}{T_0} dV - \int_{\partial_\eta B} \bar{\mathbf{H}} \log \frac{T}{T_0} dS \end{aligned} \quad (2.1)$$

where $\bar{\mathbf{T}}$ is the applied tractions over the traction boundary $\partial_{\mathbf{T}}B$. $\bar{\mathbf{H}}$ is the outward heat flux over the Neumann boundary condition $\partial_{\eta}B$. In the exploration of EQ.2.1, the authors introduce two temperatures Θ and T , which are respectively an equilibrium temperature and an external temperature, to satisfy the symmetric of variational formalism. Consequently contrary to traditional works, the Euler-Lagrange equations of Φ is symmetry. Θ follows as a scaling variable and we can obtain it by

$$\Theta = \frac{\partial E}{\partial(\rho_0\eta)}$$

where $T = \Theta$ at local thermodynamics state.

This variational formulation works for general dissipative materials including finite elastic and plastic deformation, non-Newtonian viscosity, rate-sensitivity, arbitrary flow and hardening rules, as well as heat conduction. In addition, the thermal and mechanical balance equations, the constitutive relations, as long as the equilibrium between the external temperature and the internal temperature can be followed as Euler-Lagrange equations of the following variational formulation:

$$\inf_{\phi, \dot{\mathbf{Z}}, \dot{\eta}} \sup_T \Phi(\phi, T, \dot{\eta}, \dot{\mathbf{Z}}) \quad (2.2)$$

The equilibrium derivation are well described in [Yang et al., 2006].

Energy-based variational method is an optimization strategy using a single function to describe all the intrinsic characters for the coupled thermo-mechanical boundary value problem. We do not need to define the stress-strain relation, as well as temperature-entropy relation separately, which can directly follow from the optimization with regard to internal variables and temperature. For example, a nonlinear equation about \mathbf{Z} can be obtained to calculate equivalent plastic strain from the variational method:

$$D_{\mathbf{Z}} [\Phi(\phi, T, \dot{\eta}, \dot{\mathbf{Z}})] (\delta\dot{\mathbf{Z}}) = 0$$

We might as well say that it is a mathematical transformation of well-known return-mapping method, and more convenient in the application of mathematical algorithm.

The thermo-mechanical coupling for general dissipative materials can thus be described as an optimization problem, and many mathematical algorithms, such as trust-region method, Levenberg-Marquardt algorithm, are suitable to seek a minimum or maximum value with respect to physical fields. In contrast to conventional coupled thermo-mechanical problem formulation, this variational approach intrinsically yields a symmetric stiffness matrix when adopting finite element methods based on this variational framework. Indubitably, these characteristics allow the application of a broad range of mathematical algorithms, contributing to numerical efficiency in matrix storage and nonlinear programming. Furthermore, this variational formulation seamlessly works for general standard materials. Consequently in view of these advantages, , Eq.2.1 allows to the design of robust and efficient algorithms, such as Rayleigh-Ritz method we will adopt within this chapter.

It should be noted that as an extension of this variational framework, it is suitable to do an error estimation and mesh adaptation, and the optimal mesh size distribution for finite element method can be given by variational method [Radovitzky and Ortiz, 1999].

2.1.2 Rayleigh-Ritz method

Rayleigh-Ritz method is widely used in mechanical engineering to find an approximation of the solution in partial differential equations with the second or higher orders. Simply, it supposes that the solution u can be approximated by a combination of certain independent functions ϕ_i :

$$u = \sum_{i=1}^N c_i \phi_i$$

where c_i are the unknown parameters to be determined. clearly, when $N \rightarrow \infty$, $u \rightarrow u_0$, u_0 is the real solution. Normally the choice of ϕ_i depends on the similar form of the real solution and the boundary conditions [Russak, 2002]. With a substitution of u in the variational functional, the quantity to be optimized (marked as $I(c_1, c_2, \dots, c_N)$) is rewritten as a function with a series of unknown parameters c_i . The stationary point of $I(c_1, c_2, \dots, c_N)$ is obtained if the variation $\delta I = 0$. Thereby the problem is changed as finding N variables in N nonlinear equations:

$$\frac{\partial I}{\partial c_i} = 0$$

The difficulty of Rayleigh-Ritz method is to try and choose a set of ϕ_i which can reflect well the character of solution. So mostly engineering take eigenfunctions as the shape functions.

As a foundation of this work, the Rayleigh-Ritz method will be adopted based on the foregoing variational formulation. Some applications of this method will be presented by the analysis of Couette flow, thermal layer, thermal-Couette flow and the final adiabatic shear band problem. Considering the formulation in the case of steady state, i.e. the stress, the elastic deformation and the entropy are constant, such that:

$$\dot{E} = 0; \dot{\eta} = 0$$

and $\dot{\varphi}$, $\dot{\mathbf{Z}}$, T constant in time, or

$$\ddot{\varphi} = 0, \quad \ddot{\mathbf{Z}} = 0, \quad \dot{T} = 0$$

These conditions imply the absence of work hardening for visco-plasticity models. In the following, we restrict our attention to the problem at steady state. So an Eulerian description of the potential of total power density is adopted as:

$$\Phi = \int_B \Delta \left(\frac{T}{\Theta} \text{Grad} V, \frac{T}{\Theta} \dot{\mathbf{Z}}, -\frac{\nabla T}{T} \right) dV \quad (2.3)$$

Body force and heat source are neglected.

2.2 Couette flow and thermal layer

As a first validation, we consider an isothermal Couette flow where two infinite plates, one of which subjected to a shearing velocity V_0 relatively to the other, are separated by a distance L . The viscous fluid located between the plates is considered Newtonian and incompressible, so that Navier-Stokes equation can be written as follows:

$$\frac{\partial^2 V}{\partial y^2} = 0$$

and using the boundary conditions

$$V(0) = 0; \quad V(L) = V_0;$$

the analytical velocity can be written:

$$V(y) = \frac{V_0}{L}y$$

Under steady state and without thermal conduction, the potential Φ in (2.3) reduces, for the Couette flow, to:

$$\Phi = \int_B \phi^* dS \quad \text{with} \quad \phi^* = \frac{1}{2}\mu\left(\frac{\partial V}{\partial y}\right)^2 \quad (2.4)$$

where μ represents the fluid viscosity. We adopt the following polynomial form to describe velocity fields:

$$V(y) = \sum_{i=0}^N c_i y^i \quad (2.5)$$

which is simplified through the boundary conditions as:

$$V(y) = \left(\frac{V_0}{L} - \sum_{i=2}^N c_i L^{i-1} \right) y + \sum_{i=2}^N c_i y^i \quad (2.6)$$

where c_i ($i = 2, \dots, N$) is an unknown parameter to be defined. Adopting the velocity field (2.6), the variational modelling of Couette flow becomes:

$$\inf_{c_i} \Phi(V) \quad (2.7)$$

So defining the velocity of Couette flow reduces to an optimization problem with respect to coefficients c_i . These coefficients can be calculated by the corresponding Euler-lagrange equation of (2.7), yielding $c_i = 0$ ($i = 2, \dots, N$). The analytical solution is retrieved.

Next, the variational formulation is validated by a simple conduction problem. Consider a 1D layer with fixed temperature boundary conditions:

$$T(0) = T_0; \quad T(L) = T_1;$$

The corresponding total power density is:

$$\Phi = \int_B -\chi dS \quad \text{with} \quad \chi = \frac{1}{2} \Theta \lambda \left(\frac{\nabla T}{T} \right)^2 \quad (2.8)$$

Where λ is thermal conductivity. Θ is the equilibrium temperature introduced to satisfy the symmetry property of variational formulation. Note that $\Theta = T$ in steady state. Hence the variational model of the thermal layer is written as

$$\sup_T \Phi$$

Similar to the forgoing Couette flow problem, we adopt the following trial temperature field satisfying the boundary conditions:

$$T(y) = T_0 + \left(\frac{T_1 - T_0}{L} - aL \right) y + ay^2$$

Using Galerkin method, we recover the analytical solution:

$$T(y) = T_0 + \frac{T_1 - T_0}{L} y \quad y \in [0, L]$$

2.3 Thermal Couette flow

Merging the above two examples, the Couette flow with thermal effect is next considered. In FIG.2.1, we consider two plates at constant temperature T_0 and T_1 . The bottom plate is fixed while the top plate is moving at constant velocity V_0 .

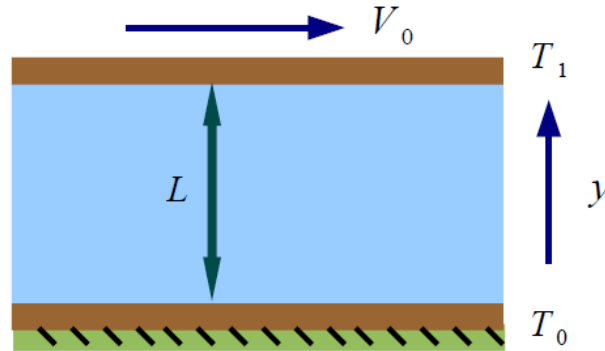


Figure 2.1: 1D thermal Couette flow problem

2.3.1 Analytical solutions

In general, for viscous non-Newtonian incompressible fluid, we define the constitutive model as follows:

$$\tau = \mu \dot{\gamma}_0 \left(\frac{\dot{\gamma}}{\dot{\gamma}_0} \right)^m$$

where m is the strain rate sensibility exponent, γ and τ are separately shear strain and shear stress. Hence the conservation of mass, the conservation of linear momentum and the conservation of energy simplify to as follows:

$$\begin{aligned} \operatorname{div}V &= 0 \\ \operatorname{div}\tau &= 0; \quad P = \text{const}; \\ -\lambda \frac{\partial^2 T}{\partial y^2} &= \tau \dot{\gamma} \end{aligned}$$

where P represents the pressure, constant in our problem. The analytical velocity and temperature are obtained as:

$$\begin{aligned} V(y) &= \frac{V_0}{L}y \\ T(y) &= -\frac{1}{2} \frac{\mu}{\lambda \dot{\gamma}_0^{m-1}} \left(\frac{V_0}{L}\right)^{m+1} y^2 + \left(\frac{T_1 - T_0}{L} + \frac{1}{2} \frac{\mu}{\lambda \dot{\gamma}_0^{m-1}} \left(\frac{V_0}{L}\right)^{m+1} L\right) y + T_0 \end{aligned}$$

2.3.2 Variational formulations

Considering the thermal Couette flow in steady state, the total power density in EQ.2.3 has two contributions: the viscous potential and the conduction potential, defined as:

$$\Phi(V, T) = \int_B \left(\frac{1}{m+1} \frac{\mu}{\dot{\gamma}_0^{m-1}} \left(\frac{T}{\Theta} \frac{\partial V}{\partial y} \right)^{m+1} - \frac{1}{2} \Theta \lambda \left(\frac{\nabla T}{T} \right)^2 \right) dy \quad (2.9)$$

For the facilitation of calculation, the following dimensionless formulas are adopted:

$$\bar{V} = \frac{V}{V_0}; \quad \bar{y} = \frac{y}{L}; \quad \bar{T} = \frac{T}{T_{ref}}; \quad \bar{\Theta} = \frac{\Theta}{T_{ref}}; \quad T_{ref} = \frac{\mu L^2}{\lambda \dot{\gamma}_0^{m-1}} \left(\frac{V_0}{L}\right)^{m+1}$$

The density power (2.9) is then reduced to

$$\bar{\Phi}(\bar{V}, \bar{T}) = \int_0^1 \left(\frac{1}{m+1} \frac{\bar{\mu}}{\bar{\dot{\gamma}}_0^{m-1}} \left(\frac{\bar{T}}{\bar{\Theta}} \frac{\partial \bar{V}}{\partial \bar{y}} \right)^{m+1} - \frac{1}{2} \bar{\Theta} \left(\frac{\nabla \bar{T}}{\bar{T}} \right)^2 \right) d\bar{y}$$

In the same way, by recourse to the boundary conditions, the velocity and temperature can be rewritten as

$$\begin{aligned} \bar{V}(y) &= (1 - \bar{a})\bar{y} + \bar{a} \bar{y}^2 \\ \bar{T}(y) &= \bar{T}_0 + (\bar{T}_1 - \bar{T}_0 - \bar{c})\bar{y} + \bar{c} \bar{y}^2 \end{aligned}$$

where \bar{a} , \bar{c} are the unknown parameters in dimensionless form. So the variational modelling of thermal Couette flow is defined as:

$$\inf_{\bar{a}} \sup_{\bar{c}} \bar{\Phi}(\bar{V}, \bar{T}) \quad (2.10)$$

Consequently, the thermal Couette problem turns to a mathematical optimization: a

Table 2.1: Comparisons with the parameters a and c ($a = \bar{a} \frac{V_0}{L^2}$; $c = \bar{c} \frac{T_{ref}}{L^2}$)

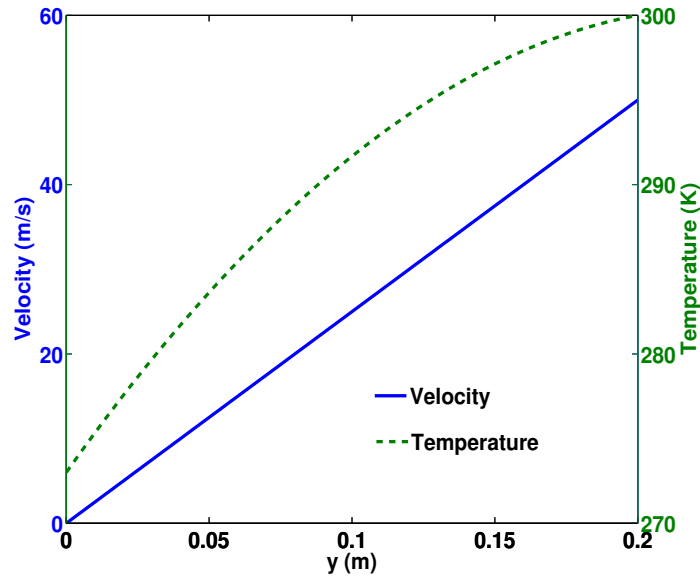
	variational modelling	analytical solutions
a (1/ms)	-2.84×10^{-13}	0
c (K/m ²)	-517.16	-517.16

saddle point for \bar{a} and \bar{c} . Taking variations with respect to \bar{a} and \bar{c} , we can obtain the corresponding mechanical and thermal balance equations. Using the following material parameters:

$$\mu = 0.157 \text{ Pa} \cdot \text{s}; \quad \lambda = 0.6 \text{ Wm}^{-1} \text{K}^{-1}; \quad m = 0.5; \quad \dot{\gamma}_0 = 1 \text{ s}^{-1}$$

$$L = 0.2 \text{ m}; \quad V_0 = 50 \text{ m/s}; \quad T_0 = 273 \text{ K}; \quad T_1 = 300 \text{ K};$$

TAB.2.1 presents the comparisons of a and c between analytical solutions and variational modelling, validating the feasibility of this variational modelling. FIG.2.2 presents profiles of velocity and temperature: the velocity has a linear form with a slope $\frac{V_0}{L}$, while the temperature in the fluid between the plates are gradually increasing with a parabolic form from the cooler plate to the upper plate. But if we choose V_0 smaller, the distribution of temperature is more linear.

**Figure 2.2:** Profiles of velocity and temperature in the thermal Couette flow

2.4 Fully formed adiabatic shear band

Adiabatic shear band is a complex thermo-mechanical phenomenon with thermal softening. It occurs easily in thermal viscoplastic materials subject to high strain rate. Generally its initiation and propagation are a precursor to material failure. Here we simplify the shear localization model as a 1D problem illustrated in FIG.2.3: a slab of thickness $2H$ subject to a simple shearing velocity V_0 , and isothermal conditions at $y = \pm H$ are considered. The material is representative of steel having a thermo-viscoplastic behaviour as described in [Leroy and Molinari, 1992]. The constitutive relation is written as:

$$\tau = \tau_0 \exp\left(-\beta\left(\frac{T}{T_0} - 1\right)\right) \left(\frac{\dot{\gamma}}{\dot{\gamma}_0}\right)^m \quad (2.11)$$

τ_0 and $\dot{\gamma}_0$ are the referenced stress and strain rate. T_0 is a reference temperature, here chosen equal to the imposed temperature at $y = \pm H$. β scales the thermal softening. m is the strain rate sensitivity. The following hypothesis are required in this study:

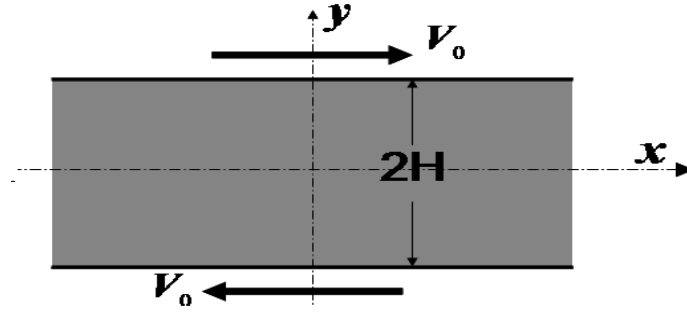


Figure 2.3: 1D shear band problem [Leroy and Molinari, 1992]

- It is an idealized, well established shear band;
- The velocity does not depend on X direction, i.e. $\vec{V} = V(y)\vec{e}_x$
- Body force and external heat supply are neglected.
- Material obeys a $J2$ von Mises law.
- It is asymptotic regime in time direction: no hardening is considered.

We consider the case when stress arrives at steady state. Consequently, the Cauchy stress is uniform in y direction, and its form is as follows:

$$\begin{bmatrix} 0 & \sigma_{xy} & 0 \\ \sigma_{xy} & 0 & 0 \\ 0 & 0 & 0 \end{bmatrix}$$

The relation between shear strain rate and equivalent strain rate is derived as:

$$V_{,y} = \sqrt{3}\dot{\epsilon}^P$$

Considering the shear band problem in steady state, the elastic deformation and the entropy arrived at a steady state. Supposing the velocity and the temperature are imposed on the boundary of the shear slab, the formulation EQ.2.3 is reduced to:

$$\Phi(V, T) = \int_{-H}^H \Psi^*\left(\frac{T}{\Theta}V_{,y}\right) - \chi\left(-\frac{T_{,y}}{T}\right)dy \quad (2.12)$$

where the dissipated pseudo-potential Ψ^* is defined as follows:

$$\Psi^*\left(\frac{T}{\Theta}V_{,y}\right) = \frac{1}{m+1} \frac{\tau_0}{(\dot{\gamma}_0)^m} \exp\left[-\beta\left(\left(\frac{\Theta}{T_0}\right) - 1\right)\right] \left(V_{,y} \frac{T}{\Theta}\right)^{m+1} \quad m \in [0, 1] \quad (2.13)$$

and χ is thermal conduction conformed to Fourier law, described in (2.8). Yet we neglect the viscoelastic potential in ϕ^* . In the same manner, the problem in FIG.2.3 is written as an optimization of (2.12) as follows:

$$\inf_V \sup_T \Phi(V, T) \quad (2.14)$$

Taking variation with respect to velocity, we can obtain the mechanical equilibrium equation, while the heat equation is obtained from the stationary condition on T (see Appendix A). In addition, thermal equilibrium requires that $\Theta = T$. Leroy and Molinari have shown that an exact solution exists for the problem in FIG. 2.3 when the material flow law is given by (2.11) [Leroy and Molinari, 1992]. Here we adopt the material parameters in TAB. 2.2.

Introducing the non-dimensional variables as follows:

$$\bar{y} = \frac{y}{H}; \quad \bar{T} = \frac{T}{T_0}; \quad \bar{t} = \frac{t}{t_C} \quad \text{with} \quad t_C = \frac{\rho_0 C H^2}{\lambda}$$

$$\bar{V} = \frac{V}{H/t_C}; \quad \bar{\tau} = \frac{\tau}{\tau_R} \quad \text{with} \quad \tau_R = \tau_0 (\dot{\gamma}_0 t_C)^{-m}$$

the total pseudo-potential (2.13) reduces to:

$$\Phi(\bar{V}, \bar{T}) = \tau_R \frac{H}{t_C} \int_{-1}^1 \left(\frac{1}{m+1} \exp(-\beta(\bar{\Theta} - 1)) \left(\frac{\bar{T}}{\bar{\Theta}} \bar{V}_{,\bar{y}}\right)^{m+1} - \frac{1}{2} \kappa \bar{\Theta} \left(\frac{\bar{T}_{,\bar{y}}}{\bar{T}}\right)^2 \right) d\bar{y} \quad (2.15)$$

where $\kappa = \frac{T_0 \rho_0 C}{\tau_R}$.

Table 2.2: Material property for HY-100 steel

T_0 (K)	300	ρ (kg/m ³)	7800
C (J/kgK)	500	λ (W/mK)	54
T_0	300	τ_0 (MPa)	500
$\dot{\gamma}_0$ (s ⁻¹)	1000	m	0.012
β	0.33	k	0.40

2.4.1 Analytical solutions

Molinari and Wright gave the similar theoretical expressions of the profiles of velocity and temperature in the band. In addition, Wright recurs to the constitutive models widely used in the engineering to point out the generality of these formulations. Here we review this analytical work and analyse the influences of material parameters to shear bandwidths.

Using the above non-dimensional variables, the equilibrium equations are written as:

$$\frac{\partial \tau}{\partial y} = 0$$

$$-\frac{\partial^2 T}{\partial y^2} = \tilde{\kappa} \tau \frac{\partial V}{\partial y}$$

where $\tilde{\kappa} = \frac{1}{\kappa}$. Leroy and Molinari [Leroy and Molinari, 1992] obtained the analytical solutions at a steady state for exponential softening law. The temperature in the layer can then be written as follows:

$$T = T_b + \frac{m}{\beta} \log[\operatorname{sech}^2(\frac{Zy}{2})]$$

and the velocity is :

$$V = \frac{m}{\beta \tilde{\kappa} \tau} \tanh(\frac{Z}{2}y)$$

Where Z is an unknown parameter reflecting well the length of localization zone, thus We might as well define the bandwidth h is equal to $\frac{2}{Z}$, as a measure parameter to estimate the profiles of velocity and temperature in the layer. Combined with the boundary condition, it can be obtained implicitly through the following nonlinear equation:

$$Z - \sqrt{\frac{2\beta\tilde{\kappa}}{m} \left(\frac{mZ}{\beta\tilde{\kappa}V_0} \tanh(\frac{Z}{2}) \right)^{(1+\frac{1}{m})} \cosh(\frac{Z}{2})} = 0$$

FIG.2.4 shows the influences of imposed velocity V_0 , strain rate sensibility exponent m , thermal softening coefficient β and the inverse of heat conduction parameter $\tilde{\kappa}$ (all in non-dimensional values) on bandwidth h . We can see that except that the bandwidth is increasing when m increases, yet it is decreasing as the other three parameters increase.

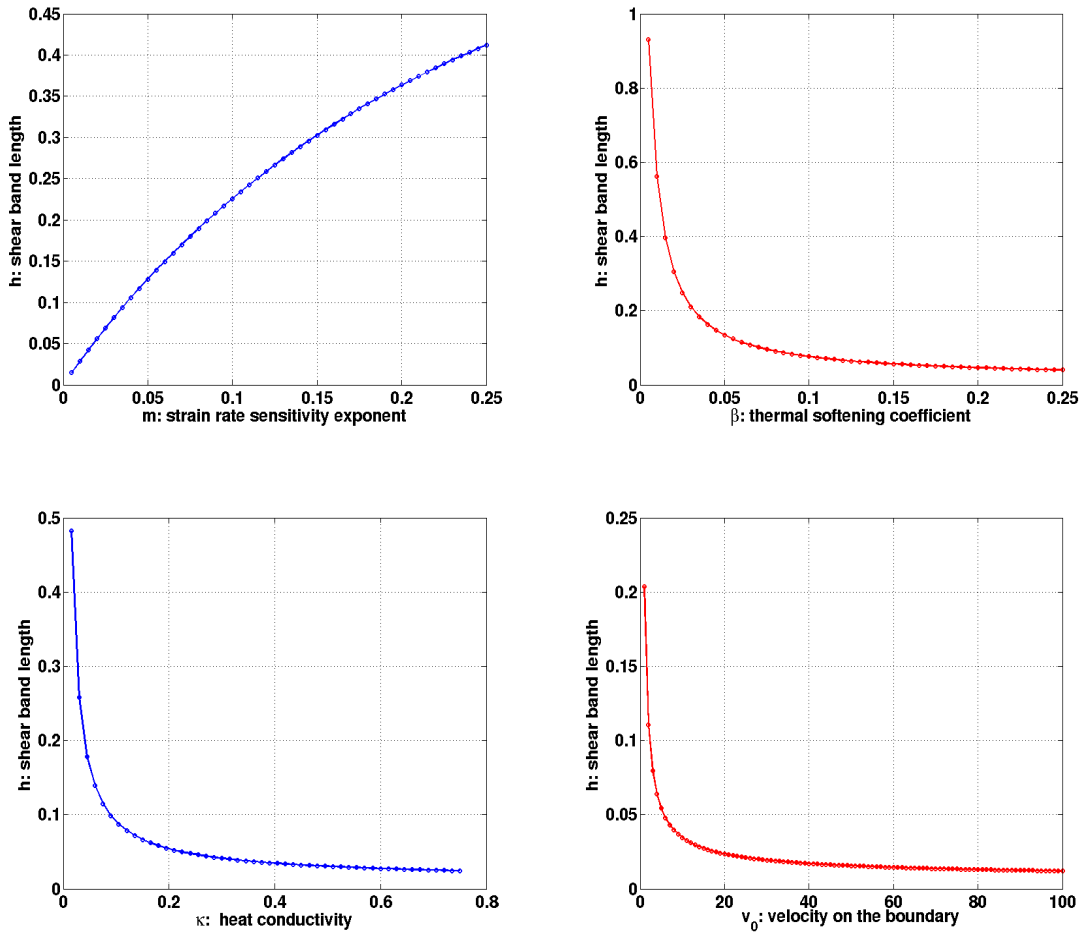


Figure 2.4: Influences of m , V_0 , β and $\tilde{\kappa}$ on bandwidth

2.4.2 Variational modelling with Rayleigh-Ritz method

We recall the boundary conditions for the simple shear problem in FIG.2.3:

$$V|_{\pm H} = V_0; \quad T|_{\pm H} = T_0$$

Here accounting for the analytical forms of physical profiles in variational formulation EQ.2.1, we will build our energy-based variational modelling of fully formed shear band from two views: the total power density with shear band width to be optimized and the one with shear band width and central temperature to be optimized.

2.4.2.1 Shear band width and penalty method

For a fully formed adiabatic shear band, the width, denoted as h , is a certain and unique value. If we just consider the original formulas for velocity and temperature, the pseudo-potential is written as the form of h . Yet the stationary point of ψ with respect to h does

not mean that it simultaneously chooses the optimization values of the pseudo-potential on the corresponding velocity and temperature. We assume that there are two shear widths: kinematic width h_V and thermal width h_T to measure the profiles of velocity and temperature. Here the analytical solutions obtained by Leroy and Molinari are applied and written as follows:

$$V(y) = V_0 \frac{\tanh(y/h_V)}{\tanh(H/h_V)}, \quad T(y) = T_0 - \frac{2m}{\beta} T_0 \ln \frac{\cosh(y/h_T)}{\cosh(H/h_T)} \quad (2.16)$$

Two length-like parameters (h_V and h_T) have been introduced. Owing to symmetry, the actual widths are twice these values. In the following, h_V and h_T will nevertheless be referred to as shear band widths.

A penalty method is introduced to fulfil the condition $h_V = h_T$. The energy-based variational modelling is changed to a constrained optimization problem as follows:

$$Stat_{h_V, h_T} \left[\Phi + \frac{1}{2} A (h_V - h_T)^2 \right] \quad (2.17)$$

where A is a penalty coefficient, an ideally infinite constant. Thus the shear localization problem is changed to an optimization form of the pseudo-potential, and shear band width is the corresponding stationary point. Then many mathematical optimized methods can be applied to search these unknown parameters associated with the steady velocity and temperature.

We choose the following algorithm to solve EQ.2.17. In effect, the variation of Φ with respect to h_V is as follows:

$$\frac{\partial \Phi}{\partial h_V} = \tau_R \frac{H}{t_C} \int_{-1}^1 \tau \frac{\partial^2 V}{\partial y \partial h_V} d\bar{y} \quad (2.18)$$

Because the conservation of linear momentum is

$$div \tau = 0$$

the stress tensor is constant in y direction, and then

$$\frac{\partial \Phi}{\partial h_V} = \tau_R \frac{H}{t_C} \tau \frac{\partial^2 V}{\partial h_V} \Big|_{-1}^1 = 0 \quad (2.19)$$

We obtain that the resolution of profiles of velocity and temperature are changed to a nonlinear equation because of $h_V = h_T$. Yet some convergence problem exists when we use this form of optimization. FIG.2.5 presents the profiles of $\frac{\partial \Phi}{\partial h_T}$ with \bar{h}_T ($\bar{h}_T = \frac{h_T}{H}$) increased. Apparently, when \bar{h}_T is close to 1, the derivation limited to 0. Due to the character of function \tanh : homogeneous when $h_V > 2.5$, there will be more than one solution in our variational modelling. Yet it merely exists an unique physical solution in $0 < \bar{h} < 1$ for a fully formed ASB. As a consequence, Newton-Raphson method does not seem to work well for this nonlinear problem, initial value will have a large influence on the algorithm. Here we choose the bisection method to calculate the bandwidth, which naturally limit the solution in the section $[0, 1]$.

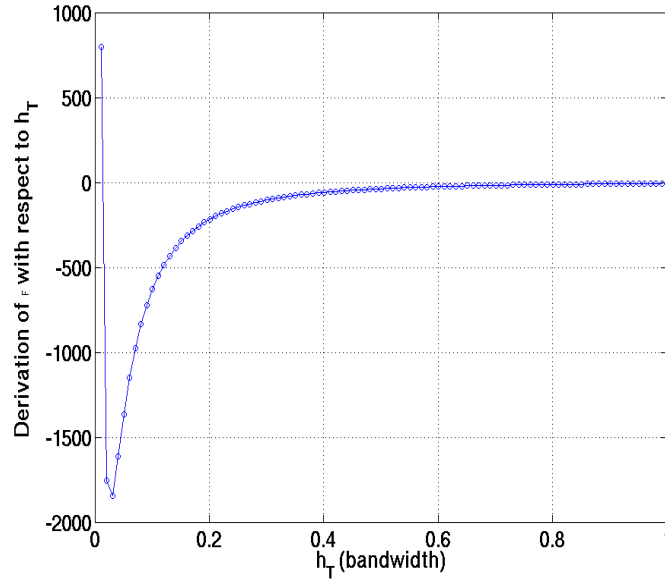


Figure 2.5: Derivation of ϕ with respect to h_T with $h_V = h_T$

2.4.2.2 Shear band width and central temperature

Although the penalty method can enforce the constraint condition, the choice of penalty coefficient is difficult to decide. Too lenient or too severe values will influence the convergence of feasible solution. Here combined with the boundary condition, we rewrite the analytical profiles of velocity and temperature as follows:

$$V(y) = V_0 \frac{\tanh(y/h)}{\tanh(H/h)}, \quad T(y) = T_{max} - (T_{max} - T_0) \frac{\ln(\cosh(y/h))}{\ln(\cosh(H/h))} \quad (2.20)$$

where h is shear band width, T_{max} is central temperature. After the substitution of (2.20) in (2.15), the pseudo-potential has two characteristic parameters h and T_{max} ; Besides (2.18), its optimization of total power density with respect to T_{max} is equal to the heat equation. The variational model (2.14) is equal to :

$$\underset{h, T_{max}}{Stat} \Phi(h, T_{max})$$

Moreover, the introduction of new parameter T_{max} avoids the dependence on material properties and gives us a more general description of velocity and temperature in the slab. FIG.2.6 illustrates the profile diagram of $\Phi(h, T_{max})$ when $H = 1.25$ mm and $V_0 = 0.01108$ m/s. Our energy-based variational modelling simplifies the thermo-mechanical coupled problem as an optimization problem associated with the band properties, which brings a saddle point to describe an adiabatic shear band. This gives us a good advantage in the application of mathematical optimization to the simulation of shear localization problem. In the next part, we will show the comparisons of this modelling based on the two foregoing methods.

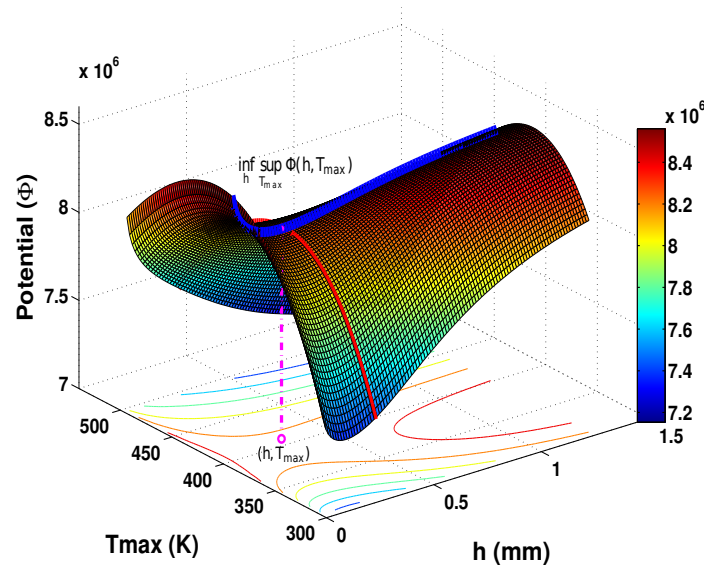


Figure 2.6: Modelling of adiabatic shear band by energy-based variational approach

2.4.3 Results and analysis

In our calculation, in view of the strong non-linearity of Euler-Lagrange equations of (2.14), we choose an improved version of Newton-Raphson method, the trust-region method, to calculate the stationary problem and obtain the shear band width h and central temperature T_{max} . TAB.2.3 shows the non-dimensional solutions \bar{h}_V , \bar{h}_T and T_{max} from the two methods of variational modelling in different material properties, which are in good agreement with the analytical solutions [Leroy and Molinari, 1992]. FIG.2.7 presents the profiles of velocity and temperature ($H = 1.25$ mm, $V_0 = 0.1$ m/s) in the steady state of the slab, the material parameters are chosen in TAB.2.2. Here the segment of the localization is $[-0.0448$ mm, 0.0448 mm], the central temperature is $893.3K$ when shear band arrives to the stability.

Table 2.3: Shear band width (dimensionless) and central temperature ($\beta = 0.38; V_0 = 0.1108$ m/s)

	Variational model		Analytical solutions	
	\bar{h}_V	$[\bar{h} \quad T_{max}]$	$[\bar{h} \quad T_{max}]$	
$m = 0.12; \kappa = 1/0.24$	0.3126	[0.3126 775.0]	[0.3126 775.0]	
$m = 0.012; \kappa = 1/0.40$	0.0310	[0.0311 896.6]	[0.0311 896.6]	
$m = 0.06; \kappa = 1/0.32$	0.1535	[0.1535 851.3]	[0.1535 851.3]	

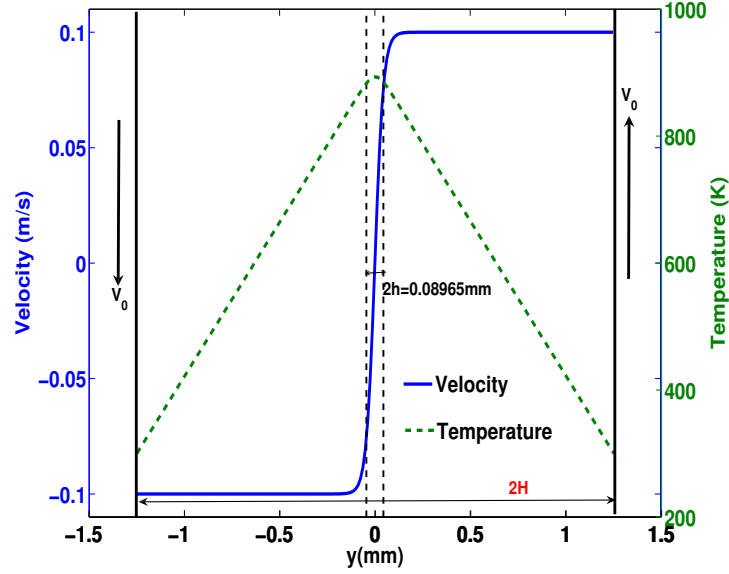


Figure 2.7: Profiles of velocity and temperature in steady state

FIG.2.8 illustrates the influence of the imposed velocity V_0 on h and T_{max} . With the velocity increased, the shear band width h decreases and the central temperature in the band increases. From this figure, we can see that the increasing speed of the shear band width diminishes when $V_0 > 0.1108$ m/s. Obviously in a thermal softening material, a higher strain rate causes a smaller band width, and also brings more dissipation and heat generation in the band. In addition, the time of the formation of the shear band is so short that the heat cannot go out of the layer by conduction, leading to a higher central temperature. The influences of thermal conductivity λ on h and T_{max} are also analysed in FIG.2.9: the shear band width increases almost linearly with λ , while the central temperature decreases in a non linear way. This conclusion also validates that adiabatic shear band is a misnomer, as described in CHAP.1. Heat conduction plays an important role in the final process of ASB formation, determining on the steady localization length and central temperature.

Moreover, we discovered that the average stress can be obtained from the following derivation:

$$\begin{aligned}
 \frac{\partial \Phi}{\partial V_0} &= \int_{-H}^H \frac{\partial \Phi}{\partial \dot{\epsilon}^P} \frac{\partial \dot{\epsilon}^P}{\partial V_0} dy \\
 &= \int_{-H}^H \sqrt{3} \tau \frac{1}{\sqrt{3}} \frac{\partial \tilde{V}(y)}{\partial y} dy \\
 &= \tau (\tilde{V}(H) - \tilde{V}(-H)) \\
 &= 2\tau
 \end{aligned} \tag{2.21}$$

The above relation holds exactly for the analytical solution (constant shear stress). For ap-

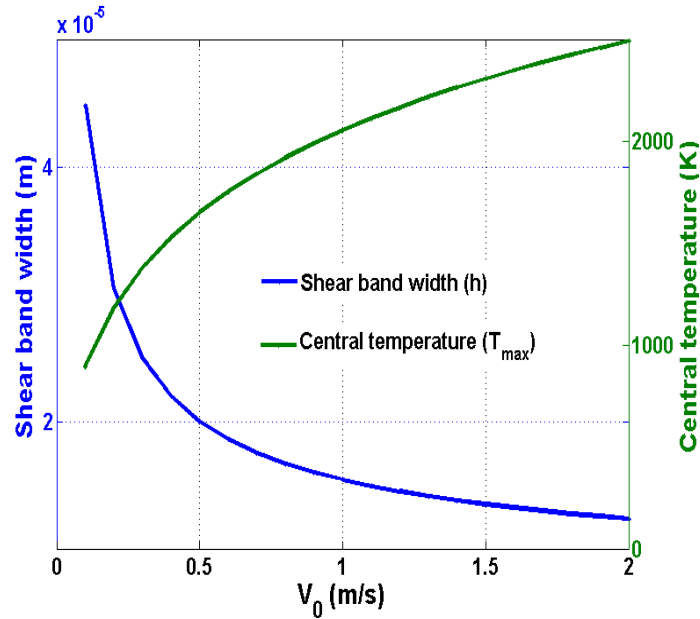


Figure 2.8: Influences of the imposed velocity V_0 on the shear band width and the central temperature

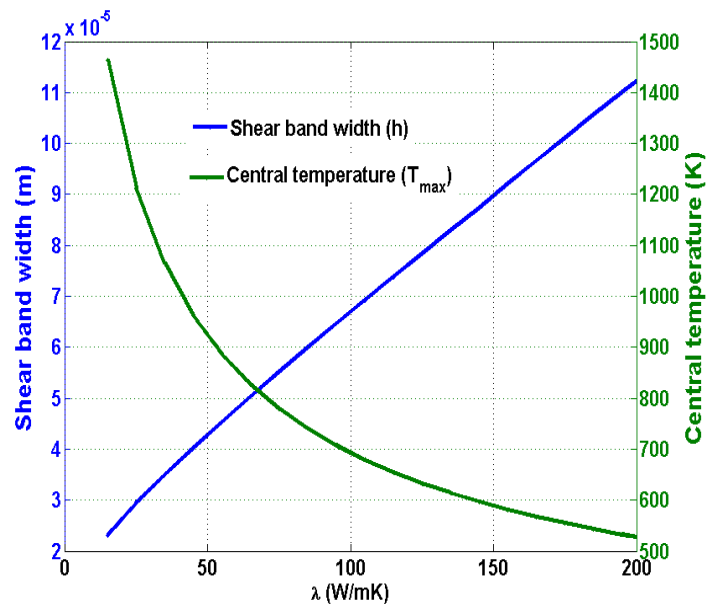


Figure 2.9: Influences of thermal conductivity λ on the shear band width and the central temperature in the steady state

proximate solutions, we can define the half of derivation of pseudo-potential with respect to the imposed velocity V_0 as average stress. FIG.2.10 shows the comparison of every point stress calculated by our modelling and the average stress. Theoretically, the stress

calculated should be equal to each other. For $V_0 = 1 \text{ m/s}$, $H = 1.25 \text{ mm}$, the maximum error is the order of 1×10^{-6} .

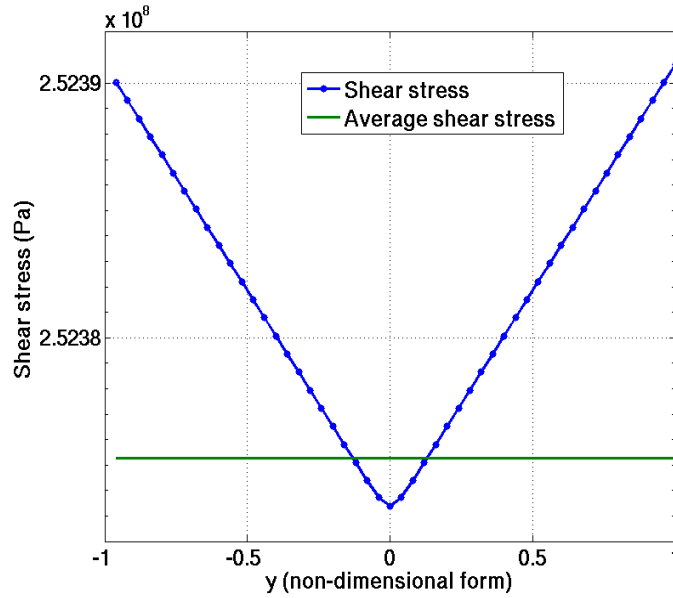


Figure 2.10: Comparison of average stress and stress

2.4.4 Extension to various constitutive relations

For arbitrary flow laws where the strain rate can be expressed as the form of stress and temperature in [Wright and Ravichandran, 1997], Wright introduced two auxiliary functions, which are the characteristics of the materials, to define strain rate sensibility exponent m and thermal softening coefficient β , and obtained the canonical aspects of adiabatic shear band. Here in this section, although the formations of (2.20) originates from the work for exponential softening law in [Leroy and Molinari, 1992], we apply the boundary conditions to eliminate the dependence of analytical formulations on material parameters, such as m and β , and then transform the solutions of thermo-mechanical field quantities as an optimization problem with respect to two variables (shear band width and central temperature). This character will bring a good advantage in the application of variational modelling to different constitutive models. We will use two popular models in mechanical engineering to validate the feasibility of material modelling on various constitutive laws.

2.4.4.1 Power law

For simplicity, we choose a flow law ([Clifton and Molinari, 1983]) defined as

$$\sigma = K \left(\frac{T}{T_0} \right)^\nu \left(\frac{\dot{\epsilon}}{\dot{\epsilon}_0} \right)^m$$

which K , ν are material parameters. Neglecting the elastic property of material and assuming that the material obeys on von Mises law, we can get

$$\dot{\bar{\epsilon}}_p = \frac{1}{\sqrt{3}} V_{,y}$$

where $\bar{\epsilon}_p$ is cumulated plastic strain. So the dissipation potential ψ^* is obtained:

$$\psi^*\left(\frac{T}{\Theta} V_{,y}\right) = \frac{1}{m+1} \frac{K}{\dot{\epsilon}_0^m} \left(\frac{\Theta}{T_0}\right)^\nu \left(\frac{1}{\sqrt{3}} V_{,y} \frac{T}{\Theta}\right)^{m+1} \quad m \in [0, 1]$$

Using this expression, and applying canonical formulations of velocity and temperature (2.20), we can get the Euler-Lagrange equations with respect to two variables h and T_{max} . Supposing that the problem is quasi-static and adiabatic, Molinari [Clifton and Molinari, 1983] described the criteria of temperature localization with respect to this simple flow law. They pointed out that adiabatic shear band will occur when

$$\nu + m < 0$$

Combined with the properties of CRS 1018, we choose the material parameters as following:

$$\nu = -0.38; m = 0.012; T_0 = 300 \text{ K}; \dot{\epsilon}_0 = 577.35 \text{ s}^{-1};$$

$$K = 866 \text{ Mpa}, \lambda = 54 \text{ W/mK}$$

As a validation tool, FEM based on the variational formulation is applied to analyse the evolution of velocity and temperature in the shear slab [Stainier and Ortiz, 2010, Stainier, 2011a]. In contrast with the traditional methods for solving thermo-mechanical problems, our tangent matrix of FEM is symmetric taking advantage of the symmetry of bilinear form of total power density. Likewise, hardening effect is neglected in FEM model, yet we consider the elastic effect in the numerical simulation. However, a fine mesh is needed in localization zone to avoid the drawback of mesh dependence.

FIG.2.11 shows the evolution of the temporary profiles of velocity and temperature when $V_0 = 0.1108\text{m/s}$ and $H = 1.25\text{mm}$. With the time increased, the form of velocity changes from linear to nonlinear, and step by step arrives at the steady form, which is consistent with the analytical solutions in steady state obtained by variational modelling. Similarly, the temperature forms are gradually convergent to its form in steady state. As a note, shear band width h is just a characteristic length factor of shear localization. The choice of h stems from the property of tangent hyperbolic function. In FEM, we use the following formulation to define the transient evolution of band width:

$$V(h) \simeq V_0 \tanh(1)$$

which originates from the analytical form of velocity. Applying this formula, FIG.2.12 shows the corresponding evolution of shear band width. As FIG.2.11 describes, the shear band width decreases with time increased, and drops rapidly before 0.02s, and then step by

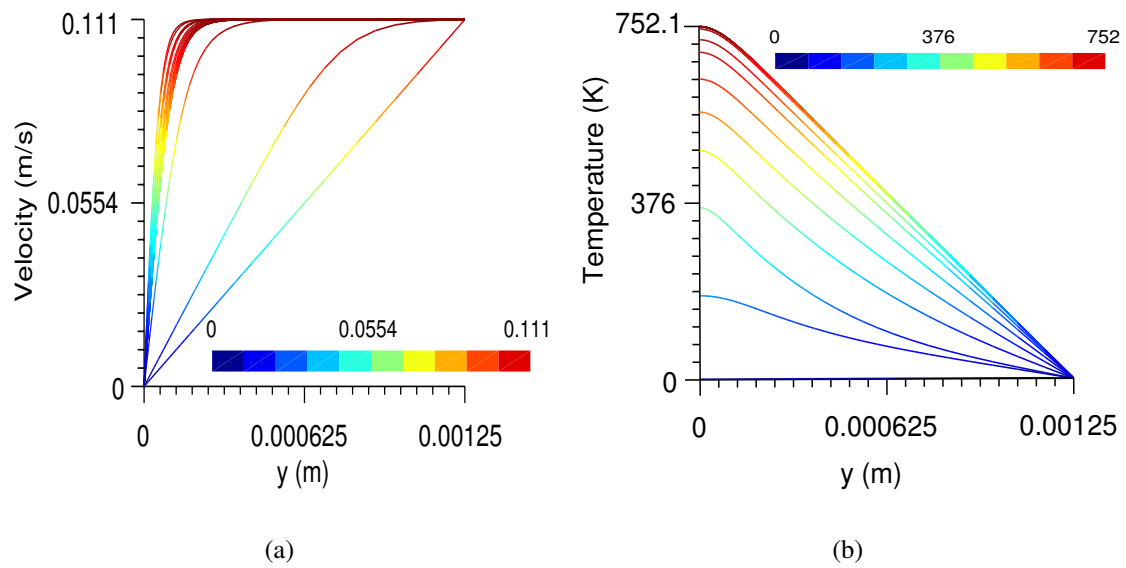


Figure 2.11: Evolutions of the velocity and the temperature in the layer obtained by FEM ($V_0 = 0.1108\text{m/s}$ and $H = 1.25\text{mm}$)

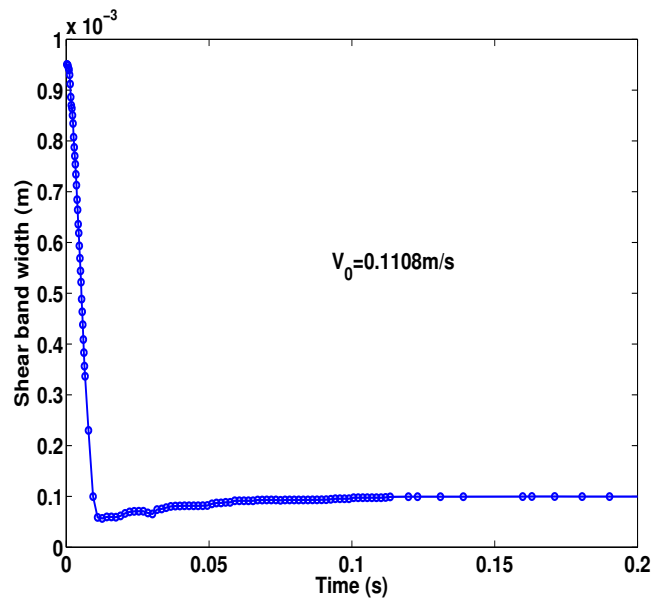


Figure 2.12: Time evolution of shear band width obtained by FEM ($V_0 = 0.1108\text{m/s}$ and $H = 1.25\text{mm}$)

step it arrives at a convergent solution when $t > 0.06\text{s}$. On the other part, the shear band width and central temperature in steady state are calculated by our variational modelling. FIG.2.13 gives the comparisons of the profiles of velocity and temperature in steady state

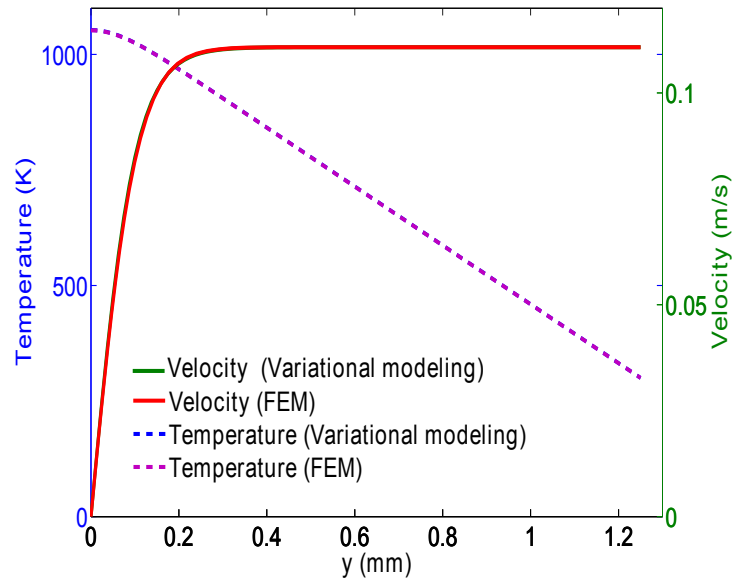


Figure 2.13: Profiles of velocity and temperature in steady state ($V_0 = 0.1108\text{m/s}$ and $H = 1.25\text{mm}$)

Table 2.4: Comparisons of shear band width h and central temperature T_{max} with FEM

	variational modelling	FEM
h (mm)	0.0991	0.0997
T_{max} (K)	1052.8	1052.1

with FEM in half of domain. Clearly, there is a good coherence with FEM. Meanwhile, we give TAB.2.4 the comparisons of shear band width and central temperature between FEM and variational method when $V_0 = 0.1108\text{m/s}$ and $H = 1.25\text{mm}$. The error approximation is controlled in 0.6% for the shear band width. Consequently, this example proposes the efficiency of our approach.

2.4.4.2 Johnson-Cook model

When considering high strain rate loading, the Johnson-Cook (JC) model is considered as the most simple and widely used model to represent material flow strength behaviour about the strain rate, large equivalent strain and temperature. It is defined as following:

$$\sigma_y(\dot{\bar{\epsilon}}^P, \bar{\epsilon}^P, T) = (A + B(\bar{\epsilon}^P)^n) \left(1 + c \log\left(\frac{\dot{\bar{\epsilon}}^P}{\dot{\bar{\epsilon}}_0}\right)\right) (1 - T^{*q})$$

The five parameters A , B , c , n and q are constant and obtained from experiments. $\dot{\bar{\epsilon}}_0$ is the reference effective strain rate determined from quasi-static test. T^* defines thermal

softening effect in function of melting temperature T_m and reference temperature T_0 .

$$T^* = \begin{cases} 0 & \text{if } T < T_0 \\ \frac{T - T_0}{T_m - T_0} & \text{if } T_0 < T < T_m \\ 1 & \text{if } T > T_m \end{cases} \quad (2.22)$$

For testing the independence of our modelling in steady state, we neglect the hardening part in JC model, choosing $B = 0$ in the example. Considering the existence of a ratio β of conversion of deformation energy into heat, the total variational modelling in steady state can be restated as:

$$\begin{aligned} \Phi = \int_{-H}^H A_d (1 - T^*(\Theta))^q \frac{T}{\Theta} \dot{\epsilon}^P + A (1 - T^*(\Theta))^q c \dot{\epsilon}_0 \\ \left(\frac{T}{\Theta} \frac{\dot{\epsilon}^P}{\dot{\epsilon}_0} \log\left(\frac{T}{\Theta} \frac{\dot{\epsilon}^P}{\dot{\epsilon}_0}\right) - \frac{T}{\Theta} \frac{\dot{\epsilon}^P}{\dot{\epsilon}_0} + 1 \right) - \chi\left(-\frac{T_y}{T}, \Theta\right) dy \end{aligned}$$

where $A_d \leq A$. The choice of A_d effects on the ratio of plastic energy transformed to heat β . If $A_d = A$, the classical Taylor-Quinney coefficient is equal to unity.

Firstly variational FEM is used to simulate the formation of ASB with the material parameters as TAB.2.5 described. We do not consider the hardening effect in steady state.

Table 2.5: Material properties for Ti-6Al-4V (in steady state)

Material property (Ti-6Al-4V) in steady state			
A (MPa)	792	A_d (MPa)	792
q	1.03	λ (W/mK)	54
c	0.014	$\dot{\epsilon}_0$ (s^{-1})	1
T_0 (K)	300	T_m (K)	1793
C_0 (J/K)	477	ρ (kg/m^3)	7830
ν	0.3	E (Gpa)	217.5

FIG.2.14 is the stress evolution of the band when $H = 1.25mm$; $V_0 = 0.1m/s$. The shear stress corresponds to the stress prevailing at the boundary ($y = \pm H$). At first the slab behaves elasticity. When plasticity develops, the stress level initially has a slight decrease because of the small effect of thermal softening. At some stage, the thermal softening occupies the process and induces the strain localization, and the stress drops rapidly. The steady state develops when $t > 0.1s$. Meanwhile shear band width decreases with the time and gradually evolves towards a constant. TAB.2.6 is the results of steady shear band width and central temperature compared with the above variational model, which has a good agreement with FEM.

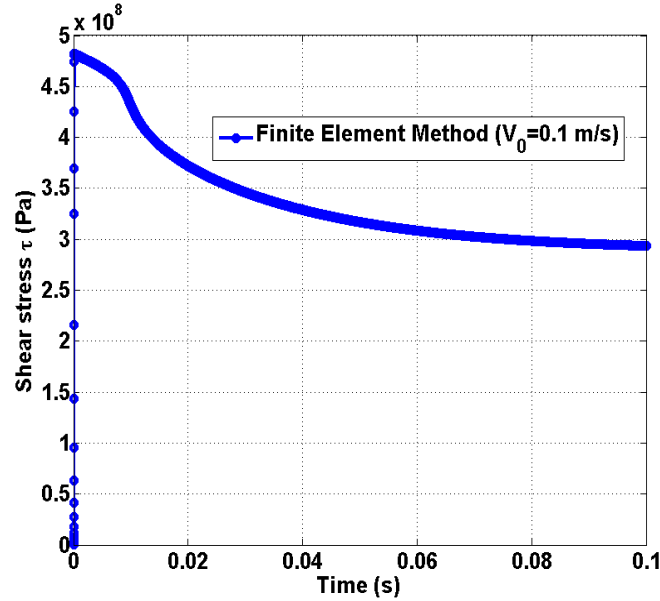


Figure 2.14: Evolutions of shear stress (JC model) by FEM ($V_0 = 0.1\text{m/s}$ and $H = 1.25\text{mm}$)

Table 2.6: Comparisons of shear band width h and central temperature T_{max} with FEM (JC Model)

	Variational modelling	FEM
h (mm)	0.042121	0.0426819
T_{max} (K)	952.8	938.7

2.4.5 Thermal boundary condition

Slab width size H is a known parameter in the foregoing energy-based variational modelling. Numerical analysis illustrates that ASB band width h and central temperature T_{max} increase when H is increased (FIG.2.15), isothermal boundary conditions $T = T_0$ and constant velocity $V = V_0$ are presented at $y = H$.

If we separately look at the mechanical part of our ASB problem, the profile of velocity for a slab with H_1 ($H_1 > h_r$) should be predicted the same as the one obtained with H_r in FIG.2.16(a), where the r subscript is used to denote a reference solution. Unfortunately, profiles of temperature obtained with different slab widths present a large difference, owing to isothermal boundary conditions (FIG.2.16(b)). Because of the strongly localized temperature, these isothermal boundary conditions are physically not very realistic, even under high strain-rate loading. In this section, we thus proceed to include heat exchange, with the objective of avoiding the direct dependency of results on slab width H . Our ap-

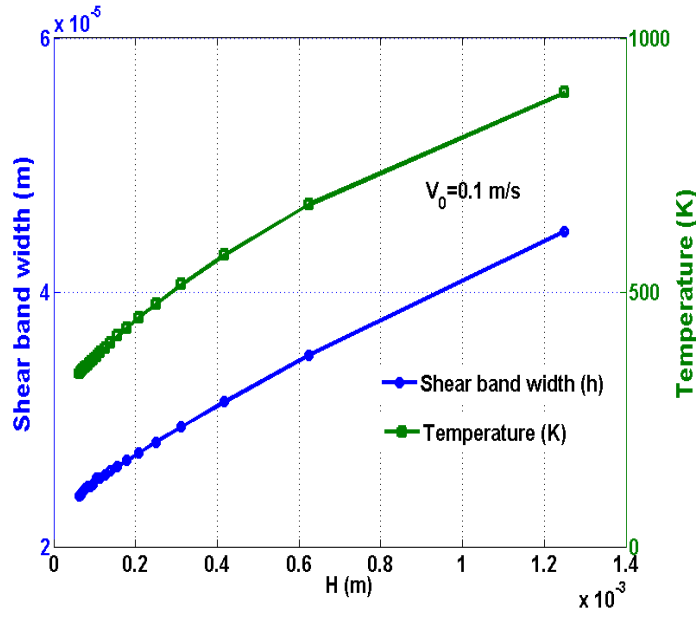


Figure 2.15: Influences of different slab widths on bandwidths and central temperatures (without heat exchange on $y = \pm H$)

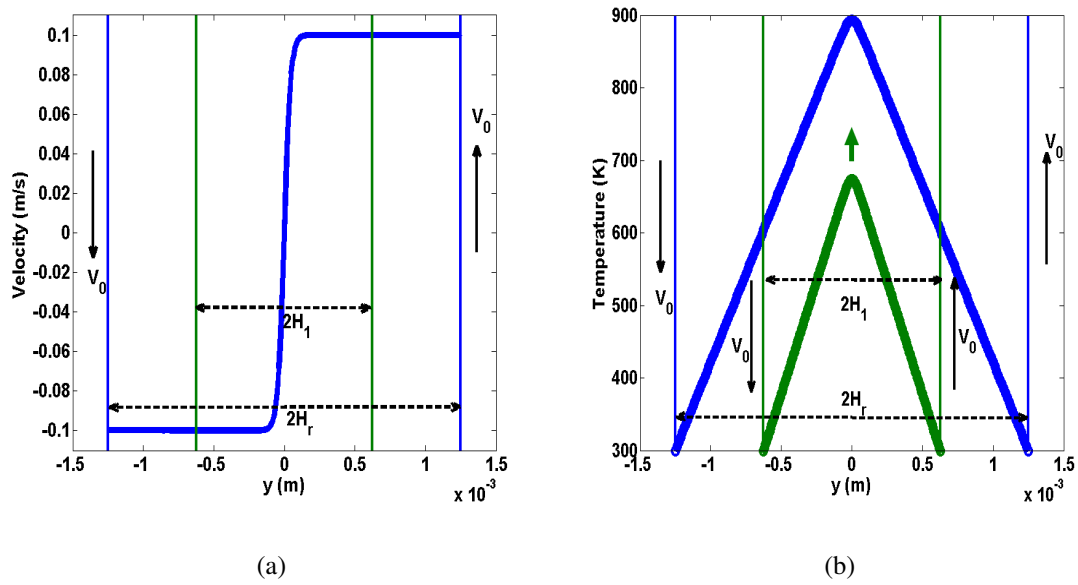


Figure 2.16: Profiles of velocity (a) and temperature (b) in a layer

proach is similar to the mixed boundary condition proposed by [Leroy and Molinari, 1992]:

$$\frac{\partial T}{\partial y} + \frac{1}{\alpha}(T - T_0) = 0 \text{ on } y = \pm H$$

where α is a known film parameter. The boundary is isothermal when $\alpha = 0$ and adiabatic when $\alpha = +\infty$.

Denoting T_{ext} the boundary temperature (now different from the outer temperature T_0), the trial temperature profile is written as:

$$T(y) = T_{max} - (T_{max} - T_{ext}) \frac{\log(\cosh(y/h))}{\log(\cosh(H/h))}$$

The trial velocity field remains unchanged. We also introduce the following heat exchange dissipation potential:

$$W_{tr} = \frac{1}{2} \frac{c}{\theta_1} (T_{ext} - T_0)^2 \quad \text{when } y = \pm H$$

where $\theta_1 = T_{ext}$ in steady state, and c is an exchange coefficient satisfying:

$$c = +\infty \quad \text{when } H_r = 1.25 \text{ mm}$$

i.e the conditions is isothermal: $T = T_0$. The total potential can be written as:

$$\Phi_t(h, T_{max}, T_{ext}, c) = \Phi - 2W_{tr}$$

where Φ is described in (2.1), here we take exponential law as an example. The variational modelling for adiabatic shear band problem with heat exchange is then described by the following optimization problem:

$$\underset{T_{ext}, h, T_{max}}{Stat} \Phi_t(h, T_{max}, T_{ext}, c) \quad (2.23)$$

Stationarity equation with respect to T_{ext} amounts to imposing a mixed boundary condition:

$$-\lambda \frac{\partial T}{\partial y} = c(T_{ext} - T_0)$$

consequently the relationship between exchange coefficient c and film parameter α proposed by Leroy [Leroy and Molinari, 1992] is derived as

$$\frac{\lambda}{\alpha} = c$$

and we will retrieve isothermal boundary conditions ($T_{ext} = T_0$) when $c = +\infty$.

Contrarily to conventional work, we will treat the exchange coefficient c as an unknown parameter, which will be determined by an optimization condition of total pseudo potential, as well to additionally consistent the bandwidth with respect to different slab width H (and a given loading velocity V_0). We will consider as reference solution of the profiles obtained from $H_r = 1.25 \text{ mm}$ and $V_0 = 0.1 \text{ m/s}$, with isothermal boundary conditions ($c = +\infty$). These profiles are characterized by $h = h_r$ and $T_{max} = T_{max,r}$. Yet it seems that it does not work due to the problem having three optimized conditions for 4

parameters: bandwidth h , maximum temperature T_{max} , external temperature T_{ext} and exchange coefficient c . As the aforementioned objectives through the introduction of c , one aspect is to ameliorate our modelling with introducing heat exchange, and other aspect is to satisfy the consistency of bandwidth with respect to different slab width. Consequently we then look at solutions obtained for $h_r \leq H \leq H_r$, with mixed boundary conditions, seeking for a value of exchange coefficient c yielding a matching temperature profile for $-H \leq y \leq H$, as illustrated in FIG.2.17. This constraint corresponds to the following condition:

$$T_{ext} = T_{max,r}(V_0) - (T_{max,r}(V_0) - T_0) \frac{\log(\cosh(H/h_r))}{\log(\cosh(H_r/h_r))}$$

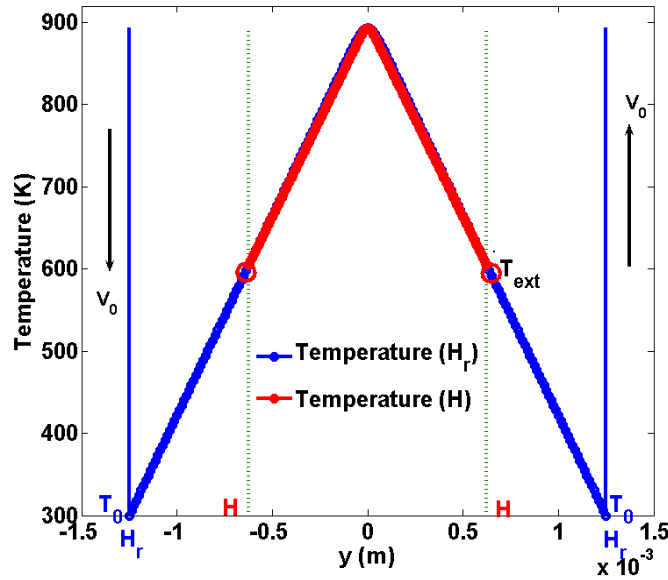


Figure 2.17: Profiles of temperature on different slab widths

Under the above constraint, shear band width and central temperature remain remarkably constant over a wide range of domain width, as shown in FIG.2.18. Unavoidably, there are some small fluctuations about bandwidths when H comes closer to the reference bandwidths, yet less than 0.05.

FIG.2.19 presents the corresponding evolution of exchange coefficient c with slab width H . It seems that a linear relation exists between $\log(H_r - H)$ and $\log(c)$. Consequently, we would like to find a fitted formula to summarize the relationships among slab width, loading and exchange coefficient. Here referring to the profiles of exchange coefficient with H , a polynomial method is applied to find its curve fitting, which can be illustrated as follows for the reference slab width $H_r = 1.25 \text{ mm}$:

$$\log(c) = a(V_0)\log(H_r - H) + b(V_0) \quad (2.24)$$

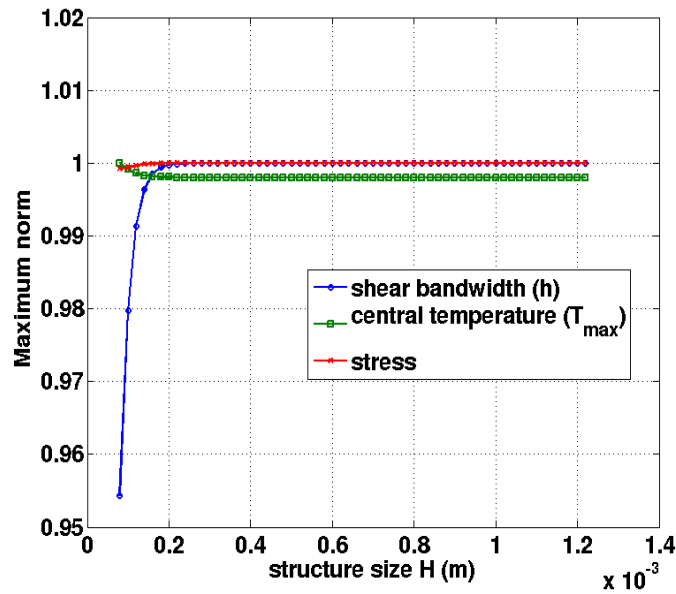


Figure 2.18: Shear band width, central temperature and central stress for different slab widths ($V_0 = 0.1 m/s$)

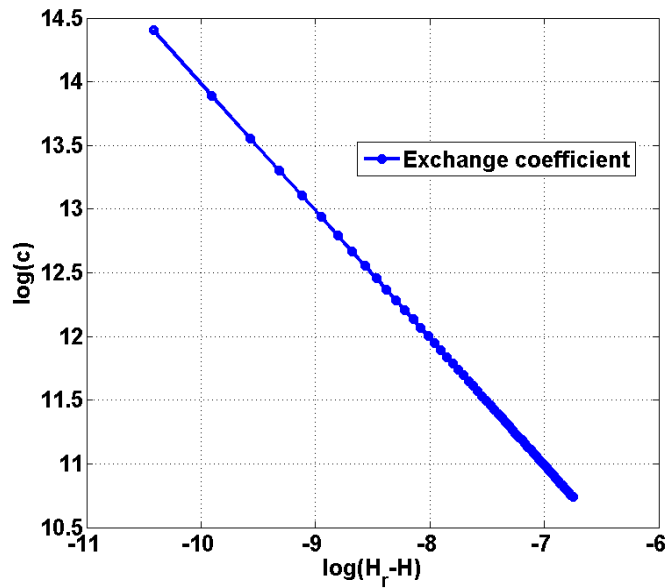


Figure 2.19: Exchange coefficient for different slab widths

Normally, $a(V_0)$ and $b(V_0)$ are the fitted parameters associated with the loading velocity. Yet numerical implementations obtained that they are basically constant with the imposed velocity V_0 , and:

$$a(V_0) = -1; \quad b(V_0) = 3.9889$$

Note that the slab width should be limited to $h_r(V_0) \leq H \leq H_r$.

As a consequence, a variational model considering heat exchange in ASB formation is built through a constraint optimization method, and exchange coefficient c is observed as an internal optimized parameter. Here the corresponding c can be directly calculated from the formula (2.24) if slab width is known, and we will use it in the incremental variational modelling.

Nusselt number is a dimensionless number of heat transfer parameter, which can be calculated as follows:

$$Nu = \frac{cH}{\lambda} = \frac{H}{\alpha}$$

It is a ratio of convection to conduction on the boundary, and a larger Nu reflects more active convection. FIG.2.20 is the evolution of Nusselt number changing with slab width H . When H augments, Nusselt number is increasing, especially for the case that H is near to H_r where exchange coefficient is infinite.

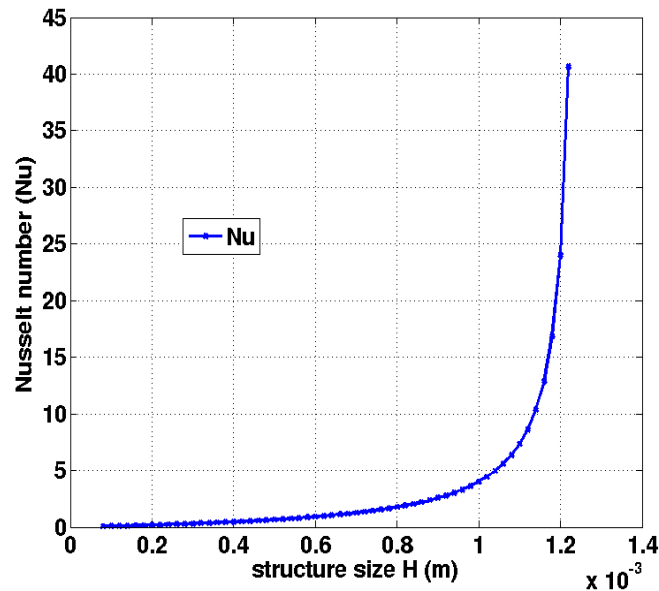


Figure 2.20: Nusselt number when $H_r = 1.25\text{mm}$

2.5 Conclusions

For general thermo-viscoplastic materials, an energy-based variational modelling was proposed and successfully applied to the simulation of adiabatic shear band in a slab subject to a constant simple shear. In accordance with the analytical lines: mechanical problem, thermo-mechanical problem in non-Newtonian fluid and thermo-viscoplastic problem with thermal softening, we derived and validated the variational modellings of Couette flow, thermal layer, thermal Couette flow and adiabatic shear band. In common,

we analysed the thermo-mechanical field profiles by means of an optimization with one or two types of parameters, largely simplifying the calculations. Moreover on one part, the shear band width and central temperature are obtained and in good agreement with [Leroy and Molinari, 1992]. These characteristics of ASB also lay a good foundation for estimating an approximate mesh size if we apply Finite Element Method to simulate ASB problem; on the other part, applying this modelling, we also discussed the influences of material parameters and the loading condition on shear band width and temperature. The evolution of profiles of velocity and temperature in shear slab are presented by means of FEM, as well as the development process of shear band width: it decreases with time increased, and step by step converges to the analytical solution obtained by variational modelling. Thus it validates that our modelling works for various material constitutive models.

As a final part, thermal boundary condition is considered to have a consistent band-width with respect to slab width. We added two unknown parameters: exchange coefficient c and temperature T_{ext} in the optimized pseudo-potential, and then a numerical formula for c is fitted by means of variational modelling, yet it depends on the reference structure.

The simple 1D example proves the feasibility and efficiency of the variational modelling in steady state. It gives us a good preparation for analysing the evolution of band-width, central temperature in the layer and stress by a Rayleigh-Ritz method. Obviously if we consider the update form of this variational formulation, this work can be extended to the transient state, as shown in next chapter. In addition, how to apply this modelling in multiple dimensions will give us a large challenge for future work.

Chapter 3

Variational modelling in transient state

Abstract :

An incremental variational modelling of adiabatic shear band structure in transient state is developed for general constitutive models, including elasticity, work hardening, heat conduction and thermal boundary condition. The evolutions of bandwidth, maximum temperature and stress are analysed under monotonic and cyclic shear loading, and are in good agreement with the results obtained by Finite Element Method.

Résumé :

Une modélisation variationnelle incrémentale des bandes de cisaillement adiabatique en régime transitoire est développée pour les modèles généraux constitutives, incluant l'élasticité, l'écrouissage, la conduction thermique et la condition thermique aux frontières. Les évolutions de la largeur de bande, de la température centrale et de la contrainte sont analysées subissant la chargement monotone et cyclique, et en accord avec les résultats de la méthode des éléments finis.

Contents

3.1	Variational updates	58
3.1.1	Variational framework	58
3.1.2	Finite element method	61
3.2	Thermo-visco-plastic variational modelling	63
3.2.1	Variational modelling for exponential softening law	63
3.2.1.1	Variational formulation	63
3.2.1.2	Numerical validation	65
3.2.2	Influence of material parameters	70
3.2.2.1	Strain rate sensibility m	72
3.2.2.2	Thermal conductivity λ	72
3.2.2.3	Thermal softening coefficient β	74
3.2.2.4	Imposed velocity V_0	75
3.2.3	Extension to various constitutive model	75
3.2.4	Variational modelling with hardening	76
3.2.4.1	Variational formulation	78
3.2.4.2	Validation and parameter analysis	79
3.2.5	Variational modelling with thermal boundary condition	81
3.2.5.1	Variational modelling	82
3.2.5.2	Validation and parameter analysis	83
3.3	Thermo-elasto-visco-plastic variational modelling	85
3.3.1	Variational modelling	86
3.3.2	Numerical validation	89
3.3.3	Average stress analysis	94
3.4	Conclusions	96

Adiabatic shear band is the result of a thermo-mechanical instability leading to large deformation and high temperature in a narrow band, normally a few tens of micrometers [Wright, 2002]. In general, the development of ASB proceeds in three steps:

- stage I: the deformation in shear is homogeneous, and strain hardening of material overcomes the thermal softening effect.
- stage II: after the maximum of stress, a diffuse instability develops due to the prominence of the thermal softening, the deformation begins to be slightly heterogeneous.
- stage III: strong instability develops and the deformation localizes in a narrow band. Fracture may occur in this stage. Under certain circumstances, when the hardening is saturated and the heat production caused by plastic is removed by heat conduction, a steady state may develop in the final stage.

In the present chapter, we will illustrate these three stages of ASB formation by means of an energy-based variational modelling.

For the same thermo-mechanical problem described as CHAP.2: a slab subject to a simple shearing velocity, we will extend the variational framework from steady state to transient state, thus describing the evolution of thermo-mechanical profiles by an energy-based variational method. The outline of this work is described as follows:

From simple to complex, we first consider the variational modelling in thermo-viscoplastic material, yet neglecting elastic and hardening property, which is equivalent to the formation of ASB directly entering into second stage. Since no analytical solution exists in transient domain, finite element method based on variational framework is introduced and applied as a comparative tool. The evolutions of bandwidth, maximum temperature and equivalent shear stress are analysed and validated by FEM. Furthermore, an expected result is obtained that the bandwidth decreases with the time and converges to a constant value in steady state. In similar manner, we also proposed the variational modellings for power law and Johnson-Cook law with hardening factor, which achieves a good agreement with FEM simulation.

Based on the analysis of exchange coefficient in CHAP.2, a variational modelling including thermal boundary condition is proposed afterwards for thermo-viscoplastic material to have a consistent bandwidth with respect to different slab widths. The temperature on the boundary increases with the time, evolving towards a constant value in steady state, which also embodies that thermal conduction in the process of adiabatic shear band structure becomes more and more important.

Considering the accuracy and development of our variational modelling, introducing elastic effect calls for no delay in the energy-based variational method. Taking the widely used Johnson-Cook model as a constitutive relation, we separate the imposed displacement as two parts: elastic displacement and plastic displacement, and propose a variational formulation of adiabatic shear banding structure including elasticity, hardening and conduction. Some simple examples are presented in this part to validate our modelling, and a good correspondence is obtained compared with FEM.

3.1 Variational updates

The variational framework proposed by Yang et al.[Yang et al., 2006] also includes a time-discretized incremental variational problem, and it can be applied to the 1D shear band problem, yielding an incremental optimization problem.

3.1.1 Variational framework

In particular, considering a time increment $[t_n, t_{n+1}]$, and assuming that $[\mathbf{F}_n, T_n, \mathbf{F}_n^p]$ is known, we proceed to obtain the variational update at time t_{n+1} . T_n presents absolute temperature at time t_n , and \mathbf{F} is the gradient of deformation:

$$\mathbf{F} = \frac{\partial \mathbf{x}}{\partial \mathbf{X}}$$

where \mathbf{x} is the current configuration vector, and \mathbf{X} is the original Lagrangian vector. We consider the conventional multiplicative decomposition of deformation gradient:

$$\mathbf{F} = \mathbf{F}^e \mathbf{F}^p$$

where \mathbf{F}^e and \mathbf{F}^p are respectively elastic and plastic parts. The spatial velocity gradient can be written as

$$\mathbf{L} = \dot{\mathbf{F}} \cdot \mathbf{F}^{-1} = \dot{\mathbf{F}}^e (\mathbf{F}^e)^{-1} + \mathbf{F}^e \dot{\mathbf{F}}^p (\mathbf{F}^p)^{-1} (\mathbf{F}^e)^{-1}$$

In another view, we can decompose \mathbf{L} into its symmetric and anti-symmetric parts:

$$\mathbf{L} = \frac{1}{2}(\mathbf{L} + \mathbf{L}^T) + \frac{1}{2}(\mathbf{L} - \mathbf{L}^T) = \mathbf{D} + \mathbf{W}$$

We suppose that the thermal-viscoplastic material obeys on J2 von Mises law, \mathbf{F}^p then satisfies the following rule:

$$\dot{\mathbf{F}}^p \mathbf{F}^{p-1} = \dot{\epsilon}^p \mathbf{M} \quad (3.1)$$

which

$$\dot{\epsilon}^p = \bar{\epsilon}^p \mathbf{M}$$

where $\bar{\epsilon}^p$ is the cumulated plastic deformation, and \mathbf{M} is the direction of cumulated plastic strain tensor, satisfying the following conditions:

$$\begin{aligned} tr(\mathbf{M}) &= 0 \\ \mathbf{M} \cdot \mathbf{M} &= \frac{3}{2} \\ \mathbf{M}^T &= \mathbf{M} \end{aligned} \quad (3.2)$$

So the gradient of plastic deformation \mathbf{F}_{n+1}^p is written as:

$$\mathbf{F}_{n+1}^p = \exp[(\bar{\epsilon}_{n+1}^p - \bar{\epsilon}_n^p) \mathbf{M}] \mathbf{F}_n^p \quad (3.3)$$

Following the work in [Yang et al., 2006], the total pseudo-potential for the thermo-mechanical coupled problem is then:

$$\Phi_n = \int_{-H}^H \left[\mathcal{W}_n - \Delta t \chi \left(\frac{1}{T_{n+1}} \frac{\partial T_{n+1}}{\partial y} \right) \right] dy \quad (3.4)$$

where \mathcal{W}_n is the optimized potential with respect to $\bar{\epsilon}_{n+1}^p$ and \mathbf{M} :

$$\begin{aligned} \mathcal{W}_n(\mathbf{F}_{n+1}, T_{n+1}; \mathbf{F}_n, T_n, \mathbf{F}_n^p, \bar{\epsilon}_n^p) &= \inf_{\bar{\epsilon}_{n+1}^p, \mathbf{M}} [W(\mathbf{F}_{n+1}, T_{n+1}, \mathbf{F}_{n+1}^p, \bar{\epsilon}_{n+1}^p) \\ &\quad - W(\mathbf{F}_n, T_n, \mathbf{F}_n^p, \bar{\epsilon}_n^p) + \rho_0 \eta_n (T_{n+1} - T_n) \\ &\quad + \int_{t_n}^{t_{n+1}} \Psi^* \left(\frac{T_{n+1}}{T_n} \frac{\Delta \bar{\epsilon}^p}{\Delta t}; \bar{\epsilon}^p, T(t) \right) dt] \end{aligned} \quad (3.5)$$

It should be emphasized that the equilibrium temperature Θ at $t = t_{n+1}$ is replaced by T_n in the incremental variational formulation. Consistency of this scheme can be validated when $\Delta t \rightarrow 0$. ρ_0 is mass density per unit undeformed volume, and $W(\mathbf{F}_{n+1}, T_{n+1}, \mathbf{F}_{n+1}^p, \bar{\epsilon}_{n+1}^p)$ is the free energy, written as:

$$\begin{aligned} W(\mathbf{F}_{n+1}, T_{n+1}, \mathbf{F}_{n+1}^p, \bar{\epsilon}_{n+1}^p) &= W^e(\mathbf{F}_{n+1}, \mathbf{F}_{n+1}^p, T_{n+1}) + W^{th}(T_{n+1}) \\ &\quad + W^p(\mathbf{F}_{n+1}, \mathbf{F}_{n+1}^p, T_{n+1}, \bar{\epsilon}_{n+1}^p) \end{aligned}$$

where W^e , W^p and W^{th} are the elastic energy, the stored plastic energy and the heat storage capacity of the material [Stainier and Ortiz, 2010]. Normally we choose elastic energy as:

$$W^e(\mathbf{C}^e) = \mu \|\text{dev}[\boldsymbol{\epsilon}^e]\|^2 + f(J) \quad (3.6)$$

where $\boldsymbol{\epsilon}^e = \frac{1}{2} \log(\mathbf{C}^e)$. \mathbf{C}^e is the elastic right Cauchy-Green tensor, equal to $\mathbf{F}^{eT} \mathbf{F}^e$, and $J = \det[\mathbf{F}] = \sqrt{\det[\mathbf{C}^e]}$. The heat storage capacity is as follows:

$$W^{th}(T_{n+1}) = \rho_0 C_0 T_{n+1} \left(1 - \log\left(\frac{T_{n+1}}{T_0}\right) \right) \quad (3.7)$$

where C_0 is heat capacity, T_0 is the reference temperature. The form of W^p depends on the flow rule, and an uniform formulation for the stored plastic energy [Stainier and Ortiz, 2010] is used in our variational modelling of FEM:

$$W^p(\bar{\epsilon}^p, T) = \frac{n}{n+1} \frac{\sigma_0(T)}{b} (1 + b \bar{\epsilon}^p)^{\frac{1}{n}+1} + \hat{\sigma}_0(T) \left[\bar{\epsilon}^p + \frac{1}{d} \exp(-d \bar{\epsilon}^p) \right] \quad (3.8)$$

$\sigma_0(T)$ and $\hat{\sigma}_0(T)$ are the linear softening functions with respect to temperature. The parameters in the formulas (n , b , d and linear softening factors) can be obtained by simple tensile/compressible experimental tests. In addition, the notations Ψ^* and χ are the same as previously described in CHAP.2: the dissipation pseudo-potential and the Fourier pseudo-potential. The entropy η_n is defined by :

$$\rho_0 \eta_n = - \frac{\partial W}{\partial T_n}(\mathbf{F}_n, T_n, \mathbf{F}_n^p, \bar{\epsilon}_n^p)$$

and $\Delta\bar{\epsilon}^p = \bar{\epsilon}_{n+1}^p - \bar{\epsilon}_n^p$.

According to the optimization condition about $\bar{\epsilon}^p$, we can update the internal variable $\bar{\epsilon}^p$ through the convex dissipation pseudo-potential:

$$\frac{\partial W(\mathbf{F}_{n+1}, T_{n+1}, \mathbf{F}_{n+1}^p, \bar{\epsilon}_{n+1}^p)}{\partial \bar{\epsilon}_{n+1}^p} + \frac{\partial \tilde{\Psi}^*}{\partial \dot{\bar{\epsilon}}_{n+1}^p} + \Delta t \frac{\partial \tilde{\Psi}^*}{\partial \bar{\epsilon}_{n+1}^p} = 0 \quad (3.9)$$

where $\tilde{\Psi}^* = \int_{t_n}^{t_{n+1}} \Psi^* \left(\frac{T_{n+1}}{T_n} \frac{\Delta \bar{\epsilon}^p}{\Delta t}; \bar{\epsilon}^p, T(t) \right) dt$.

In the incremental variational potential, \mathcal{W} appears as a thermo-elastic pseudo-potential. The first Piola-Kirchhoff stress can be written as:

$$\frac{\partial \mathcal{W}'_n}{\partial \mathbf{F}_{n+1}} = \mathbf{P}_{n+1}$$

and the heat equation in adiabatic form is given by taking the variation about T :

$$\frac{\partial \mathcal{W}'_n}{\partial T_{n+1}} = -\rho_0 \Delta \eta + \frac{\Delta t}{T_{n+1}} D_{int} = 0$$

where D_{int} is the internal dissipation.

In continuum mechanics, there are several types of strain measures to present material movement, such as right Cauchy-Green strain \mathbf{C} , defined as $\mathbf{C} = \mathbf{F}^T \mathbf{F}$, and \mathbf{D} is strain rate tensor; Green-Lagrange strain tensor \mathbf{E} , defined as $\mathbf{E} = \frac{1}{2}(\mathbf{C} - \mathbf{I})$; logarithmic strain \mathbf{E}^N , defined as $\mathbf{E} = \frac{1}{2} \log(\mathbf{C})$. If we choose these different strains to describe the terms in energy \mathcal{W}'_n , we can also obtain the relative stress forms: Cauchy stress $\boldsymbol{\sigma}$, second Piola-Kirchhoff stress \mathbf{S} by \mathcal{W}'_n according to:

$$\int_V \boldsymbol{\sigma} : \mathbf{D} dV = \int_V \mathbf{S} : \dot{\mathbf{E}} dV = \int_{V_0} \mathbf{P} : \dot{\mathbf{F}} dV_0 \quad (3.10)$$

In general, the deformation gradient \mathbf{F} is written as:

$$\mathbf{F}_{n+1} = \mathbf{I} + \frac{\partial \mathbf{u}_{n+1}}{\partial \mathbf{x}}$$

For the shear band problem on 1D, \mathbf{F} can be reduced to:

$$\mathbf{F}_{n+1} = \begin{bmatrix} 1 & \frac{\partial u_{n+1}}{\partial y} & 0 \\ 0 & 1 & 0 \\ 0 & 0 & 1 \end{bmatrix}$$

As a consequence, the shear band problem in the variational framework is written as:

$$\inf_{u_{n+1}} \max_{T_{n+1}} \Phi_n(u_{n+1}, T_{n+1}; u_n, T_n, \mathbf{F}_n^p, \bar{\epsilon}_n^p) \quad (3.11)$$

When the time step tends towards 0, Euler-Lagrange equations of (3.11) are consistent with continuous mechanical and thermal equilibrium equations.

3.1.2 Finite element method

Coupled thermo-mechanical problem is always an issue of great contention because of its widespread occurrence and application in mechanical engineering. For the coupling between the conservation of linear momentum and the first law of thermodynamics, seeking for a crafty coupling algorithm has a large influence on the efficiency and accuracy of numerical simulation. In general, there are two types existing in this domain:

- strongly coupled problem: recalled as monolithic scheme. all the profiles, i.e displacement and temperature are included in a nonlinear structure. Consequently the same time-stepping is used in mechanical and thermal evolution, and the coupled terms involve the system non-symmetry. The strong point of monolithic scheme is its stability, i.e. the solution is unconditionally stable in the fully implicit algorithm. Yet because of large composition including displacement and temperature, once we use some numerical discretized approaches such as FEM, meshfree method, the calculation of system is enormous to process a good accuracy. Moreover, the different time step for the displacement and temperature may be better for numerical modelling, especially for the localization problem.
- weakly coupled problem: recalled as staggered scheme. The resolution of mechanical problem and thermal problem proceed interactively. When solving the mechanical equation, we regard it as isothermal, and inversely if solving thermal equation, mechanical part is constant. Necessarily for the weakly coupled problem, the stability of its time discretization should be limited to some conditions. A number of papers proposed some stability techniques to reduce the expense of unconditional stability [Armero and Simo, 1992, Armero and Simo, 1993, Simo, 1991]. The drawbacks of monolithic scheme are the strong points of staggered scheme. For the different physics, we can arrange different time step and different node density according to the need of computational accuracy.

Practically, some engineers neglect thermal conduction effect in heat equation for dynamic high strain rate loading, then treat the problem as adiabatic, so the temperature can be calculated as an internal parameter in the calculation. Yet for our shear localization problem, thermal conduction plays an important role in the final term of the formation of adiabatic shear band, which influences the steady shear band width and central temperature. Unfortunately this nonlinear term makes the numerical implication more complicated. Here our FEM modelling is built on the strongly coupled problem.

Non-symmetric system causes a lot of inconvenience in the numerical method, yet except for our FEM based on energy-based variational modelling. Thanks to the symmetry of the bilinear form of variational pseudo-potential, the tangent matrix of the FEM is also symmetrical, which is different from the traditional thermo-mechanical problem, and this character brings some algorithmic advantages. In the FEM model, elastic potential, stored plastic potential and stored thermal potential are chosen as (3.6), (3.8) and (3.7).

For the dissipation pseudo-potential Ψ^* , Stainier [Stainier and Ortiz, 2010] proposed a general form of time discretization which is composed of rate-independent part and

rate-dependent part:

$$\Psi^*(\dot{\bar{\epsilon}}^p, \bar{\epsilon}^p, T) = \sigma_y(\bar{\epsilon}^p, T)\dot{\bar{\epsilon}}^p + \frac{m}{m+1}\sigma_v(T)\dot{\epsilon}_0\left(\frac{\dot{\bar{\epsilon}}^p}{\dot{\epsilon}_0}\right)^{\frac{1}{m}+1} \quad (3.12)$$

where the critical stress σ_y is

$$\sigma_y(\bar{\epsilon}^p, T) = \sigma_1(T)(1 + b'\bar{\epsilon}^p)^{\frac{1}{n}} + \hat{\sigma}_1(T)[1 - \exp(-d'\bar{\epsilon}^p)]$$

The terms $\sigma_1(T)$, $\hat{\sigma}_1(T)$ and $\sigma_v(T)$ have a similar linear thermal softening effect, described as :

$$\sigma_1(T) = \sigma_1(T_0)[1 - \omega_1(T - T_0)]$$

Using the experimental results, we can proceed the identifications of constitutive parameters in these formulas to have a good correspondence of strain-stress curves. The constitutive relations of Aluminium, Titanium and Tantalum are validated by this variational modelling.

The time discretization of dissipation pseudo-potential is very important in FEM, inappropriate discrete terms will cause that the incremental Euler-Lagrange equation is not consistent with the heat equation. For instance, if we simply take a generalized mid-point rule for a fully implicit approach, the consistency can not be obtained. Thereby [Stainier, 2011a] proposed a consistent approximation for its time-discretization as follows:

$$\begin{aligned} \frac{1}{\Delta t} \int_{t_n}^{t_{n+1}} \Psi^* \left(\frac{T_{n+1}}{T_n} \frac{\Delta \bar{\epsilon}^p}{\Delta t}; \bar{\epsilon}^p, T(t) \right) dt &\approx \frac{T_n}{T_{n+1}} \Psi^* \left(\frac{T_{n+1}}{T_n} \frac{\Delta \bar{\epsilon}^p}{\Delta t}; \bar{\epsilon}_{n+\theta}^p, T_n \right) \\ &+ \frac{\Delta T}{T_{n+1}} \Psi^* \left(\frac{T_{n+1}}{T_n} \frac{\Delta \bar{\epsilon}^p}{\Delta t}; \bar{\epsilon}_{n+\theta}^p, T_{n+\alpha} \right) \end{aligned}$$

The parameters have $\alpha \in [0, 1]$ and $\theta \in [0, 1]$, normally we choose it equal to 0.5, a mid-point rule for the time integration.

Based on the incremental variational potential (3.4), it is easy to derive the incremental equations by standard finite element method. The displacement and temperature are relatively described as a linear form of shape functions. Here for the simulation of shear localization, we should firstly give an approximation of the localization length in order to have a good accuracy in localized zone. Yet it causes a large expense in computation, even if for 1D shear band problem.

For illustrating the evolution of shear band width and comparing it with our variational modelling by Rayleigh-Ritz method, we choose two parameters to measure the shear localization: the kinematic width h_V obtained from the velocity distribution and the thermal width h_T obtained from the temperature distribution at every time step. Referring to the analytical formulation, they are approximated as follows:

$$\begin{aligned} h_{V_{n+1}} &\quad \text{such that} \quad V_{n+1}(h_{V_{n+1}}) \simeq V_0 \tanh(1) \\ h_{T_{n+1}} &\quad \text{such that} \quad T(h_T) \simeq T_{max} - (T_{max} - T_0) \frac{\log(\cosh(1))}{\frac{H}{h_T} - \log 2} \end{aligned}$$

We should say that two formulas are merely an approximation according to the profiles of velocity and temperature, since no heat affected zone is considered in the thermal width.

As the problem in CHAP.2 described, we consider a shear slab subject to a simple shearing velocity for general thermo-viscoplastic materials, and a constant velocity V_0 is imposed on $y = \pm H$. Yet body force is neglected in the modelling. We will present our modelling in two parts from simple to complex: the modelling without elasticity and the modelling considering it.

3.2 Thermo-visco-plastic variational modelling

According to the definition of entropy, we can write η as:

$$\rho_0 \eta(T_{n+1}) = \rho_0 C_0 \log\left(\frac{T_{n+1}}{T_0}\right)$$

We recall the total incremental pseudo-potential described as follows:

$$\begin{aligned} \Phi_n(\dot{\bar{\epsilon}}_{n+1}^p, \bar{\epsilon}_{n+1}^p, T_{n+1}) &= \int_{-H}^H [W^p(\bar{\epsilon}_{n+1}^p, T_{n+1}) - W^p(\bar{\epsilon}_n^p, T_n) + W^{th}(T_{n+1}) - W^{th}(T_n) \\ &\quad + \rho_0 \eta(T_n)(T_{n+1} - T_n) + \Delta t \Psi^*\left(\frac{T_{n+1}}{T_n} \dot{\bar{\epsilon}}_{n+1}^p, \bar{\epsilon}_n^p, T_n\right) \\ &\quad - \Delta t \frac{1}{2} \lambda T_n \left(\frac{\partial T_{n+1}}{\partial y} \frac{1}{T_{n+1}}\right)^2] dy \end{aligned} \quad (3.13)$$

In addition, we write the equivalent plastic strain as follows:

$$\dot{\bar{\epsilon}}_{n+1}^p = \frac{1}{\sqrt{3}} \frac{\partial V_{n+1}}{\partial y}$$

Using a substitution of $\dot{\bar{\epsilon}}_{n+1}^p$ in pseudo-potential (3.13), the variational update for the adiabatic shear band is:

$$\inf_{V_{n+1}} \sup_{T_{n+1}} \Phi_n(V_{n+1}, T_{n+1}, V_n, T_n) \quad (3.14)$$

For simplicity, we might as well firstly suppose that the temperature is isothermal on the boundary:

$$T = T_0 \quad \text{on } y = \pm H$$

3.2.1 Variational modelling for exponential softening law

3.2.1.1 Variational formulation

We derived the incremental dissipation potential for an exponential softening law as follows:

$$\Psi^*(\dot{\bar{\epsilon}}_{n+1}^p, \bar{\epsilon}_n^p, T_n) = \frac{1}{m+1} \frac{\tau}{\dot{\gamma}_0^m} \exp\left(-\beta\left(\frac{T_n}{T_0} - 1\right)\right) \left(\frac{\partial V_{n+1}}{\partial y}\right)^{m+1}$$

where m and β are respectively the strain rate sensitivity exponent and the thermal softening coefficient. Obviously it is convex with respect to velocity. Neglecting the heat affected zone, and supposing that the distributions of velocity and temperature satisfy the canonical expressions at each time step, we choose two paths to describe their profiles at $t = t_{n+1}$:

- kinematic width $h_{V_{n+1}}$ and dynamic width $h_{T_{n+1}}$ as unknown parameters:

$$V(y) = V_0 \frac{\tanh(y/h_{V_{n+1}})}{\tanh(H/h_{V_{n+1}})}, \quad T(y) = T_0 - \frac{2m}{\beta} T_0 \ln \frac{\cosh(y/h_{T_{n+1}})}{\cosh(H/h_{T_{n+1}})} \quad (3.15)$$

In addition, at every time step, there is an additional condition for two parameters:

$$h_{V_{n+1}} = h_{T_{n+1}}$$

Because its canonical expressions originate from [Leroy and Molinari, 1992], and material parameters are included in the formulas, this method is just used in exponential softening law. So the problem (3.14) is changed to seek the stationary point of total potential:

$$\underset{h_{V_{n+1}}, h_{T_{n+1}}}{Stat} \Phi_n(h_{V_{n+1}}, h_{T_{n+1}}) \quad \text{with} \quad h_{V_{n+1}} = h_{T_{n+1}} \quad (3.16)$$

As CHAP.2 described: $\frac{\partial \Phi}{\partial h_{V_{n+1}}} = 0$, the optimizations of Φ with respect to two parameters are consequently transformed to a nonlinear equation:

$$\left. \frac{\partial \Phi_n}{\partial h_{T_{n+1}}} \right|_{h_{V_{n+1}} = h_{T_{n+1}}} = 0$$

Here, we list this method to give the readers a different idea in the transformation of variational modelling from steady state to transient state. Yet this model is restricted to the exponential softening law because of the formulation of temperature profile, merely working without hardening coefficient. The later examples show that the modelling in constitutive relations with hardening has different bandwidth h_V and h_T even if when it arrives at a relatively steady state. So we mostly choose the next method for the adiabatic shear banding simulations. But some results are also given in the numerical validation to show its feasibility for exponential law.

- In order to extend our modelling to different constitutive laws, we adopt a similar approach as in CHAP.2 through the introduction of another parameter T_{max} :

$$V_{n+1}(y) = V_0 \frac{\tanh(y/h_{V_{n+1}})}{\tanh(H/h_{V_{n+1}})}, \quad (3.17a)$$

$$T_{n+1}(y) = T_{max_{n+1}} - (T_{max_{n+1}} - T_0) \frac{\ln(\cosh(y/h_{T_{n+1}}))}{\ln(\cosh(H/h_{T_{n+1}}))} \quad (3.17b)$$

Here we do not impose the consistency of kinematic width and thermal width at each time step which is contrast to the aforegoing modelling. The incremental variational modelling is written as:

$$\underset{h_{V_{n+1}}, h_{T_{n+1}}, T_{max_{n+1}}}{Stat} \Phi_n(h_{V_{n+1}}, h_{T_{n+1}}, T_{max_{n+1}}) \quad (3.18)$$

Physically there is no shear band happening in the early stage, so we give a constraint condition for this modelling according to the character of function $\tanh(x)$:

$$\text{if } \bar{h}_V > 2.5 \quad \bar{h}_v = 2.5 \text{ and } \bar{h}_V = \bar{h}_T \quad (3.19)$$

Where $\bar{h} = \frac{h}{H}$. Consequently nonlinear equations are built by the stationary conditions of total pseudo-potential. Compared with the first method, it is more complicated, yet more general in the terms of constitutive relations owing to the independence of temperature formula on m and β .

It is important to note that: in contrast to previous approaches, the shear band width figures among the unknowns, and will be determined by numerical optimization. It is an important feature, since this width at every time step is controlled by the combined effect of internal dissipation and conduction, and we will use an example to illustrate that it can evolve as the shear band evolves towards its stationary structure.

In general, there is no shear localization for the profile of velocity at initial time if we choose small time step. Consequently initial condition is described as follows:

$$h_0 = H$$

3.2.1.2 Numerical validation

Although we work on the simplified problem in 1D thermal viscoplastic material, the complicated constitutive relations and the coupled thermo-mechanical terms make the theoretical analysis of adiabatic shear band out of the way. Therefore FEM is applied to validate our energy-based variational modelling.

FIG.3.1 shows the results of the profiles of velocity and temperature in the layer ($H = 1.25\text{mm}$, $V_0 = 0.01108\text{m/s}$, $T_0 = 300\text{K}$). As the time increases, the profiles of velocity change from a linear form to a nonlinear form, and step by step concentrate on the central zone, arriving at a steady state when the time reaches 0.1 s . The stationary shear band width is 0.247 mm , and $T_{max} = 395\text{K}$. Two shear band widths are chosen to measure the shear localization: the kinematic width h_V and the thermal width h_T . It should be noted that two formulas are merely an approximation of kinematic and thermal widths and do not represent a physical bandwidth, since no heat affected zone is considered in the thermal width. Yet the approximated formula of h_V can reflect well the length of shear localization in velocity.

We also analyse the evolution of the shear band when the imposed velocity is $V_0 = 1\text{m/s}$ (FIG.3.2). The average shearing strain rate at $V_0 = 1\text{m/s}$ is 800s^{-1} , and the one close

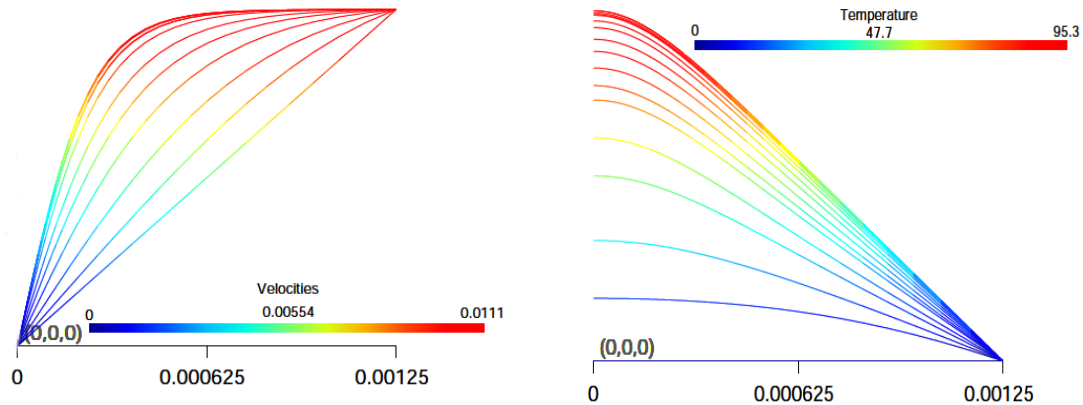


Figure 3.1: Evolution of the profiles of velocity and temperature by FEM ($V_0 = 0.01108m/s$)

to the loading edge is 0, but the higher shearing strain rate is on the center of the band, as $64845s^{-1}$ at steady state. Consequently lots of higher strain are just concentrated into a shear localization domain, which of length here is $h = 0.01542mm$ for the slab width $H = 1.25mm$. Moreover, compared with $V_0 = 0.01108m/s$, the time for reaching a steady state is shorter, the shear band width is smaller, and central temperature is higher ($T_{max} = 2053.4K$), which is in agreement with the analytical solution. In addition, we can observe a heat affected zone in the process of the shear band formation because of the locally lower strain and local annealing due to the temperature increase [Dinzart and Molinari, 1998]. Yet this transient effect is less obvious in the case of $V_0 = 0.01108m/s$.

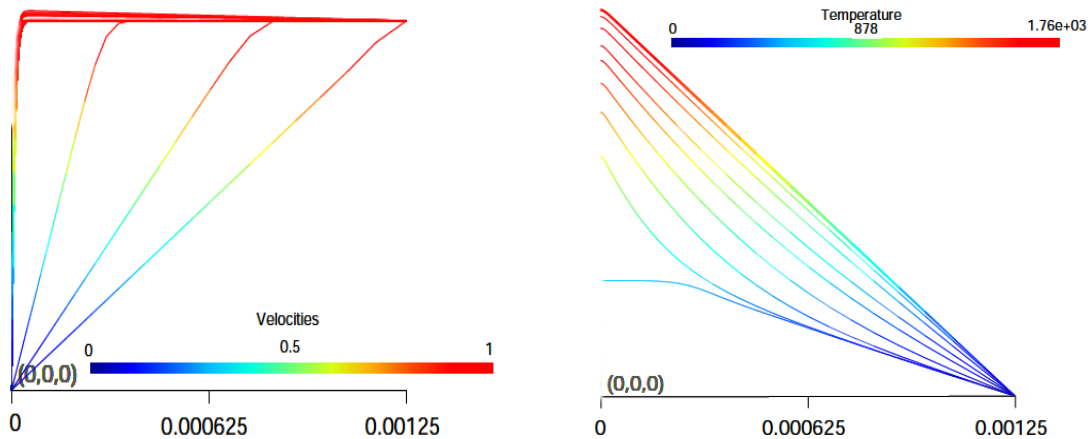


Figure 3.2: Evolution of the profiles of velocity and temperature by FEM ($V_0 = 1m/s$)

FIG.3.3 presents the convergence of kinematic width and thermal width when $H = 1.25mm$, $V_0 = 0.01108m/s$, $T_0 = 300K$. With the time increased, the two widths decrease gradually and tend towards the same stationary value, which are consistent with the analytical solutions. Although FEM shows a relative precise solution, the expense of com-

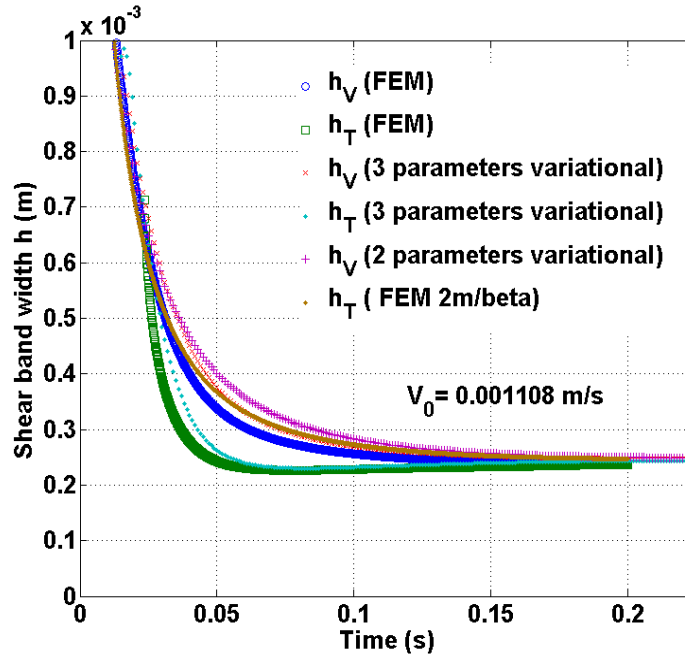


Figure 3.3: Convergence of the shear band width ($V_0 = 0.01108m/s$)

putational time in standard FEM is enormous. Taking the calculation of $V_0 = 1m/s$ as an example, firstly we should do an examination of the bandwidth, the large variation of displacement in sharply tiny width demands the refined mesh in localized zone, and the complicated constitutive relations lead to a slow speed of convergence in this thermo-mechanical problem.

It seems that the drawbacks in standard FEM have little influences on our variational modelling. We use a Rayleigh-Ritz method to avoid mesh dependence, and the profiles of velocity and temperature are controlled by kinematic width h_V and thermal width h_T , which are the stationary points of the total pseudo potential. Therefore the problem of ASB is changed to two or three nonlinear equations, which smartly decrease the calculation. Yet because we adopt the uniform form of temperature profiles, heat affect zone is neglected in the evolution of temperature. For the second method in our modelling, the problem is changed to a constrained optimization, we resource to some mathematical methods, such as internal penalization and external penalization to solve it.

FIG.3.4 shows the evolution of velocity profiles and temperature profiles compared with the analytical stationary solutions when $H = 1.25mm$, $V_0 = 0.01108m/s$, $T_0 = 300K$. Here the time step is chosen as $\Delta t = 10^{-3}s$. Results obtained by Rayleigh-Ritz approach are consistent with those obtained by FEM. With the time increased, the profiles of velocity and temperature are well convergent to the steady one.

In addition, returning to FIG.3.3, we can get the comparison of the convergence of shear band width, which in Rayleigh-Ritz method accords well with one by FEM. The evolutions of bandwidths are in agreement with the results by FEM. Furthermore, compu-

tation time is reduced compared to that of FEM. Therefore Rayleigh-Ritz method presents a higher efficiency without mesh.

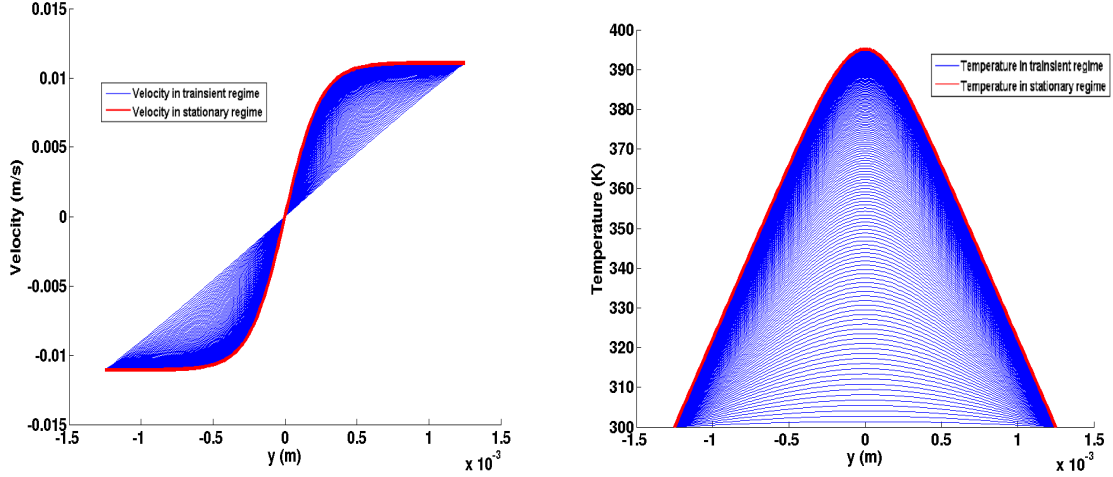


Figure 3.4: Evolution of the profiles of velocity and temperature by Rayleigh-Ritz method ($V_0 = 0.01108m/s$)

FIG.3.5 also presents the evolutions of bandwidths at $V_0 = 1m/s$. The formation of adiabatic shear band largely depends on the imposed velocity. The time for arriving its steady state is decreasing with V_0 increased: the ASB at $V_0 = 0.01108m/s$ arrives at steady state when $t = 0.07s$, yet the one at $V_0 = 1m/s$ is steady when $t = 0.02s$. The steady bandwidth decreases when the imposed velocity increases. Physically, when the dynamic velocity is higher, heat conduction effect is more clear, as it has not enough time to get out of the band, thus the zone is more localized, the bandwidth is shorter. The phenomenon of heat affected zone appears more clearly in the case of high velocity, so the approximated error is larger than the one at low velocity. Yet the kinematic width calculated by our modelling is in good agreement with FEM, and the modelling with three variables (h_V, h_T and T_{max}) represents the evolution of bandwidth better than the one with two variables (h_V and h_T) at high velocity.

We also give the evolution of maximum temperature in transient state (FIG.3.6). Before ASB forms, the increase of temperature is almost linear. With the time increased, the increasing speed of temperature is gradually slow, and finally arrives at a steady state. Substantially the form of evolution of central temperature is identical to $\tanh(x)$. This result shows that the central temperature calculated by FEM in the process of ASB formation is a little higher than one by Rayleigh-Ritz method. For thermal visco-plastic material, if there is no hardening factor such as exponential softening law, the material enters into material instability more quickly. FIG.3.7 and FIG.3.8 show the stress evolution respectively at $V_0 = 0.01108m/s$ and $V_0 = 1m/s$. The formation of shear band is regarded as the process of a sharp stress collapse in a short time. Normally because of high loading rate, the time in elasticity is so short that we almost can not see its influences in the figures of stress evolution by FEM. However, in the form of log coordinate,

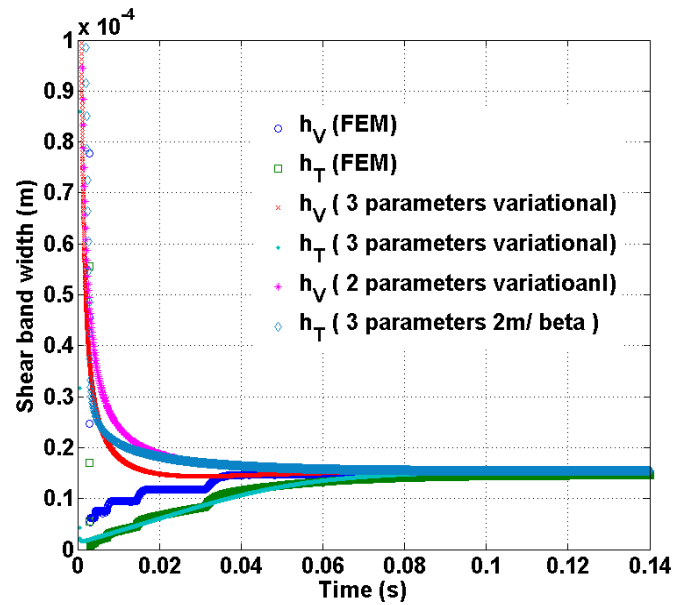


Figure 3.5: Convergence of the bandwidths by Rayleigh-Ritz method ($V_0 = 1m/s$)

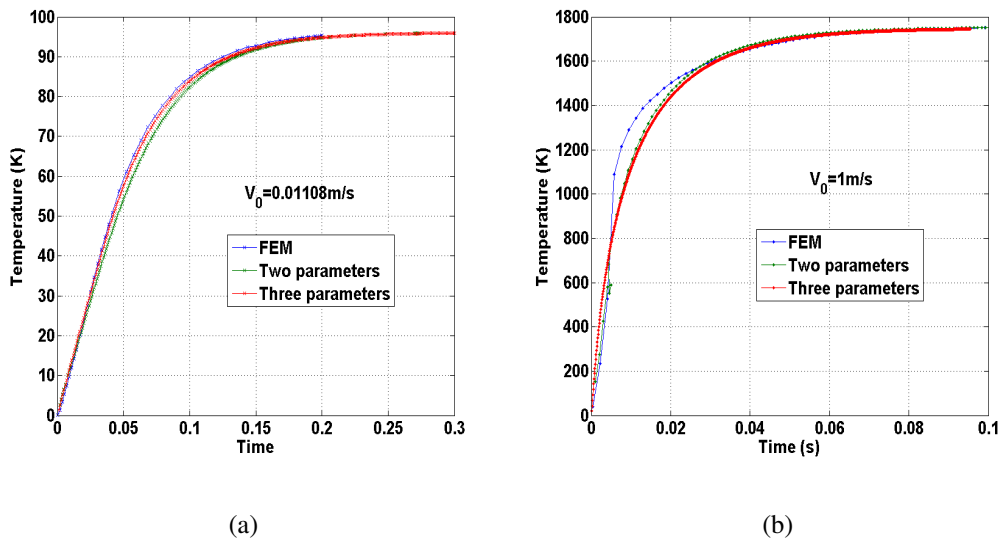


Figure 3.6: Evolution of the maximum temperature at $V_0 = 0.01108m/s$ (a) and $V_0 = 1m/s$ (b)

FEM simulation well reports that the material goes through elastic deformation, plasticity, small instability and dropping abruptly. In our variational modelling, the trend of curve, the maximum stress in evolution and the stress arriving at steady state are also in good agreement with FEM, especially the ones at low loading rate (FIG.3.7). In addition, at

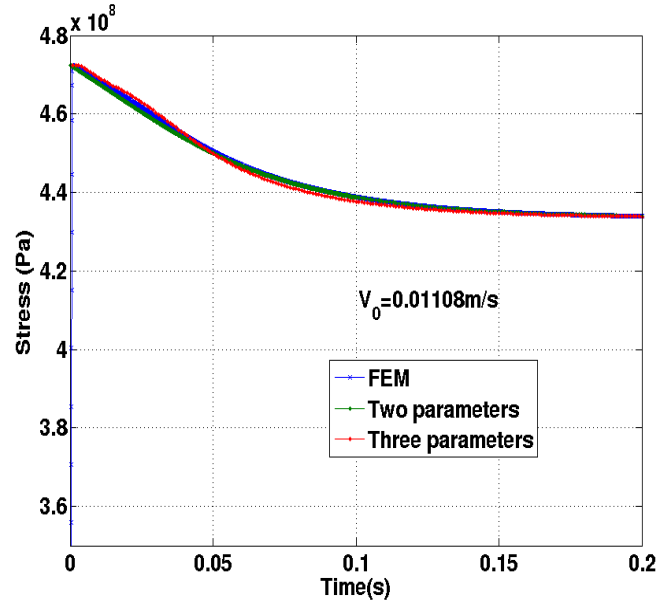


Figure 3.7: Evolution of stress in exponential softening law at $V_0 = 0.01108m/s$

high strain rate, the stress evolution calculated by two variables is less precise than one by three variables. Using two scalars to reflect the profile of temperature can compensate the effect brought by the negligence of heat affected zone. In view of the conservation of linear momentum in quasi-static case, the distribution of stress is theoretically homogeneous in the band, yet there is some approximation error in numerical simulation. Consequently we choose the central point as a compared point in stress curves (also for FEM).

We also studied the influence of time step on the stress evolution in Rayleigh-Ritz method (FIG.3.9). The choice of initial time step brings some inaccuracy because of the constrained optimization and the negligence of elasticity in the ASB formation. Similar to the other numerical methods, the choice of time step is very important to the numerical implementation of ASB, because their initiation and propagation always happen in a short time at high strain rate. If we choose it too large, the process of stress evolution is not precisely simulated. Contrastively if the time step is too small, the expense of calculation is unaffordable. In the beginning, we give a wrong approximation of stress state under the circumstance of neglecting elasticity and hardening. Pre-estimation of material state is necessary in our present variational modelling.

3.2.2 Influence of material parameters

As we all know, shear localization always occurs at high strain rates in the dissipative mechanisms. The constitutive behaviours are complicated and often not well characterized. For the sake of computational simplicity, some simplified constitutive relations are applied in the code. For example, some material parameters are neglected, or we consid-

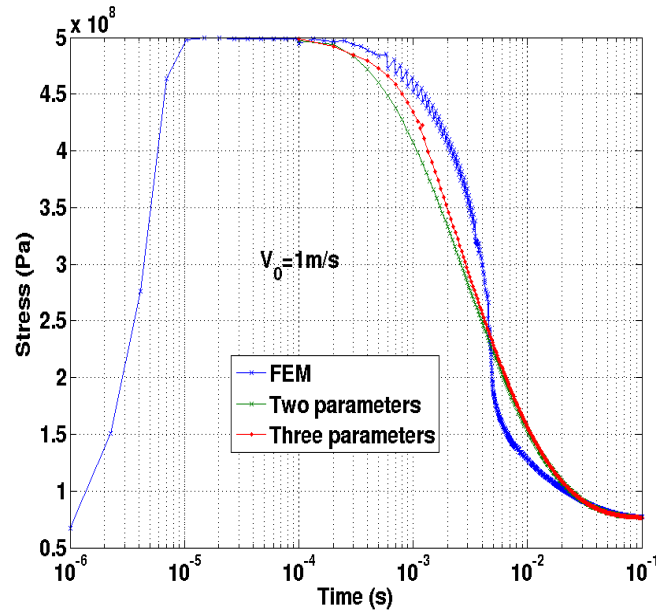


Figure 3.8: Evolution of stress in exponential softening law at $V_0 = 1\text{ m/s}$

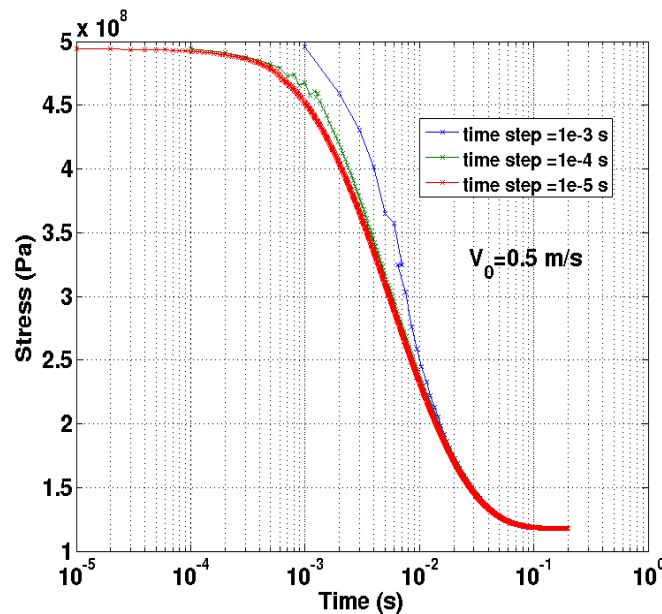


Figure 3.9: Influence of time step on stress evolution in exponential softening law at $V_0 = 0.5\text{ m/s}$

ered that the material has a constant flow stress, even some references eliminate thermal softening coefficient β . So studying the influence of material parameters in constitutive relations is interesting to build a simplified material model for the formation of ASB.

In this part, based on this optimized model, we will gradually analyse the effects of

material parameters, such as strain rate sensitivity m , heat conductivity λ and loading magnitudes, to the characters of ASB formation.

3.2.2.1 Strain rate sensibility m

Strain rate sensibility exponent is an important factor to reflect the resistance to prevent necking during a deformation of a plastic material. It depends on loading rate. Usually we use the following formula to test it:

$$m = \frac{\partial \ln \sigma}{\partial \ln \dot{\epsilon}}$$

Here fixing the other parameters in constitutive law, we amplify or reduce m to study its influence on the characters of ASB.

FIG.3.10 shows evolutions of stress with different m at $V_0 = 0.5m/s$, $H = 1.25mm$. We choose three values $m = 0.012$, $m = 0.05$ and $m = 0.1$ to compare the process of localization formation. The value of strain rate sensibility has a large influence on yield stress. If m is larger, the initial yield stress is smaller, and the smooth instability sustains longer, then the strong sharply stress collapse happens later, the variations of stress from initial state to final steady state is smaller. Therefore the localization phenomenon is less clear than that of smaller m . For instance, when $m = 0.1$, the character of ASB in steady state is $h = 0.30795mm$, yet $h = 0.039662mm$ when $m = 0.012$. Since we consider an ideal thermal visco-plastic material, no damage is considered. We found that the formation time of ASB and central temperature is little influenced by different m . The material almost arrives at steady state at the same time as seen in FIG.3.10.

3.2.2.2 Thermal conductivity λ

Thermal conduction is always a hot point in the research of ASB. Some researchers neglect this part in numerical simulation, and then calculate adiabatic temperature as an internal parameter. This largely simplifies the calculation and improves the convergence for thermal-mechanical coupling. As we repeatedly emphasized in CHAP.2, the engineers pointed out that thermal conduction played an important role in the final term of ASB, the bandwidth also depends on this part. Here we will use our variational modelling to validate this conclusion.

FIG.3.11 presents the evolutions of stress with different thermal conduction coefficient λ ($V_0 = 0.5m/s$, $H = 1.25mm$). Three values are chosen ($\lambda = 54 Wm^{-1}K^{-1}$, $25 Wm^{-1}K^{-1}$, $10 Wm^{-1}K^{-1}$) in the figure. In the initial state of stress evolution, the differences of three curves are so little that it is hard to distinguish which one. The stress evolutions in different thermal conductivity are mostly identical in first term. Yet as time increases, the effect of λ gradually presents clear, which can be visualized at the end of quick stress collapse. The material arrives at steady state more quickly if thermal conductivity coefficient is larger, and the steady stress is larger. In addition, the localization is more serious as λ decreases, bandwidth is smaller and central temperature is higher. For

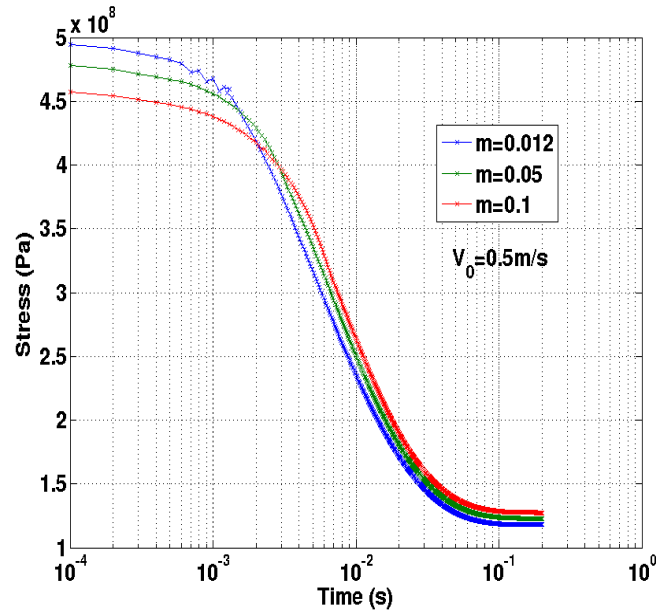


Figure 3.10: Influence of m on stress evolution in exponential softening law at $V_0 = 0.5\text{m/s}$

example, $h = 0.022298\text{mm}$, $T_{max} = 2654\text{K}$ when $\lambda = 10\text{Wm}^{-1}\text{K}^{-1}$, yet $h = 0.039662\text{mm}$, $T_{max} = 1648\text{K}$ when $\lambda = 54\text{Wm}^{-1}\text{K}^{-1}$. We do not consider the melting point of steel, the value is not physical but enough to illustrate the influence of thermal conduction.

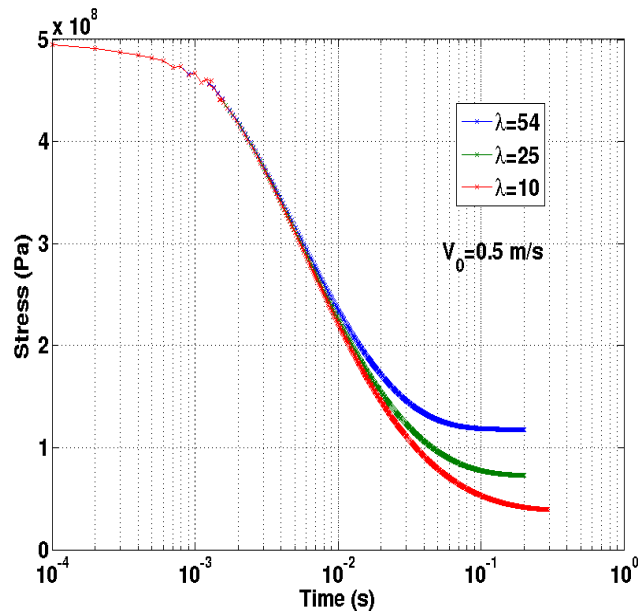


Figure 3.11: Influence of λ on stress evolution in exponential softening law at $V_0 = 0.5\text{m/s}$

3.2.2.3 Thermal softening coefficient β

As we known, the occurrence of ASB is the result of competition between strain hardening and thermal softening. As the effect of softening overcomes the hardening and gradually plays a more important role, ASB initiates and sharpens. Thermal softening coefficient is an index to reflect the resistance of material to temperature. Some references [Tzavaras and Gurtin, 1987, Zhu and Batra, 1991, Yadav et al., 2001] analysed the influence of this parameter on the shear band development in metals subjected to high shear, tensile or compression strain rate. Experimental results showed that there is more possibility to occur instability phenomenon when the thermal softening value is larger. Here we study this effect using our variational modelling.

FIG.3.12 presents the evolutions of stress with different thermal softening coefficients β ($V_0 = 0.5\text{m/s}, H = 1.25\text{mm}$). According to three curves obtained by $\beta = 0.33$, $\beta = 0.2$ and $\beta = 0.1$, the magnitudes of thermal softening coefficient do not have a large influence on the initial maximum flow stress, they almost keep the same value, verifying that the effect softening is slight in the first state. Yet the material enters into strong instability at later time. If β is larger, shear localization initiates earlier, the degree of stress collapse is more serious and the duration of instability propagation are different. Therefore we deduce that the larger thermal softening coefficient causes the occurrence of ASB more easily, and the bandwidth is shorter at steady state. For instance, $h = 0.06965\text{mm}$ when $\beta = 0.1$, and $h = 0.039662\text{mm}$ when $\beta = 0.33$. This conclusion is in good agreement with experimental observations.

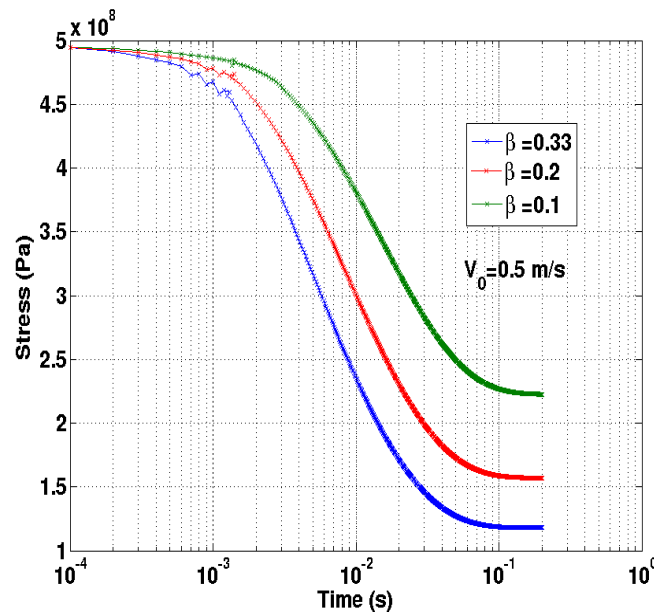


Figure 3.12: Influence of β on stress evolution in exponential softening law at $V_0 = 0.5\text{m/s}$

3.2.2.4 Imposed velocity V_0

Shear localization easily occurs at high strain rate. Obviously, because of the high loading rate, there is not enough time for heat to get out of the band by thermal conduction, and high temperature is localized in tiny width. Yet rightly due to this condition, numerical simulation of this phenomenon is complicated because strong instability causes a convergent difficulty in mesh modelling and nonlinear algorithm. Here based on our validated modelling without mesh, we use an example to study the influence of dynamic loading in the formation of ASB.

FIG.3.13 presents the stress evolution with different imposed velocities V_0 on the boundary $y = \pm H$. For the structure size $H = 1.25mm$, three velocities are considered to illustrate its influence on stress evolution. The strong instability is easier to occur at higher strain rate loading, and in the initial state the material arrives at the stress larger than that of smaller shear rate. When the stresses at $V_0 = 1m/s$ and the one at $V_0 = 0.5m/s$ arrive at steady state, the large stress collapse at $V_0 = 0.01108m/s$ still does not happen. In addition, the degree of instability is more serious at higher strain rate. Therefore the localization phenomenon occurs easily and appears easily at high imposed velocity, because large deformation concentrates on a tiny bandwidth. That is also the reason why the adiabatic shear band seems as a discontinuous surface in macroscopic scale.

Finally we might as well illustrate that high strain rate loading is not necessary to shear localization happening, slow strain rate loading sometimes can also cause ASB. Moreover it is not a sufficient condition for ASB neither. For some thermal visco-plastic materials subjected to high shear rate loading, fracture may play a dominant role before strong instability occurs due to the complicated microscopic property, or it breaks down before ASB arrives at steady state.

In summary, according to the analysis of the influence of material parameters, such as strain rate sensibility exponent m , heat conductivity λ , thermal softening coefficient β and loading velocity V_0 , we can find that ASB forms easily for thermal visco-plastic materials having small m and large β subjected to high strain rate loading. Furthermore the thermal conductivity mainly takes effect at the end of ASB formation.

3.2.3 Extension to various constitutive model

In similar manner to that in steady state, we apply the boundary conditions and introduce the maximum temperature to eliminate the dependence of canonical profiles on material parameters. Thus here we will use the well-known power law to illustrate and validate the feasibility of this thermo-viscoplastic constitutive model.

Neglecting hardening parameter in power law, $W^p = 0$, we derive that the dissipative pseudo-potential is as follows:

$$\Psi^*(\dot{\bar{\epsilon}}^p, \bar{\epsilon}^p, T) = \frac{1}{m+1} \frac{\tau_0}{\dot{\gamma}_0^m} \left(\frac{T}{T_0}\right)^{-v} \left(\frac{\partial V}{\partial y}\right)^{m+1} \quad (3.20)$$

where v is thermal softening coefficient, and thermal conduction obeys on Fourier's law.

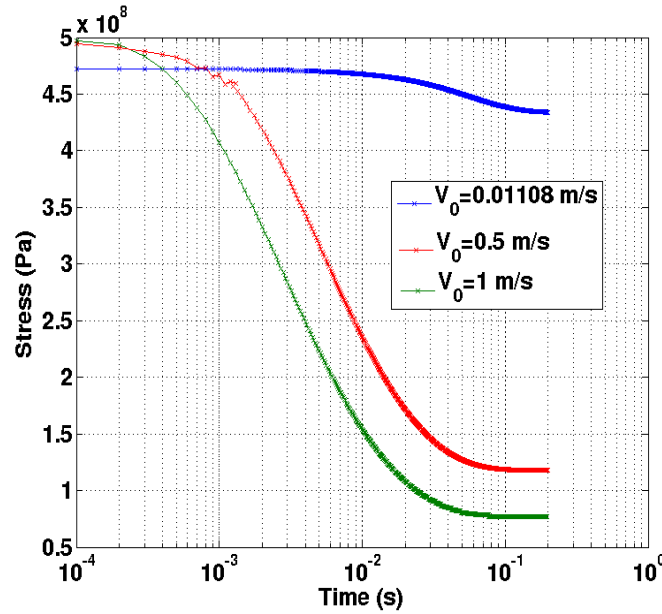


Figure 3.13: Influence of V_0 on stress evolution in exponential softening law

After substituting (3.20) into total incremental potential (3.13), and using the canonical formulations of velocity and temperature, the problem of ASB in transient state is written as an optimization problem about three parameters h_V , h_T and T_{max} at every time step. By means of similar algorithm to that in exponential softening law, we get the kinematic width, thermal width and central temperature to describe the profiles of velocity and temperature, and then calculate the corresponding stress evolution.

FIG.3.14 and FIG.3.15 show that the stress evolution respectively at $V_0 = 0.01108m/s$ and $V_0 = 0.5m/s$. Small instability, large decrease of stress and gradually arriving at steady state are well described in the curves. The stress evolutions have a good correspondence with the ones by FEM, especially for lower strain rate (FIG.3.14). Undergoing higher strain rate, the smaller time step can better represent the formation of ASB. We can also discover that the localization happens more seriously if the imposed velocity is higher, the stress variations express more clearly. Moreover, the formulations of velocity and temperature have achieved satisfactory results in power law, similar to the results in FIG.3.4. We do not list this comparison, which actually agree well with FEM. Consequently, our energy-based variational modelling also works well on power law, meanwhile we validate the canonical aspects of formulations of velocity and temperature through variational method.

3.2.4 Variational modelling with hardening

In view of the comparisons with FEM, our variational method is feasible in exponential softening law and power law, and it can represent well the evolution of bandwidth,

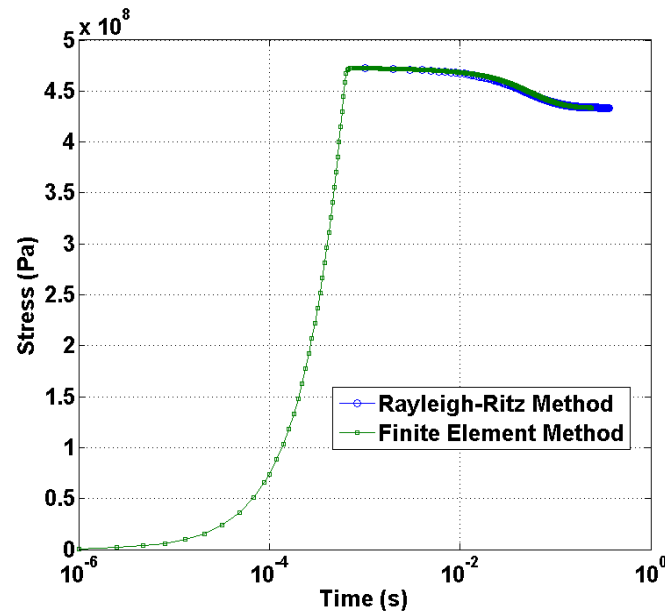


Figure 3.14: Evolution of stress in power law at $V_0 = 0.01108m/s$

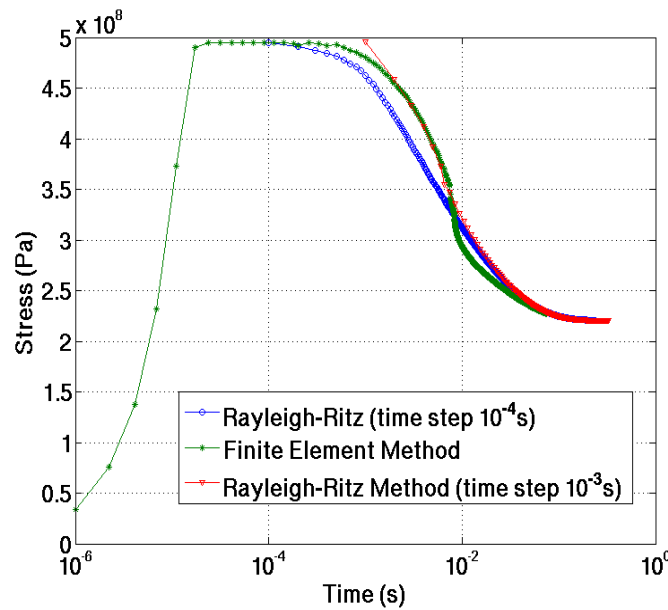


Figure 3.15: Evolution of stress in power law at $V_0 = 0.5m/s$

maximum temperature and stress in the process of ASB formation. Yet previous work was restricted to an ideal thermo-visco-plastic behaviour, where hardening factor was neglected in constitutive relations, thus the first stage of ASB naturally did not exist in the stress evolution. Here we extend the modelling to the widely used Johnson-Cook model

and propose a variational modelling of adiabatic shear band for thermo-visco-plasticity at high-strain rate. Yet elasticity is temporarily neglected in this part.

3.2.4.1 Variational formulation

The main difference with the foregoing modellings will be the presence of a stored plastic energy W^P in total incremental pseudo-potential. In view of the effective yield stress expressed in Johnson-Cook model, we derive W^P as follows:

$$W^P = (A_s \bar{\epsilon}^P + \frac{B_s}{n+1} (\bar{\epsilon}^P)^{n+1}) (1 - \theta^{*q}) \quad (3.21)$$

and the dissipation pseudo-potential is restated as:

$$\Psi^* \left(\dot{\bar{\epsilon}}^P; \bar{\epsilon}^P; T_n \right) = (1 - \theta^{*q}) ([A_d + B_d (\bar{\epsilon}^P)^n] \dot{\bar{\epsilon}}^P + [A + B (\bar{\epsilon}^P)^n] C \dot{\epsilon}_0 (\dot{\epsilon}^* \ln(\dot{\epsilon}^*) - \dot{\epsilon}^* + 1)) \quad (3.22)$$

Where $\dot{\epsilon}^* = \frac{\dot{\bar{\epsilon}}^P}{\dot{\epsilon}_0}$. The corresponding material parameters are illustrated in steady state. These expressions result in an effective yield limit with $A = A_s + A_d, B = B_s + B_d$, which is identical to that of JC model. Yet the ratio of the intrinsic rate of the total plastic to heat power will depend on the decomposition of yield stress into stored and dissipated potential. The dimensionless function θ^* is the form as EQ.2.22.

If we choose the same profiles as the ones restated in (3.17), the equivalent plastic strain in W^P can be expressed as:

$$\bar{\epsilon}_{n+1}^P = \bar{\epsilon}_n^P + \Delta t \dot{\bar{\epsilon}}_{n+1}^P$$

Thus a problem appears: if we also use the canonical velocity profiles in Rayleigh-Ritz method, a recursion will be introduced in the algorithm, which will bring the enormous calculation. Therefore according to $\dot{\bar{\epsilon}}^P = \frac{1}{\sqrt{3}} \frac{\partial v}{\partial y}$, we proceed a similar approach to describe the characters of ASB, yet instead using a profile of displacement as follows:

$$U_{n+1}(y) = U_{0_{n+1}} \frac{\tanh(y/h_{V_{n+1}})}{\tanh(H/h_{V_{n+1}})} \quad (3.23)$$

and $U_{0_{n+1}} = U_{0_n} + \Delta t V_0$, which represents a displacement loading imposed on the boundary $y = \pm H$ at $t = t_{n+1}$.

For thermal visco-plastic materials, our variational update of ASB formation is then described as follows:

$$\begin{aligned} & \inf_{U_{n+1}} \sup_{T_{n+1}} \Phi_n(U_{n+1}, T_{n+1}) \\ & \quad \Updownarrow \\ & \underset{h_{V_{n+1}}, h_{T_{n+1}}, T_{max_{n+1}}}{Stat} \Phi_n(h_{V_{n+1}}, h_{T_{n+1}}, T_{max_{n+1}}) \end{aligned} \quad (3.24)$$

The similar initial condition and constraints for the case without the occurrence of localization are necessary in the calculation.

3.2.4.2 Validation and parameter analysis

In our validation, we choose the widely used titanium alloy Ti-6Al-4V to do the simulation, the material parameters are described in TAB.3.1 ([Bouchnak, 2010]). As A_s and B_s chosen in the table, we consider that the Taylor-Quiney parameter is equal to 1, all the intrinsic plastic energy transformed to heat, so $A_d = A$, $B_d = B$. We imposed the isothermal conditions on the boundary $y = \pm H$, always $T_b = 300K$. Owing to the introduction of

Table 3.1: Material properties for Ti-6Al-4V (in transient state)

material property (Ti-6Al-4V)			
A (MPa)	983	B (MPa)	348
A_s (MPa)	0	B_s (MPa)	0
n	0.32	q	0.69
c	0.024	$\dot{\epsilon}_0$	0.1
T_0 (K)	293	T_m (K)	1943
C_0	580	ρ_0 (kg/m^3)	4428

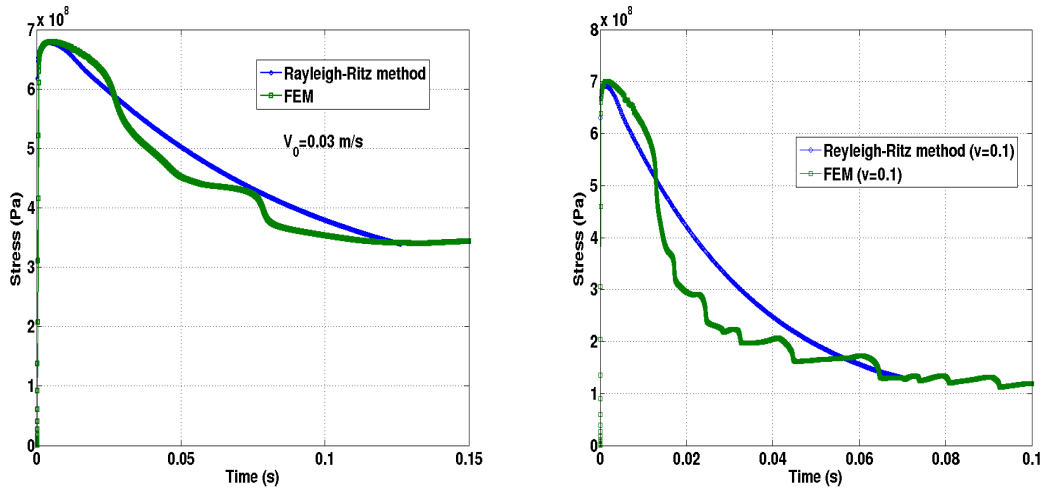


Figure 3.16: Evolution of stress in JC model without elasticity in the layer $H = 1.25mm$

the hardening parameter, the stress state in Johnson-Cook model is different from those in exponential softening law and power law, which can arrive at a steady state. Yet the speed of stress decreasing is slower after the strong stress collapses. FIG.3.16 shows the comparison of the stress evolution with FEM in the band $H = 1.25mm$ at $V_0 = 0.03m/s$ and $V_0 = 0.1m/s$. With the time increased, material firstly goes through the hardening dominant part, stress continuously increases and arrives at a maximum. Gradually the effect of thermal softening is more controlled, stress begins decreasing slowly, and suddenly it has

a large descend, material is in strong instability and ASB forms. Finally the bandwidth arrives at relative steady state. The results of Rayleigh-Ritz method accord well with those of FEM. The maximum stress, the trend of stress and the time of ASB forming are in good correspondence with FEM. In other terms, the formation of ASB depends strongly on imposed velocity, the evolution of stress at higher V_0 arrives at a relatively steady state more quickly. Furthermore the localization is more serious, and the bandwidth is smaller, central temperature is higher than ones at slower imposed velocity.

If the layer width H is smaller, we found that our variational modelling works better. FIG.3.17 is the comparison of stress evolutions in $H = 0.325\text{mm}$ at the same imposed velocity. The whole process of formation of ASB is in good agreement with FEM.

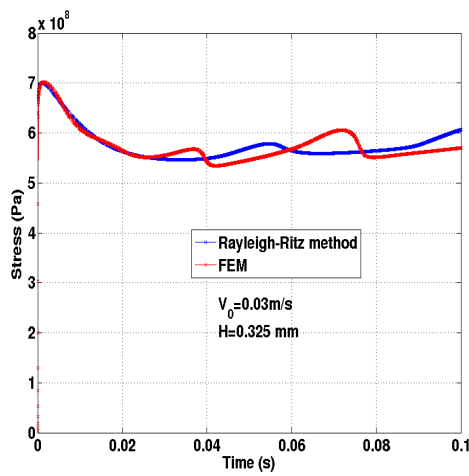


Figure 3.17: Evolution of stress in JC model without elasticity with $H = 0.325\text{mm}$

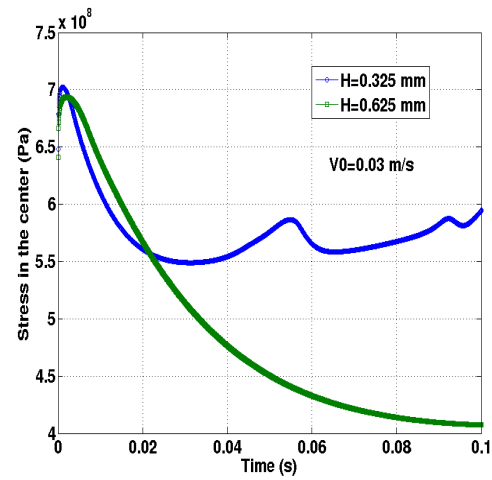


Figure 3.18: Comparison of stress evolution in JC model without elasticity in different layer widths ($V_0 = 0.03\text{m/s}$)

If we consider that the layer is isothermal on $y = \pm H$, same velocity will introduce the different localization character in different layer width, not only in the variations of stress collapse as FIG.3.18 described, but also in the bandwidth and central temperature evolution. The localization level is more serious with longer H , and it arrives at relatively stable stage later. Normally, it is difficult to keep isothermal boundary condition for the layer subjected to a high strain rate loading. Some heat exchange will create on $y = \pm H$, which is also why we introduce the variational modelling with thermal boundary conditions in transient state (next part). Yet here we can find that the profiles of displacement and temperature also have a good approximation for the variational modelling with hardening in transient state.

We also analyse the evolutions of bandwidth and central temperature about $V_0 = 0.03\text{m/s}$, $H = 0.325\text{mm}$ (FIG.3.19 and FIG.3.20). We introduce two bandwidths: kinematic bandwidth h_V and thermal bandwidth h_T to describe the profiles of displacement and temperature, and there is another parameter T_{max} to control its evolution for temperature. We should repeat that shear band width in our variational modelling, such as h_V or

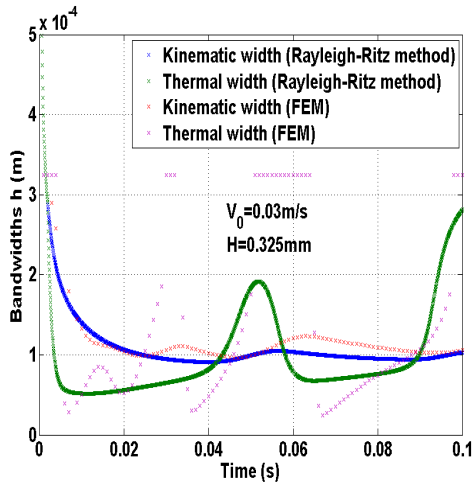


Figure 3.19: Evolution of bandwidth (h) in JC model without elasticity in $H = 0.325\text{mm}$

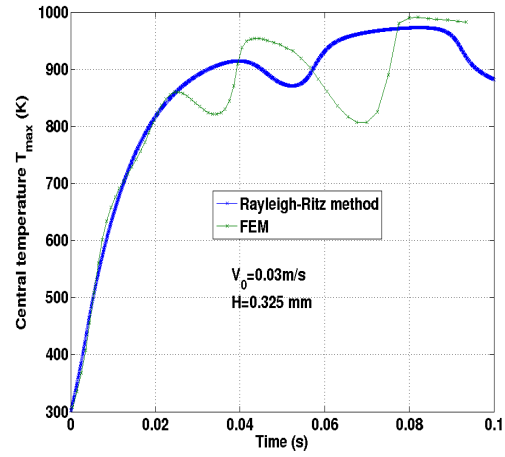


Figure 3.20: Evolution of central temperature (T_{max}) in JC model without elasticity in $H = 0.325\text{mm}$

h_T , is a parameter to measure the physical field. Yet if we understand h_V from its profile and the character of $\tanh(x)$, it is a length of the domain having large displacement gradient, so comparatively it is more reliable to measure a physical localization. As FIG.3.17 described, the stress evolution at $V_0 = 0.03\text{m/s}$ arrives at a relatively steady state approximately at $t = 0.025\text{s}$. The evolution of kinematic length has a good agreement with that by FEM, especially ahead of $t = 0.03\text{s}$. Afterwards it fluctuates at the shear band width, but for h_T it is a strong instability after the bandwidth arrives at steady state. Correspondingly, we have a good approximation of central temperature before steady state, which continuously increases. Yet it is irregular as thermal width begins fluctuating owing to the effect of hardening part. These results illustrate that our variational modelling with hardening factor is feasible in predicting bandwidth, temperature and stress in transient state.

By means of this variational modelling, the influence of hardening factor on stress evolution is analysed for a layer subject to a shearing velocity. Two values $n = 0.1$ and $n = 0.32$ are introduced to do the comparison (FIG.3.21). Smaller hardening factor induces higher effect of hardening and larger maximum stress, yet it lasts shorter. Furthermore, smaller bandwidth and higher central temperature happened in $n = 0.1$ compared with that of $n = 0.32$, the localization is more serious. We might as well say that the smaller strain hardening coefficient causes ASB more easily.

3.2.5 Variational modelling with thermal boundary condition

Similar to the description in CHAP.2, high loading makes the boundary hard to keep isothermal condition. This is also why the foregoing analysis in transient state can not have the same bandwidth with different layer width. At steady state, we proposed a fitted

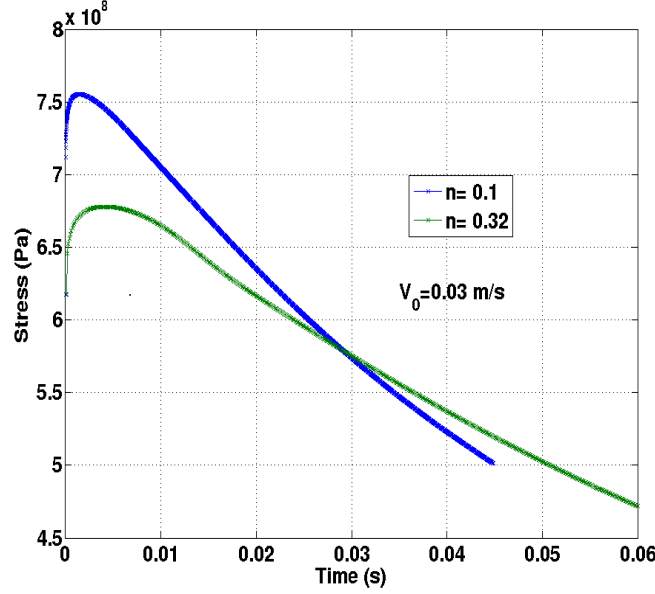


Figure 3.21: Influence of hardening factor on stress evolution in JC model without elasticity ($V_0 = 0.03\text{m/s}$, $H = 1.25\text{mm}$)

formula for exchange coefficient on the boundary. In this section, we will apply this result to discuss the evolution of thermal boundary in transient state based on variational modelling.

3.2.5.1 Variational modelling

Supposing T_{ext_n} as the boundary temperature at $t = t_n$, the incremental transformed potential is described as follows:

$$W_{tr_{n+1}} = \frac{1}{2} \frac{c}{T_{ext_n}} (T_{ext_{n+1}} - T_0)^2 \quad \text{when } y = \pm H \quad (3.25)$$

where c is exchange coefficient, which will be calculated as the formula in CHAP.2. Therefore we also choose $H_r = 1.25\text{mm}$ as a reference width: when $H = H_r$, $c = \infty$ and the thermal boundary condition is isothermal.

The canonical profiles of temperature depend on $T_{ext_{n+1}}$ besides the other parameters $h_{T_{n+1}}$, $T_{max_{n+1}}$, written as:

$$T_{n+1}(y) = T_{max_{n+1}} - (T_{max_{n+1}} - T_{ext_{n+1}}) \frac{\ln(\cosh(y/h_{T_{n+1}}))}{\ln(\cosh(H/h_{T_{n+1}}))} \quad (3.26)$$

As a consequence, the variational update of the ASB is restated as an optimization problem with respect to four parameters:

$$\underset{T_{ext_{n+1}}, h_{V_{n+1}}, h_{T_{n+1}}, T_{max_{n+1}}}{Stat} [\Phi_{t_{n+1}}(T_{ext_{n+1}}, h_{V_{n+1}}, h_{T_{n+1}}, T_{max_{n+1}}) - 2W_{tr_{n+1}}] \quad (3.27)$$

Note that the calculation of $T_{ext_{n+1}}$ in incremental modelling is different from the one in stationary modelling. It will be obtained from the optimizations of total pseudo-potential with respect to four parameters instead of directly solving it through the profile of temperature with reference width. This variational modelling with heat exchange is intended to obtain a consistent bandwidth with different slab widths, and then better illustrate the ASB physical environment. Four nonlinear equations will be derived to describe the constitutive equations.

3.2.5.2 Validation and parameter analysis

If we donot consider exchange potential in the variational modelling, the bandwidth and stress evolutions are presented in FIG.3.22 and FIG.3.23. The kinematic width and thermal width converge to different values with different slab widths, and the stresses at steady state are different. In addition, it seems that the localization is more serious with longer slab width, as the example in FIG.3.18 . Simply we choose exponential softening law to

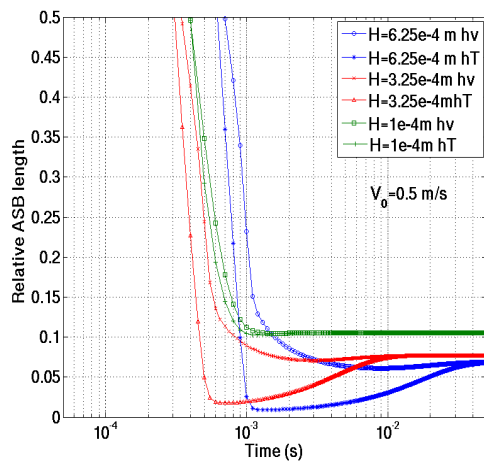


Figure 3.22: Evolution of bandwidth (h) in power model with different H (no exchange on $y \pm H$ and $V_0 = 0.5m/s$)

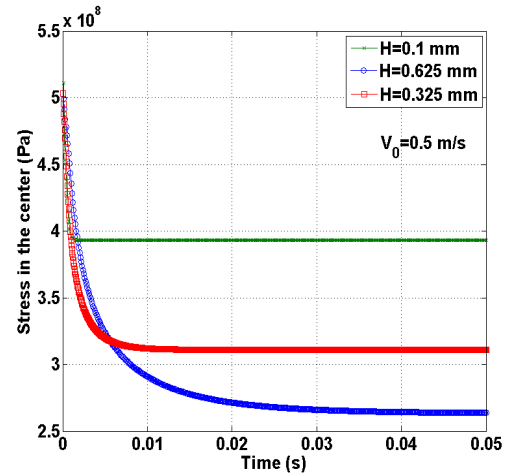


Figure 3.23: Evolution of stress in power model with different H (no exchange on $y \pm H$ and $V_0 = 0.5m/s$)

validate the modelling with thermal boundary condition.

By means of the variational modelling (3.27), we analyse the ASB problem imposed on $V_0 = 0.1m/s, H = 0.625mm$. The profiles of velocity and temperature evolve as shown in FIG.3.24. The velocity distribution goes from linear term to nonlinear term, and arrives at steady state. It seems that their forms are similar to the ones in the modelling without heat exchange. Yet for temperature profiles, at first the material is in adiabatic state, the temperature distribution is isothermal in the slab at the first term, and then the central temperature is gradually higher than the other part because of localized deformation in the central part. When the time increases, it converges to the steady profile which is in good agreement with the solution calculated by the variational modelling at steady state.

FIG.3.25 shows the corresponding evolution of T_{max} and T_{ext} at $V_0 = 0.1\text{ m/s}$. This also accords well with the conclusions in the analysis of influence of thermal conductivity: it plays a weak role in the first and second terms of ASB formation, and is gradually clear in the final term.

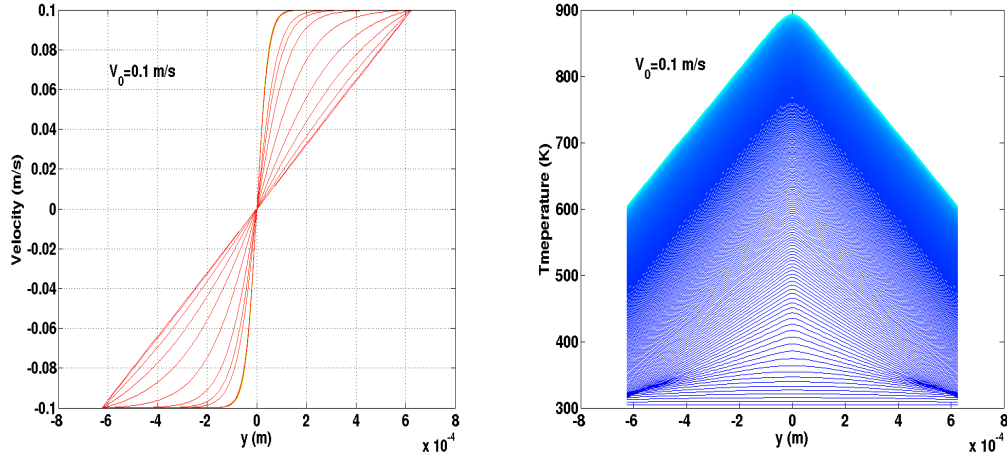


Figure 3.24: Evolution of the profiles of velocity and temperature by Rayleigh-Ritz method in exponential softening law ($V_0 = 0.1\text{ m/s}$)

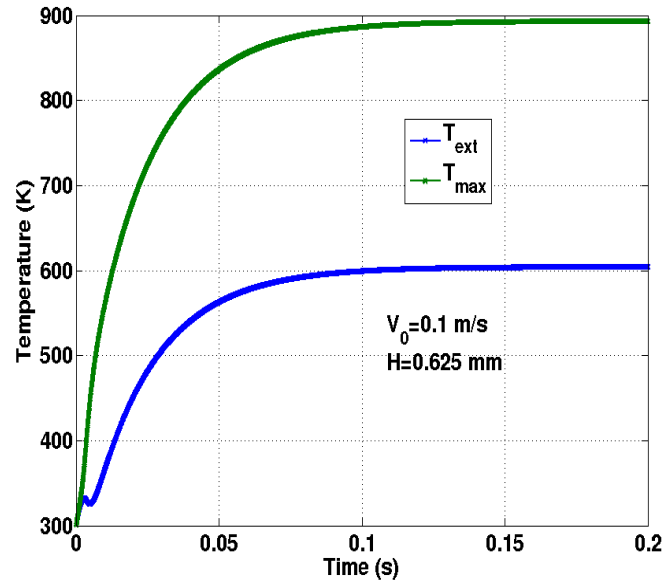


Figure 3.25: Evolution of central temperature and external temperature by Rayleigh-Ritz method in exponential softening law ($V_0 = 0.1\text{ m/s}$)

Thanks to the introduction of heat exchange on the boundary, a variational modelling is built to obtain a bandwidth independent to slab width, which we can validate

in FIG.3.26. The bandwidth converges to the same value with $H = 1.25\text{mm}$ and $H = 0.625\text{mm}$. Yet the convergent speed varies with H , it seems that the smaller H arrives at steady state more quickly than that of longer length, which makes a different stress evolution with different slab widths (FIG.3.27). The falling gradient with $H = 0.625\text{mm}$ is larger than that with $H = 1.25\text{mm}$, the stress arrives at the same value with $H = 1.25\text{mm}$ and $H = 0.625\text{mm}$ (because of identical bandwidth and maximum temperature).

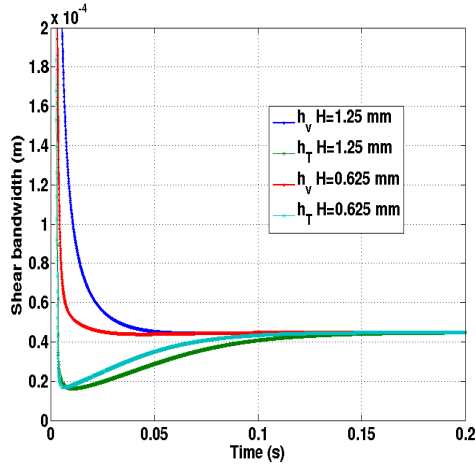


Figure 3.26: Evolution of bandwidth (h) in exponential softening model with different H ($V_0 = 0.1\text{m/s}$)

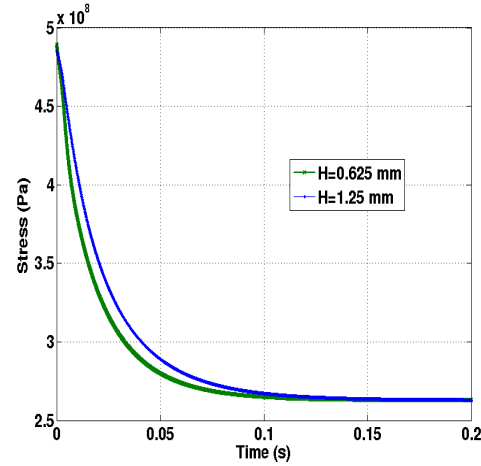


Figure 3.27: Evolution of stress in exponential softening model with different H ($V_0 = 0.1\text{m/s}$)

3.3 Thermo-elasto-visco-plastic variational modelling

In the foregoing work, we proposed and validated the feasibility of variational modelling including hardening or thermal boundary condition. ASB problem is changed to an optimization problem with respect to several parameters in this framework. One advantage of this algorithm is that it reduces the large calculation quantity brought by numerical methods (FEM, meshfree...), the other is that the bandwidth and central temperature can be obtained through the modelling, giving a basic prediction for some discontinuous modellings. Yet in the analysis, our modelling depends strongly on the time step: if it is too small, the material which should be elastic state is calculated as in hardening part due to the negligence of elasticity. Moreover this simplified factor limits the application of our modelling, such that some unloading case can not be simulated using the described modelling, preventing the development of modelling from 1D to 2D or 3D. For example, the application of our variational modelling, such as using our canonical aspects as a discontinuous element or embedding it in standard FEM, can not move a step with a modelling without elasticity. Thus it is mandatory to build a variational modelling with elasticity.

3.3.1 Variational modelling

Similarly considering a layer subjected to a simple shearing velocity V_0 , we suppose the loading displacement can be written as:

$$U_0 = U_0^e + U_0^p$$

U_0^e is an elastic part, and U_0^p is a plastic part. The strain rate is given by:

$$\dot{\boldsymbol{\varepsilon}} = \begin{bmatrix} 0 & \dot{\boldsymbol{\varepsilon}}^e & 0 \\ \dot{\boldsymbol{\varepsilon}}^e & 0 & 0 \\ 0 & 0 & 0 \end{bmatrix} + \begin{bmatrix} 0 & \dot{\boldsymbol{\varepsilon}}^p & 0 \\ \dot{\boldsymbol{\varepsilon}}^p & 0 & 0 \\ 0 & 0 & 0 \end{bmatrix}$$

where $\boldsymbol{\varepsilon}^e$ is the elastic strain, considered as uniform in the layer:

$$\boldsymbol{\varepsilon}^e = \frac{1}{2} \frac{U_0^e}{H}$$

and $\boldsymbol{\varepsilon}^p$ is the plastic strain. As we know for $J2$ von Mises law, the relation between equivalent plastic strain $\bar{\boldsymbol{\varepsilon}}^p$ and shearing plastic strain $\boldsymbol{\gamma}^p$ is:

$$\dot{\bar{\boldsymbol{\varepsilon}}}^p = \sqrt{\frac{2}{3}} \dot{\boldsymbol{\varepsilon}}^p \cdot \dot{\boldsymbol{\varepsilon}}^p = \frac{1}{\sqrt{3}} \dot{\boldsymbol{\gamma}}^p$$

Equivalent plastic strain is continuously increasing no matter the material is loading or unloading. So we introduce another parameter equivalent displacement \bar{U}_0^p as:

$$\dot{U}_0^p = \alpha \dot{\bar{U}}_0^p \quad \text{with } \dot{\bar{U}}_0^p \geq 0 \quad (3.28)$$

where α is a scalar, choosing 1 or -1. We postpone to discuss the determination of its sign before the proposition of elastic-plastic condition in the following. We describe the profile of shear plastic strain using (3.23) :

$$\boldsymbol{\gamma}_{n+1}^p(y) = \bar{U}_{0n+1}^p \frac{1 - \tanh^2(y/h_{V_{n+1}})}{h_{V_{n+1}} \tanh(H/h_{V_{n+1}})} \quad (3.29)$$

and the profile of temperature is chosen the same as the foregoing form with two parameters ($h_{T_{n+1}}$ and $T_{max_{n+1}}$). Different from the incremental variational pseudo-potential, the elastic potential W^e should be included in total variational formulation:

$$W^e = \frac{1}{2} \lambda \text{tr}(\boldsymbol{\varepsilon}^e) \cdot \text{tr}(\boldsymbol{\varepsilon}^e) + \mu \|\text{dev}(\boldsymbol{\varepsilon}^e)\|^2 = \mu \frac{1}{2} \left(\frac{U_0^e}{H} \right)^2$$

We recall that the total pseudo-potential is written as:

$$\begin{aligned} \Phi_n(\boldsymbol{\varepsilon}_{n+1}^e, \dot{\bar{\boldsymbol{\varepsilon}}}_{n+1}^p, \bar{\boldsymbol{\varepsilon}}_{n+1}^p, T_{n+1}) &= \int_{-H}^H [W^e(\boldsymbol{\varepsilon}_{n+1}^e) - W^e(\boldsymbol{\varepsilon}_n^e) + W^p(\bar{\boldsymbol{\varepsilon}}_{n+1}^p, T_{n+1}) - W^p(\bar{\boldsymbol{\varepsilon}}_n^p, T_n) \\ &\quad + W^{th}(T_{n+1}) - W^{th}(T_n) + \Delta t \Psi^* \left(\frac{T_{n+1}}{T_n} \dot{\bar{\boldsymbol{\varepsilon}}}_{n+1}^p, \bar{\boldsymbol{\varepsilon}}_n^p, T_n \right) \\ &\quad + \rho_0 \eta(T_n)(T_{n+1} - T_n) - \Delta t \frac{1}{2} \lambda T_n \left(\frac{\partial T_{n+1}}{\partial y} \frac{1}{T_{n+1}} \right)^2] dy \quad (3.30) \end{aligned}$$

In our variational modelling with elasticity, we use the formulas of W^p and Ψ^* described in Johnson-Cook law. Additionally, the incremental form of U_0 is described using the explicit formula:

$$U_{0_{n+1}} = U_{0_n} + V_0 \cdot \Delta t \quad (3.31)$$

and the equivalent plastic strain is similarly described:

$$\bar{\epsilon}_{n+1}^p = \bar{\epsilon}_n^p + \Delta t \dot{\bar{\epsilon}}_{n+1}^p \quad (3.32)$$

Using the equilibrium equation that stress is homogeneous in the layer, the derivation of Φ_n with respect to $\bar{U}_{0_{n+1}}^p$ is:

$$\begin{aligned} f \equiv \frac{\partial \Phi_n}{\partial \bar{U}_{0_{n+1}}^p} &= -\frac{\partial W_{n+1}^e}{\partial U_{0_{n+1}}^e} \alpha \cdot 2H + \int_{-H}^H \frac{\partial W_{n+1}^p}{\partial \bar{U}_{0_{n+1}}^p} + \Delta t \frac{\partial \Psi_{n+1}^*}{\partial \bar{U}_{0_{n+1}}^p} dy \\ &= -\frac{\partial W_{n+1}^e}{\partial U_{0_{n+1}}^e} \alpha \cdot 2H + \int_{-H}^H \left(\frac{\partial W_{n+1}^p}{\partial \bar{\epsilon}_{n+1}^p} + \frac{\partial \Psi_{n+1}^*}{\partial \dot{\bar{\epsilon}}_{n+1}^p} \right) \cdot \frac{\partial \bar{\epsilon}_{n+1}^p}{\partial \bar{U}_{0_{n+1}}^p} dy \\ &\cong -\frac{\partial W_{n+1}^e}{\partial U_{0_{n+1}}^e} \alpha \cdot 2H + 2[\tau_{y_{n+1}}] \end{aligned} \quad (3.33)$$

Moreover $\frac{\partial W_{n+1}^e}{\partial U_{0_{n+1}}^e} = \mu \frac{U_{0_{n+1}}^e}{H^2}$, so (3.33) can be physically described as:

$$\frac{\partial \Phi_n}{\partial \bar{U}_{0_{n+1}}^p} = -2\alpha\tau_e + 2[\tau_{y_{n+1}}]$$

Consequently, the traditional elastic-plastic condition can be transformed as an optimization of our variational modelling:

$$\inf_{\alpha, \bar{U}_{0_{n+1}}^p} \Phi(h_{V_{n+1}}, h_{T_{n+1}}, T_{max_{n+1}}, \bar{U}_{0_{n+1}}^p) \quad (3.34)$$

Considering the convexity of Φ_n with respect to $\bar{U}_{0_{n+1}}^p$, we obtain the sign of α :

$$\alpha = \text{sign}(U_{0_{n+1}}^{e,trial}) \quad \text{with} \quad U_{0_{n+1}}^{e,trial} = U_{0_{n+1}} - U_{0_n}^p \quad (3.35)$$

and the elastic loading-unloading condition accounting for the optimization condition (3.34) follows as:

$$f^{trial} \equiv \frac{\partial \Phi}{\partial \bar{U}_{0_{n+1}}^p}(\bar{U}_{0_n}^p, h_{v_n}, h_{T_n}, T_{max_n}) > 0 \quad (3.36)$$

when (3.36) is satisfied, the material is in elasticity. Actually we can give the geometrical interpretation of this condition in the view of mathematical optimization, as FIG.3.28 described: accounting for the constraint condition $\bar{U}_{0_{n+1}}^p \geq \bar{U}_{0_n}^p$, firstly we determine whether the solution of $f = 0$ exists through the gradient of total potential with respect to $\bar{U}_{0_{n+1}}^p$. If

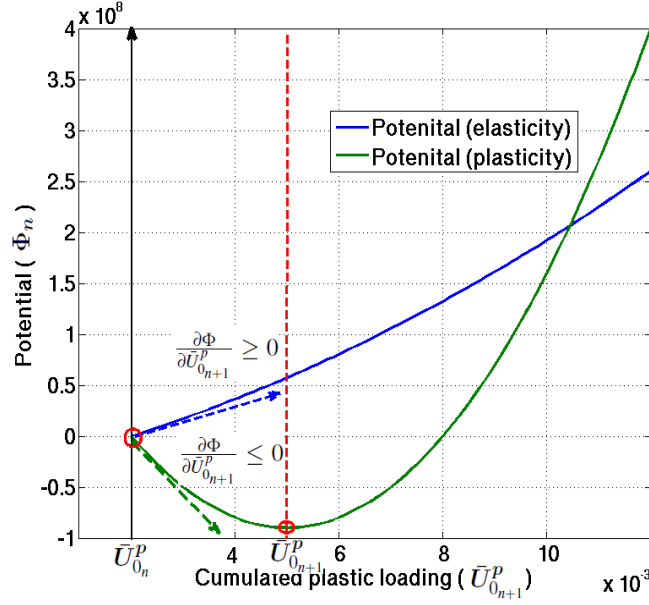


Figure 3.28: Optimization of total potential with respect to cumulated plastic loading

it is positive, the minimum is $\bar{U}_{0_{n+1}}^P = \bar{U}_{0_n}^P$ because of the convexity of potential, otherwise there must be a $\bar{U}_{0_{n+1}}^P > 0$ making $f = 0$. As a result, a condition stemmed as Kuhn-Tucker relation is proposed for our variational modelling:

$$\bar{U}_{0_{n+1}}^P \geq 0; \quad f \leq 0; \quad \bar{U}_{0_{n+1}}^P f = 0 \quad (3.37)$$

Two cases in elasticity for thermo-mechanical problem are considered: elastic under loading and unloading. For simplicity, we distinguish them through $\bar{U}_{0_{n+1}}^P$:

- If $\bar{U}_{0_{n+1}}^P = 0$, elastic loading;
- otherwise: unloading state (thermal problem).

The variation modelling for 1D simple shear band is stated as follows:

- if $f^{trial} = \frac{\partial \Phi_n}{\partial \bar{U}_{0_{n+1}}^P}(\bar{U}_{0_n}^P, h_{V_n}, h_{T_n}, T_{max_n}) > 0$, the ASB problem is described as:

$$\bar{U}_{0_{n+1}}^P = \bar{U}_{0_n}^P; \quad \text{and} \quad \begin{cases} \text{if } \bar{U}_{0_{n+1}}^P = 0; & h_{V_{n+1}} = h_{V_n}; h_{T_{n+1}} = h_{T_n}; T_{max_{n+1}} = T_{max_n}; \\ \text{else} & Stat_{h_{T_{n+1}}, T_{max_{n+1}}} \Phi_{n+1}(\bar{U}_{0_n}^P, h_{V_n}, h_{T_{n+1}}, T_{max_{n+1}}) \end{cases} \quad (3.38)$$

- if $\frac{\partial \Phi_n}{\partial \bar{U}_{0_{n+1}}^P}(h_{V_n}, h_{T_n}, T_{max_n}) \leq 0$, the ASB problem is described as:

$$\bar{U}_{0_{n+1}}^P, h_{V_{n+1}}, h_{T_{n+1}}, T_{max_{n+1}} \quad Stat \quad \Phi_{n+1}(\bar{U}_{0_{n+1}}^P, h_{V_{n+1}}, h_{T_{n+1}}, T_{max_{n+1}}) \quad (3.39)$$

For the second case, we tried to resolve the above modelling and found that it had a slow convergence to the stationary point, especially for the first state having no shear band initiation. Therefore we adopt the distributed strategy to simplify the problem, described in ALG.1. Here C is a constant, smaller than 1. The choice of C decides on the accuracy

Algorithm 1 Algorithm in plastic state for 1D variational modelling at each step $t_n \rightarrow t_{n+1}$

```

inf $\bar{U}_{0_{n+1},1}^P$   $\Phi_n(\bar{U}_{0_{n+1},1}^P, h_{V_n}, h_{T_n}, T_{max_n});$ 
Stat $_{h_{V_{n+1}}, h_{T_{n+1}}, T_{max_{n+1}}}$   $\Phi_{n+1}(\bar{U}_{0_{n+1},1}^P, h_{V_{n+1}}, h_{T_{n+1}}, T_{max_{n+1}});$ 
 $i = 1;$   $d_0 = \bar{U}_{0_{n+1},1}^P - \bar{U}_{0_n}^P;$   $d = d_0;$ 
while  $|d| > Cd_0$  do
 $h_{V_n} = h_{V_{n+1}};$   $h_{T_n} = h_{T_{n+1}};$   $T_{max_n} = T_{max_{n+1}};$ 
inf $\bar{U}_{0_{n+1},i+1}^P$   $\Phi_n(\bar{U}_{0_{n+1},i+1}^P, h_{V_n}, h_{T_n}, T_{max_n});$ 
Stat $_{h_{V_{n+1}}, h_{T_{n+1}}, T_{max_{n+1}}}$   $\Phi_{n+1}(\bar{U}_{0_{n+1},i+1}^P, h_{V_{n+1}}, h_{T_{n+1}}, T_{max_{n+1}});$ 
 $d = \bar{U}_{0_{n+1},i+1}^P - \bar{U}_{0_{n+1},i}^P;$ 
 $\bar{U}_{0_{n+1},i}^P = \bar{U}_{0_{n+1},i+1}^P;$ 
 $i = i + 1;$ 
end while

```

and the efficiency of algorithm, normally we choose $C = 0.1$ because of the small time step, and in the following subject we will show its influence on the algorithm and exhibit that the choice is reasonable.

3.3.2 Numerical validation

A same problem of Titanium alloy (Ti-6Al-4V) is repeatedly analysed in the ongoing work, yet elasticity is considered using the variational modelling. Besides the material property parameters already given in TAB.3.1, we use the following elastic property: Young's modulus $E = 1.14 \times 10^{11}$ Pa and Poisson ratio $\nu = 0.3$, so:

$$\mu = \frac{1}{2} \frac{E}{1 + \nu} = 5.4231 \times 10^{10} \text{ Pa}$$

FIG.3.29 shows the stress evolution at $V_0 = 0.03m/s$ and $V_0 = 0.1m/s$. Besides the comparison with FEM, we also compared the results with the modelling without elasticity at $V_0 = 0.03m/s$. Firstly, the variational modelling with elasticity reflects a more complete process of the stress evolution in the band, when we choose time step as $10^{-4}s$, the material should be in elastic state according to FEM result, yet for the modelling without elasticity, it shows its drawback that the beginning is in plasticity, although the rest part shows a correspondence with FEM. So comparatively, the result of our thermo-elasto-viscoplastical modelling accords well with FEM: material goes though elasticity, and enters into hardening part, stress increases slowly and gradually arrives at a maximum value. Then thermal softening part plays a determinant role in the band, stress begins decreasing

slowly, yet suddenly has a large drop, the shear band is forming and the bandwidth is in steady state relatively. In addition, thanks to the introduction of elasticity, variational modelling has a better agreement compared with the modelling without elasticity in particular the stress in the second stage. These results validate that our proposed modelling is feasible to measure material state.

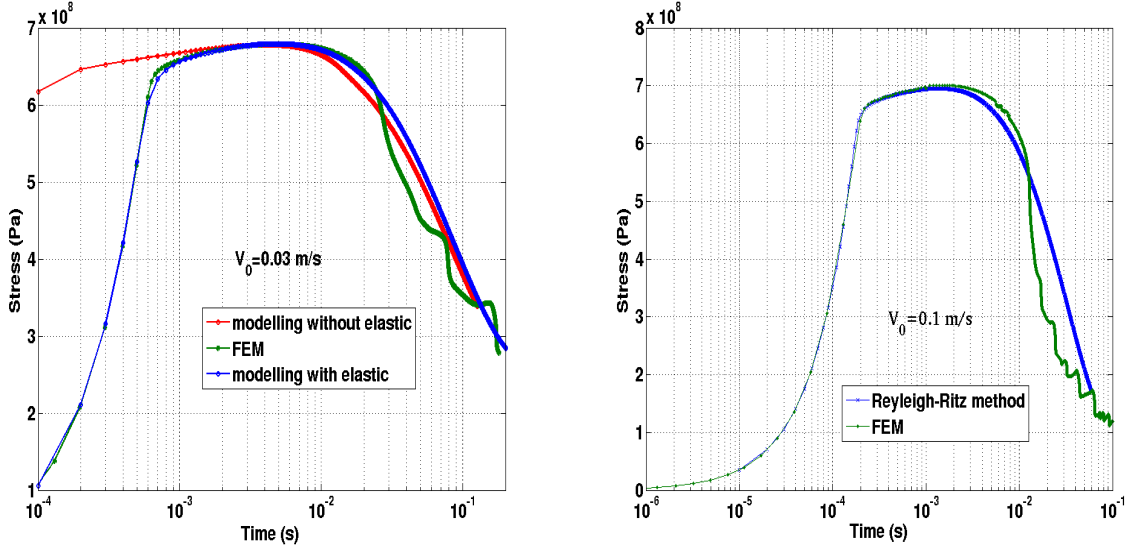


Figure 3.29: Comparison of stress evolution with FEM in JC law ($V_0 = 0.03m/s$ and $V_0 = 0.1m/s$)

We also analyse the evolution of equivalent plastic displacement \bar{U}_0^p at different imposed velocities $V_0 = 0.03m/s$ and $V_0 = 0.1m/s$ (FIG.3.30). Under monotonic loading, \bar{U}_0^p should be equal to U_0^p , which is the distributed part of the total imposed displacement at each time. In elastic state, all the loading displacement is used for elastic deformation, $\bar{U}_0^p = 0$; After the material gradually arrives at the turning point, the distribution of total displacement into equivalent plastic displacement has a quick increase, and finally it occupies all the imposed displacement. The moments, when material enters into plasticity and plastic displacement becomes completely dominant, appear earlier in higher loading rate.

Based on this validated modelling, we will do some researches on ASB behaviour under cyclic loading. The loading condition is chosen as follows:

$$U_{0_{n+1}} = U_{0_n} + \Delta t V_0 \quad \text{when } 0 < t < 0.1s; \quad (3.40)$$

except:

$$U_{0_{n+1}} = U_{0_n} - \Delta t V_0 \quad \text{when } \begin{cases} 0.01s < t \leq 0.02s; \\ 0.03s < t \leq 0.04s; \\ 0.07s < t \leq 0.08s; \end{cases} \quad (3.41)$$

FIG.3.31 shows the stress-plastic displacement (U_0^p) curves at cyclic shear loading rate ($V_0 = 0.03m/s$ and $V_0 = 0.1m/s$). The evolution of yield limit depends on the

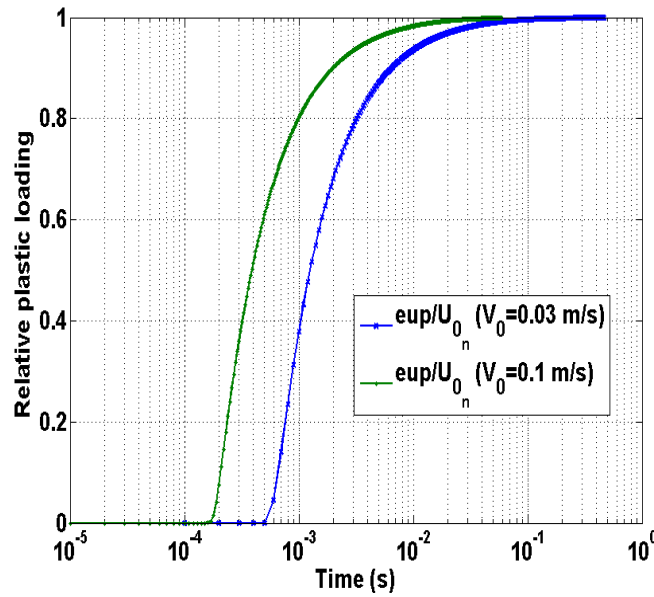


Figure 3.30: Evolution of equivalent plastic displacement in JC law ($V_0 = 0.03m/s$ and $V_0 = 0.1m/s$)

charging in the plastic regime, and an appropriate unloading can strengthen the value of yield limit (FIG.3.32). For titanium alloy(Ti-6Al-4V), material already enters into second ($V_0 = 0.03m/s$) or third term ($V_0 = 0.1m/s$) when the first unloading happens. In addition, under same loading condition, hardening part and thermal softening at $V_0 = 0.1m/s$ happened earlier than that at $V_0 = 0.03m/s$, so higher strain rate creates ASB more easily, as described in the analysis of hardening coefficient.

If we set the unloading condition happening in the first stage, flow stress is strengthened after material goes through unloading part. FIG.3.33 is a stress evolution under the unloading condition (3.40):

$$U_{0_{n+1}} = U_{0_n} - \Delta t V_0 \quad \text{when } 2 \times 10^{-3}s < t \leq 8 \times 10^{-3}s$$

material stays in hardening part in $2 \times 10^{-3}s < t \leq 8 \times 10^{-3}s$, so we can see that its flow stress is larger at $t = 8 \times 10^{-3}s$ than $t = 2 \times 10^{-3}s$, yet then thermal softening effect is gradually clear that the stress begins decreasing.

Reviewing the results under simple uniform shearing form, we analysed the influence of charging condition on shear bandwidth and central temperature (FIG.3.34 and FIG.3.35). Cyclic loading can relieve the effect of shear localization in certain time in view of the comparisons. When material is subjected to unloading, central temperature in the zone is decreasing, so h has a little rebound. Yet because we unloaded the structure at 0.01 s, the material stress enters into hardening or softening part in inverse direction. At the same time, the characters of ASB are weaker under cyclic loading than ones under monotonic loading. We can see clearly that maximum temperature is smaller than normal

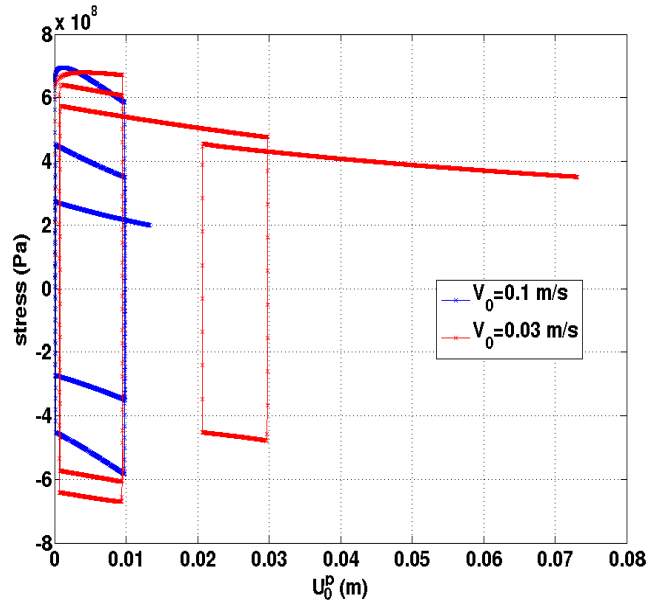


Figure 3.31: Stress-plastic displacement(U_0^P) relation under cyclic loading and simple shear loading in JC law ($V_0 = 0.03m/s$ and $V_0 = 0.1m/s$)

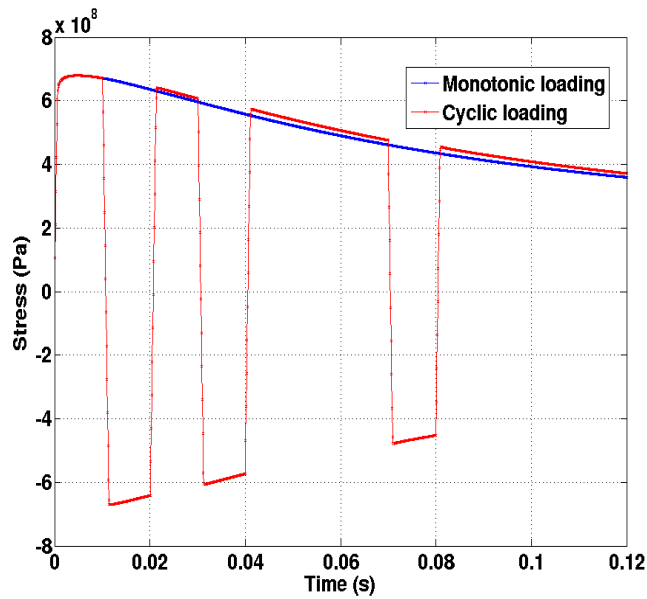


Figure 3.32: Comparison of stress evolution under cyclic loading in JC law ($V_0 = 0.03m/s$)

loading in FIG.3.35. Yet controlling the unloading time is more important to improve the material property.

In our algorithm, there is a parameter C to control the error approximation about \bar{U}_0^P ,

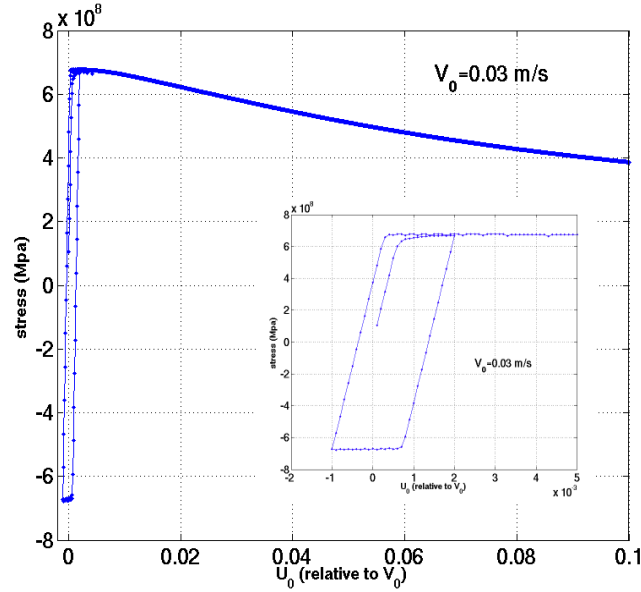


Figure 3.33: Stress-charged displacement(U_0) relation under cyclic loading in JC law ($V_0 = 0.03m/s$)

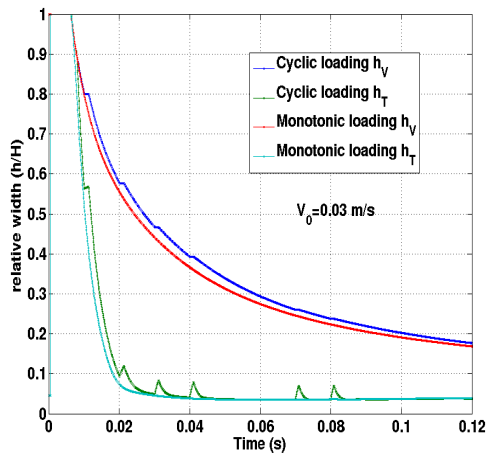


Figure 3.34: Evolution of bandwidth under cyclic loading ((3.40) and (3.41)) in JC law ($V_0 = 0.03m/s$)

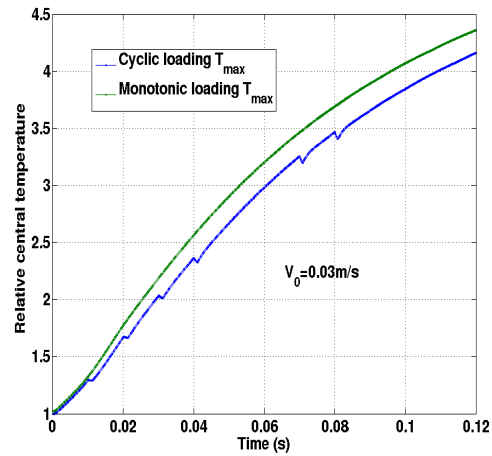


Figure 3.35: Evolution of central temperature under cyclic loading ((3.40) and (3.41)) in JC law ($V_0 = 0.03m/s$)

its choice reflects the efficiency and accuracy of our variational modelling. We analyse the influence of C on the stress evolution at $V_0 = 0.03m/s$ in FIG.3.36. Because of small time step, the change of equivalent strain is very small between two circumstances, so $C = 0.1$ and $C = 0.01$ have no large influence on the stress evolution. Although $C = 0.1$, the threshold d may be 10^{-4} . Consequently $C = 0.1$ is enough to resolve our variational

modelling, yet the choice also depends on time step.

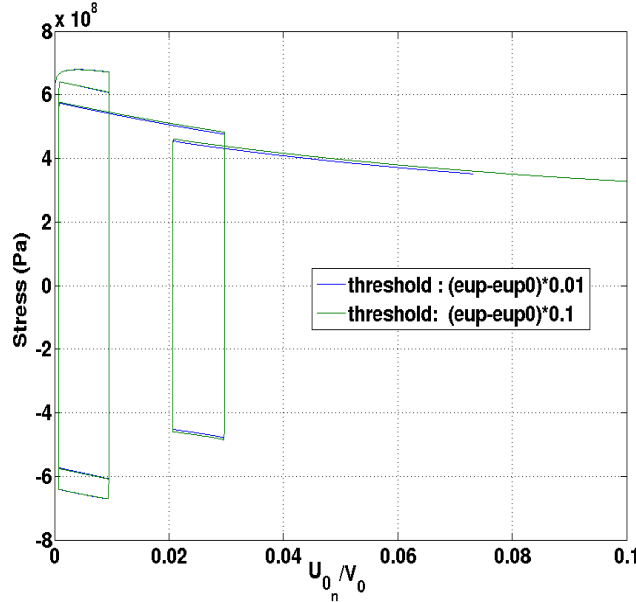


Figure 3.36: Influence of C on stress evolution under cyclic loading (3.40 and 3.41) in JC law ($V_0 = 0.03m/s$)

3.3.3 Average stress analysis

In the critical condition of plastic stage, we derived the following average stress according to the uniformity of stress in equilibrium equation:

$$[\tau_y] = \frac{1}{2} \int_{-H}^H \left[\frac{\partial W_{n+1}^p}{\partial \bar{U}_{0n+1}^p} + \Delta t \frac{\partial \Psi_{n+1}^*}{\partial \bar{U}_{0n+1}^p} \right] dy$$

Yet when we calculate the stress using numerical methods, there is some error approximation in simulation. In CHAP.2, we already discussed the approximation between average stress and point stress calculated by flow law in steady state, and got that error can be controlled in 1×10^{-6} . Here referred to the determination of material state and the future application in higher dimension, we will consider the error approximation of average stress in transient state.

As we know in the foregoing work, adiabatic shear band forms and arrives at relative steady state before $t = 0.09s$ for $V_0 = 0.03m/s$, yet for $V_0 = 0.1m/s$, the time is before $0.03s$. FIG.3.37 shows the evolution of stress error under cyclic loading. The formula of relative error presenting in the figure is as follows:

$$e^* = \max\left(1 - \frac{\tau_y(y)}{[\tau_y]}\right)$$

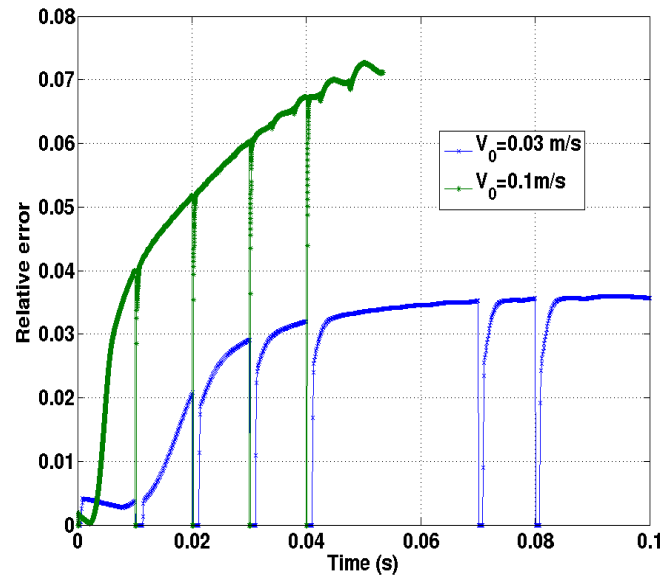


Figure 3.37: Error approximation of average stress under cyclic loading (3.40 and 3.41) in JC law

In the first and the second stage of ASB, we can control the error less than 0.005, but with the time increased, the stress in the band has a sudden dropping, and material enters into strong instability. The error in this stage has an increase with higher speed. We consider that one part of the reason is from the threshold for calculating \bar{U}_0^p , the other part is the numerical calculation: when we calculated in the program, $\tanh(x)$ and $\cosh(x)$ are simplified to calculate if $x > 60$, and numerical integration is also a source of error approximation to keep high efficiency of our algorithm. Moreover there is some error from calculating the optimization point using constrained optimized method, such as Trust-region method. Despite these disadvantages exist, the error can be controlled in 0.4% for $V_0 = 0.03\text{m/s}$ and 6% for $V_0 = 0.1\text{m/s}$ after that the stress passes through the strong collapse. In addition, we want to say that in our current study, material damage has not been yet considered in our modelling. But it will be a good aspect if including it in our future study for the perfect performance of total ASB forming and stability. We discovered that the larger error of average stress used to appear in the last part of third stage, and damage maybe occur at the same time. So it maybe bring a better stress approximation if we add damage coefficient.

The error approximation from average stress analysis influences the determination of elastic and plastic state, but this problem just exists several time steps because of error estimation. When the time step is very small, the turning point from loading to unloading maybe have a judgement error in the comparison between the trial stress and stress at last step. Only one time step happens in all the calculation we have met. However, the stress error is also very small because of tiny time step, so this influence can be neglected in the simulation of ASB forming process.

3.4 Conclusions

Based on the variational modelling in steady state proposed in CHAP.2, we aim at working on the variational updating modelling for illustrating the three stages in the formation of adiabatic shear band. In this chapter, four modellings of thermo-mechanical shear localization problem are gradually proposed to simulate the evolution of profiles of displacement or velocity and temperature in the localization zone:

- Thermo viscoplastic modelling
- Thermo viscoplastic modelling with hardening
- Thermo viscoplastic modelling with thermal boundary condition
- Thermo elasto-viscoplastic modelling

In the variational framework, Finite Element Method having symmetric tangent stiffness matrix is applied to validate our modellings, and shows its feasibility. Meanwhile it mentions that the canonical formulas of displacement and temperature work well for the prediction of ASB characters. As we all know, exponential softening law, power law and Johnson-Cook law are widely used in thermo-viscoplastic materials. Here as an application, three variational modellings in these constitutive models are derived and used to implement the formation of ASB simulation in different materials, then it reflects that canonical profiles work on various material models. In addition, we analysed the influence of material parameters for understanding well the ASB formation: strain rate sensibility exponent m , thermal softening coefficient β , thermal conductivity λ and imposed velocity V_0 . Shear localization forms more easily for thermal-viscoplastic materials with smaller m and β under higher strain rate loading.

Similar to the idea of CHAP.2, we also introduce exchange potential in the modelling to keep the conformity of bandwidth. The evolution of temperature on the boundary increases with the time, but its increasing speed is gradually decreasing. From the temperature profile in the first stage and the comparison between T_{max} and T_{ext} , we got that the conduction part plays an insignificant effect before the late part of ASB stability, which is in good agreement with experiments. As the analysis in the influence of thermal conductivity, thermal conduction is an important factor if we want to better get material bandwidth and temperature distribution at the end of third stage.

For the widely used constitutive model Johnson-Cook, hardening part and elastic part are included for decreasing the difficulty of time step choice and wide application in the variational modelling. We adopt the division of loading displacement as elastic part and plastic part, and then introduce another optimized parameter into variational potential to track the initiation and evolution of plasticity. Finally this thermo-elastic-visco-plastic modelling is validated by FEM. By means of this modelling, some examples under cyclic loading are simulated to explore the influence of ASB evolution brought by the loading condition. We found that an appropriate unloading condition can relieve the degree of localization. The characters of ASB (bandwidth h and central temperature T_{max}) are

less serious at steady state if material goes through unloading condition. Yet the error approximation of the average stress from numerical calculation may cause the turning point of loading and unloading to be misjudged, it can be avoided if time step is not chosen too tiny.

Arrived here, we have built a complete thermo-elasto-viscoplastic variational modelling for this thermo-mechanical problem in 1D, including elasticity, hardening, thermal softening, thermal conduction and thermal boundary condition. Yet 1D analysis is limited and imperfect in the numerical simulation of ASB formation, for instance, hot spot phenomenon in temperature distribution. So how to extend this complete 1D variational modelling to the one in 2D or 3D? This question will be given a response in next chapter.

Chapter 4

Variational two-scale modelling in 2D/3D

Abstract :

By means of the discontinuous interface element, a new variational two-scale model is proposed for adiabatic shear bands structure in 2D/3D in order to avoid mesh dependence. The advantage of our approach is that an inhomogeneous plastic deformation and temperature distribution in the localized region are inferred from canonical analytical expressions. The corresponding finite element implementation is also derived when we embed our 1D variational pseudo-potential of shear localization into standard FEM.

Résumé :

Un nouveau modèle variationnel à deux-échelles de la bande de cisaillement adiabatique en 2D/3D est proposé en utilisant des éléments d'interface discontinus de sorte à éviter la dépendance aux maillages. Contrairement aux travaux existants, des déformations plastiques et des températures non homogènes sont inférées par les expressions analytiques canoniques. On dérive l'implémentation de la méthode des éléments finis (MEF) quand le pseudo-potential variationnel de la localisation est inséré dans la MEF standard.

Contents

4.1	Mesh dependence in standard FEM	102
4.2	Variational two-scale method	108
4.2.1	Discontinuous approaches	108
4.2.1.1	Interface element	109
4.2.1.2	Embedded discontinuity model	110
4.2.1.3	Extended finite element method	112
4.2.2	Variational two-scale modelling	114
4.2.2.1	Linearized kinematics	114
4.2.2.2	Finite kinematics	116
4.3	Finite element implementation	118
4.3.1	Finite element modelling	118
4.3.2	Thermo-mechanical flux	121
4.4	Conclusions	124

The numerical analysis of adiabatic shear bands in 2D/3D is always a challenging subject due to the presence of large deformation and high temperature localized in tens of micrometers. At macroscopic scale, its specific characters make it seem as a discontinuous surface, yet it is not true if investigated at microscopic scale. Thus mesh dependence and alignment is a common problem for the popular FEM. Even for numerical meshless methods, the choice of node density is unavoidable.

In general, one solution to this difficulty is to refine the mesh in the localization region. The localized mesh size should be set similar to that of bandwidth, yet naturally enormous meshes make the calculation unaffordable and low efficiency. The other, popular and strongly advised in the mechanical engineering, is to build a discontinuous modelling in ASB domain based on the standard FEM. Considering that the homogeneous deformation exists in the most of structure, we set the interface elements in the predicted line where localization zone occurs, or embed the discontinuous enrichments into the shape functions of FEM, avoiding the necessity of setting the same scale of mesh size, and presenting a relatively accurate localization phenomenon occurring at a fine scale. Moreover, mesh alignment can also be prevented by enhancing the performance of isoparametric elements involving strain localization. However, a difficulty in all the solutions is that it is necessary to find a constitutive relation for traction-displacement jump and heat production (entropy) in discontinuity. Meanwhile how to describe the profiles in discontinuity and build the connection between continuous part and discontinuity is a considerable question.

By means of the proposed variational modelling including elasticity, hardening, conduction and thermal boundary condition in CHAP.3, we will extend it to 2D/3D and build our variational two-scale modelling for ASBs structure. The study is organized as follows: firstly, we give an example of ASB implemented by standard FEM to understand well the initiation and propagation of ASBs, and then points out the importance and the necessity of discontinuous models (section 1). Secondly, three modellings: interface element, embedding discontinuous model and XFEM ([Ortiz and Pandolfi, 1999, Oliver, 1996b, Areias and Belytschko, 2007]), are discussed here aimed at solving the mesh dependence problem of standard FEM. We also give the common difficulties among them, which can be solved easily with our variational modelling. As an example, interface element is applied in standard FEM to build a variational two-scale modelling (section 2), and the total pseudo-potential in variational formulation is derived having two parts: discontinuous elements merely on surface and standard elements on the other part. Thus for 2D or 3D localization problem, we successfully transfer it as a 1D problem and a line or surface fields of standard element. Considering the implementation of the modelling by FEM, we simply give the formulations of internal force and entropy in this two-scale modelling (section 3). Meanwhile the tangent components are also derived for Newton-Raphson iteration.

4.1 Mesh dependence in standard FEM

A simple pre-notched bar (FIG.4.1) is considered to analyse the orientation and propagation of ASBs, which is also mentioned in [Areias and Belytschko, 2007]. We impose a shearing velocity on top of structure, but fix the displacement in normal direction. Moreover another constraint condition is applied on the bottom side: it is all fixed. Material properties are also described as follows:

$$E = 210 \text{ GPa}; \quad \nu = 0.3; \quad \sigma_0 = 800 \times 10^6 \text{ Pa};$$

$$T_{melt} = 493 \text{ K}; \quad \rho_0 = 7850 \text{ Kg/m}^3; \quad c = 460 \text{ JKg}^{-1}\text{K}^{-1}; \quad k = 30 \text{ NK}^{-1}\text{s}^{-1}$$

for simplicity we consider the linear thermal softening of flow stress. The corresponding yield stress is written as:

$$y = \sigma_0 \left(1 - \frac{\theta}{200}\right) (1 + \dot{\epsilon}^{0.05})$$

where $\theta = T - T_r$, T_r is reference temperature. Here we analyse the bar subjected to a

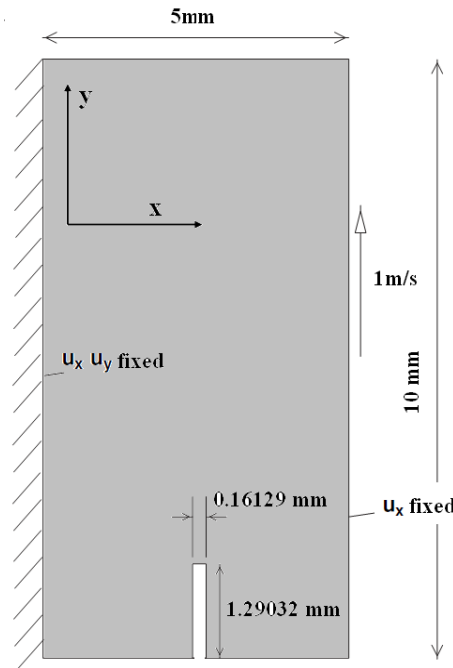


Figure 4.1: Pre-notched bar [Areias and Belytschko, 2007]

high velocity $\dot{u}_y = 1 \text{ m/s}$ in quasi-static state.

For understanding the thermal conduction effect in the orientation of ASB, we separate adiabatic case and conduction case in the simulation. The loading velocity is so high that easily causing the small bandwidth in the plate. Therefore standard FEM will demand fine mesh to track the physical properties in the localization region. Yet building

an appropriate mesh model needs a good prediction of bandwidth, otherwise mesh dependence will happen if setting the large mesh size in the localized zone. We illustrate this point through four different mesh models: 622 elements, 1877 elements, 4105 elements and 7184 elements. In addition, considering that localization zone normally occur in front of notched domain, we set different mesh sizes to analyse its influence. Here 1 element, 3 element, 5 element and 7 element are arranged in front of pre-notched bar in x for the corresponding four mesh models.

In adiabatic case, FIG.4.2 shows the distributions of displacement profiles in front of the pre-notched zone under different mesh sizes. ASB completely exists in the bar for four mesh models. Obviously, the material states depend strongly on the mesh sizes. The larger grid is, the later shear localization forms, and the wider the bandwidth occurs. For four mesh models, they arrive at the relatively steady states separately at $t = 0.0006s$, $t = 0.0003s$, $t = 0.0002s$ and $t = 0.000127s$. Note that the steady state is defined that the stress has small fluctuations with the time evolved.

Accordingly, FIG.4.3 gives the steady states of temperature profiles for the pre-notched bar subjected to a high shearing velocity. With the grid size decreases, the band is less clear, we almost can not see its existence for the finest mesh. So we predict that the bandwidth evolves towards 0 if mesh is more refined at adiabatic case. There is not a steady value for the bandwidth, which is converse to experimental result. Consequently, the model at adiabatic case is insufficient in the analysis of ASB problem.

FIG.4.4 shows the evolution of reaction force in six different mesh sizes. Besides the four mesh models used in the foregoing analysis, we add two new mesh models (1004 elements and 1068 elements), which merely refine the front of pre-notch (separately arranged by 2 elements and 4 elements in x direction) in the simulation. The localized refinement can also improve the precision of the simulation, we found that the model with 1068 elements has a good agreement with the model with 7184 elements. The model with smaller mesh sizes in front of pre-notch enters the instability state earlier, and the corresponding yield force is smaller. Its collapse occurs more precipitously, so material arrives at steady state faster and its value is consequently smaller.

Mesh dependence is presented clearly in adiabatic case, not just on the critical force, but also on the bandwidth. The model with smaller mesh size can produce a strong discontinuous phenomenon more easily. This urges us to make an inquiry in introducing thermal conduction and explore whether it brings a good effect into mesh dependence or not.

FIG.4.5 and FIG.4.6 show the distribution of the temperature profiles (θ) and the equivalent plastic strain profiles under different mesh sizes at a relatively steady state. In view of the above analysis in adiabatic case, we choose three mesh models: 622 elements, 1877 elements and 1068 elements (merely localized refinement). The reference temperatures are separately chosen as $T_r = 30K$, $T_r = 15K$ and $T_r = 30K$. Apparently compared with the ones in adiabatic case, the conduction factor can alleviate effectively the mesh dependence in shear localization. Although the time for arriving at steady state is different ($t = 0.0006s$, $t = 0.0003s$ and $t = 0.0002s$), the bandwidth seems having a little influence. The second one and third one almost keep consistency with the bandwidths for 1877 ele-

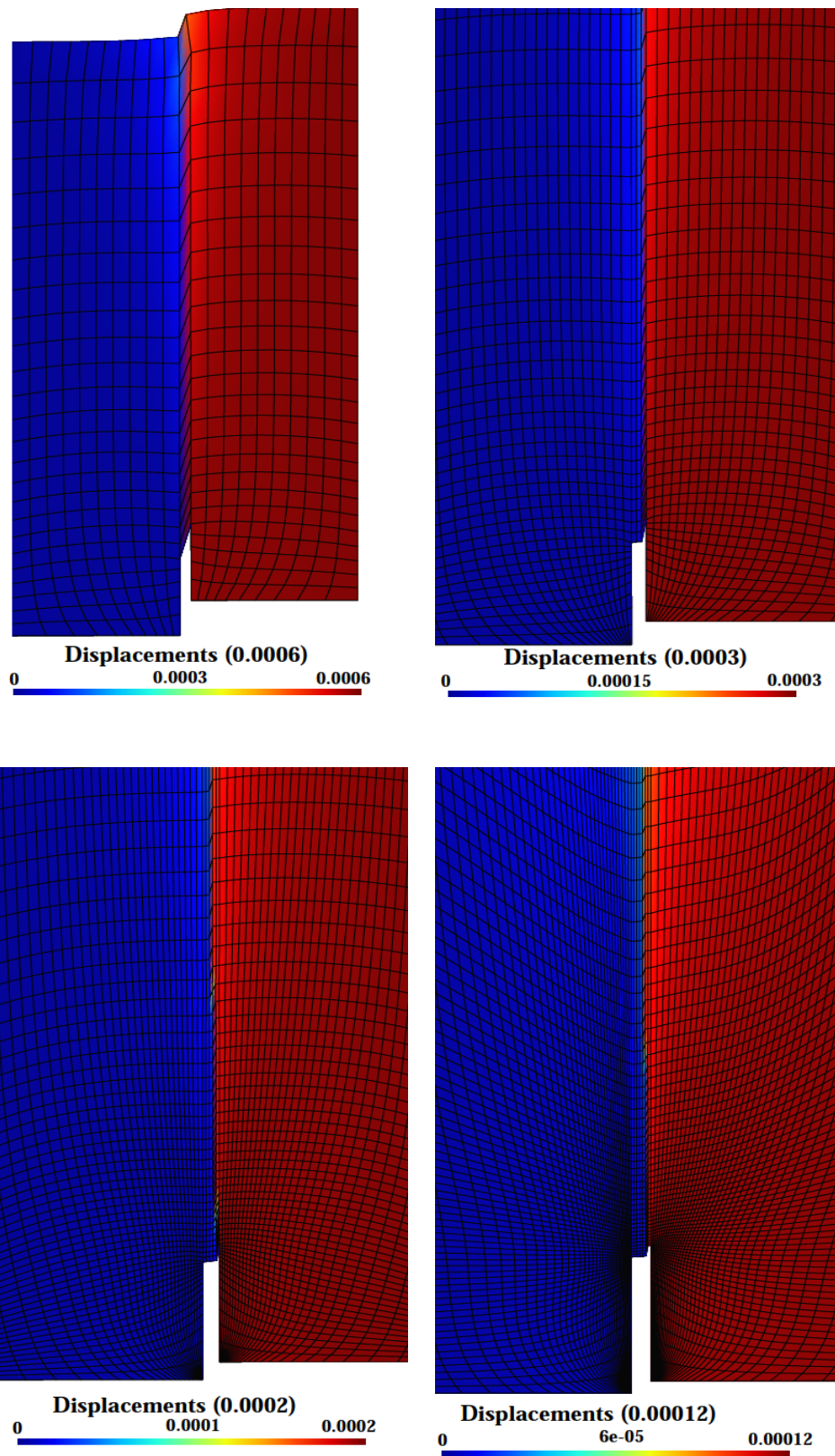


Figure 4.2: Displacement profiles under different mesh sizes at relatively steady state (adiabatic case)

Energy-based variational modelling of adiabatic shear band structure

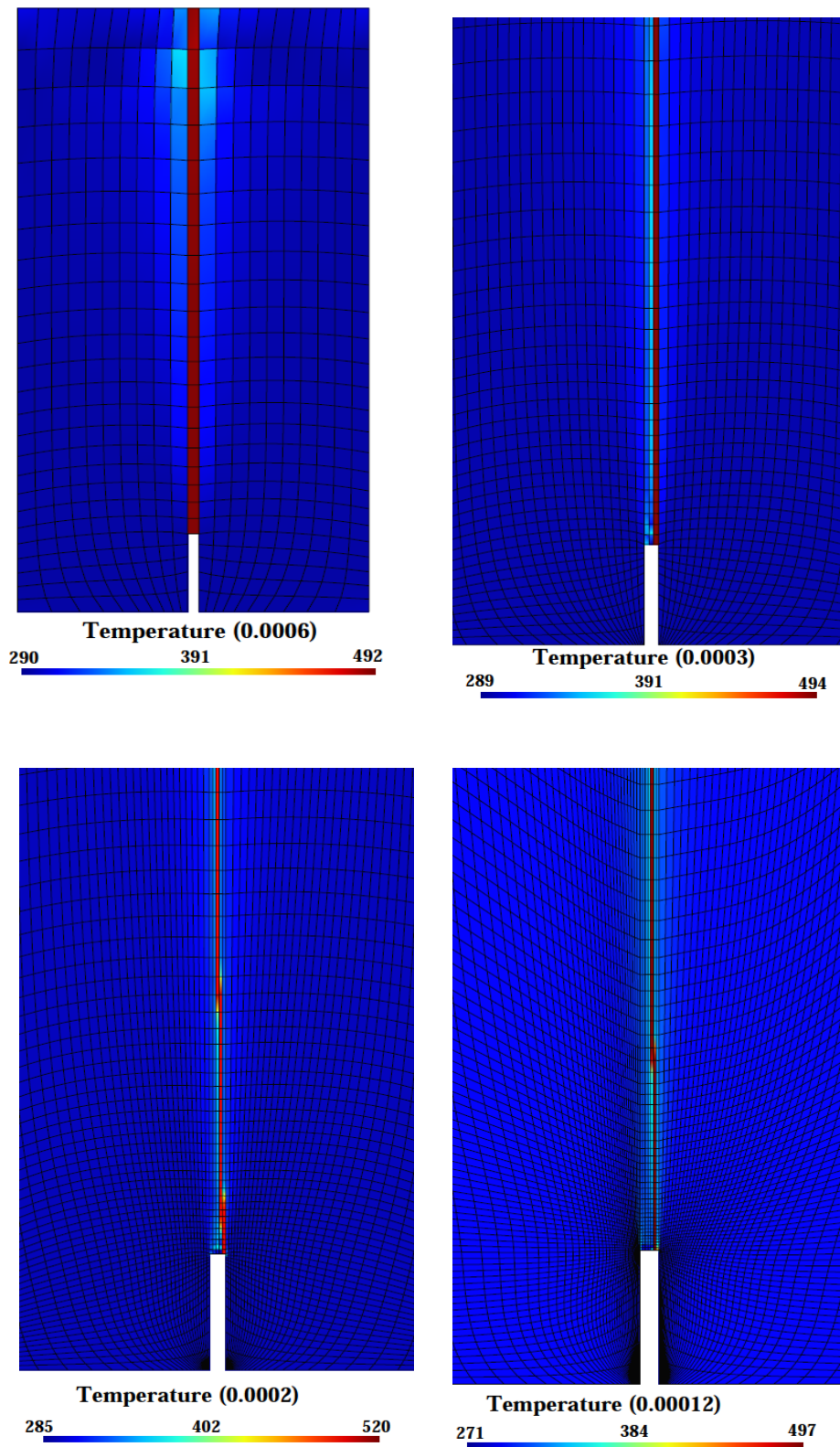


Figure 4.3: Temperature profiles under different mesh sizes at relative steady state (adiabatic case)

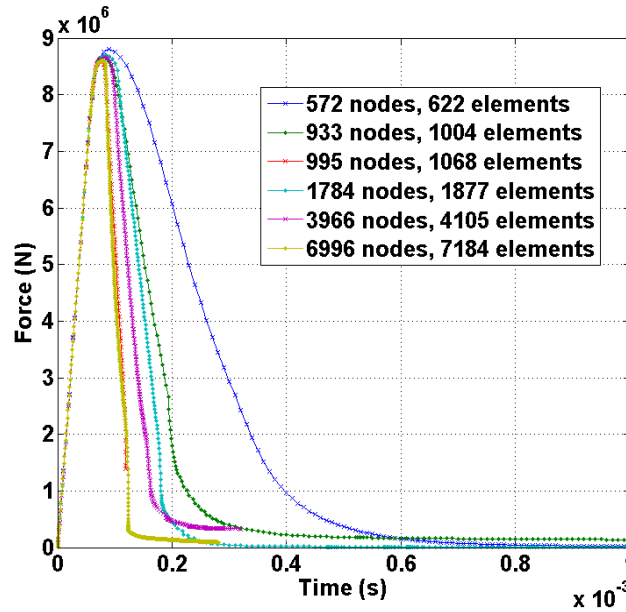


Figure 4.4: Evolution of reaction force for different mesh sizes in adiabatic case

ments and 1064 elements. The evolutions of reaction force in the modelling with thermal conduction are also analysed under different mesh sizes in FIG.4.7. Firstly, the critical force, as well as the steady force, keeps more consistency for different mesh models than that in adiabatic case, except for the first one having 622 element. The collapses of stress in 1877 elements and 1064 elements seem having a good correspondence. Yet as the models with the same mesh size in width (in front of pre-notch), they have some little differences in the speed of force dropping. Therefore for standard FEM, good simulation of ASB problem does not only need an appropriate mesh size in localization zone, but also the consideration of thermal conduction is necessary, which plays a critical role in the final term of force evolution.

From the thermo-mechanical analysis of pre-notched bar subjected to a shearing velocity, ASB phenomenon is a discontinuous phenomenon in macroscopic sight. It seems that there is a breaking band between two sides of notch, and large deformation and high temperature mainly occur in localization zone, yet the other part almost goes through a homogeneous profiles. Standard FEM can give us an approximate result with respect to its orientation, propagation, but it is unacceptable in the costing if we set the mesh size which can reflect well the localization property. Moreover, it might cause a certain ill-posedness. So some engineers recourse to reconstruct the mesh model in localization zone to decrease the time cost, which has reached a high state of maturity [Jirasek and Belytschko, 2002]. Yet the expense of mesh refinement is an unavoidable drawback, meanwhile it also brings a lot of challenges in mesh creation for dynamic fracture or interacting cracks.

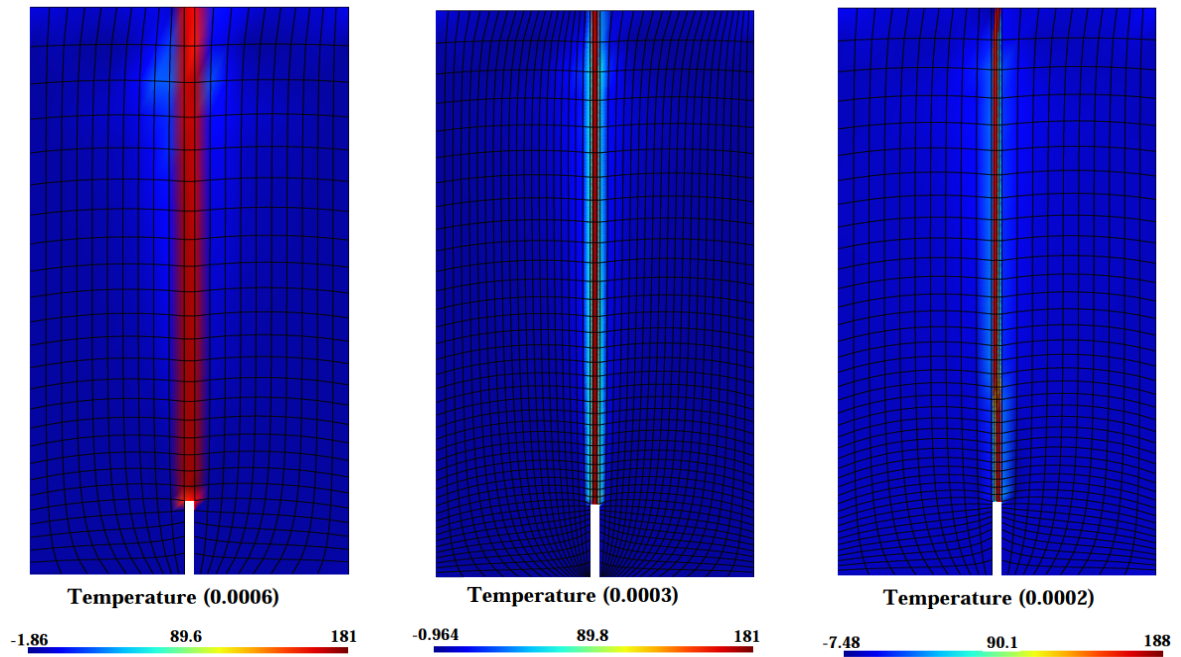


Figure 4.5: Temperature profiles under different mesh sizes at relatively steady state (modelling with thermal conduction)

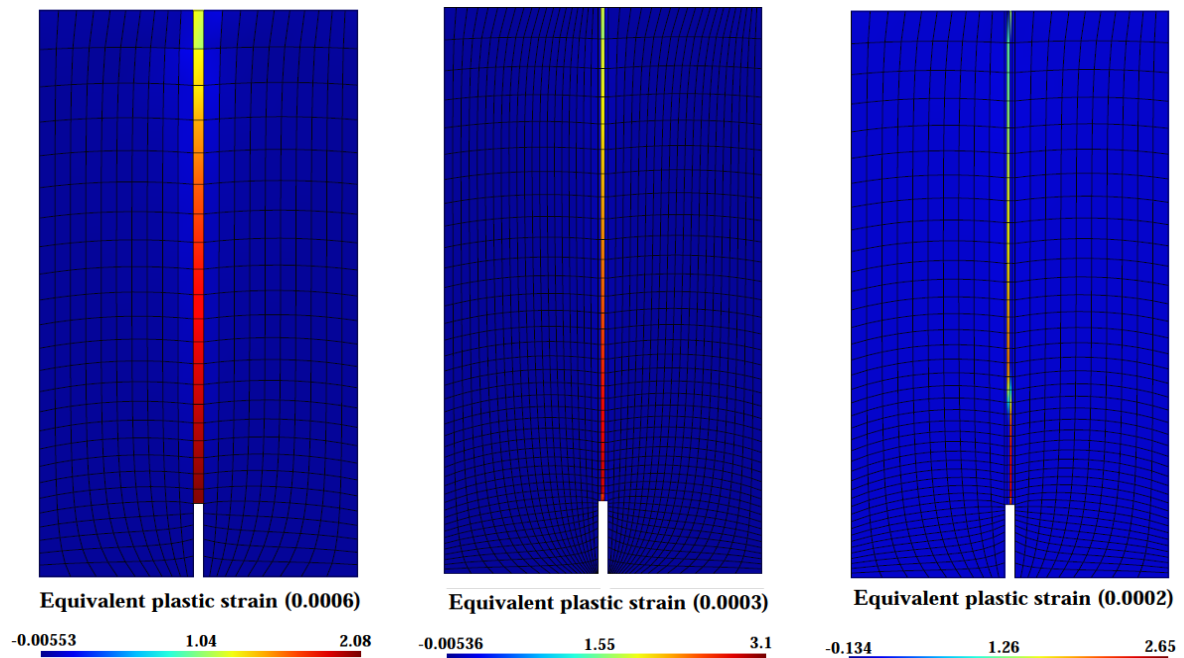


Figure 4.6: Equivalent plastic strain profiles under different mesh sizes at relatively steady state (modelling with thermal conduction)

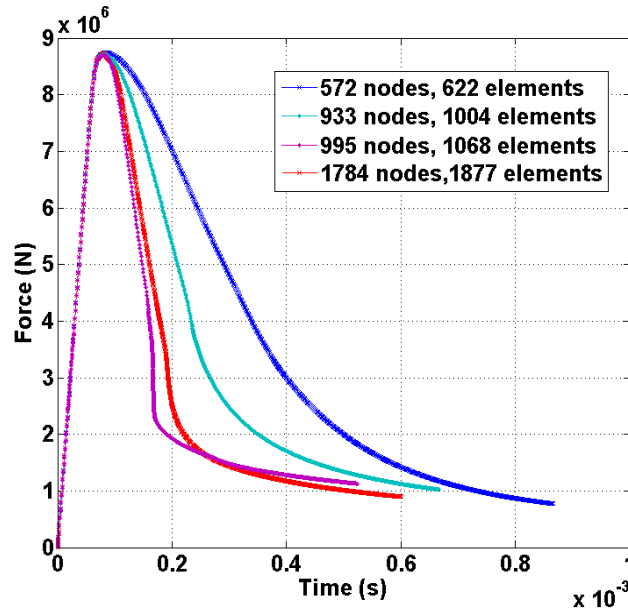


Figure 4.7: Evolution of reaction force for different mesh sizes (modelling with thermal conduction)

4.2 Variational two-scale method

In this study, we briefly revised the development of discontinuous modellings for adiabatic shear bands structure, and then proposed our variational two-scale model through interface elements.

4.2.1 Discontinuous approaches

Discontinuities are always of considerable interest in nonlinear solid mechanics, such as shear bands, multi-physical interactions. Engineers have developed some discontinuous methods to remove the unsuitable features: mesh alignment and mesh dependence in standard FEM. Some enrichments of approximated shape functions are introduced to capture the discontinuity profiles. For these discontinuous modellings, Jirasek classifies it into two categories [Jirasek and Belytschko, 2002]: explicit models of discontinuities and implicit models. The first one employs the discontinuous field by moving the mesh coinciding with discontinuity or by describing special enrichment techniques. Yet implicit model arranges the coefficient to introduce a representation of discontinuity, for instance done by smeared crack models. Here we will simply illustrate the discontinuous methods: interface element, embedded discontinuous models and extended finite element method, and point out the application of our 1D variational models for ASBs.

4.2.1.1 Interface element

Interface element was firstly proposed by Ortiz and co-workers [Ortiz and Camacho, 1996] to solve computational crack and fracture propagation in 2D, and then extended in 3D fracture mechanics as a cohesive element model [Ortiz and Pandolfi, 1999]. Recently, by means of this discontinuous method, Yang [Yang et al., 2005] applied the variational modelling with the interface element to the simulation of ASB formation. The main idea of this modelling is the coupling between cohesive surface deformation and decohesion.

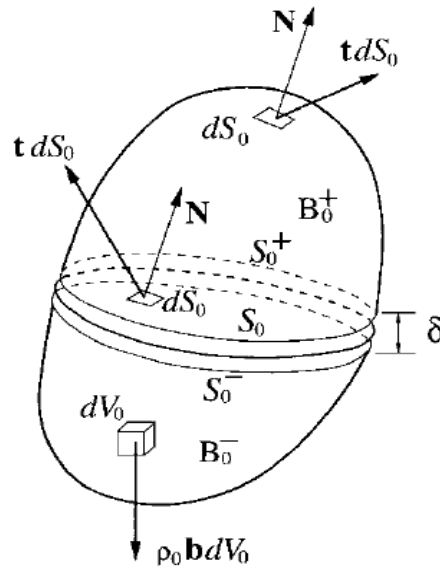


Figure 4.8: Interface element [Ortiz and Pandolfi, 1999]

Simply, interface element can be described in FIG.4.8. We suppose that there is a localization zone in domain B_0 , and the surface S_0 splits the body into two domains B_0^+ and B_0^- . As localized band occurs, the corresponding nodes on S_0 are also separated as two nodes on S_0^- and S_0^+ . The original normal direction on S_0 is defined by \mathbf{N} and the deformed one is defined as \mathbf{n} , traction force denoted by \mathbf{t} . The property of \mathbf{t} is

$$\mathbf{t} = \mathbf{P} \cdot \mathbf{N}$$

\mathbf{P} is the first Piola-Kichhroff stress conjugate to deformation gradient \mathbf{F} . So for keeping the modelling consistency on interface, the following condition should be satisfied:

$$[[\mathbf{P} \cdot \mathbf{N}]] = [[\mathbf{t}]] = 0 \quad \text{on } S_0^\pm$$

the symbol $[[\cdot]]$ means the jumping profiles. Therefore the deformation power can be obtained by the above condition and equilibrium equation as follows:

$$P^D = \sum \int_{B_0^\pm} \mathbf{P} \cdot \dot{\mathbf{F}} dV_0 + \int_{S_0} \mathbf{t} \cdot [[\dot{\varphi}]] dS_0 \quad (4.1)$$

where φ is the deformation mapping in finite configuration. So clearly the simulation of localization region concentrates on the discontinuous surface S_0 and the decohesion traction. If we works on 2D ASB problem, surface S_0 will be transformed as a line. Therefore for variational method, the importance of the interface element modelling is to find an effective free energy ϕ on S_0 satisfying:

$$\mathbf{t} = \frac{\partial \phi}{\partial \delta}$$

where we denote $\delta = [[\varphi]]$, \mathbf{t} furnishes the conjugate stress measure. Normally for the sake of avoiding mesh alignment, we adopt a coordinate transformation to the energy modelling on sliding and normal displacement (δ_n and δ_S). so:

$$\mathbf{t} = \frac{\partial \phi}{\partial \delta_n}(\delta_n, \delta_S, \mathbf{q})\mathbf{n} + \frac{\partial \phi}{\partial \delta_S}(\delta_n, \delta_S, \mathbf{q})\frac{\delta_S}{\delta_S}$$

\mathbf{q} is internal variable, such as equivalent plastic strain; $\delta_S = |\delta_S|$. Normally there is another variable in ϕ_n : deformation on surface $F^||$, Ortiz [Ortiz and Pandolfi, 1999] neglected it for simplicity. A key benefit of the potential structure of the cohesive law is that it reduces the identification of cohesive law from \mathbf{t} to total potential. Yet we should emphasize that the choice of ϕ depends on the constitutive law of traction force \mathbf{t} and displacement jump ϕ under loading conditions. Ortiz and co-workers used a standard J-integral as the critical energy release rate in ϕ to analyse crack propagation and cohesive law.

In contrast to use cohesive law, Yang [Yang et al., 2005] applied the same constitutive relation to describe the behaviour of strain-localization elements, and introduced a band thickness to build the relation between the displacement jumping and deformation gradient. In addition, the pseudo potential with this surface deformation is also considered and derived.

For the shear localization problems in thermo-mechanical coupling, the temperature of the surrounding volumes should also be included in free energy, and to some extent, the heat entropy will be a determined factor for the formulation of energy potential. Strain localization element method is comparatively easier in the analysis of ASB problem, and it fits well into the finite element analysis, and all the process to add interface element is actually like a mixed boundary condition. Yet it demands that the cracks and shear bands develop along the existing interface element edges.

4.2.1.2 Embedded discontinuity model

One reason for mesh dependence in strain localization problem is the large deformation gradient concentrated in tiny length, and standard finite element mesh can only capture its property through continuously refining the mesh in localization zone. So if we can add some discontinuous terms in the approximations of the profiles to reflect well its characters on every localized grid, normal mesh size can also track the physical aspect of localization problems.

Ortiz [Ortiz et al., 1987] redefined the shape functions aiming at reproducing the localized modes in bifurcation analysis. Termed as weak discontinuities, the high strain gradients can be expressed in the form of finite band width. Thereby a prediction of band thickness limits the development of this model. Yet if the strain jumping is so tiny that we can regard it as zero, we might as well say that material appears a strong discontinuity. The zero band width in constitutive model makes the embedded discontinuity independent on the characteristic length, as the works in [Larsson et al., 1996, Hughes and Krishna, 1998, Oliver et al., 1999, Oliver, 1996a], and the corresponding profiles of deformations will be adopted the one without the term of band width.

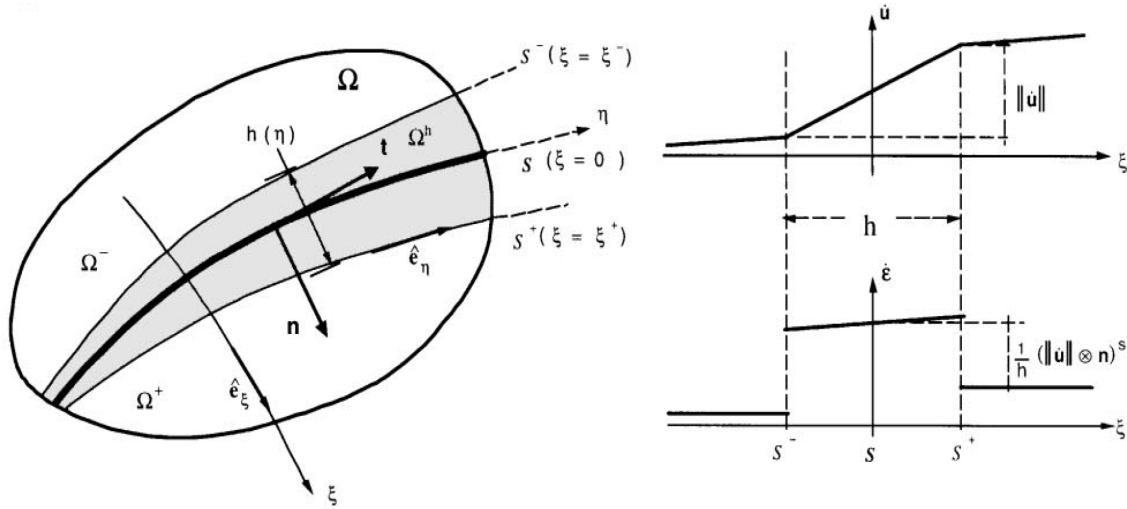


Figure 4.9: Definition of discontinuity part [Oliver, 1996b]

We suppose that there is a localization region on surface S (FIG.4.9) in the sub-domain $\Omega^h \subset \Omega$, and two modellings are divided by the length of localization domain h . When h is finite, weak discontinuity shows as FIG.4.9 demonstrated. Strong discontinuity occurs if $h \rightarrow 0$, and the strain rate will be $\delta_S([\dot{\mathbf{u}}] \otimes \mathbf{n})^S$ in this case, where δ_S is a line Dirac's delta-function. To satisfy the consistency of modelling, the governing equations for this boundary value problem should include the traction continuity besides the equilibrium equations, regarding as external imposed boundary conditions:

$$\sigma_{\Omega \setminus S}^+ \cdot \mathbf{n} = \sigma_{\Omega \setminus S}^- \cdot \mathbf{n} = \sigma_S \cdot \mathbf{n} \quad \mathbf{x} \subseteq S$$

In addition, for representing well the high strain rate in one element, an enrichment regards to displacement jumping should be added in standard FEM approximation, as the following described([Oliver et al., 1999]):

$$\dot{\mathbf{u}}(\mathbf{x}, t) = \dot{\hat{\mathbf{u}}}(\mathbf{x}, t) + H_S[[\dot{\mathbf{u}}]](\mathbf{x}, t) \quad (4.2)$$

where $\dot{\hat{\mathbf{u}}}(\mathbf{x}, t)$ is continuous C^0 displacement fields, and then kinematic strain rate is derived as([Oliver et al., 1999]):

$$\dot{\boldsymbol{\varepsilon}}(\mathbf{x}, t) = \nabla^S \dot{\hat{\mathbf{u}}} + H_S \nabla^S [[\dot{\mathbf{u}}]] + \mu_S \frac{1}{h(\eta)} ([\dot{\mathbf{u}}] \otimes \mathbf{n})^S \quad (4.3)$$

Function H_S is a step function: 1 in Ω^+ , 0 in Ω^- . μ_S is a collocation function placed in S : if $\mathbf{x} \subseteq S$, $\mu_S(\mathbf{x}) = 1$, and otherwise $\mu_S(\mathbf{x}) = 0$. For the case of strong discontinuity, the last term $\mu_S/h(\eta)$ limits to δ_S . For simplifying the numerical simulation, normally we set a characteristic function in enrichment to distinguish the elements crossed by localization parts.

Two crucial points [Rabczuk, 2007] are always discussed in the models of strain localization: the detection of loss of material stability and the constitutive models for the traction-separation law to capture the localized behaviour. For the first one, engineers prefer to adopt the mathematical condition of loss of ellipticity to judge the localization state. Oliver worked on the bifurcation propagation through this method and got the critical normal direction. Yet how to decide the transition of ASB from weak discontinuity to strong discontinuity is a considerable question. Based on the above enrichment, he proposed the variable bandwidth model using the hardening/softening law to control material states. For the second one, experimental results are also needed in discontinuous modelling to define the corresponding traction-separation law.

Embedded discontinuity method does not need to add new freedom degree, so the implementation process is more convenient. However, due to the discontinuous enrichment on the element boundaries, the nonconforming displacement approximation appears easily in the simulation. Consequently, extended finite element method is interesting to be applied, which can intrinsically get a conforming model.

4.2.1.3 Extended finite element method

In strain localization problem, discontinuity can also be introduced through a discontinuous partition of unity, called as extended finite element method (XFEM). Different from the forgoing models, it adds additional freedoms to control the approximation of partition of unity besides the discontinuous enrichment. Additionally Level-set method is also applied in this discontinuous model to represent and track the motion of discontinuity.

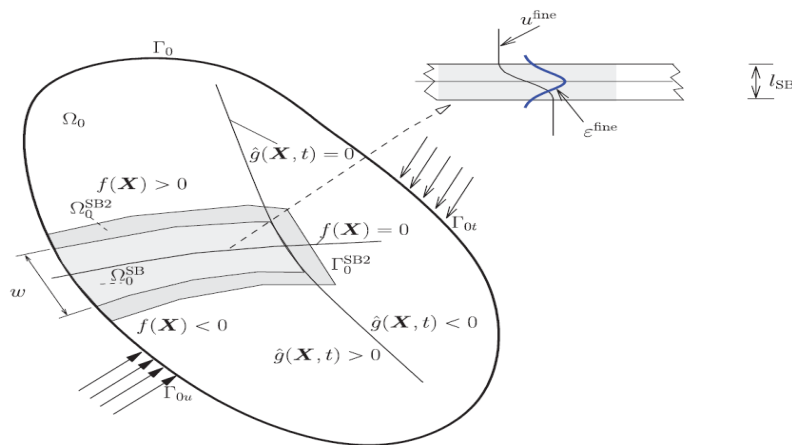


Figure 4.10: Shear band in XFEM [Areias and Belytschko, 2006]

FIG.4.10 shows a shear band width ω in Ω_0^{SB2} crossed on Ω_0 in the initial configuration. Level set functions $f(\mathbf{F})$ and $\hat{g}(\mathbf{X}, t)$ are to decide the shear localization area and front side. So the band is defined by

$$\{\mathbf{X} \in \Omega_0^{SB} \mid |f(\mathbf{X})| < \omega(\mathbf{X}) \text{ and } \hat{g}(\mathbf{X}, t) > 0\}$$

and $\Omega_0^{SB2} - \Omega_0^{SB}$ is a neutral domain, at least one layer of elements existed. The displacement for the element containing shear band can be written as:

$$\mathbf{u}(\mathbf{X}, t) = \sum_{k=1}^4 N_K(\mathbf{X}) \mathbf{u}_K(t) + [M_{m_K}(\mathbf{X}) - M_{m_K}(\mathbf{X}_K)] \mathbf{t} \alpha_K(t)$$

where \mathbf{u}_K is nodal displacement, and \mathbf{t} is the spatial unit vector tangent to the shear band. N_K is the shape function for standard FEM, and M_m is the enrichment function for localization element. Similarly, the temperature can be written as

$$T(\mathbf{X}, t) = \sum_{K=1}^4 N_K(\mathbf{X}) T_K(t) + M_T(\mathbf{X}) \beta(t)$$

M_T is the enrichment for temperature. Yet how to capture the localization character using the enrichment is important. In [Areias and Belytschko, 2006], they choose the mechanical enrichment as $\tanh(\frac{2}{l_B} f(\mathbf{X}))$, l_B is the shear band length known as a material parameter. For simulating the dynamic evolution of ASB width, they choose the linear function (the ratio of signed distance function to bandwidth) as the enrichment of displacement in [Areias and Belytschko, 2007]. Contrarily to other discontinuous methods, they introduce the minimum energy principle to identify the bandwidth in the shape enrichment. On the other hand, a symmetry linear function respecting the central line of ASB is enhanced in temperature approximation. The stability analysis of ellipticity is a critical condition to track level set and growth of band localization.

Based on the normal freedoms on standard FEM, XFEM adds new coefficients α and β on every nodal points to approximate the magnitude of discontinuity in every element. Therefore the number of resolved quantities is greater than that in normal discontinuous methods, but a good accuracy by XFEM can be obtained because of the conforming displacement approximation and the introduction of bandwidth calculation. Additionally, we donot need to set mesh direction along the occurrence of ASB, largely simplifying the mesh modelling. Consequently the described forgoing problems in localization zone, such as mesh alignment or dependence are overcome by discontinuous enrichment in XFEM.

Whichever discontinuous methods we adopts, good and adequate representation of displacement and temperature fields in ASB region are necessary conditions in all the localized modellings. In addition, two common additional laws should be intrinsically or directly illustrated in models:

- Traction-separation flow

- Heat production (entropy) on ASB zone

In 1D transient state, our variational modelling in CHAP.3 can inherently build these flow laws through the total pseudo-potential with internal variables h and T_{max} . Furthermore, canonical formulations of displacement and temperature can also be constructed as the enrichments in the foregoing three discontinuous models. Thus in next part, we will give the application of 1D variational modelling in interface elements.

4.2.2 Variational two-scale modelling

Material represents the discontinuous phenomenon at macroscopic scale owing to the shear localization zone with large deformation and high temperature in a tiny scale, actually it is not at microscopic scale. Here referred to the strain localized finite element used in [Yang et al., 2006], we will derive our variational two-scale modelling combined with the work in CHAP.3 in the terms of linearized kinematics and finite configuration. Yet initially, we suppose that the length on the normal direction of interface element is a constant, and the localization phenomenon will happen in this certain distance.

4.2.2.1 Linearized kinematics

We suppose the displacement jump $[[\mathbf{u}]]$ happened on S_0^- and S_0^+ , which has a certain distance H in the localized domain (FIG.4.8). In addition, H is so small that can be negligible compared with mesh sizes in other parts. The middle plane is S , and the normal direction is \mathbf{n} , so the strain can be defined as:

$$\boldsymbol{\varepsilon} = \boldsymbol{\varepsilon}_e + \boldsymbol{\varepsilon}_p$$

where

$$\boldsymbol{\varepsilon}_e = \boldsymbol{\varepsilon}^{\parallel} + \frac{[[\mathbf{u}]] \cdot \mathbf{n}}{H} \mathbf{n} \otimes \mathbf{n} + \frac{1}{2}(\boldsymbol{\gamma}^e \otimes \mathbf{n} + \mathbf{n} \otimes \boldsymbol{\gamma}^e)$$

$\boldsymbol{\varepsilon}^{\parallel}$ is the membrane strain within discontinuity plane. $\boldsymbol{\gamma}^e$ is the shearing elastic strain, which we restate as homogeneous through thickness, such that:

$$\dot{\boldsymbol{\gamma}}^e = \frac{\dot{u}^{te}}{H} \mathbf{t} \quad \text{and} \quad \boldsymbol{\gamma}^e \cdot \mathbf{n} = 0$$

where u^{te} is unknown parameter depending on the displacement jumping. \mathbf{t} is the unit vector aligned with $[[\dot{\mathbf{u}}]]^t = [[\dot{\mathbf{u}}]] - (([[\dot{\mathbf{u}}]] \cdot \mathbf{n})\mathbf{n}$, and plastic strain is denoted as:

$$\boldsymbol{\varepsilon}_p = \frac{1}{2}(\boldsymbol{\gamma}^p(\eta) \otimes \mathbf{n} + \mathbf{n} \otimes \boldsymbol{\gamma}^p(\eta)) \quad \text{and} \quad \boldsymbol{\gamma}^p(\eta) \cdot \mathbf{n} = 0$$

where $\dot{\boldsymbol{\gamma}}^p(\eta) = \dot{\boldsymbol{\gamma}}^p(\eta)\mathbf{t}$. Thereby for keeping the consistency with the global profile, the following conditions should be satisfied:

$$\int_0^H \mathbf{n} \cdot \boldsymbol{\varepsilon} \cdot \mathbf{n} d\eta = [[\mathbf{u}]] \cdot \mathbf{n}$$

$$\int_0^H (\dot{\gamma}^e + \dot{\gamma}^p(\eta)) d\eta = [[\dot{\mathbf{u}}]] - ([[\dot{\mathbf{u}}]] \cdot \mathbf{n}) \mathbf{n} = [[\dot{\mathbf{u}}]]^t$$

Simply, we note $u^n = [[\mathbf{u}]] \cdot \mathbf{n}$ and $\dot{u}^t = [[\dot{\mathbf{u}}]] \cdot \mathbf{t}$.

The total potential of interface element is written as:

$$\Phi(u, T) = \int_{B_0^\pm} \phi(u, T) dV + \int_S \phi(\varepsilon^\parallel, T, [[\mathbf{u}]], T_b) dS \quad (4.4)$$

Where T_b is the temperature of the surrounding matrix, and the potential in discontinuity ϕ is equal to:

$$\phi(\varepsilon^\parallel, T, [[\mathbf{u}]], T_b) = \int_0^H \phi_1(\varepsilon^\parallel, u^n, u^t, \gamma^p(\eta), T_b, T) d\eta \quad (4.5)$$

How to decide the form of ϕ is the main work in this modelling. Considering a time increment $[t_n, t_{n+1}]$, and supposing $[\varepsilon_n^\parallel, [[\mathbf{u}]]_n, T_{b_n}]$ is known, we adopt the work in CHAP.3 and define the incremental potential as:

$$\phi_{n+1}(\varepsilon_{n+1}^\parallel, [[\mathbf{u}]]_{n+1}, T_{b_{n+1}}) = \underset{h_{V_{n+1}}, h_{T_{n+1}}, T_{max_{n+1}}, \bar{u}_{n+1}^{tP}}{Stat} \phi_{n+1}^* \quad (4.6)$$

where

$$\begin{aligned} \phi_{n+1}^* &= \int_{-\frac{H}{2}}^{\frac{H}{2}} W^e(\varepsilon_{n+1}^e, u_{n+1}^t, \varepsilon_{n+1}^\parallel, u_{n+1}^n) - W^e(\varepsilon_n^e, u_n^t, \varepsilon_n^\parallel, u_n^n) \\ &+ W^p(\bar{\varepsilon}_{n+1}^p, T_{n+1}) - W^p(\bar{\varepsilon}_n^p, T_n) + W^{th}(T_{n+1}) - W^{th}(T_n) + \rho_0 \eta_n (T_{n+1} - T_n) \\ &+ \Delta t \Psi^* \left(\frac{T_{n+1}}{T_n} \bar{\varepsilon}_{n+1}^p, \bar{\varepsilon}_n^p, T_n \right) - \Delta t \frac{1}{2} \lambda T_n \left(\frac{\partial T_{n+1}}{\partial \eta} \frac{1}{T_{n+1}} \right)^2 d\eta \end{aligned}$$

Moreover, it stands for the case that velocity and temperature are inhomogeneous in the band approximated as the canonical formulations. According to the optimization conditions, the following formulations can be received:

$$\frac{\partial \phi_{n+1}^*}{\partial h_{V_{n+1}}} = 0; \quad \frac{\partial \phi_{n+1}^*}{\partial h_{T_{n+1}}} = 0; \quad \frac{\partial \phi_{n+1}^*}{\partial T_{max_{n+1}}} = 0; \quad \frac{\partial \phi_{n+1}^*}{\partial \bar{u}_{n+1}^{tP}} = 0;$$

Normally we consider the perturbations:

$$\begin{aligned} \varepsilon_{n+1}^\parallel &\rightarrow \varepsilon_{n+1}^\parallel + \delta \varepsilon_{n+1}^\parallel; & [[\mathbf{u}]]_{n+1} &\rightarrow [[\mathbf{u}]]_{n+1} + \delta [[\mathbf{u}]]_{n+1}; \\ T_{max_{n+1}} &\rightarrow T_{max_{n+1}} + \delta T_{max_{n+1}}; & h_{T_{n+1}} &\rightarrow h_{T_{n+1}} + \delta h_{T_{n+1}}; \\ \bar{u}_{n+1}^{tP} &\rightarrow \bar{u}_{n+1}^{tP} + \delta \bar{u}_{n+1}^{tP}; & T_{b_{n+1}} &\rightarrow T_{b_{n+1}} + \delta T_{b_{n+1}}; \\ h_{V_{n+1}} &\rightarrow h_{V_{n+1}} + \delta h_{V_{n+1}}; \end{aligned}$$

so the variation of ϕ_n^* is described as

$$\begin{aligned} \delta\phi_{n+1}^* = & \frac{\partial\phi_{n+1}^*}{\partial\varepsilon_{n+1}^{\parallel}}\delta\varepsilon_{n+1}^{\parallel} + \frac{\partial\phi_{n+1}^*}{\partial u_{n+1}^n}\mathbf{n}\delta[[\mathbf{u}]]_{n+1} + \frac{\partial\phi_{n+1}^*}{\partial u_{n+1}^t}\mathbf{t}\delta[[\mathbf{u}]]_{n+1} + \frac{\partial\phi_{n+1}^*}{\partial T_{b_{n+1}}}\delta T_{b_{n+1}} \\ & + \frac{\partial\phi_{n+1}^*}{\partial h_{v_{n+1}}}\delta h_{v_{n+1}} + \frac{\partial\phi_{n+1}^*}{\partial h_{T_{n+1}}}\delta h_{T_{n+1}} + \frac{\partial\phi_{n+1}^*}{\partial T_{max_{n+1}}}\delta T_{max_{n+1}} + \frac{\partial\phi_{n+1}^*}{\partial \bar{u}_{n+1}^{tp}}\delta \bar{u}_{n+1}^{tp} \end{aligned}$$

Considering the stationary condition about $h_{v_{n+1}}$, $h_{T_{n+1}}$, $T_{max_{n+1}}$ and \bar{u}_{n+1}^{tp} , we can write the variations of ϕ_{n+1} as:

$$\delta\phi_{n+1} = \frac{\partial\phi_{n+1}^*}{\partial\varepsilon_{n+1}^{\parallel}}\delta\varepsilon_{n+1}^{\parallel} + \frac{\partial\phi_{n+1}^*}{\partial u_{n+1}^n}\mathbf{n}\delta[[\mathbf{u}]]_{n+1} + \frac{\partial\phi_{n+1}^*}{\partial u_{n+1}^t}\mathbf{t}\delta[[\mathbf{u}]]_{n+1} + \frac{\partial\phi_{n+1}^*}{\partial T_{b_{n+1}}}\delta T_{b_{n+1}}$$

here $\frac{\partial\phi_{n+1}^*}{\partial T_{n+1}} = 0$. So the modelling of interface element can be built with recourse to the 1D variational modelling in CHAP.3. The potential in localized domain is transformed as the forms on discontinuous plane and the surrounding element profiles. If the localization problem is in 2D, S will be just a line.

4.2.2.2 Finite kinematics

We denote \mathbf{N} the unit vector normal to the discontinuous plane (oriented from side - to side +), and \mathbf{n} is the one in the deformed configuration. The deformation gradient \mathbf{F} is decomposed as:

$$\mathbf{F} = \mathbf{F}^e \mathbf{F}^p$$

The elastic deformation is assumed to be homogeneous through the shear band thickness, defined as:

$$\mathbf{F}^e = \mathbf{F}^{\parallel} + \frac{[[\mathbf{u}]] \cdot \mathbf{n}}{H} \mathbf{n} \otimes \mathbf{N} + \gamma^e \otimes \mathbf{N}$$

where \mathbf{F}^{\parallel} is the deformed gradient in discontinuous plane, and $\mathbf{F}^{\parallel} \mathbf{N} = \mathbf{n}$. γ^e is elastic shear deformation, written as:

$$\dot{\gamma}^e = \dot{\gamma}^e \tilde{\mathbf{t}} = \dot{\tilde{\gamma}}^e \mathbf{t} \quad (4.7)$$

where \mathbf{t} is the unit vector aligned with the tangential velocity jump $[[\dot{\mathbf{u}}]]^t$, defined as:

$$[[\dot{\mathbf{u}}]]^t = [[\dot{\mathbf{u}}]] - (([\dot{\mathbf{u}}]] \cdot \mathbf{n}) \mathbf{n}$$

and

$$\mathbf{F}^{\parallel} \mathbf{T} = \tilde{\mathbf{t}}$$

\mathbf{T} is the unit vector aligned with $\mathbf{F}^{\parallel -1} [[\dot{\mathbf{u}}]]^t$. γ^e and $\tilde{\gamma}^e$ are all scalars, which depend on $i^t = (\mathbf{F}^{\parallel -1} [[\dot{\mathbf{u}}]]^t) \cdot \mathbf{T}$. For the plastic deformation \mathbf{F}^p , we assume that it is inhomogeneous through thickness, and a general formula is defined as follows:

$$\mathbf{F}^p = \mathbf{I} + \gamma^p(\eta) \otimes \mathbf{N}$$

where $\eta \in [0, H]$. According to the above definition about \mathbf{T} , γ^e and γ^p are orthogonal to \mathbf{N} :

$$\gamma^p(\eta) \cdot \mathbf{N} = 0; \quad \gamma^e \cdot \mathbf{N} = 0;$$

The velocity is then written as:

$$\mathbf{D}^p = \dot{\mathbf{F}}^p \mathbf{F}^{p-1} = \dot{\gamma}^p(\eta) \otimes \mathbf{N}$$

and the equivalent plastic strain in J2 Von Mises law is obtained by :

$$\dot{\epsilon}^p = \sqrt{\frac{2}{3} \mathbf{D}^p \cdot \mathbf{D}^p} = \sqrt{\frac{2}{3}} \dot{\gamma}^p$$

Combined with the decomposition of \mathbf{F}^e and \mathbf{F}^p , the deformation gradient \mathbf{F} can also be described as:

$$\mathbf{F} = \mathbf{F}^{\parallel} \mathbf{F}^{\perp} \quad (4.8)$$

where

$$\mathbf{F}^{\perp} = \mathbf{I} + \frac{[[\mathbf{u}]] \cdot \mathbf{n}}{H} \mathbf{N} \otimes \mathbf{N} + \gamma^e \mathbf{T} \otimes \mathbf{N} + \gamma^p(\eta) \otimes \mathbf{N}$$

In order to be consistent with the macroscopic velocity jump, the deformation gradient must have the properties as follows:

$$\int_0^H (\dot{\gamma}^e + \dot{\gamma}^p(\eta)) d\eta = \mathbf{F}^{\parallel-1} [[\dot{\mathbf{u}}]]^t \cdot \mathbf{T}$$

$$\int_0^H \mathbf{n} \cdot \mathbf{F} \cdot \mathbf{N} d\eta = [[\mathbf{u}]] \cdot \mathbf{n}$$

Here we should mention that there is only one temperature field existed for two surfaces S_0^- and S_0^+ , contrarily a new group of displacement fields for $[[\mathbf{u}]]$ are added in our modelling. Hence the consistency of temperature in discontinuity works automatically.

If denoting $\mathbf{F}^{\parallel-1} [[\dot{\mathbf{u}}]] \cdot \mathbf{T}$ as u^t , $[[\mathbf{u}]] \cdot \mathbf{n}$ as u^n , the 1D modelling $\phi^*(\mathbf{F}^{\parallel}, u^n, u^t, T_b)$ described in (4.5) is also applied in finite kinematics. In similar manner, a new group of variables $[\mathbf{F}_{n+1}^{\parallel}, [[\mathbf{u}]]_{n+1}, T_{b_{n+1}}]$ will be calculated over time increment $[t_n, t_{n+1}]$, assuming $[\mathbf{F}_n^{\parallel}, [[\mathbf{u}]]_n, T_{b_n}]$ known. Similar to the variational derivation described in the linear kinematics, we can also prove that the variations of potential in localization can be represented through the discontinuous plane:

$$\begin{aligned} \delta\Phi_{n+1} &= \int_{B_0^\pm} \frac{\partial\Phi_{n+1}}{\partial\mathbf{F}_{n+1}} \delta\mathbf{F}_{n+1} + \frac{\partial\Phi_{n+1}}{\partial T_{n+1}} \delta T_{n+1} dv + \\ &\int_S \frac{\partial\phi_{n+1}^*}{\partial\mathbf{F}_{n+1}^{\parallel}} \delta\mathbf{F}_{n+1}^{\parallel} + \frac{\partial\phi_{n+1}^*}{\partial T_{b_{n+1}}} \delta T_{b_{n+1}} + \\ &\frac{\partial\phi_{n+1}^*}{\partial u_{n+1}^n} \mathbf{n} \delta[[\mathbf{u}]]_{n+1} + \frac{\partial\phi_{n+1}^*}{\partial u_{n+1}^t} \frac{\partial u_{n+1}^t}{\partial [[\mathbf{u}]]_{n+1}} \delta[[\mathbf{u}]]_{n+1} dS \end{aligned} \quad (4.9)$$

where the perturbations $\delta \mathbf{F}_{n+1}$, δT_{n+1} , $\delta \mathbf{F}_{n+1}^{\parallel}$, $\delta [[\mathbf{u}]]_{n+1}$ and $\delta T_{b_{n+1}}$ are arbitrary.

Combined with 1D energy-based variational modelling, we applied the strain localized finite element inferred into normal elements to reflect well the localization profiles. Contrary to the previous work, a normal deformation gradient formula is proposed including the inhomogeneous plastic strain. In addition, we also propose the variational two-scale model in view of linear deformation and finite configuration. The following feature is presented in our modelling:

$$\frac{\partial \phi^*}{\partial u^t} = \tau_{average}$$

Therefore the traction-separation law FIG.4.11(a) and the entropy created on discontinuity FIG.4.11(b) can be well demonstrated through our variational model with ordinary material property.

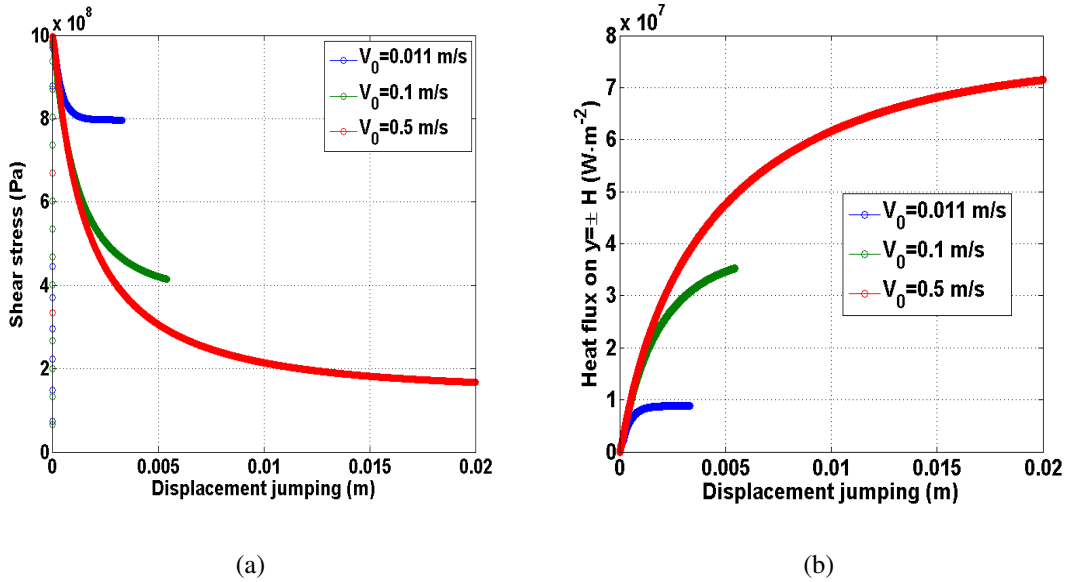


Figure 4.11: Traction-separation law (a) and heat production (b) on discontinuity for exponential softening law

4.3 Finite element implementation

4.3.1 Finite element modelling

Strain localization element fits well into the implementation of FEM. For the elements crossed by shear band, we pre-set two nodes on the same geometrical node in the reference configuration (FIG.4.3.1). Thus if the surface element S has n nodes, the total number of

nodes in strain localization element is $2n$ (S^+ and S^-). Yet the temperature freedom still keeps one in two surfaces. Overall, it is alike as a mixed boundary condition when dealing with interface element in FEM.

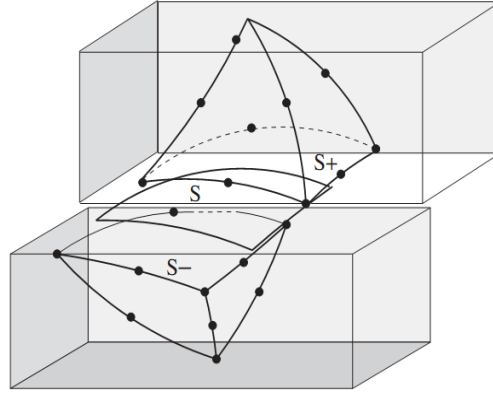


Figure 4.12: Shear band element[Ortiz and Pandolfi, 1999]

We denote $N_a(s_1, s_2)$ $a = 1, \dots, n$ as the standard shape function, where (s_1, s_2) are the natural co-ordinates of each of the surface elements in some convenient standard configuration. So the discontinuous element on the two surfaces is defined as:

$$\mathbf{X} = \sum_{a=1}^n \bar{\mathbf{X}}_a N_a(s) \quad (4.10)$$

where

$$\bar{\mathbf{X}}_a = \frac{1}{2}(\mathbf{X}_a^+ + \mathbf{X}_a^-)$$

\mathbf{X}^\pm is the co-ordinates of the nodes in the undeformed configuration of the element. The corresponding tangent basis vectors are obtained by:

$$G_\alpha(\mathbf{s}) = \sum_{a=1}^n \bar{\mathbf{X}}_a N_{a,\alpha}(s)$$

the unit normal to S (from S^- to S^+) is then:

$$\mathbf{N} = \frac{G_1 \times G_2}{|G_1 \times G_2|} \quad (4.11)$$

Similarly, the displacement jump is defined as:

$$[[\mathbf{u}]] = \sum_{a=1}^n [[\mathbf{x}]]_a N_a(s) \quad (4.12)$$

where

$$[[\mathbf{x}]]_a = \mathbf{x}_a^+ - \mathbf{x}_a^-$$

where \mathbf{x}_a^\pm are the co-ordinates of the nodes in the deformed configuration. The node force in the interface element can be written as follows:

$$\begin{aligned} f_{ia}^\pm &= \frac{\partial}{\partial x_{ia}^\pm} \int_S \phi_{n+1}(\mathbf{F}_{n+1}^\parallel, [[u]]_{n+1}, T_{b_{n+1}}) dS \\ &= \int_S \frac{\partial \phi_{n+1}}{\partial \mathbf{F}_{n+1}^\parallel} \frac{\partial \mathbf{F}_{n+1}^\parallel}{\partial x_{ia}^\pm} + \frac{\partial \phi_{n+1}}{\partial u_{n+1}^n} \frac{\partial u_{n+1}^n}{\partial x_{ia}^\pm} + \frac{\partial \phi_{n+1}}{\partial u_{n+1}^t} \frac{\partial u_{n+1}^t}{\partial x_{ia}^\pm} dS \end{aligned} \quad (4.13)$$

and the corresponding tangent matrix in mechanical part is derived as:

$$\begin{aligned} K_{iajb} &= \frac{\partial f_{ia}^\pm}{\partial x_{jb}^\pm} = \int_S \frac{\partial^2 \phi_{n+1}}{\partial \mathbf{F}_{n+1}^\parallel{}^2} \frac{\partial \mathbf{F}_{n+1}^\parallel}{\partial x_{jb}^\pm} \frac{\partial \mathbf{F}_{n+1}^\parallel}{\partial x_{ia}^\pm} + \frac{\partial \phi_{n+1}}{\partial \mathbf{F}_{n+1}^\parallel} \frac{\partial^2 \mathbf{F}_{n+1}^\parallel}{\partial x_{ia}^\pm \partial x_{jb}^\pm} + \\ &\quad \frac{\partial^2 \phi_{n+1}}{\partial u_{n+1}^n{}^2} \frac{\partial u_{n+1}^n}{\partial x_{jb}^\pm} \frac{\partial u_{n+1}^n}{\partial x_{ia}^\pm} + \frac{\partial \phi_{n+1}}{\partial u_{n+1}^n} \frac{\partial^2 u_{n+1}^n}{\partial x_{ia}^\pm \partial x_{jb}^\pm} + \\ &\quad \frac{\partial^2 \phi_{n+1}}{\partial u_{n+1}^t{}^2} \frac{\partial u_{n+1}^t}{\partial x_{jb}^\pm} \frac{\partial u_{n+1}^t}{\partial x_{ia}^\pm} + \frac{\partial \phi_{n+1}}{\partial u_{n+1}^t} \frac{\partial^2 u_{n+1}^t}{\partial x_{ia}^\pm \partial x_{jb}^\pm} dS \end{aligned} \quad (4.14)$$

In the finite element method for thermo-mechanical coupling, we adopt the same shape function to approximate the temperature profile, defined as:

$$T = \sum_{a=1}^n N_a(\mathbf{s}) T_a$$

where T_a $a = 1, \dots, n$ is the temperature at node. The nodal entropy in the interface element is described as:

$$\frac{\partial \phi_{n+1}}{\partial T_i} = \frac{\partial \phi_{n+1}}{\partial T_b} N_i \quad (4.15)$$

and regarding to (4.13), the coupling of thermal mechanics is derived as:

$$\frac{\partial f_{ia}^\pm}{\partial T_j} = \frac{\partial^2 \phi_{n+1}}{\partial u_{n+1}^t \partial T_{b_{n+1}}} \frac{\partial u_{n+1}^t}{\partial x_{ia}^\pm} N_j \quad (4.16)$$

Following (4.15), we can derive the second order of ϕ_{n+1} about temperature:

$$\frac{\partial^2 \phi_{n+1}}{\partial T_i \partial T_j} = \frac{\partial^2 \phi_{n+1}}{\partial T_b^2} N_i N_j \quad (4.17)$$

Therefore if we want to determine the specific formulations of node force and tangent matrix for interface elements, two parts of derivations should be known: thermo-mechanical flux and strain or direction derivations (in Appendix B), such as $\frac{\partial \mathbf{F}_{n+1}^\parallel}{\partial x_{ia}^\pm}$, $\frac{\partial u_{n+1}^t}{\partial x_{ia}^\pm}$.

4.3.2 Thermo-mechanical flux

In 1D variational potential ϕ_{n+1}^* , we can also write the elastic potential W_{n+1}^e as:

$$W_{n+1}^e = W_{1_{n+1}}^e(\mathbf{F}^{\parallel}, u_{n+1}^n) + W_{2_{n+1}}^e(u_{n+1}^t, \bar{u}_{n+1}^{tP})$$

According to the definition of deformation gradient, $\mathbf{F}_{n+1}^{\parallel}$ and u_{n+1}^n are the elastic components and independent on the internal parameters: h_V , h_T , T_{max} and \bar{u}^{tP} . So the fluxes about these two components are similar to the ones of finite elements in linear elastic problem, here we do not give its relative formulas of stress and force.

In view of (4.5), we might as well use :

$$\phi(\mathbf{F}^{\parallel}, u^n, u^t, T_b) = \phi^*(h_V^*, h_T^*, T_{max}^*, \bar{u}^{tP*}, \mathbf{F}^{\parallel}, u^n, u^t, T_b) \quad (4.18)$$

which h_V^* , h_T^* , T_{max}^* , \bar{u}^{tP*} are the optimized values making the pseudo-potential in 1D shearing problem have the optimizations with respect to displacement and temperature.

- If the material is in elasticity, the dissipation in total potential will be equal to 0, and two cases exist according to \bar{u}_n^{tP} :

- $\bar{u}_n^{tP} = 0$

In this state, material is in the initial term. The increase of loading only has influence on mechanical part, and the temperature still keeps the consistency with the surrounding temperature. So thermo-mechanical flux and their derivations are written as follows:

$$\begin{aligned} \frac{\partial \phi_{n+1}}{\partial u_{n+1}^t} &= \frac{\partial W_{2_{n+1}}^e}{\partial u_{n+1}^t}(u_{n+1}^t, \bar{u}_n^{tP}); & \frac{\partial^2 \phi_{n+1}}{\partial u_{n+1}^t{}^2} &= \frac{\partial^2 W_{2_{n+1}}^e}{\partial u_{n+1}^t{}^2}(u_{n+1}^t, \bar{u}_n^{tP}); \\ \frac{\partial \phi_{n+1}}{\partial T_{b_{n+1}}} &= 0; & \frac{\partial^2 \phi_{n+1}}{\partial u_{n+1}^t \partial T_{b_{n+1}}} &= 0; & \frac{\partial^2 \phi_{n+1}}{\partial T_{b_{n+1}}{}^2} &= 0; \end{aligned} \quad (4.19)$$

- $\bar{u}_n^{tP} \neq 0$

Material is under unloading. The total potential will illustrate a simple heat problem. The dissipation part is zero, mechanical flux and derivation agree with the ones in the initial term. Because of heat conduction, thermal flux and its derivation will have some changes:

$$\begin{aligned} \frac{\partial \phi_{n+1}}{\partial T_{b_{n+1}}} &= \frac{\partial \phi_{n+1}^*}{\partial T_{b_{n+1}}}(h_{V_n}^*, h_{T_{n+1}}^*, T_{max_{n+1}}^*, \bar{u}_n^{tP*}); \\ \frac{\partial^2 \phi_{n+1}}{\partial T_{b_{n+1}}{}^2} &= \frac{\partial^2 \phi_{n+1}^*}{\partial h_{T_{n+1}} \partial T_{b_{n+1}}} \frac{\partial h_{T_{n+1}}}{\partial T_{b_{n+1}}} + \frac{\partial^2 \phi_{n+1}^*}{\partial T_{max_{n+1}} \partial T_{b_{n+1}}} \frac{\partial T_{max_{n+1}}}{\partial T_{b_{n+1}}}; \end{aligned} \quad (4.20)$$

Two unknown parameters appear in the second order derivation about $T_{b_{n+1}}$: $\frac{\partial h_{T_{n+1}}}{\partial T_{b_{n+1}}}$, $\frac{\partial T_{max_{n+1}}}{\partial T_{b_{n+1}}}$. Here by means of the optimization conditions about $h_{T_{n+1}}$, $T_{max_{n+1}}$, we

can get:

$$\frac{\partial}{\partial T_{b_{n+1}}} \left(\frac{\partial \phi_{n+1}^*}{\partial T_{max_{n+1}}} \right) = 0; \quad \frac{\partial}{\partial T_{b_{n+1}}} \left(\frac{\partial \phi_{n+1}^*}{\partial h_{T_{n+1}}} \right) = 0; \quad (4.21)$$

Therefore a system of linear equations about two variables is built as follows:

$$\begin{bmatrix} \frac{\partial \phi_{n+1}^*}{\partial h_{T_{n+1}}^2} & \frac{\partial \phi_{n+1}^*}{\partial h_{T_{n+1}} \partial T_{max_{n+1}}} \\ \text{sym.} & \frac{\partial \phi_{n+1}^*}{\partial T_{max_{n+1}}^2} \end{bmatrix} \begin{bmatrix} \frac{\partial h_{T_{n+1}}}{\partial T_{b_{n+1}}} \\ \frac{\partial T_{max_{n+1}}}{\partial T_{b_{n+1}}} \end{bmatrix} = - \begin{bmatrix} \frac{\partial \phi_{n+1}^*}{\partial h_{T_{n+1}} \partial T_{b_{n+1}}} \\ \frac{\partial \phi_{n+1}^*}{\partial T_{max_{n+1}} \partial T_{b_{n+1}}} \end{bmatrix}$$

The corresponding values $\frac{\partial h_{T_{n+1}}}{\partial T_{b_{n+1}}}$ and $\frac{\partial T_{max_{n+1}}}{\partial T_{b_{n+1}}}$ can be obtained by simple equation solver.

- When the material is in plasticity, the derivation about h_V and \bar{u}^{tP} will be involved in thermo-mechanical flux, making the problem more complicated. Yet the formula of average stress keeps consistency with the case in elasticity:

$$\frac{\partial \phi_{n+1}}{\partial u_{n+1}^t} = \frac{\partial W_{2_{n+1}}^e}{\partial u_{n+1}^t} (u_{n+1}^t, \bar{u}_{n+1}^{tP*}) \quad (4.22)$$

The second order derivation of u_{n+1}^t will include the derivation part of \bar{u}_{n+1}^{tP*} :

$$\frac{\partial^2 \phi_{n+1}}{\partial u_{n+1}^t{}^2} = \frac{\partial^2 W_{2_{n+1}}^e}{\partial u_{n+1}^t{}^2} + \frac{\partial^2 \phi_{n+1}^*}{\partial u_{n+1}^t \partial \bar{u}_{n+1}^{tP}} \frac{\partial \bar{u}_{n+1}^{tP}}{\partial u_{n+1}^t} \quad (4.23)$$

an unknown value $\frac{\partial \bar{u}_{n+1}^{tP}}{\partial u_{n+1}^t}$ appeared in the calculation of second order of ϕ_{n+1} about u_{n+1}^t . Here we will use the optimization condition about \bar{u}_{n+1}^{tP} to analyse this component. Obviously, ϕ_{n+1} has the feature as:

$$\frac{\partial}{\partial u_{n+1}^t} \left(\frac{\partial \phi_{n+1}^* (h_V^*, h_T^*, T_{max}^*, \bar{u}_{n+1}^{tP*})}{\partial \bar{u}_{n+1}^{tP}} \right) = 0$$

Following it, we can get:

$$\frac{\partial \bar{u}_{n+1}^{tP}}{\partial u_{n+1}^t} = - \left(\frac{\partial^2 \phi_{n+1}^*}{\partial \bar{u}_{n+1}^{tP}{}^2} \right)^{-1} \frac{\partial^2 \phi_{n+1}^*}{\partial u_{n+1}^t \partial \bar{u}_{n+1}^{tP}} \quad (4.24)$$

For example, we choose the elastic potential as follows in our program:

$$W_2^e = \frac{\mu}{H} (u^t - u^{tP})^2$$

and u^{tP} is plastic displacement in 1D variational modelling, defined as:

$$\dot{u}^{tP} = \text{sign}(\dot{u}^t) \dot{\bar{u}}^{tP}$$

the following derivations can be evaluated:

$$\frac{\partial \phi}{\partial u^t} = \frac{\partial W_2^e}{\partial u^t} = \frac{2\mu}{H}(u^t - u^{tP*}); \quad \frac{\partial^2 W_2^e}{\partial u^{t2}} = \frac{2\mu}{H}; \quad \frac{\partial^2 \phi^*}{\partial \bar{u}^{tP} \partial u^t} = -\frac{2\mu}{H} \text{sign}(\dot{u}^t)$$

so:

$$\frac{\partial^2 \phi}{\partial u^{t2}} = \frac{2\mu}{H} - \left(\frac{2\mu}{H}\right)^2 \left(\frac{\partial^2 \phi^*}{\partial \bar{u}^{tP2}}\right)^{-1}$$

As a mention, all the derivations of ϕ^* is on the base of the optimization value.

Now we will work on the formulation of thermal flux. Based on the optimization conditions about the internal parameters, we can easily get that:

$$\frac{\partial \phi_{n+1}}{\partial T_{b_{n+1}}} = \frac{\partial \phi_{n+1}^*}{\partial T_{b_{n+1}}}(h_V^*, h_T^*, T_{max}^*, \bar{u}^{tP*})$$

and the corresponding second order of ϕ about T_b is

$$\begin{aligned} \frac{\partial^2 \phi_{n+1}}{\partial T_{b_{n+1}}^2} &= \frac{\partial^2 \phi_{n+1}^*}{\partial h_{V_{n+1}} \partial T_{b_{n+1}}} \frac{\partial h_{V_{n+1}}}{\partial T_{b_{n+1}}} + \frac{\partial^2 \phi_{n+1}^*}{\partial h_{T_{n+1}} \partial T_{b_{n+1}}} \frac{\partial h_{T_{n+1}}}{\partial T_{b_{n+1}}} + \\ &\frac{\partial^2 \phi_{n+1}^*}{\partial T_{max_{n+1}} \partial T_{b_{n+1}}} \frac{\partial T_{max_{n+1}}}{\partial T_{b_{n+1}}} + \frac{\partial^2 \phi_{n+1}^*}{\partial \bar{u}_{n+1}^{tP} \partial T_{b_{n+1}}} \frac{\partial \bar{u}_{n+1}^{tP}}{\partial T_{b_{n+1}}} + \frac{\partial^2 \phi_{n+1}^*}{\partial T_{b_{n+1}}^2} \end{aligned} \quad (4.25)$$

Consequently it is necessary to evaluate the derivations of $\frac{\partial h_{V_{n+1}}}{\partial T_{b_{n+1}}}$, $\frac{\partial h_{T_{n+1}}}{\partial T_{b_{n+1}}}$, $\frac{\partial T_{max_{n+1}}}{\partial T_{b_{n+1}}}$, $\frac{\partial \bar{u}_{n+1}^{tP}}{\partial T_{b_{n+1}}}$ for obtaining the value (4.25). Repeatedly, the optimization conditions about four internal parameters will be used here to solve this problem. Besides (4.21), the others optimizations are:

$$\frac{\partial}{\partial T_{b_{n+1}}} \left(\frac{\partial \phi_{n+1}^*}{\partial h_{V_{n+1}}} \right) = 0; \quad \frac{\partial}{\partial T_{b_{n+1}}} \left(\frac{\partial \phi_{n+1}^*}{\partial \bar{u}_{n+1}^{tP}} \right) = 0; \quad (4.26)$$

so a system of linear equations with four variables can be obtained by (4.26), described as follows:

$$\begin{bmatrix} \frac{\partial \phi_{n+1}^*}{\partial h_{V_{n+1}}^2} & \frac{\partial \phi_{n+1}^*}{\partial h_{V_{n+1}} \partial h_{T_{n+1}}} & \frac{\partial \phi_{n+1}^*}{\partial h_{V_{n+1}} \partial T_{max_{n+1}}} & \frac{\partial \phi_{n+1}^*}{\partial h_{V_{n+1}} \partial \bar{u}_{n+1}^{tP}} \\ & \frac{\partial \phi_{n+1}^*}{\partial h_{T_{n+1}}^2} & \frac{\partial \phi_{n+1}^*}{\partial h_{T_{n+1}} \partial T_{max_{n+1}}} & \frac{\partial \phi_{n+1}^*}{\partial h_{T_{n+1}} \partial \bar{u}_{n+1}^{tP}} \\ & & \frac{\partial \phi_{n+1}^*}{\partial T_{max_{n+1}}^2} & \frac{\partial \phi_{n+1}^*}{\partial T_{max_{n+1}} \partial \bar{u}_{n+1}^{tP}} \\ \text{sym.} & & & \frac{\partial^2 \phi_{n+1}^*}{\partial \bar{u}_{n+1}^{tP2}} \end{bmatrix} \begin{bmatrix} \frac{\partial h_{V_{n+1}}}{\partial T_{b_{n+1}}} \\ \frac{\partial h_{T_{n+1}}}{\partial T_{b_{n+1}}} \\ \frac{\partial T_{max_{n+1}}}{\partial T_{b_{n+1}}} \\ \frac{\partial \bar{u}_{n+1}^{tP}}{\partial T_{b_{n+1}}} \end{bmatrix} = - \begin{bmatrix} \frac{\partial \phi_{n+1}^*}{\partial h_{V_{n+1}} \partial T_{b_{n+1}}} \\ \frac{\partial \phi_{n+1}^*}{\partial h_{T_{n+1}} \partial T_{b_{n+1}}} \\ \frac{\partial \phi_{n+1}^*}{\partial T_{max_{n+1}} \partial T_{b_{n+1}}} \\ \frac{\partial \phi_{n+1}^*}{\partial \bar{u}_{n+1}^{tP} \partial T_{b_{n+1}}} \end{bmatrix}$$

We adopt an efficient linear solver (based on LU decomposition) to solve our linear systems, then the corresponding solutions will be entered into (4.25) to calculate the second order derivation of ϕ_{n+1}^* about $T_{b_{n+1}}$.

For the thermal mechanical coupling term $\frac{\partial^2 \phi_{n+1}}{\partial u_{n+1}^t \partial T_{b_{n+1}}}$, we can write it as:

$$\frac{\partial^2 \phi_{n+1}}{\partial u_{n+1}^t \partial T_{b_{n+1}}} = \frac{\partial^2 W_{2_{n+1}}^e}{\partial u_{n+1}^t \partial \bar{u}_{n+1}^{tP}} \frac{\partial \bar{u}_{n+1}^{tP}}{\partial T_{b_{n+1}}} \quad (4.27)$$

As an end, we should mention that all the analysis are based on the 1D variational modelling without heat exchange on the boundary, so the influence of length H on surrounding temperature is neglected for simplifying the analysis. Yet it is similar to the above analysed method in that case. Based on the above discussion, the optimized parameters will include another one: $\bar{T}_{b_{n+1}}$ which is a boundary temperature obtained by total potential. This case will be similar to the results in [Yang et al., 2005].

By means of Appendix B, every term in (4.13) and (4.14) is derived and can be substituted to calculate the nodal force and tangent matrix. It seems that every term is very complicated according to the above derivation, but we can discover that many common terms exist in the formulations. So if we can get certain parts, the tangent matrix is just a simple calculation operation. Furthermore, the corresponding integration can be implemented by numerical method, such as Gauss method. Although we have not given the numerical example in this section, the verification in theory demonstrates that this variational modelling is feasible with strain localized element.

4.4 Conclusions

In the thermo-mechanical localized problem, mesh dependence is a common phenomenon and always limits the application of numerical methods as a fatal default, such as the accuracy of solution, the convergence of numerical methods. In this study, firstly a simple pre-notched bar subjected to a shearing velocity is analysed by standard FEM. In term of adiabatic case, we found that the bandwidth tends to zero with the central mesh refined gradually. The stress evolution is largely influenced by mesh size, and the maximum stress is smaller if the grid in front of pre-notch is finer. Contrastively, this problem with thermal conduction presents less dependence compared to the one in adiabatic case. We can find that there is a steady state for stress evolution with the mesh size decreased. Subsequently, the bandwidth keeps consistency when the mesh size arrives to some extent. Yet the dense mesh creation or enormous calculation in localization zone make the standard FEM unacceptable in the simulation of ASBs structure. It needs the development of discontinuous modellings.

Then briefly, we revised three widely used methods (interface element, embedded discontinuous method and XFEM) in the application of shear localization problem. Although they bring a lot of advantages in the discontinuous modellings, there is a large challenge to find a good description of shear localization profiles and the relative constitutive components in traction-seoeration and entropy relation.

Consequently based on the energy-based variational modelling for thermo-elasto-viscoplastic materials proposed in CHAP.3, we successfully extend it in strain localized

element and propose a variational two-scale model for adiabatic shear bands. The reason that we call it two-scale modelling is that at macroscopic scale it is represented by displacement jump, yet the characters at microscopic scale are resourced to our 1D variational modelling. Compared with other discontinuous methods, the modelling has the following advantages:

- New form of deformation gradient in localization. We consider that plastic strain is inhomogeneous in the normal direction to discontinuous surface.
- Inhomogeneous temperature distribution. According to the analytical solution, “cusp” profile of temperature is applied in variational modelling.
- Intrinsically representing traction-separation and entropy relations. Adopting incremental energy potential, all the continuous relations, including flow theory, traction-separation law do not need to be defined separately, but instead can be directly obtained by the derivations of total potential.
- Shear band width calculation. We define two bandwidths in our microscopic modelling: kinematic width and thermal width, and they can be easily determined as two internal parameters of incremental potential.
- Symmetry tangent matrix in FEM.

Unfortunately we have not finished a numerical example to verify our two-scale modelling, but it does not influence our proposition of modelling. Completely theoretical analysis and finite element implementation are successfully derived, giving a good preparation for future implementation.

Chapter 5

Conclusions and perspectives

A new energy-based variational model of adiabatic shear banding structure for thermo-elasto-viscoplastic materials has been proposed and successfully tested, accounting for elasticity, work hardening and thermal conduction. In view of the widely used Johnson-Cook model, a list of parameters, such as kinematic bandwidth, thermal bandwidth and equivalent displacement loading, are introduced as the internal variables to track the dynamic evolutions of deformation and temperature in the localization region. Meanwhile as a validation of canonical aspects of modelling, the corresponding thermo-viscoplastic models for exponential law and power rate law are developed in steady and transient state. Heat exchange coefficient is considered to complete the 1D modelling as well, and its formula fitted in steady state is applied in transient state to optimize the surrounding temperature.

To present well the application of our modelling in the adiabatic shear banding structure in 2D or 3D, we resource to a discontinuous technology: interface element, and propose a variational two-scale model based on this 1D total variational potential. Not only the theoretical derivation is given to describe its function in the two-scale model, but also every term of nodal force, entropy and tangent matrix is precisely derived in CHAP.4.

5.1 Conclusions

As the foregoing work described, the main problems of adiabatic shear bands are mesh dependence and model quality, which exactly this study aims at solving. According to the proposed thermo-elasto-viscoplastic models, we applied and analysed the evolutions of bandwidth, temperature and stress in the layer subjected to a simple shearing velocity. Moreover, a variational two-scale model is proposed to extend the present 1D modelling into the simulations of ASB structure in 2D/3D. In short, a series of conclusions and advantages are received in this thesis as follows:

- A thermo-mechanical variational framework based on Rayleigh-Ritz method is a main aspect of our energy-based variational modelling. Mesh discretization is non-existent in this structure. The profiles of velocity and temperature can be simply

described as the two functions with several unknown scalars, such as central temperature, bandwidth. In steady state, heat exchange coefficient can also be obtained by means of the optimization of total potential with respect to the temperature on the boundary. In transient state, the transformation condition from elasticity to plasticity regards to another new optimized parameter: equivalent displacement loading. Thus our variational modelling makes the complicated shear localization problem concentrated on a simple mathematical optimization problem, which greatly simplifies the simulation.

- These new proposed variational models (thermo-viscoplastic model and thermo-elasto-viscoplastic model) are verified by analytical solutions or finite element method. Initially, we built the steady variational modellings for Couette flow, thermal flow and thermal Couette flow, and validated their feasibility in steady state. Then for adiabatic shear bands, we proposed a series of the corresponding variational models with regarding to different flow laws (exponential softening law, power rate law and Johnson-Cook law) in steady and transient states. Standard FEM verified that the nonlinear profiles of velocity and temperature presented well the characters of shear localization, agreeing with the FEM analysis.
- A formula for the exchange coefficient was proposed using the polynomial curve fitting method. We also analysed the influence of heat exchange on the surrounding temperature at high strain rate loading. Material is basically isothermal at the beginning, and the surrounding temperature is comparable to the central temperature. But the effect of thermal conduction is gradually evident with the time increased, and high temperature concentrates on the center of the layer at last. Appreciating to the introduction of thermal boundary condition, we can obtain that the bandwidth in steady state is independent on the layer width.
- The combination between the boundary conditions and the analytical formulations can efficiently avoid the dependence of the formulation of the temperature profile on material parameters. We verified the canonical aspect of our modelling through its applications on three flow laws (exponential softening law, power rate law and Johnson-Cook law).
- Material instability analysis are not needed in our modelling. We use the constraint optimization to control the shear band initiation and propagation.
- The evolutions of the ASBs characteristics were analysed in this study. Two kinds of bandwidths are introduced to track the profiles of velocity and temperature, yet kinematic bandwidth is more persuasive in physics and mathematics. With the time increased, shear band length has a large decrease initially, then quickly arrives at steady state. On contrast, the maximum temperature is gradually increasing and evolves towards the analytical solution (exponential softening law and power rate law). However, the speed of its increase is decreasing because of the thermal conduction. Subsequently, stress evolution obtained by our modelling in Johnson-Cook

law can well present the initiation and the propagation of adiabatic shear band. We can confirm that the occurrence of shear localization is the result of stress instability. In thermo-elasto-viscoplastic model, the evolution of equivalent displacement loading show that the plastic distribution of imposed loading increases with the time, and almost occupies the whole imposed displacement in the final term.

- The average stress can be approximated by the derivation of total potential with respect to the charging displacement. We also found that the numerical error approximation of this part is achievable to simulate the adiabatic shear structure. Exactly by means of this discovery, we proposed our thermal elasto-viscoplastic variational model, and gives a good foundation to its extension in 2D/3D.
- We analysed the influences of material parameters (thermal softening coefficient, thermal conductivity, strain rate sensibility and imposed velocity) on stress evolution. On the one hand, if velocity is higher, the strain rate sensibility m is smaller but thermal softening coefficient is higher, the shear localization region is more localized. On the other hand, we verify that the thermal conduction can not be neglected in the final term, which will influence the bandwidth at steady state.
- As an application of our 1D variational modelling, a new variational two-scale model is proposed by means of an interface element. Contrarily to other discontinuous methods, this model considers inhomogeneous plastic strain and temperature distribution in shear localization part. In addition, the relations of traction-separation and entropy on discontinuity are intrinsically derived in the total incremental energy potential. Moreover, finite element implementation is precisely derived to validate the convenience of two-scale modelling. Normally this model has a good effect on avoiding mesh dependence, yet the drawback is that the shear band path must be pre-known, otherwise the computation will be enormous.

5.2 Discussion and future work

The work in this thesis is concentrated in the variational modelling for adiabatic shear bands in quasi-static state. Here we do not need to consider the inertia effect because of the small length of layer. Although inertia factor has little influence on our strain localization model (because the element size in the localization region will be normally smaller than $10^{-3}m$), it is better to consider the dynamical variational modelling in the analysis of the external localization region. In present, Stainier [Stainier, 2011b] has already derived the dynamical form and applied it in FEM simulation, here all the results calculated by FEM have neglected the dynamical part.

The aspect of variational method is to transform the conservation laws of physical problems into a mathematical optimization problem. Consequently as the foregoing work described, the resolution of the profiles of shear localization is transformed into some non-linear equations with several optimized scalars. When we use Rayleigh-Ritz method to

avoid mesh discretization, subsequently the nonlinear parts, like \tanh , \cosh are also added into the modelling. As well as thermal conduction part, these terms strongly influence the convergence of nonlinear equations, especially in the initial term (constraint optimization). So our modelling works well if the solver of nonlinear equations is efficient. This is also the reason why we apply trust-region method to substitute the ordinary Newton-Raphson method in the study. Hence how to find the balance between the accuracy of profiles and convenient solver is a worthy considerable question.

In addition, our variational modelling can well simulate the initiation and propagation of shear bands structure. Yet this process is complicated in the implementation, and it will bring some difficulties in the application of 1D modelling. Although the analytical formulations present their completeness in the simulation of ASBs formation (from linear form to nonlinear form), it might as well do some attempt to compare the one adding the linear perturbation analysis and the present modelling in the calculation aspect, and choose the better one for our simulation.

Generally speaking, high temperature near to the melting point and large deformation gradient are the common characters in the final term of ASBs. Naturally, damage will be an inevitable phenomenon in this term. Yet we neglect its influence in this study. Perspectively, it will have a good aspect to built an energy-based variational modelling with damage factor.

For the application of our 1D variational modelling, we built a discontinuous model resorting to the strain localized element, and the corresponding finite element implementation is derived but has not been verified in program. Here in the future work of adiabatic shear bands structure in 2D or 3D, the first thing is to validate the new variational two-scale models through some simple examples, such as the pre-notched bar described in CHAP.4, hat-shaped specimen. However, this model depends on the prediction of shear band path, so it will be powerless once meeting the ASBs in the popular experiment: thick-walled cylinder. Extended finite element method will be a good direction to solve the unknown path problem. Some work has been done in the reference if the enrichment of the profiles of displacement and temperature are largely simplified. We can apply our verified analytical formulations as the enrichments to present the approximation of physical profiles, and the corresponding bandwidth evolution is tracked through our proposed total incremental update potential. A good accuracy of the results simulated by the XFEM based on our 1D variational model will be expected in perspective.

Conclusions et perspectives

Un nouveau modèle de la structure de BCA dans les matériaux thermo-élasto-viscoplastiques a été proposé et validé par une approche énergétique variationnelle en prenant en compte l'élasticité, l'écroutissement et la conduction de chaleur. Compte tenu de la loi Johnson-Cook, une liste de paramètres, tels que la largeur de bande cinématique, la largeur de bande thermique et le chargement en déplacement équivalent, sont présentés comme des variables internes pour suivre les évolutions de déformation et de température dans la zone localisée. Afin de valider les aspects canoniques du modèle, les lois thermo-viscoplastiques correspondantes (loi exponentielle et loi de puissance) sont développées en régime stationnaire et transitoire. Le coefficient de transfert de chaleur est ainsi considéré pour compléter la modélisation 1D, et sa formule est établie en régime stationnaire. Nous l'appliquons pour optimiser les températures aux frontières en régime transitoire.

Dans le but d'appliquer un modèle variationnel en 2D/3D, nous recourons à une méthode discontinue: les éléments d'interface, et proposons un modèle variationnel à deux échelles basé sur le potentiel 1D incrémental. La dérivation théorique est non seulement donnée pour décrire sa fonction dans le modèle à deux échelles, mais chaque terme de la force nodale, de l'entropie et de la matrice tangente est également dérivé précisément au CHAP.4.

Conclusions

Les problèmes principaux des Bandes de Cisaillement Adiabatique comme décrit ci-dessus, sont la dépendance au maillage et la qualité du modèle soit exactement ce que cette étude vise à résoudre. En utilisant le modèle thermo-élasto-viscoplastique, nous avons analysé les évolutions des largeurs de bandes, la température au cœur et la contrainte dans la couche soumise à une vitesse de cisaillement simple. De plus, un modèle variationnel à deux échelles est proposé pour faire évoluer les applications de notre modèle de la structure de BCA de 1D à 2D/3D. En bref, une série des conclusions et des avantages sont reçues dans cette étude:

- Un cadre thermo-mécanique variationnel basé sur la méthode de Rayleigh-Ritz est un aspect essentiel de notre modélisation énergétique variationnelle. La discrétisation maillage est inexistante dans cette structure. Les profils de vitesse et de température peuvent être simplement décrits comme les deux fonctions avec plusieurs scalaires inconnus, tels que la température centrale et la largeur de bande. Le coefficient de

transfert de chaleur est aussi obtenu en régime stationnaire par l'optimisation de potentiel total par rapport à la température aux frontières. De plus, la transformation de l'état élastique à l'état plastique est contrôlée par un nouveau paramètre d'optimisation: le chargement en déplacement équivalent. Ainsi, notre modélisation variationnelle rend le problème de localisation complexe concentrée sur un problème d'optimisation mathématique simple, ce qui simplifie grandement la simulation numérique.

- Ces nouveaux modèles variationnels (modèle thermo-viscoplastique et modèle thermo-élasto-viscoplastique) sont vérifiés par des solutions analytiques ou la méthode des éléments finis. Au départ, nous avons construit les modélisations variationnelles en régime stationnaire pour l'écoulement de Couette, l'écoulement thermique et l'écoulement de Couette thermique, et avons validé leur faisabilité. De plus, nous avons proposé une série de modèles variationnels concernent les lois d'écoulement différents (loi adoucissement exponentielle, loi de puissance et loi Johnson-Cook) en régime stationnaire et transitoire. La MEF standard vérifie que les profils non-linéaire de vitesse et de température présentent bien les caractères de localisation de cisaillement.
- Une formule du coefficient de transfert a été obtenu par la méthode polynomiale. Nous avons également analysé l'influence de l'échange de chaleur à la température ambiante dans la couche soumise à une vitesse de déformation élevée. Le matériau est essentiellement isotherme au début, et la température aux bords est comparable à la température centrale. Cependant l'effet de la conduction thermique apparait progressivement quand le temps augmente, et enfin la température élevée se concentre sur le centre de la couche. Grâce à l'introduction d'une condition limite thermique, on peut obtenir que la largeur de bande en régime stationnaire est indépendante de la largeur de la couche.
- La combinaison entre les conditions aux limites et les formulations analytiques peuvent efficacement éviter la dépendance de la formulation du profil de température aux paramètres matériaux. Par conséquent, l'aspect canonique de notre modélisation a été vérifié à travers des applications des lois d'écoulement différents (loi adoucissement exponentielle, loi de puissance et loi Johnson-Cook).
- L'analyse de l'instabilité matérielle n'est pas nécessaires dans notre modélisation. Nous utilisons l'optimisation sous contrainte pour contrôler l'initiation et la propagation des BCAs.
- Les évolutions des caractéristiques de BCAs ont été analysées dans cette étude. La largeur de bande d'un point de vue cinématique est plus facile à appréhender que celle d'un point de vue physiques ou mathématiques. Elle a une forte diminution d'abord, puis évolue lentement, et enfin arrive au cas stationnaire (simplement pour la loi exponentielle et la loi de puissance). Au contraire, la température centrale élève progressivement et évolue vers la solution analytique. Cependant,

l'augmentation de température diminue en raison de la conduction thermique. Par la suite, l'évolution de la contrainte obtenue par notre modélisation de Johnson-Cook représente bien l'initiation et la propagation des BCAs. Les résultats illustrent que l'apparition de localisation de cisaillement est le fruit de l'instabilité de contrainte. De plus, l'évolution du chargement déplacement équivalent montre que la contribution plastique augmente avec le temps, et presque occupe tout le déplacement imposé dans la dernière étape.

- La contrainte moyenne est approchée par la dérivation de potentiel par rapport au chargement en déplacement. Nous avons trouvé que l'erreur numérique de cette partie est réalisable pour simuler la structure de cisaillement adiabatique. A partir de cette conclusion, un modèle thermo-élasto-viscoplastique variationnel a été proposé, ce qui donne une bonne base pour son extension en 2D/3D.
- Les influences des paramètres matériaux (le coefficient d'adoucissement thermique, la conductivité thermique, la sensibilité de vitesse de déformation et la vitesse imposée) à l'évolution de contrainte sont analysées par le modèle variationnelle. D'une part, si la vitesse est plus élevée, la sensibilité de vitesse de déformation m est plus petite mais le coefficient d'adoucissement thermique λ est plus élevé et la zone de localisation de cisaillement est plus localisée. D'autre part, on vérifie que la conduction thermique est un facteur important dans les analyses de BCA, ce qui va influencer la largeur de bande en régime stationnaire.
- Comme application de notre modélisation variationnelle en 1D, un nouveau modèle variationnel à deux échelles est proposé au moyen des éléments d'interface. Contrairement à d'autres méthodes discontinues, il considère la déformation plastique et la distribution de température inhomogène dans la zone localisée. En outre, les lois de traction-séparation et de l'entropie de discontinuité sont intrinsèquement dérivées par le potentiel incrémental. La mise en oeuvre des éléments finis représente précisément la commodité du modèle à deux-échelles. Normalement ce modèle est un bon moyen pour éviter la dépendance de maillage, mais l'inconvénient est que le chemin des BCAs doit être pré-connu, sinon le calcul sera énorme.

Discussion et travaux futurs

Le travail dans cette étude se concentre sur la modélisation variationnelle pour des BCAs dans l'état quasi-statique. Nous n'avons pas besoin d'examiner l'effet d'inertie en raison de la faible largeur de la couche. Même si le facteur d'inertie a peu d'influence à notre modèle de localisation (car la taille de l'élément dans la région de localisation est inférieur à 10^{-3} m), c'est préférable d'envisager la modélisation dynamique variationnelle. Actuellement, Stainier [Stainier, 2011b] a déjà tiré la formulation variationnelle dynamique et l'a appliqué dans la simulation des éléments finis. Cependant tous les résultats calculés par la méthode des éléments finis ont négligé l'inertie.

L'avantage de la méthode variationnelle est de transformer les lois de conservation des problèmes physiques comme un problème d'optimisation mathématique. Par conséquent, la résolution des profils de BCA s'est présentée par des équations non-linéaires avec plusieurs scalaires optimisées comme décrit ci-dessus. En utilisant la méthode de Rayleigh-Ritz pour éviter la discrétisation de maillage, les parties nonlinéaires, comme \tanh et \cosh , sont ainsi introduites dans la modélisation. Ces termes influent fortement la convergence des algorithmes en plus de la conduction thermique, en particulier dans la période initiale (optimisation contrainte). Ainsi, si le solveur d'équations non-linéaires est efficace, notre modèle fonctionne bien. C'est aussi la raison pour laquelle nous appliquons l'algorithme à régions de confiance pour remplacer la méthode Newton-Raphson dans la simulation. Comment trouver l'équilibre entre la précision des profils et le solveur pratique est une question considérable.

En outre, la modélisation variationnelle peut ainsi simuler l'initiation et la propagation de la structure des BCAs au moyen de l'optimisation contrainte. Cependant ce processus est compliqué à la mise en oeuvre, et il apportera des difficultés dans les applications de notre modélisation en 1D. Bien que les formulations analytiques représentent leur intégralité (de la forme linéaire à la forme non-linéaire), c'est raisonnable de faire une tentative de comparer le modèle ajoutant une perturbation linéaire et la modélisation présente, et de choisir le meilleur dans la simulation.

D'une manière générale, une température élevée proche du point de fusion et un grand gradient de déformation sont des caractères communs dans le terme final de BCA. Naturellement, les endommagements seront un phénomène inévitable enfin de la formation de BCA. Cependant nous négligeons son influence dans cette étude. Il sera intéressant par la suite de construire une modélisation énergétique variationnelle ayant un facteur d'endommagement.

Afin d'appliquer notre modélisation variationnelle 1D à 2D/3D, nous avons construit un modèle discontinu au moyen de l'élément localisé, et la mise en oeuvre des éléments finis est dérivée, pourtant elle n'a pas été numériquement vérifiée. Dans les travaux futurs, la première chose à faire est de valider le modèle variationnel à deux échelles à travers des exemples numériques, par exemple la barre pré-entaillée comme décrit dans CHAP.4, l'éprouvette de chapeau. Cependant, ce modèle dépend de la prévision du chemin des BCAs. Il sera ainsi impuissant dans le modèle de l'expérience de cylindre. La méthode étendue des éléments finis (XFEM) sera une bonne direction pour résoudre le problème de BCA du chemin inconnu. Des travaux ont été réalisés dans la référence si les enrichissements des profils de vitesse et de température sont simplifiés. Nous pouvons appliquer les formulations canoniques qui sont vérifiées dans cette étude à présenter les profils physiques. De plus l'évolution de la largeur de bande est suivie par l'optimisation de potentiel total incrémental. En perspective, une bonne précision des résultats numériques par la XFEM sera atteinte basée sur la modélisation variationnelle en 1D.

Appendix A

Verification of variational modelling

The total power density potential (2.12) in CHAP.2 is a formulation of the coupled thermo-mechanical problem for rate-dependency and thermal softening material, here we skilfully present the conservation of laws as an optimization problem with respect to velocity and temperature. For completeness, in this appendix we will show this equality through variational calculation. Taking variation of velocity to (2.12), we obtain:

$$\begin{aligned}
 0 = D_V \Phi(V, T)(\delta V) &= \int_{-H}^H \frac{1}{m+1} \frac{\tau_0}{(\dot{\gamma}^0)^m} \exp\left\{-\beta\left(\frac{\Theta}{T_0} - 1\right)\right\} \left(\frac{T}{\Theta}\right)^{m+1} (m+1) \left(\frac{\partial V}{\partial y}\right)^m \frac{\partial \delta V}{\partial y} dy \\
 &= \left[\frac{\tau_0}{(\dot{\gamma}^0)^m} \exp\left\{-\beta\left(\frac{\Theta}{T_0} - 1\right)\right\} \left(\frac{T}{\Theta}\right)^{m+1} \left(\frac{\partial V}{\partial y}\right)^m \delta V \right]_{-H}^H \\
 &\quad - \int_{-H}^H \frac{\partial}{\partial y} \left(\frac{\tau_0}{(\dot{\gamma}^0)^m} \exp\left\{-\beta\left(\frac{\Theta}{T_0} - 1\right)\right\} \left(\frac{T}{\Theta}\right)^{m+1} \left(\frac{\partial V}{\partial y}\right)^m \right) \delta V dy \\
 &= - \int_{-H}^H \frac{\partial}{\partial y} \left(\frac{\tau_0}{(\dot{\gamma}^0)^m} \exp\left\{-\beta\left(\frac{\Theta}{T_0} - 1\right)\right\} \left(\frac{T}{\Theta}\right)^{m+1} \left(\frac{\partial V}{\partial y}\right)^m \right) \delta V dy
 \end{aligned}$$

So:

$$\frac{\partial}{\partial y} \left(\frac{\tau_0}{(\dot{\gamma}^0)^m} \exp\left\{-\beta\left(\frac{\Theta}{T_0} - 1\right)\right\} \left(\frac{T}{\Theta}\right)^{m+1} \left(\frac{\partial V}{\partial y}\right)^m \right) = 0 \quad (\text{A.1})$$

By means of the thermal equilibrium $\Theta = T$ and the formula of material flow stress, (A.1) reduce to :

$$\frac{\partial \tau}{\partial y} = 0$$

The conservation of linear momentum is retrieved.

Next we do the variation of (2.12) with respect to temperature, with the result:

$$\begin{aligned}
0 = D_T \Phi(V, T)(\delta T) &= \int_{-H}^H \frac{\tau_0}{(\dot{\gamma}^0)^m} \exp\left\{-\beta\left(\frac{\Theta}{T_0} - 1\right)\right\} \frac{T^m}{\Theta^{m+1}} \left(\frac{\partial V}{\partial y}\right)^{m+1} \delta T dy \\
&+ \int_{-H}^H \lambda \Theta \left(\frac{\partial T}{\partial y} \frac{1}{T}\right) \left(\frac{\partial \delta T}{\partial y} \frac{1}{T} - \frac{\delta T}{T^2} \frac{\partial T}{\partial y}\right) dy \\
&= \int_{-H}^H \frac{\tau_0}{(\dot{\gamma}^0)^m} \exp\left\{-\beta\left(\frac{\Theta}{T_0} - 1\right)\right\} \frac{T^m}{\Theta^{m+1}} \left(\frac{\partial V}{\partial y}\right)^{m+1} \delta T dy \\
&+ \int_{-H}^H \lambda \Theta \left(\frac{\partial T}{\partial y} \frac{1}{T^3}\right) \frac{\partial T}{\partial y} \delta T dy - \left[\lambda \Theta \frac{\partial T}{\partial y} \delta T\right]_{-H}^H \\
&+ \int_{-H}^H \lambda \Theta \frac{\partial}{\partial y} \left(\frac{\partial T}{\partial y} \frac{1}{T^2}\right) \delta T dy
\end{aligned}$$

According to the isothermal boundary condition and $\Theta = T$, we observe:

$$\frac{\tau_0}{(\dot{\gamma}^0)^m} \exp\left\{-\beta\left(\frac{\Theta}{T_0} - 1\right)\right\} \left(\frac{\partial V}{\partial y}\right)^{m+1} \frac{1}{T} + \frac{\lambda}{T^2} \left(\frac{\partial T}{\partial y}\right)^2 + \lambda \Theta \frac{\partial}{\partial y} \left(\frac{\partial T}{\partial y} \frac{1}{T^2}\right) = 0$$

So:

$$\frac{\tau_0}{(\dot{\gamma}^0)^m} \exp\left\{-\beta\left(\frac{\Theta}{T_0} - 1\right)\right\} \left(\frac{\partial V}{\partial y}\right)^{m+1} + \lambda \frac{\partial^2 T}{\partial y^2} = 0$$

The conservation of energy was then validated through taking the variation of temperature.

Appendix B

Additional derivation in interface element

As shown in the derivation of nodal force and tangent matrix, some strain or displacement formulas should be known for the sake of obtaining the specific tensor expression. The work in this part will be concentrated on these derivations. We should emphasize that the following analysis is based on the variational modelling on 3D. Referred to the definition of the in-plane deformation, we can write it as:

$$\mathbf{F}^{\parallel} = \mathbf{g}_i \otimes \mathbf{G}^i$$

where \mathbf{g}_i denote the tangent basis vectors in the deformed configuration, and $\mathbf{g}_3 = \mathbf{n}$, which is unit normal direction. \mathbf{G}^i is the contravariant coordinate about \mathbf{G}_i and $\mathbf{G}_3 = \mathbf{N}$. Then we can derive that:

$$\mathbf{F}^{\parallel -1} = \mathbf{G}_i \otimes \mathbf{g}^i$$

similarly, \mathbf{g}^i is the dual basis, we can write it as:

$$\mathbf{g}^1 = \frac{\mathbf{g}_2 \times \mathbf{g}_3}{|\mathbf{g}_1 \times \mathbf{g}_2|}; \quad \mathbf{g}^2 = \frac{\mathbf{g}_3 \times \mathbf{g}_1}{|\mathbf{g}_1 \times \mathbf{g}_2|}; \quad \mathbf{g}^3 = \mathbf{n}; \quad (\text{B.1})$$

According to the discretization of finite element to displacement, we have ([Yang et al., 2005]):

$$\frac{\partial \mathbf{F}_{mk}^{\parallel}}{\partial x_{ia}^{\pm}} = \frac{1}{2} \delta_{mi} N_{a,\alpha} G^{\alpha k} + \frac{1}{2} \frac{\partial n_m}{\partial \bar{x}_{ia}} G^{3k} \quad (\text{B.2})$$

where

$$\frac{\partial n_m}{\partial \bar{x}_{ia}} = \frac{e_{irs}}{|\mathbf{g}_1 \times \mathbf{g}_2|} (g_{2r} N_{a,1} - g_{1r} N_{a,2}) (\delta_{ms} - n_m n_s) \quad (\text{B.3})$$

where δ is Kronecker delta, and e_{irs} is the alternating symbol. Furthermore the second order of unit normal vector can be derived as:

$$\begin{aligned} \frac{\partial^2 n_m}{\partial \bar{x}_{jb} \partial \bar{x}_{ia}} &= -\frac{e_{jhl} e_{irs}}{|\mathbf{g}_1 \times \mathbf{g}_2|^2} n_l (g_{2h} N_{b,1} - g_{1h} N_{b,2}) (g_{2r} N_{a,1} - g_{1r} N_{a,2}) \\ &\quad (\delta_{ms} - n_m n_s) + \frac{e_{irs}}{|\mathbf{g}_1 \times \mathbf{g}_2|} [\delta_{ms} \delta_{rj} (N_{b,2} N_{a,1} - N_{a,2} N_{b,1}) - \\ &\quad (g_{2r} N_{a,1} - g_{1r} N_{a,2}) (\frac{\partial n_m}{\partial \bar{x}_{jb}} n_s + n_m \frac{\partial n_s}{\partial \bar{x}_{jb}})] \end{aligned} \quad (\text{B.4})$$

and the following term should also be known for calculating the tangent stiffness matrix:

$$\frac{\partial^2 \mathbf{F}_{mL}^{\parallel}}{\partial x_{ia}^{\pm} \partial x_{jb}^{\pm}} = \frac{1}{4} \frac{\partial^2 \mathbf{F}_{mL}^{\parallel}}{\partial \bar{x}_{ia} \partial \bar{x}_{jb}} = \frac{1}{4} \frac{\partial^2 n_m}{\partial \bar{x}_{jb} \partial \bar{x}_{ia}} G^{3k} \quad (\text{B.5})$$

By means of (4.12), we get:

$$u^n = \sum_{a=1}^n [[x_m]]_a N_a(\mathbf{s}) n_m \quad (\text{B.6})$$

and the displacement jump in tangent direction is:

$$[[\mathbf{u}]]^t = [[\mathbf{u}]] - u^n \mathbf{n} = \sum_{a=1}^n ([[x]]_a N_a - \mathbf{n} \sum_{a=1}^n [[x_m]]_a N_a(\mathbf{s}) n_m) \quad (\text{B.7})$$

so

$$u^t = |\mathbf{F}^{\parallel}|^{-1} |[[\mathbf{u}]]^t| = \sqrt{A} \quad \text{where } A = \sum_{k=1}^{n_1} (G_{\beta k} g^{\beta h} [[u_h]]^t)^2; \quad (\text{B.8})$$

where n_1 is the dimension number, equal to 3. From the above formulas, we can obtain that:

$$\frac{\partial u^t}{\partial x_{ia}^{\pm}} = A^{-\frac{1}{2}} \sum_{k=1}^{n_1} G_{\beta k} g^{\beta h} [[u_h]]^t \left(\frac{\partial g^{\beta h}}{\partial x_{ia}^{\pm}} G_{\beta k} [[u_h]]^t + g^{\beta h} G_{\beta k} \frac{\partial [[u_h]]^t}{\partial x_{ia}^{\pm}} \right) \quad (\text{B.9})$$

where

$$\frac{\partial [[u_h]]^t}{\partial x_{ia}^{\pm}} = \pm \delta_{hi} N_a - \left(\sum_{a=1}^n [[x_m]]_a N_a n_m \right) \frac{\partial n_h}{\partial x_{ia}^{\pm}} - \delta_{mi} (\pm N_a n_m n_h + [[x_m]]_a N_a \frac{\partial n_m}{\partial x_{ia}^{\pm}} n_h) \quad (\text{B.10})$$

and

$$\frac{\partial u^n}{\partial x_{ia}^{\pm}} = \pm \delta_{mi} N_a n_m + \delta_{mi} [[x_m]]_a N_a \frac{\partial n_m}{\partial x_{ia}^{\pm}} \quad (\text{B.11})$$

Based on the expression in (B.1), the derivations of g^i can also be expressed as the index notations for tensors, yet here we do not describe them in the paper.

In similar manner, for calculating the tangent stiffness matrix, the second order derivation of u^t should be derived.

$$\begin{aligned}
\frac{\partial^2 u^t}{\partial x_{jb}^{\pm} \partial x_{ia}^{\pm}} &= -\frac{1}{2} A^{-\frac{3}{2}} \left(\sum_{k=1}^{n_1} g^{\beta h} G_{\beta k} [[u_h]]^t \left(\frac{\partial g^{\beta h}}{\partial x_{jb}^{\pm}} G_{\beta k} [[u_h]]^t + g^{\beta h} G_{\beta k} \frac{\partial [[u_h]]^t}{\partial x_{jb}^{\pm}} \right) \right) \\
&\quad \left(\sum_{k=1}^{n_1} g^{\beta h} G_{\beta k} [[u_h]]^t \left(\frac{\partial g^{\beta h}}{\partial x_{ia}^{\pm}} G_{\beta k} [[u_h]]^t + g^{\beta h} G_{\beta k} \frac{\partial [[u_h]]^t}{\partial x_{ia}^{\pm}} \right) \right) + \\
&\quad A^{-\frac{1}{2}} \sum_{k=1}^{n_1} \left[\left(\frac{\partial g^{\beta h}}{\partial x_{jb}^{\pm}} G_{\beta k} [[u_h]]^t + g^{\beta h} G_{\beta k} \frac{\partial [[u_h]]^t}{\partial x_{jb}^{\pm}} \right) \left(\frac{\partial g^{\beta h}}{\partial x_{ia}^{\pm}} G_{\beta k} [[u_h]]^t \right. \right. \\
&\quad \left. \left. + g^{\beta h} G_{\beta k} \frac{\partial [[u_h]]^t}{\partial x_{ia}^{\pm}} \right) + g^{\beta h} G_{\beta k} [[u_h]]^t \left(\frac{\partial^2 g^{\beta h}}{\partial x_{jb}^{\pm} \partial x_{ia}^{\pm}} G_{\beta k} [[u_h]]^t \right. \right. \\
&\quad \left. \left. + \frac{\partial g^{\beta h}}{\partial x_{ia}^{\pm}} G_{\beta k} \frac{\partial [[u_h]]^t}{\partial x_{jb}^{\pm}} + \frac{\partial g^{\beta h}}{\partial x_{jb}^{\pm}} G_{\beta k} \frac{\partial [[u_h]]^t}{\partial x_{ia}^{\pm}} + g^{\beta h} G_{\beta k} \frac{\partial^2 [[u_h]]^t}{\partial x_{jb}^{\pm} \partial x_{ia}^{\pm}} \right) \right] \quad (\text{B.12})
\end{aligned}$$

where

$$\begin{aligned}
\frac{\partial^2 [[u_h]]^t}{\partial x_{jb}^{\pm} \partial x_{ia}^{\pm}} &= \delta_{mj} (\mp N_b n_m - [[x_m]]_b N_b \frac{\partial n_m}{\partial x_{jb}^{\pm}}) \frac{\partial n_h}{\partial x_{ia}^{\pm}} - \left(\sum_{a=1}^n [[x_m]]_a N_a n_m \right) \frac{\partial^2 n_h}{\partial x_{jb}^{\pm} \partial x_{ia}^{\pm}} \\
&\quad \mp \delta_{mi} N_a \left(\frac{\partial n_m}{\partial x_{jb}^{\pm}} n_h + n_m \frac{\partial n_h}{\partial x_{jb}^{\pm}} \right) - \delta_{mi} [[x_m]]_a N_a \left(n_h \frac{\partial^2 n_m}{\partial x_{jb}^{\pm} \partial x_{ia}^{\pm}} + \frac{\partial n_m}{\partial x_{ia}^{\pm}} \frac{\partial n_h}{\partial x_{jb}^{\pm}} \right) \\
&\quad \mp \delta_{mj} \delta_{ab} N_b n_h \frac{\partial n_m}{\partial x_{ia}^{\pm}} \quad (\text{B.13})
\end{aligned}$$

and the second order of u^n with respect to \mathbf{x} is described as

$$\frac{\partial^2 u^n}{\partial x_{jb}^{\pm} \partial x_{ia}^{\pm}} = \pm \delta_{mi} N_a \frac{\partial n_m}{\partial x_{jb}^{\pm}} + \delta_{mi} \left(\pm \delta_{mj} \delta_{ab} N_b \frac{\partial n_m}{\partial x_{ia}^{\pm}} + [[x_m]]_a N_a \frac{\partial^2 n_m}{\partial x_{jb}^{\pm} \partial x_{ia}^{\pm}} \right) \quad (\text{B.14})$$

List of Figures

1.1	Adiabatic shear band in the bulk material ([Odeshi et al., 2006])	3
1.2	Voids and micro-cracks (Ti-6Al-4V alloy [Bai et al., 1994]) in adiabatic shear band	4
1.3	Stress-strain curves at High-speed photographs of the grid pattern(Ti-6Al-4V alloy in [Liao and Duffy, 1998])	6
1.4	Temperature profile measured across an ASB at a late stage of deformation [Marchand and Duffy, 1988])	10
1.5	Schematic view of thin-walled tube ([Dinzart and Molinari, 1998])	12
2.1	1D thermal Couette flow problem	31
2.2	Profiles of velocity and temperature in the thermal Couette flow	33
2.3	1D shear band problem [Leroy and Molinari, 1992]	34
2.4	Influences of m , V_0 , β and $\tilde{\kappa}$ on bandwidth	37
2.5	Derivation of ϕ with respect to h_T with $h_V = h_T$	39
2.6	Modelling of adiabatic shear band by energy-based variational approach	40
2.7	Profiles of velocity and temperature in steady state	41
2.8	Influences of the imposed velocity V_0 on the shear band width and the central temperature	42
2.9	Influences of thermal conductivity λ on the shear band width and the central temperature in the steady state	42
2.10	Comparison of average stress and stress	43
2.11	Evolutions of the velocity and the temperature in the layer obtained by FEM ($V_0 = 0.1108\text{m/s}$ and $H = 1.25\text{mm}$)	45
2.12	Time evolution of shear band width obtained by FEM ($V_0 = 0.1108\text{m/s}$ and $H = 1.25\text{mm}$)	45
2.13	Profiles of velocity and temperature in steady state ($V_0 = 0.1108\text{m/s}$ and $H = 1.25\text{mm}$)	46
2.14	Evolutions of shear stress (JC model) by FEM ($V_0 = 0.1\text{m/s}$ and $H = 1.25\text{mm}$)	48
2.15	Influences of different slab widths on bandwidths and central temperatures (without heat exchange on $y = \pm H$)	49
2.16	Profiles of velocity (a) and temperature (b) in a layer	49
2.17	Profiles of temperature on different slab widths	51

2.18	Shear band width, central temperature and central stress for different slab widths($V_0 = 0.1m/s$)	52
2.19	Exchange coefficient for different slab widths	52
2.20	Nusselt number when $H_r = 1.25mm$	53
3.1	Evolution of the profiles of velocity and temperature by FEM ($V_0 = 0.01108m/s$)	66
3.2	Evolution of the profiles of velocity and temperature by FEM ($V_0 = 1m/s$)	66
3.3	Convergence of the shear band width ($V_0 = 0.01108m/s$)	67
3.4	Evolution of the profiles of velocity and temperature by Rayleigh-Ritz method ($V_0 = 0.01108m/s$)	68
3.5	Convergence of the bandwidths by Rayleigh-Ritz method ($V_0 = 1m/s$)	69
3.6	Evolution of the maximum temperature at $V_0 = 0.01108m/s$ (a) and $V_0 = 1m/s$ (b)	69
3.7	Evolution of stress in exponential softening law at $V_0 = 0.01108m/s$	70
3.8	Evolution of stress in exponential softening law at $V_0 = 1m/s$	71
3.9	Influence of time step on stress evolution in exponential softening law at $V_0 = 0.5m/s$	71
3.10	Influence of m on stress evolution in exponential softening law at $V_0 = 0.5m/s$	73
3.11	Influence of λ on stress evolution in exponential softening law at $V_0 = 0.5m/s$	73
3.12	Influence of β on stress evolution in exponential softening law at $V_0 = 0.5m/s$	74
3.13	Influence of V_0 on stress evolution in exponential softening law	76
3.14	Evolution of stress in power law at $V_0 = 0.01108m/s$	77
3.15	Evolution of stress in power law at $V_0 = 0.5m/s$	77
3.16	Evolution of stress in JC model without elasticity in the layer $H = 1.25mm$	79
3.17	Evolution of stress in JC model without elasticity with $H = 0.325mm$	80
3.18	Comparison of stress evolution in JC model without elasticity in different layer widths ($V_0 = 0.03m/s$)	80
3.19	Evolution of bandwidth (h) in JC model without elasticity in $H = 0.325mm$	81
3.20	Evolution of central temperature (T_{max}) in JC model without elasticity in $H = 0.325mm$	81
3.21	Influence of hardening factor on stress evolution in JC model without elasticity ($V_0 = 0.03m/s, H = 1.25mm$)	82
3.22	Evolution of bandwidth (h) in power model with different H (no exchange on $y \pm H$ and $V_0 = 0.5m/s$)	83
3.23	Evolution of stress in power model with different H (no exchange on $y \pm H$ and $V_0 = 0.5m/s$)	83
3.24	Evolution of the profiles of velocity and temperature by Rayleigh-Ritz method in exponential softening law ($V_0 = 0.1m/s$)	84

3.25	Evolution of central temperature and external temperature by Rayleigh-Ritz method in exponential softening law ($V_0 = 0.1m/s$)	84
3.26	Evolution of bandwidth (h) in exponential softening model with different $H(V_0 = 0.1m/s)$	85
3.27	Evolution of stress in exponential softening model with different $H(V_0 = 0.1m/s)$	85
3.28	Optimization of total potential with respect to cumulated plastic loading .	88
3.29	Comparison of stress evolution with FEM in JC law ($V_0 = 0.03m/s$ and $V_0 = 0.1m/s$)	90
3.30	Evolution of equivalent plastic displacement in JC law ($V_0 = 0.03m/s$ and $V_0 = 0.1m/s$)	91
3.31	Stress-plastic displacement(U_0^p) relation under cyclic loading and simple shear loading in JC law ($V_0 = 0.03m/s$ and $V_0 = 0.1m/s$)	92
3.32	Comparison of stress evolution under cyclic loading in JC law ($V_0 = 0.03m/s$)	92
3.33	Stress-charged displacement(U_0) relation under cyclic loading in JC law ($V_0 = 0.03m/s$)	93
3.34	Evolution of bandwidth under cyclic loading ((3.40) and (3.41)) in JC law ($V_0 = 0.03m/s$)	93
3.35	Evolution of central temperature under cyclic loading ((3.40) and (3.41)) in JC law ($V_0 = 0.03m/s$)	93
3.36	Influence of C on stress evolution under cyclic loading (3.40 and 3.41) in JC law ($V_0 = 0.03m/s$)	94
3.37	Error approximation of average stress under cyclic loading (3.40 and 3.41) in JC law	95
4.1	Pre-notched bar [Areias and Belytschko, 2007]	102
4.2	Displacement profiles under different mesh sizes at relatively steady state (adiabatic case)	104
4.3	Temperature profiles under different mesh sizes at relative steady state (adiabatic case)	105
4.4	Evolution of reaction force for different mesh sizes in adiabatic case . . .	106
4.5	Temperature profiles under different mesh sizes at relatively steady state (modelling with thermal conduction)	107
4.6	Equivalent plastic strain profiles under different mesh sizes at relatively steady state (modelling with thermal conduction)	107
4.7	Evolution of reaction force for different mesh sizes (modelling with thermal conduction)	108
4.8	Interface element [Ortiz and Pandolfi, 1999]	109
4.9	Definition of discontinuity part [Oliver, 1996b]	111
4.10	Shear band in XFEM[Areias and Belytschko, 2006]	112
4.11	Traction-separation law (a) and heat production (b) on discontinuity for exponential softening law	118

4.12 Shear band element[Ortiz and Pandolfi, 1999]	119
-------------------------------------------------------------	-----

List of Tables

2.1	Comparisons with the parameters a and c ($a = \bar{a} \frac{V_0}{L^2}$; $c = \bar{c} \frac{T_{ref}}{L^2}$)	33
2.2	Material property for HY-100 steel	36
2.3	Shear band width (dimensionless) and central temperature ($\beta = 0.38$; $V_0 = 0.1108$ m/s)	40
2.4	Comparisons of shear band width h and central temperature T_{max} with FEM	46
2.5	Material properties for Ti-6Al-4V (in steady state)	47
2.6	Comparisons of shear band width h and central temperature T_{max} with FEM (JC Model)	48
3.1	Material properties for Ti-6Al-4V (in transient state)	79

Bibliography

- [Areias and Belytschko, 2006] Areias, P. M. A. and Belytschko, T. (2006). Two-scale shear band evolution by local partition of unity. *International Journal for Numerical Methods in Engineering*, 66(5):878–910.
- [Areias and Belytschko, 2007] Areias, P. M. A. and Belytschko, T. (2007). Two-scale method for shear bands : Thermal effects and variable bandwidth. (March):658–696.
- [Armero and Simo, 1992] Armero, F. and Simo, J. C. (1992). A new unconditionally stable fractional step method for non-linear coupled thermomechanical problems. *International Journal for Numerical Methods in Engineering*, 35:737–766.
- [Armero and Simo, 1993] Armero, F. and Simo, J. C. (1993). A priori stability estimates and unconditionally stable product formula algorithms for nonlinear coupled thermo-plasticity. *International Journal of Plasticity*, 9:749–782.
- [Bai et al., 1994] Bai, Y., Xue, Q., Xu, Y., and Shen, L. (1994). Characteristics and microstructure in the evolution of shear localization in Ti-6Al-4V alloy. *Mechanics of Materials*, 17(2-3):155–164.
- [Batra and Chen, 1999] Batra, R. C. and Chen, L. (1999). Shear band spacing in gradient-dependent thermoviscoplastic materials. *Computational Mechanics*, 23(1):8–19.
- [Batra and Kim, 1992] Batra, R. C. and Kim, C. H. (1992). Analysis of shear banding in twelve materials. *International Journal of Plasticity*, 8(4):425–452.
- [Batra and Ko, 1992] Batra, R. C. and Ko, K. I. (1992). An adaptive mesh refinement technique for the analysis of shear bands in plane strain compression of a thermoviscoplastic solid. *Computational Mechanics*, 10(6):369–379.
- [Batra and Wei, 2006] Batra, R. C. and Wei, Z. (2006). Shear band spacing in thermoviscoplastic materials. *International Journal of Impact Engineering*, 32(6):947–967.
- [Batra and Wei, 2007] Batra, R. C. and Wei, Z. G. (2007). Instability strain and shear band spacing in simple tensile/compressive deformations of thermoviscoplastic materials. *International Journal of Impact Engineering*, 34(3):448–463.

- [Batra and Zhang, 2008] Batra, R. C. and Zhang, G. (2008). Modified Smoothed Particle Hydrodynamics (MSPH) basis functions for meshless methods, and their application to axisymmetric Taylor impact test. *Journal of Computational Physics*, 227(3):1962–1981.
- [Batra and Zhang, 2004] Batra, R. C. and Zhang, G. M. (2004). Analysis of adiabatic shear bands in elasto-thermo-viscoplastic materials by modified smoothed-particle hydrodynamics (MSPH) method. *Journal of Computational Physics*, 201(1):172–190.
- [Belytschko et al., 1988] Belytschko, T., Fish, J., and Engelmann, B. E. (1988). A finite element with embedded localization zones. *Computer methods in applied mechanics and engineering*, 70:59–89.
- [Belytschko et al., 2000] Belytschko, T., Liu, W. K., and Moran, B. (2000). *Nonlinear finite elements for continua and structures*.
- [Bodin, 1996] Bodin, L. (1996). *Bandes de cisaillement en thermo-viscoplasticité dynamique: applications à l’usinage et à la rupture ductile des métaux*. PhD thesis, Université de Metz.
- [Bouchnak, 2010] Bouchnak, T. B. (2010). *Etude du comportement en sollicitations extrêmes et de l’usinabilité d’un nouvel alliage de titane aéronautique: le Ti555-3*. PhD thesis, Paris institute of technology.
- [Chen and Batra, 1999] Chen, L. and Batra, R. C. (1999). Effect of material parameters on shear band spacing in work-hardening gradient dependent thermoviscoplastic materials. *International Journal of Plasticity*, 15:551–574.
- [Chichili et al., 2004] Chichili, D. R., Ramesh, K., and Hemker, K. J. (2004). Adiabatic shear localization in α -titanium: experiments, modeling and microstructural evolution. *Journal of the Mechanics and Physics of Solids*, 52(8):1889–1909.
- [Clifton and Molinari, 1983] Clifton, R. and Molinari, A. (1983). Localisation de la déformation viscoplastique en cisaillement simple: résultats exacts en théorie non linéaire. *C.R.Acad.Sci.Paris*, 2:1–4.
- [Dilello and Olmstead, 1997] Dilello, J. A. and Olmstead, W. E. (1997). Temporal evolution of shear band thickness. 45(3):345–359.
- [Dilello and Olmstead, 2003] Dilello, J. A. and Olmstead, W. E. (2003). Numerical solution of shear localization in Johnson – Cook materials. 35:571–580.
- [Dinzart and Molinari, 1998] Dinzart, F. and Molinari, A. (1998). Structure of adiabatic shear bands in thermo-viscoplastic materials. 17:923–938.
- [Fancello et al., 2006] Fancello, E. A., Ponthot, J.-P., and Stainier, L. (2006). A variational formulation of constitutive models and updates in non-linear finite viscoelasticity. *International Journal for Numerical Methods in Engineering*, 65(11):1831–1864.

- [Gioia and Ortiz, 1996] Gioia, G. and Ortiz, M. (1996). The two-dimensional structure of dynamic boundary layers and shear bands in thermoviscoplastic solids. *J.Mech.Phys.Solids*, 44(2):251–292.
- [Glimm et al., 1996] Glimm, J. G., Plohr, B. J., and Sharp, D. H. (1996). Mechanics of materials tracking of shear band I. The one-dimensional case. 24:31–41.
- [Grady, 1994] Grady, D. E. (1994). Dissipation in adiabatic shear bands. *Mechanics of Materials*, 17:289–293.
- [Guduru et al., 2001] Guduru, P., Rosakis, A., and Ravichandran, G. (2001). Dynamic shear bands: an investigation using high speed optical and infrared diagnostics. *Mechanics of Materials*, 33(7):371–402.
- [He, 1997] He, J. (1997). Equivalent theorem of Hellinger-Reissner and Hu-Washizu variational principles. *Journal of Shanghai University (English Edition)*, 1(1):36–41.
- [Hong et al., 2010] Hong, C., Tao, N., Huang, X., and Lu, K. (2010). Nucleation and thickening of shear bands in nano-scale twin/matrix lamellae of a Cu–Al alloy processed by dynamic plastic deformation. *Acta Materialia*, 58(8):3103–3116.
- [Hughes and Krishna, 1998] Hughes, T. J. R. and Krishna, G. (1998). A study of strain localization in a multiple scale framework-The one-dimensional problem. *Computer methods in applied mechanics and engineering*, 7825(97):193–222.
- [Jirasek and Belytschko, 2002] Jirasek, M. and Belytschko, T. (2002). Computational Resolution of Strong Discontinuities. In *Fifth World Congress on Computational Mechanics*.
- [Khan et al., 2004] Khan, A. S., Sung Suh, Y., and Kazmi, R. (2004). Quasi-static and dynamic loading responses and constitutive modeling of titanium alloys. *International Journal of Plasticity*, 20(12):2233–2248.
- [Larsson et al., 1996] Larsson, R., Runesson, K., and Sture, S. (1996). Soil based on regularized. *International Journal of Solids and Structures*, 33(2):3081–3101.
- [Leroy and Molinari, 1992] Leroy, Y. M. and Molinari, A. (1992). Stability of steady states in shear zones. *J.Mech.Phys.Solids*, 40(1):181–212.
- [Li et al., 2010] Li, D. H., Yang, Y., Xu, T., Zheng, H. G., Zhu, Q. S., and Zhang, Q. M. (2010). Observation of the microstructure in the adiabatic shear band of 7075 aluminum alloy. *Materials Science and Engineering: A*, 527(15):3529–3535.
- [Li et al., 2003] Li, Q., Xu, Y., and Bassim, M. N. (2003). Dynamic mechanical properties in relation to adiabatic shear band formation in titanium alloy-Ti17. *Materials Science and Engineering: A*, 358(1-2):128–133.

- [Li et al., 2000] Li, S., Hao, W., and Liu, W. K. (2000). Mesh-free simulations of shear banding in large deformation. *International Journal of Solids and Structures*, 37(48-50):7185–7206.
- [Li et al., 2001] Li, S., kam Liu, W., Qian, D., and Guduru, P. R. (2001). Dynamic shear band propagation and micro-structure of adiabatic shear band. *computational methods in applied mechanics and engineering*, 191:73–92.
- [Li and Liu, 2000] Li, S. and Liu, W. K. (2000). Numerical simulations of strain localization in inelastic solids using mesh-free methods. (January 1999):1285–1309.
- [Li et al., 2002] Li, S., Liu, W. K., Rosakis, A. J., Belytschko, T., and Hao, W. (2002). Mesh-free Galerkin simulations of dynamic shear band propagation and failure mode transition. *International Journal of Solids and Structures*, 39(5):1213–1240.
- [Liao and Duffy, 1998] Liao, S. C. and Duffy, J. (1998). Adiabatic shear bands in a Ti-6Al-4V titanium alloy. *J.Mech.Phys.Solids*, 46(11):2201–2231.
- [Longère et al., 2005] Longère, P., Dragon, A., Trumel, H., and Deprince, X. (2005). Adiabatic shear banding-induced degradation in a thermo-elastic/viscoplastic material under dynamic loading. *International Journal of Impact Engineering*, 32(1-4):285–320.
- [Love and Batra, 2006] Love, B. M. and Batra, R. C. (2006). Determination of effective thermomechanical parameters of a mixture of two elastothermoviscoplastic constituents. *International Journal of Plasticity*, 22(6):1026–1061.
- [Magness et al., 1994] Magness, L. S., Armstrong, R. W., Batra, R. C., Meyers, M. A., and Wright, T. W. (1994). High strain rate deformation behaviors of kinetic energy penetrator materials during ballistic impact. *Mechanics of materials*, 17(2-3):147–154. eng.
- [Marchand and Duffy, 1988] Marchand, A. and Duffy, J. (1988). An experimental study of the formation process of adiabatic shear bands in a structural steel. *Journal of the Mechanics and Physics of Solids*, 36(3):251–283.
- [Marsden and Hughes, 1983] Marsden, J. E. and Hughes, T. J. R. (1983). *Mathematical foundations of elasticity*.
- [Martinez et al., 2007] Martinez, F., Murr, L. E., Ramirez, A., Lopez, M., and Gaytan, S. M. (2007). Dynamic deformation and adiabatic shear microstructures associated with ballistic plug formation and fracture in Ti-6Al-4V targets. *Materials Science and Engineering: A*, 454-455:581–589.
- [Medyanik et al., 2007] Medyanik, S. N., Liu, W. K., and Li, S. (2007). On criteria for dynamic adiabatic shear band propagation. *Journal of the Mechanics and Physics of Solids*, 55(7):1439–1461.

- [Mercier, 1997] Mercier, S. (1997). *Etude de la formation et de la propagation d'une bande de cisaillement adiabatique*. PhD thesis, Université de Metz.
- [Meyer and Manwaring, 1986] Meyer, L. W. and Manwaring, S. (1986). *Metallurgical Applications of Shock-Wave and High-Strain-Rate Phenomena*.
- [Meyers et al., 2001] Meyers, M., Nesterenko, V. F., LaSalvia, J. C., and Xue, Q. (2001). Shear localization in dynamic deformation of materials: microstructural evolution and self-organization. *Materials Science and Engineering: A*, 317(1-2):204–225.
- [Meyers et al., 2003] Meyers, M., Xu, Y., Xue, Q., Pérez-Prado, M., and McNelley, T. (2003). Microstructural evolution in adiabatic shear localization in stainless steel. *Acta Materialia*, 51(5):1307–1325.
- [Moës et al., 1999] Moës, N., Dolbow, J., and Belytschko, T. (1999). A finite element method for crack growth without remeshing. *International journal for numerical methods in engineering*, 150(February):131–150.
- [Molinari, 1997] Molinari, A. (1997). Collective behaviour and spacing shear bands. 45(9):1551–1575.
- [Molinari and Clifton, 1987] Molinari, A. and Clifton, R. J. (1987). Analytical characterization of shear localization in thermoviscoplastic materials. *Journal of Applied Mechanics*, 54:806–812.
- [Murr et al., 2009] Murr, L. E., Ramirez, A. C., Gaytan, S. M., Lopez, M. I., Martinez, E. Y., Hernandez, D., and Martinez, E. (2009). Microstructure evolution associated with adiabatic shear bands and shear band failure in ballistic plug formation in Ti–6Al–4V targets. *Materials Science and Engineering: A*, 516(1-2):205–216.
- [Needleman and Tvergaard, 1992] Needleman, A. and Tvergaard, V. (1992). Analysis of plastic flow localization in metals. *Applied Mechanics Reviews*, 45:3–18.
- [Nemat-Nasser et al., 2001] Nemat-Nasser, S., Guo, W., Nesterenko, V. F., Indrakanti, S. S., and Gu, Y. (2001). Dynamic response of conventional and hot isostatically pressed Ti -6Al - 4V alloys : experiments and modeling. *Mechanics of Materials*, 33:425–439.
- [Nemat-Nasser and Li, 1998] Nemat-Nasser, S. and Li, Y. (1998). Flow stress of f.c.c polycrystals with application to ofhc cu. *Acta Materialia*, 46(2):565–577.
- [Nesterenko et al., 1998] Nesterenko, V., Meyers, M., and Wright, T. (1998). self-organization in the initiation of adiabatic shear bands.pdf. *Acta Materialia*, 46(1):327–340.
- [Odeshi et al., 2005] Odeshi, A., Bassim, M., Al-Ameeri, S., and Li, Q. (2005). Dynamic shear band propagation and failure in AISI 4340 steel. *Journal of Materials Processing Technology*, 169(2):150–155.

- [Odeshi et al., 2006] Odeshi, A. G., Bassim, M. N., and Al-Ameeri, S. (2006). Effect of heat treatment on adiabatic shear bands in a high-strength low alloy steel. *Materials Science and Engineering: A*, 419(1-2):69–75.
- [Oliver, 1996a] Oliver, J. (1996a). Modelling strong discontinuities in solid mechanics via strain softening constitutive equations. Part 1: Fundamentals. *International Journal for Numerical Methods in Engineering*, 39(January):3575–3600.
- [Oliver, 1996b] Oliver, J. (1996b). Modelling strong discontinuities in solid mechanics via strain softening constitutive equations. Part2: Numerical simulation. *International Journal for Numerical Methods in Engineering*, 39(February):3601–3623.
- [Oliver et al., 1999] Oliver, J., Cervera, M., and Manzoli, O. (1999). Strong discontinuities and continuum plasticity models : the strong discontinuity approach. *International Journal of Plasticity*, 15:319–351.
- [Ortiz and Camacho, 1996] Ortiz, M. and Camacho, G. T. (1996). Computational modelling of impact damage in brittle materials. *International Journal of Solids and Structures*, 33:2899–2938.
- [Ortiz et al., 1987] Ortiz, M., Leroy, Y. M., and Needleman, A. (1987). A finite element method for localized failure analysis. *Computer methods in applied mechanics and engineering*, 61:189–214.
- [Ortiz and Pandolfi, 1999] Ortiz, M. and Pandolfi, A. (1999). Finite-deformation irreversible cohesive elements for three-dimensional crack-propagation analysis. *International Journal for Numerical Methods in Engineering*, 44(9):1267–1282.
- [Ortiz and Stainier, 1999] Ortiz, M. and Stainier, L. (1999). The variational formulation of viscoplastic constitutive updates. *Computer Methods in Applied Mechanics and Engineering*, 171(3-4):419–444.
- [Peirs et al., 2008] Peirs, J., Verleysen, P., and Degrieck, J. (2008). The use of hat-shaped specimens for dynamics. (11).
- [Peirs et al., 2010] Peirs, J., Verleysen, P., Degrieck, J., and Coghe, F. (2010). The use of hat-shaped specimens to study the high strain rate shear behaviour of Ti–6Al–4V. *International Journal of Impact Engineering*, 37(6):703–714.
- [Rabczuk, 2007] Rabczuk, T. (2007). Discontinuous modelling of shear bands using adaptive meshfree methods. *computational methods in applied mechanics and engineering*, (August 2007).
- [Rabczuk et al., 2007] Rabczuk, T., Areias, P., and Belytschko, T. (2007). A simplified mesh-free method for shear bands with cohesive surfaces. (October 2006):993–1021.

- [Rabczuk and Samaniego, 2008] Rabczuk, T. and Samaniego, E. (2008). Discontinuous modelling of shear bands using adaptive meshfree methods. *Computer Methods in Applied Mechanics and Engineering*, 197(6-8):641–658.
- [Radovitzky and Ortiz, 1999] Radovitzky, R. and Ortiz, M. (1999). Error estimation and adaptive meshing in strongly nonlinear dynamic problems. *Computer Methods in Applied Mechanics and Engineering*, 172:203–240.
- [Ranc et al., 2008] Ranc, N., Taravella, L., Pina, V., and Herve, P. (2008). Temperature field measurement in titanium alloy during high strain rate loading—Adiabatic shear bands phenomenon. *Mechanics of Materials*, 40(4-5):255–270.
- [Russak, 2002] Russak, I. B. (2002). Calculus of variations MA 4311 lecture notes. Technical report.
- [Simo, 1991] Simo, J. C. (1991). Nonlinear stability of the time-discrete variational problem of evolution in nonlinear heat conduction, plasticity and viscoplasticity. *computational methods in applied mechanics and engineering*, 88:111–131.
- [Stainier, 2006] Stainier, L. (2006). Approche variationnelle en thermomécanique des solides.
- [Stainier, 2011a] Stainier, L. (2011a). Consistent incremental approximation of dissipation pseudo-potentials in the variational formulation of thermo-mechanical constitutive updates. *Mechanics Research Communications*, 38(4):315–319.
- [Stainier, 2011b] Stainier, L. (2011b). Energy-based variational approach for thermo-mechanical coupling under dynamic conditions. In *Int. Conf. on Computational Methods for Coupled Problems in Science and Engineering*, Kos, Greece.
- [Stainier et al., 2002] Stainier, L., Cuitiño, A. M., and Ortiz, M. (2002). A micromechanical model of hardening , rate sensitivity and thermal softening in bcc single crystals. *Journal of the Mechanics and Physics of Solids*, 50:1511–1545.
- [Stainier et al., 2005] Stainier, L., Fancello, E. A., and Ponthot, J.-p. (2005). A variational framework for nonlinear viscoelastic and viscoplastic models in finite deformation regime. In *Mecánica Computacional*, volume XXIV, pages 455–465.
- [Stainier and Ortiz, 2010] Stainier, L. and Ortiz, M. (2010). Study and validation of a variational theory of thermo-mechanical coupling in finite visco-plasticity. *International Journal of Solids and Structures*, 47(5):705–715.
- [Teng et al., 2007] Teng, X., Wierzbicki, T., and Couque, H. (2007). On the transition from adiabatic shear banding to fracture. *Mechanics of Materials*, 39(2):107–125.
- [Tzavaras and Gurtin, 1987] Tzavaras, A. E. and Gurtin, C. M. E. (1987). Effect of Thermal Softening in Shearing of Strain-Rate Dependent Materials. *Archive for Rational Mechanics and Analysis*, 99(4):349–374.

- [Wilson and Batra, 1998] Wilson, N. M. and Batra, R. C. (1998). Adiabatic shear bands in plane strain deformations of a WHA. *International Journal of Plasticity*, 14(1-3):43–60.
- [Wright, 1995] Wright, T. W. (1995). scaling laws for adiabatic shear bands. *International Journal of Solids and Structures*, 32(17):4–9.
- [Wright, 2002] Wright, T. W. (2002). *The physics and mathematics of adiabatic shear band*. Cambridge Monographs on Mechanics.
- [Wright, 2003] Wright, T. W. (2003). On the speed of an unconstrained shear band in a perfectly plastic material. *International Journal of Solids and Structures*, 40(4):871–879.
- [Wright and Ockendon, 1992] Wright, T. W. and Ockendon, H. (1992). A model for fully formed shear bands. Technical report.
- [Wright and Ockendon, 1996] Wright, T. W. and Ockendon, H. (1996). A scaling law for the effect of inertia on the formation of adiabatic shear bands. *International Journal of Plasticity*, 12(7):927–934.
- [Wright and Ravichandran, 1997] Wright, T. W. and Ravichandran, G. (1997). Canonical aspects of adiabatic shear band. 13(4):309–325.
- [Xue et al., 2008] Xue, Q., Bingert, J., Henrie, B., and Gray, G. (2008). EBSD characterization of dynamic shear band regions in pre-shocked and as-received 304 stainless steels. *Materials Science and Engineering: A*, 473(1-2):279–289.
- [Xue et al., 2002] Xue, Q., Meyers, M. A., and Nesterenko, V. F. (2002). Self-organization of shear bands in titanium and Ti–6Al–4V alloy. *Acta Materialia*, 50:575–596.
- [Xue et al., 2004] Xue, Q., Meyers, M. A., and Nesterenko, V. F. (2004). Self organization of shear bands in stainless steel. *Materials Science and Engineering: A*, 384(1-2):35–46.
- [Xue et al., 2003] Xue, Q., Nesterenko, V. F., and Meyers, M. A. (2003). Evaluation of the collapsing thick-walled cylinder technique for shear-band spacing. *International Journal of Impact Engineering*, 28(3):257–280.
- [Yadav et al., 2001] Yadav, S., Repetto, E. A., Ravichandran, G., and Ortiz, M. (2001). A computational study of the influence of thermal softening on ballistic penetration in metals. *International Journal of Impact Engineering*, 25(8):787–803.
- [Yang et al., 2005] Yang, Q., Mota, A., and Ortiz, M. (2005). A class of variational strain-localization finite elements. *International Journal for Numerical Methods in Engineering*, 62(8):1013–1037.

- [Yang et al., 2006] Yang, Q., Stainier, L., and Ortiz, M. (2006). A variational formulation of the coupled thermo-mechanical boundary-value problem for general dissipative solids. *Journal of the Mechanics and Physics of Solids*, 54(2):401–424.
- [Zhang, 1994] Zhang, X. (1994). On the propagation of a shear band in a steel tube. *Journal of Engineering Materials and Technology*, 116(April):155–161.
- [Zhou et al., 2006] Zhou, F., Wright, T. W., and Ramesh, K. (2006). The formation of multiple adiabatic shear bands. *Journal of the Mechanics and Physics of Solids*, 54(7):1376–1400.
- [Zhu and Batra, 1991] Zhu, Z. G. and Batra, R. C. (1991). Shear band development in a thermally softening viscoplastic body. *Computer & Structures*, 39(5):459–472.